Gisela Grupe · George C. McGlynn
Editors

Isotopic Landscapes in Bioarchaeology

Springer

Isotopic Landscapes in Bioarchaeology

Gisela Grupe • George C. McGlynn
Editors

Isotopic Landscapes in Bioarchaeology

Proceedings of the International Workshop "A Critical Look at the Concept of Isotopic Landscapes and its Application in Future Bioarchaeological Research", Munich, October 13–15, 2014

Springer

Editors
Gisela Grupe
Biozentrum
LMU München
Martinsried
Germany

George C. McGlynn
Staatssammlung f. Anthropologie
und Paläoanatomie
München, Bayern
Germany

ISBN 978-3-662-48338-1 ISBN 978-3-662-48339-8 (eBook)
DOI 10.1007/978-3-662-48339-8

Library of Congress Control Number: 2016932309

Springer Heidelberg New York Dordrecht London

Printed on acid-free paper

Springer-Verlag GmbH Berlin Heidelberg is part of Springer Science+Business Media (www.springer.com)

Preface

Isotopic landscapes ("isoscapes"), spatially and temporally defined stable isotopic patterns in geological and ecological settings, are indispensable tracers for the monitoring of the flow of matter through geo/ecological systems. The analysis of stable isotopes of the elements nitrogen, carbon, oxygen, strontium, and lead is now routinely employed as a tool in bioarchaeology for the purpose of reconstructing biodiversity, palaeodiet, palaeoecology, palaeoclimate, migration, and trade. The quest to better understand past human and animal movement and patterning in prehistoric and historic times has benefited substantially from developments, especially in the field of radiogenic isotope research.

The beginnings of stable isotope research in bioarchaeology date back to the 1980s, which means that we now have a foundation of more than 30 years of research. It is now commonly agreed upon that the explanatory power of stable isotopic ratios not only depends on a firm, testable hypothesis, but more importantly on the cooperative networking of scientists from both natural and social sciences. Application of multi-isotopic tracers potentially generates isotopic patterns with multiple dimensions, which may firmly characterize a find, but can no longer be interpreted by conservative statistics alone. Many efforts were, and still are, dedicated to decomposition research because molecules and crystals in archaeological tissues will nearly always be altered to a certain degree.

Stable isotope analysis of archaeological finds also gained significant benefits from the insights generated by examining the role stable isotopes play as natural tracers in modern ecology. Expectedly, things did not become easier, but rather more complex, primarily due to the growing understanding of the stable isotope flux through the bio-, hydro-, and geosphere, the substantial influence of physiological particularities and diet, and also the eminent danger of false-positive results brought about by diagenetic signals skewing the original biological signal. As a result, the question might be addressed whether isotopic landscapes in bioarchaeology actually exist at all—are we dealing with an ecogeological reality, or simply a concept, and is this concept really a silver bullet for providing needed answers?

Stable isotopes of light elements (hydrogen, carbon, nitrogen, oxygen, sulphur) are routinely measured for the reconstruction of individual and collective vertebrate dietary behaviour. In the case of human finds, diet is instead used as a vehicle for assessing past subsistence economies. Dietary reconstructions based on faunal remains provide information about habitat preference, feeding and herding management of domesticates, palaeoflora, and past climatic conditions, all of which are parameters that increase our understanding of human activities in the past. Stable oxygen isotopes and stable isotopes of heavy elements such as strontium and lead in particular are very helpful in identifying immigrated humans, imported animals, or objects that are not local to a specific site. Many colleagues active in this field share the experience that, in addition to their own research questions, there is a flood of inquiries from archaeologists with regard to whether dietary preferences of individuals or groups of people can be distinguished from each other, or if it is possible to identify individuals who immigrated to a certain site, and if so, whether it is possible to define the place of origin of these immigrants. These same questions also apply to animals.

No doubt, the answer to these questions will be yes, preceded by the word probably or possibly. However, subtle differences in dietary behaviour may not be assessed at all by stable isotope analysis, and even less subtle differences might remain undetected due to physiological reasons. Many immigrants to a site remain undetected because of an overall geographic redundancy of isotopic ratios. Specifying persons as locals or immigrants may in fact be incorrect because of a general misconception of how environmental isotopic signals are generated, and how they are transferred into the consumer's hard tissue. To put it short: sample processing protocols and the methods of mass spectrometry have long been established and validated, but the interpretation of the measurement data remains a tricky process. In this respect, colleagues from the natural sciences should perhaps undertake more efforts to better explain the method and its potential to their colleagues from the archaeological sciences to avoid expectations which are too high to be fulfilled or even met at all (let alone that both time and money could be saved or that alternative methodological approaches could be more promising). Measurement data seem to be astoundingly exact, yet should certainly only be handled as "proxy data" (or "uncertain data" in terms of computer sciences), especially when gathered from archaeological finds.

This book is dedicated to the proceedings of an international workshop entitled "A critical look at the concept of isotopic landscapes and its application in future bioarchaeological research", held from October 13 to October 15, 2014, in Munich, Germany. The meeting was financially supported by the German Research Foundation (Deutsche Forschungsgemeinschaft, DFG) and was organized within the frame of the DFG Research Unit "Transalpine Mobility and Culture Transfer" (FOR 1670; see www.for1670-transalpine.uni-muenchen.de). The meeting was augmented by a round-table discussion on biomineralization, organized and financed by the Center of Advanced Studies (CAS) of the Ludwig-Maximilian-University Munich. The research group FOR 1670 is a multidisciplinary

consortium aiming at the isotopic mapping of a specific reference region of eminent historical importance, namely the Inn-Eisack-Etsch passage which crosses the Alps and thereby connects South and North Europe. This transalpine route uses the Brenner Pass, which is the lowest pass across the Alps, and was in use as early as the Mesolithic as evidenced by numerous archaeological sites.

The meta-level of this project, however, addresses more general questions concerning archaeological isoscapes, which necessitate an in-depth discussion with specialists from the academic disciplines involved. Are archaeological skeletal finds really suitable for the generation of an isotopic map of a certain region of interest? How do diet, physiology, and ecogeography influence stable isotopic ratios? Do archaeological isotopic landscapes exist at all? What do we learn from modern isotopic mappings, such as the "Global network of isotopes in precipitation/rivers" projects (GNIP and GNIR, respectively)? Is it possible to mineralogically validate the isotopic data in a way that diagenetic alterations influencing these data can be excluded? Is a "multi-isotope fingerprint" superior to single isotopic ratios for provenance analyses, and how can modern data mining methods combined with a similarity search help in deciphering these fingerprints? And, specifically, what about cremated finds? For extensive prehistoric periods, cremating the dead was the major if not exclusive burial custom. Due to the high degree of fragmentation and thereby increased osteological efforts necessary for robust anthropological and archaeozoological diagnoses, less attention is frequently paid to cremations opposed to unburnt skeletal finds. Stable isotopes of light elements are thermally unstable, but radiocarbon dating of cremated finds can be successful—this is a breakthrough in bioarchaeological research, but how is this possible?

Expert contributions to these questions were presented on the workshop and are published in this book under the general headline of "Isotopic landscapes in bioarchaeology". We would like to stress that despite this concentration on contributions by natural scientists, a major contextual aspect must not be neglected which, however, was not in the focus of this conference, namely the concept underlying terms such as "mobility" versus "migration" or "import". Stable isotope analysis is not an end in itself, but a useful tool for answering questions which are also generated by the social sciences, and a firm exploration of potentials and limits is indispensable.

According to the pertinent methodological questions, this volume is divided into four parts that are nonetheless related to each other contextually due to the nature of the subject. Part I focuses on the rather neglected substrate of cremations, their anthropology, mineralogy, and radiocarbon dating. Geological aspects of isotopic landscapes are addressed in Part II, and the ecological aspects of isotopic landscapes are dealt with in Part III. Part IV, finally, addresses innovative methods of processing multi-isotope signatures by computer scientists. Preceding the chapters is a contribution by Elizabeth Harper on the more general topic of biomineralization, presented on the aforementioned round table at the Center of Advanced Studies of the LMU.

The workshop, the round table, and therefore this book could not have been realized without financial support by the Deutsche Forschungsgemeinschaft and the

Center of Advanced Studies. We are most indebted to Dr. Michael Apel, Director of the Museum of Man and Nature in Munich, who hosted the workshop in the conference room of his museum at Nymphenburg Castle. Special thanks go to our staff members who were of tremendous help in the organization, namely Monika Retzbach-Boulesnam, Dr. Andrea Grigat (scientific coordinator of the Research Group FOR 1670), M.Sc. Julia Niggemeyer, and M.Sc. Nils Turner.

Participants of the workshop in front of the Museum "Man and Nature". *Photo*: J. Niggemeyer

Martinsried, Germany — Gisela Grupe
München, Germany — George C. McGlynn
March 2015

Contents

List of Contributors

Johannes A.C. Barth Department of Geography and Geosciences, GeoZentrum Nordbayern, FAU Erlangen-Nürnberg, Erlangen, Germany

James H. Burton Department of Anthropology, University of Wisconsin, Madison, WI, USA

Gisela Grupe Ludwig-Maximilians-Universität München, Biozentrum, Martinsried, Germany

Rachel Hahn Department of Anthropology, University of Wisconsin, Madison, WI, USA

Elizabeth M. Harper Department of Earth Sciences, University of Cambridge, Cambridge, UK

Stefan Hölzl RiesKraterMuseum Nördlingen, Nördlingen, Germany

Dorrit E. Jacob Department of Earth and Planetary Sciences, Macquarie University, North Ryde, NSW, Australia

Department of Geosciences, Johannes Gutenberg University, Mainz, Germany

Balazs Kocsis Sektion Kristallographie, Ludwig-Maximilians-Universität München, Munich, Germany

Hans-Peter Kriegel Lehr-und Forschungseinheit für Datenbanksysteme, Ludwig-Maximilians-Universität München, Munich, Germany

Peer Kröger Lehr-und Forschungseinheit für Datenbanksysteme, Ludwig-Maximilians-Universität München, Munich, Germany

Christina Lihl Institut für Grundwasserökologie, Helmholtz-Zentrum München, Ingolstädter Landstr, Neuherberg, Germany

Cheryl Makarewicz Institut für Ur- und Frühgeschichte, Christan-Albrechts-Universität Kiel, Kiel, Germany

Markus Mauder Lehr-und Forschungseinheit für Datenbanksysteme, Ludwig-Maximilians-Universität München, Munich, Germany

Christoph Mayr Institut für Geographie, Friedrich-Alexander Universität Erlangen-Nürnberg, Erlangen, Germany

Paläontologie und Geobiologie, Ludwig-Maximilians-Universität München, Munich, Germany

George McGlynn Staatssammlung für Anthropologie und Paläoanatomie, Munich, Germany

Jacqueline I. McKinley Wessex Archaeology, Salisbury, UK

Eirini Ntoutsi Lehr-und Forschungseinheit für Datenbanksysteme, Ludwig-Maximilians-Universität München, Munich, Germany

Wolfgang Schmahl Sektion Kristallographie, Ludwig-Maximilians-Universität München, Munich, Germany

Frank Söllner Department für Geo- und Umweltwissenschaften, Ludwig-Maximilians-Universität München, Munich, Germany

Bruno Streit Department of Ecology and Evolution, Goethe University Frankfurt, Frankfurt/Main, Germany

Anita Toncala Ludwig-Maximilians-Universität München, Biozentrum, Martinsried, Germany

Peter Tropper Institute of Mineralogy and Petrography, University of Innsbruck, Innsbruck, Austria

Robert van Geldern Department of Geography and Geosciences, GeoZentrum Nordbayern, FAU Erlangen-Nürnberg, Erlangen, Germany

Mark van Strydonck Royal Institute for Cultural Heritage (KIK-IRPA), Brussels, Belgium

Igor Villa Centro Universitario Datazione e Archeometria, Università di Milano Bicocca, Milano, Italy

Institute of Geological Sciences, University of Bern, Bern, Switzerland

Stefan Ziegler Department of Ecology and Evolution, Goethe University Frankfurt, Frankfurt/Main, Germany

WWF Germany, Berlin, Germany

Unanswered Questions in the Evolution of Biomineralisation

Elizabeth M. Harper

Introduction

Organisms have been building hard parts since the Late Precambrian. In fact representatives of all Kingdoms are able to biomineralise in the form of granules, plates, tubes, shells, bones or teeth. Biomineralised structures are mainly composites consisting of a mineralised component dispersed in an organic matrix and show an extraordinary diversity of microstructural arrangements and combinations. This wealth of diversity has stimulated a huge amount of interest and research, attracting the attention of biologists, materials scientists, archaeologists and palaeontologists and is increasingly using highly sophisticated techniques and interdisciplinary research to delve into the intricacies (e.g. DiMasi and Gower 2014).

Research on patterns of biomineralisation has been used in unravelling relationships between organisms (Bieler et al. 2014) or understanding functional morphology (e.g. Carter and Schneider 1997) and also for gaining an understanding for more applied uses, such as using bones or shells as geochemical proxies for assessing environmental parameters on both geological (Branson et al. 2013; Bell et al. 2014) and archaeological (Richards and Hedges 1999; Privat et al. 2002) timescales. The ability of organisms to produce low-density materials with a range of superior mechanical properties (toughness, high resistance to brittle failure) has implications in the synthesis of novel materials (Kaplan 1998; De Paula et al. 2010) and medical applications (Liao et al. 2000; Berland et al. 2005). Finally, our increasing concern about increased acidity in ocean waters has focused attention on the high dependency of many invertebrate taxa on building and maintaining their shells (Ries et al. 2009; Kroeker et al. 2013; Hyun et al. 2014).

E.M. Harper (✉)
Department of Earth Sciences, University of Cambridge, Downing Street, Cambridge CB2 3EQ, UK
e-mail: emh21@cam.ac.uk

G. Grupe, G.C. McGlynn (eds.), *Isotopic Landscapes in Bioarchaeology*,
DOI 10.1007/978-3-662-48339-8_1

In such a field of active multidisciplinary research, it is difficult to provide an overall synthesis of the state of knowledge or to give an exhaustive sense of questions which need answers. However, this contribution attempts to highlight areas of research that are interesting in the context of understanding the very evolution of hard parts. It is a personal rather than definitive account and, as such, dwells on molluscan matters.

Are We Seeing the First Biomineralisers?

The beginnings of biomineralised hard parts, as recognised by the appearance of skeletal body fossils, are famously abrupt, heralding the start of the credible fossil record at the start of the Phanerozoic. If we want to tackle questions as to when, where and how biomineralisation started and to tease apart evidence for what selection pressures and enabling conditions were, we need an accurate fossil record.

Much has been done in the last decade to synthesise data on the fossil record of the first biomineralisers (Zhuravlev and Wood 2008; Wood 2011; Wood and Zhuravlev 2012). But such compilations are critically dependent on the quality of the fossil record itself. Here, more than perhaps elsewhere in the fossil record, the vagaries of taphonomic loss of original mineralogy, microstructure and detail are of great importance. It is notable that 'small shelly fossils' are relatively robust, complex objects. It seems unlikely that hard parts evolved in quite such an 'advanced' form and suggests perhaps that by their first appearance in the fossil record both the biochemical machinery and selection pressures necessary for the evolution of hard parts were already in place. Even earlier hard parts may have been made of very small units or have been very weakly mineralised, perhaps made of unstable mineral phases, or perhaps just from binding together abiotic grains supplied by the local sediments. The circumstances in which we might be able to recognise early products of biomineralisation are heavily dependent on lagerstätten (e.g. Zhang et al. 2014), and either lack of opportunity or failure to recognise these may impede our recognition of the earliest biomineralised structures.

We might perhaps expect early hard parts to rely on agglutination of raw materials from the abiotic environment. Bengtson (1994) and Lipps (1992) point out that agglutinated skeletons have been widespread amongst a wide range of protists and metazoans (molluscs, phoronids, polychaetes and insects) since the Cambrian, and McIlroy et al. (2001) describe agglutinated tubes from the Ediacaran that are interpreted by them as foraminifera. These agglutinated hard parts rely on producing sticky surfaces on to which grains can be 'planted'. For example in bivalves, many modern and fossil anomalodesmatans attach sediment grains to the outsides of their shells by arenophilic threads, secreted by glands in the mantle (Sartori and Harper 2009). Such agglutinated structures are easy and, presumably, metabolically cheap ways to make skeletons. The potential for building really substantial hard parts by agglutination is highlighted by the modern bivalves *Granicorium* and *Samarangia*. These animals have smooth, relatively thin

aragonite shells but build themselves extraordinary 'concrete overcoats' complete with radial ornament fashioned by what is effectively early diagenesis, perhaps mediated by bacteria, of mucus-bound sediment particles (Taylor et al. 1999; Braithwaite et al. 2000). These extraordinary shells had been previously overlooked; indeed overzealous preparators had routinely 'scraped them clean'. How capable are we of recognising such biomineralisation in the fossil record?

Many taxa biomineralise by means of laying down crystals onto a thin flexible organic sheet, for example the periostracum of molluscs and brachiopods. The periostracum functions both to separate the site of shell formation from the ambient fluid and also to form the template onto which the shell is then secreted, as well as other secondary functions such as retarding shell dissolution (Taylor and Kennedy 1969; Harper 1997). It is, however, becoming increasingly clear, in bivalves at least, that this sheet forms not just the template *onto* which calcium carbonate is deposited but also that calcification occurs within the sheet itself (Checa and Harper 2010; Checa et al. 2014). Early calcification occurs in the form of isolated spikes, but subsequently the inner layer of the periostracum becomes fully mineralised as the outermost layer of the bivalve shell. In the case of the palaeoheterodont *Neotrigonia*, 'spike' formation occurs deep within the periostracal groove at the very early stages of periostracum formation long before it reaches the shell margin (Checa et al. 2014). It is plausible to suggest this also as a model for early shell formation, but again this form of very basic biomineralisation would be difficult to recognise in fossil material.

Aside from the problems of recognising biomineralised structures as such, taphonomic problems also make identification of original mineralogies and microstructures less certain. Nevertheless, original microstructure may be determined from the surface topography of phosphatic internal moulds (Runnegar 1985), although the interpretation of these has not always been straightforward; see Vendrasco et al. (2011) for discussion. Such mouldic preservation requires original mineralogy to be inferred, in the case of early molluscs as aragonite. In other instances, where replaced shell material is present, suggestion of original mineralogy may be made using elemental analysis, ghost fabrics, isotopic evidence or from relying on phylogenetic inference (see Wood and Zhuravlev 2012).

The above points notwithstanding, the record of the evolution of well-recognised hard parts shows that biomineralisation evolved in a wide range of taxa, employing a number of different biominerals over a, geological speaking, rather narrow time interval. Zhuravlev and Wood (2008) recognise a window of time from the late Ediacaran to the Middle Ordovician when the majority of biomineralising groups are recognised in the fossil record with hard parts. Earlier instances are known, for example the Neoproterozoic modular *Namapoikia* (Wood et al. 2002) and scales of the earliest known mineralising protist (Cohen et al. 2011) from the mid-Neoproterozoic of Canada. During that time interval mineralised skeletal parts appear in taxa as disparate as single-celled organisms, sponges, corals, trilobites, annelids and chordates. The mineral phase of these hard parts is commonly calcium carbonate, silica or calcium phosphate, with the ability to secrete each evolved a number of times. Knoll (2003) estimates, for example, that calcium

carbonate hard parts have evolved at least 20 times in the Metazoa alone. It is also interesting that most major mineralisers arise at this time; there are few major mineralising clades which have evolved since the early Palaeozoic, although scleractinians which evolved from naked corals started to secrete aragonite in the Triassic (Stanley and Fautin 2001) and calcifying coccoliths in the Triassic (Siesser 1993) are obvious exceptions. Thomas and Reif (1993) document the myriad of different ways in which skeletons are achieved by organisms, and Thomas et al. (2000) show that 80 % of these are exploited by the Middle Cambrian.

Why Did Biomineralisation Evolve?

Clearly biomineralisation is polyphyletic, but this sudden explosion into a wealth of taxonomic and mineralogical diversity suggests strongly that the 'time was right' in the particular narrow window of geological time at the end of the Precambrian and the beginning of the Phanerozoic. But it is far from clear why this was the case. Was it because there was a sudden urgent selection pressure towards biomineralisation or might there have long been an ongoing advantage for organisms to possess hard parts, but that environmental conditions prevented or impeded their evolution until some 'trigger' event?

What Were the Selection Pressures Which Favoured Biominerlisation?

It seems intuitively obvious that many instances of biomineralisation produce structures whose primary functions are support (e.g. the vertebrate skeleton), crushing offensive weapons (e.g. jaws in worms and vertebrates, claws in many arthropod groups) or protection (shells of molluscs, brachiopods and the mineralised carapaces of some arthropods). Biominerals, however, may have other functions, such as the highly sophisticated double calcite lenses of trilobite eyes (Gál et al. 2000) or the 'love darts' in pulmonate snails (Hasse 2002). Although these two examples are almost certainly a derived, secondary use of biomineralisation, it may be less easy in other instances what functionality has been co-opted.

A common explanation for the evolution of hard parts is to appeal to a common selection pressure and the evolution of early predators (Vermeij 1990; Bengtson 1994; Knoll 2003; Porter 2011). The suggestion, therefore, is that they were primarily defensive. Alternative suggestions have been linked to the need to expel toxic calcium ions (Simkiss 1977) or that increase in body size allowed by increasing oxygen levels required support (Nicol 1966; Vermeij 1990). There is good evidence that Cambrian seas hosted a range of predators, as evidenced by the recognition of preserved gut contents (Conway Morris 1977), functional

morphology (Daley et al. 2013), coprolite contents (Shen et al. 2014) and healed injuries (Conway Morris and Jenkins 1985) or borings (Bengtson and Yue 1992). At least some of the hard parts produced at this time appear defensive, for example shells that contain and protect soft tissues, although again it is not easy to determine that this was their initial function. However, I am not wholly convinced of the view of Knoll (2003, p. 339) that 'The diverse skeletons of Cambrian organisms share only one principal feature in common—they would have protected their owners against the bilaterian animal predators that took shape during the Cambrian explosion'. It is not obvious that all Cambrian hard parts are defensive. Some, for example chaetognath jaws, may even have been offensive, and whereas exoskeletons might offer either a place to hide or at least deflect blows, it is difficult to envisage most endoskeletons in this way. In much the same way as the explanation for lack of healed injuries in bivalve organism (Vermeij 1983), predators repelled by an internal skeleton will already have caused substantial soft tissue damage, with the result that even if the initial predation attempt is unsuccessful leakage of body fluids and metabolites will attract secondary predators or scavengers. In these instances perhaps it is more probable that support was the primary function. The only exception to this might be for more modular organisms, such as sponges and cnidarians, where predation is more akin to grazing (Rotjan and Lewis 2009) and small spicules embedded in the soft parts may deter or limit such attacks, though here again the arrangement of the megascleres, even in Cambrian forms, for example *Eiffelia* (Botting and Butterfield 2005), provides a rigid framework for support.

What Were the Environmental Facilitators Which Allowed Biomineralisation?

If there are advantages in possessing hard parts, did some environmental change in the Late Precambrian/early Phanerozoic facilitate their multiple acquisition? Various authors have suggested links with ocean chemistry changes. Widely cited events are phosphate spikes (e.g. Cook and Shergold 1984), increasing calcium levels (Brennan et al. 2004) and carbonate shifts (Riding 1982; Zhuravlev and Wood 2008), but it is difficult to reconcile these with the broad array of mineral types being used (Knoll 2003). Perhaps a more overarching solution comes with the idea of increasing levels of increasing atmospheric oxygen (e.g. Canfield et al. 2007) or at least increasing ventilation of oxygen through seawater (Butterfield 2009), necessary to fuel the metabolic costs of biomineralising or perhaps the recognition of major perturbations to the carbon cycle at the Pre-Cambrian/Cambrian transition (Knoll 2003).

What Influences the Mineralogy Exploited?

Lowenstam and Weiner (1989) list over 60 different minerals which have been recognised as being used by organisms and the list is growing, for example the addition of greigite (Fe_3S_4) from the foot scales of an extraordinary hydrothermal vent gastropod (Warén et al. 2003). However, the vast majority of hard parts are composed of a number of polymorphs of calcium carbonate, calcium phosphate or hydrated silica. Neontological and palaeontological evidence suggests that the mineralogy used by particular clades is usually fixed, implying a strict genetic control. There are, however, reports of 'unexpected' mineralogies in fossil material, e.g. aragonite in early brachiopods (Balthasar et al. 2011) and apparent primary calcite in a Cretaceous scleractinian coral (Stolarski et al. 2007), and there is also evidence that in particular rather extreme experimental conditions of altered seawater composition animals may be induced to secrete skeletal material of a different mineralogy (Checa et al. 2007).

It has often been suggested that for calcium carbonate secreters, taxa first utilise and then retain the mineralogy which is compatible with the seawater chemistry in which they evolve (Wilkinson 1979; Stanley and Hardie 1998; Porter 2007). In a detailed survey, Wood and Zhuravlev (2012) show that there are clear patterns in the mineralogy developed in late Precambrian and Cambrian biomineralisers. The aragonite-facilitating seas of the Ediacaran/early Cambrian were populated either by aragonitic or high magnesium calcite secreters, whereas in the subsequent 'calcite' sea these calcareous organisms were joined only by those secreting low magnesium calcite. These authors go on further to dissect the utilisation of aragonite and high magnesium calcite, discovering that there is some degree of ecological separation: aragonite (and later low magnesium calcite) was used by sessile unattached taxa (including some motile) whilst those which were sessile and attached tended to use high magnesium calcite. It is perhaps implicit here that there must have been particular benefits for these ecological associations, but exactly what these were is not clear. Wood and Zhuravlev (2012) also note that early Cambrian small shelly fossils utlilised calcium phosphate, at a time coincident with the seawater phosphate spike noted by Cook and Shergold (1984). These early phosphatisers are interpreted as sessile cnidarians or lophotrochozoans, but later calcium phosphate became prevalent in highly energetic motile forms, i.e. amongst the chordates, some arthropods and the chaetognaths. Wood and Zhuravlev (2012) interpret this preference for calcium phosphate in active groups to be associated with the lower solubility of this mineral (compared to carbonates) in lower pH extracellular fluids which accompany such activity.

The Calcite Versus Aragonite Problem

Aside from the deep time aspects of polymorph choice, another aspect of some interest is understanding clades in which both low magnesium calcite and aragonite secretions are possible and that shells are produced with distinct layers of each. On occasion, bivalves also may produce the metastable carbonate Vaterite, for example in the shells of the freshwater *Corbicula fluminea*, but this is clearly pathogenic (Spann et al. 2010). Understanding the distribution of calcite and aragonite question has long been pondered by mollusc workers (reviewed in Harper 2000) but is also an issue for bryozoologists (Taylor et al. 2014).

Within molluscs it seems clear the primitive mineralogy was wholly aragonitic (Taylor 1973; Vendrasco et al. 2011) and there is good biochemical evidence to show that the choice of polymorph is strictly controlled by the organism by the presence of specific proteins within the organic matrix (Falini et al. 1996). However, a range of modern and fossil gastropods and bivalves also secrete both aragonite and calcite. This is clearly a polyphyletic trait—both in terms of the classes but also within. For example, in the bivalves there are at least four clades which secrete continuous layers of calcite (Carter 1980). The patterns of this expression are interesting. Although some infaunal bivalves do lay down calcite, it is a peculiarity of some individuals and in the form of patches rather than continuous shell layers (Carter et al. 1998). Continuous shell layers of calcite are restricted to epifaunal taxa, and, interestingly, the first appearance of calcite within these clades was always in the outer shell layer and no bivalve has ever entirely lost aragonite from the shell. The pattern observed in gastropods is very similar (Taylor and Reid 1990).

Explanations for the evolution of calcitic microstructures in molluscs fall into two types: (1) physiological and (2) adaptive. Lowenstam (1954) and Carter et al. (1998) suggested a physiological control suggesting that cold water taxa have higher calcite:aragonite ratios. However, this has been demonstrated unambiguously in relatively few cases (Taylor and Reid 1990) and it is difficult to explain the persistence of wholly aragonitic taxa (including all those which are infaunal) in either high latitude or deep sea faunas or why the temperature effect should only influence the outer shell layers, although Carter et al. (1998) suggest that it is the temperature that initially facilitates the deposition of calcite but go on to suggest that this may then be the basis for selection where it is advantageous. The idea that calcitic shell layers are in some way adaptive is tantalising. Taylor and Reid (1990) provide a very elegant hypothesis that explains the development in outer shell layers as an anti-dissolution trait based on the lower solubility of calcite compared to aragonite. They go on to show that calcitic shell layers are particularly prevalent and well developed in molluscs that live intertidally, an environment where there are marked diurnal changes in solubility of calcium carbonate driven by the changes in photosynthetic activities of marine algae (Daniel and Boyden 1975). It is, however, puzzling that freshwater and deep sea molluscs, which inhabit environments with more aggressive dissolution, do not appear to have evolved this

adaptation, and experimental dissolution work by Harper (2000) has shown that merely comparing inorganic properties of minerals is not a reliable guide to their physical properties: crystal size and organic matrix content all also influence solubility with the result that some aragonitic microstructures, such as nacre, are actually relatively insoluble.

What Are the Metabolic Costs of Biomineralisation?

Many of our questions about why particular mineralogies and microstructures were or are used by particular taxa might be better answered if we know more about the relative costs of biomineralisation. These are not easy questions to tackle experimentally, and, as in all of these instances, even if we know the metabolic costs for say coccoliths, it does not automatically follow that we would be able to apply those to such disparate organisms as molluscs or corals. It is also relevant to consider other aspects of the organism's biology and the relative importance of biomineralisation in their overall energy budgets. Although the metabolic rate of brachiopods is very low (Peck et al. 1997) and they make relatively thin shells, these, along with calcareous spicules within the tissue, make up >90 % of the dry weight of the animal (Peck 2008), and, therefore, the energy budget allocated to biomineralisation must be proportionately high, particularly compared with bivalves which physiologically are much more active.

Despite our general lack of knowledge on the topic, metabolic costs are often cited as explanations as to why certain shell microstructures are utilised and not others. For example it has been suggested that even though molluscan nacre is famously, tough and crack resistant, it has been lost in certain lineages because it is metabolically expensive to produce (Palmer 1983). There is a persistent suggestion that the major physiological cost of 'shell' secretion is making the organic matrix and that the cost of the mineral phase is negligible (Palmer 1983, 1992; Bengtson 1994, 2004; Wood 2011), but it is not clear that this is necessarily so, or if it is universal. Perhaps again, most work has been done on molluscs where it is known that there is very wide range variation in organic matrix content between different microstructures (from 0.1 % to over 8 % dry weight of shell). Palmer's work on gastropods showed that those taxa with more organic-rich microstructures grew and repaired faster than those with less.

The assumption that the mineral phase is easy to produce has not been tested. Wood and Zhuravlev (2012) go further and suggest that low magnesium calcite is cheaper to produce than either high magnesium calcite or aragonite based on their lattice energies (Mackenzie et al. 1983), but again it is not clear that this is necessarily true, nor the same for all biomineralising groups. Although biomineralisation pathways are, as yet, incompletely understood, it is clear that not all pathways are the same and that biominerals are not identical to their inorganic counterparts, for example in the inclusion of macromolecules within the crystals. The three crystallisation pathways discussed by Weiner and Addadi (2011) all

require movement of ions from an external or body fluid (which may often be by active transport, pumping against concentration gradients). Weiner and Addadi show that of three considered pathways, biomineralisation involves transport of material in a transient disordered state, sometimes in membrane-bound vesicles, to the site of the final crystallisation. These processes are likely to involve active transport.

Final Remarks

Scientists have been researching biomineralised structures for many decades, but some groups, such as bivalve molluscs, because of their economic or ecological importance have been extensively studied in this respect (Boggild 1930; Taylor et al. 1969, 1973; Carter 1990), other groups less well so. Even in taxa that are historically well studied, research is very active. New analytical techniques are opening new avenues for research (DiMasi and Gower 2014) and the prospect of reaching a much deeper understanding of the genetic controls involved in shell manufacture (Sleight et al. 2015).

It is important that we recognise that processes or patterns are likely to differ to some greater or lesser extent between groups of biomineralisers and apply information learnt about one group uncritically to another. The answers to many of the questions posed in this contributions are interwoven with one another, and their solutions will be found by collaborations between different disciplines.

Acknowledgements I was very grateful to be invited to take part in the Round Table discussion. 'Biomineralization—Lessons from the past and for the future' which proved a stimulating and thought-provoking session, really showing us how much more there is to learn.

References

Balthasar U, Cusack M, Faryma L, Chung P, Holmer LE, Jin J, Percival IG, Popov LE (2011) Relic aragonite from Ordovician-Silurian brachiopods: implications for the evolution of calcification. Geology 39:967–970

Bell DB, Jung SJA, Kroon D, Lourens LJ, Hodell DA (2014) Local and regional trends in Plio-Pleistocene δ18O records from benthic foraminifera. Geochem Geophys Geosyst 15:3304–3321

Bengtson S (1994) The advent of animal skeletons. In: Bengtson S (ed) Early life on earth, Nobel symposium 84. Columbia University Press, New York, NY, pp 412–425

Bengtson S (2004) Early skeletal fossils. In: Lipps H, Wagooner BM (eds) Neoproterozoic–Cambrian biological revolutions, vol 10. The Paleontological Society Papers, Austin, pp 67–77

Bengtson S, Yue Z (1992) Predatorial borings in late Precambrian mineralized exoskeletons. Science 257:267–369

Berland S, Delattre O, Borzeix S, Catonné Y, Lopez E (2005) Nacre/bone interface changes in durable nacre endosseous implants in sheep. Biomaterials 26:2767–2773

Bieler R, Mikkelsen PM, Collins TM, Glover EA, González VL, Graf DL, Harper EM, Healy J, Kawauchi GY, Sharma PP, Staubach S, Strong EE, Taylor JD, Tëmkin I, Zardus JD, Clark S, Guzmán A, McIntyre E, Sharp P, Giribet G (2014) Investigating the bivalve tree of life – an exemplar-based approach combining molecular and novel morphological characters. Invertebr Syst 28:32–115

Boggild OB (1930) The shell structure of the molluscs. Det Kongelige Danske Videnskabernes Selskrabs Skrifter, Naturvidenskabelig og Mathematisk Afdeling 2:231–326

Botting JP, Butterfield NJ (2005) Reconstructing early sponge relationships by using the Burgess Shale fossil *Eiffelia globosa*, Walcott. Proc Natl Acad Sci U S A 102:1554–1559

Braithwaite CJR, Taylor JD, Glover EA (2000) Marine carbonate cements, biofilms, biomineralization, and skeletogenesis: some bivalves do it all. J Sediment Res 70:1129–1138

Branson O, Redfern SAT, Tyliszczak T, Sadekov A, Langer G, Kimoto K, Elderfield H (2013) The coordination of Mg in foraminiferal calcite. Earth Planet Sci Lett 383:134–141

Brennan ST, Lowenstein TK, Horita J (2004) Seawater chemistry and the advent of biocalcification. Geology 32:473–476

Butterfield NJ (2009) Oxygen, animals and oceanic ventilation: an alternative view. Geobiology 7:1–7

Canfield DE, Poulton SW, Narbone GM (2007) Late-Neoproterozoic deep-ocean oxygenation and the rise of animal life. Science 315:92–95

Carter JG (1980) Environmental and biological controls of bivalve shell mineralogy and microstructure. In: Rhoads DC, Lutz RA (eds) Skeletal growth of aquatic organisms. Plenum Press, New York, pp 69–113

Carter JG (1990) Skeletal biomineralization: patterns, processes and evolutionary trends. Van Nostrand and Reinhold, New York

Carter JG, Schneider JA (1997) Condensing lenses and shell microstructure in *Corculum* (Mollusca, Bivalvia). J Paleontol 71:56–61

Carter JG, Barrera E, Tevesz MJS (1998) Thermal potentiation and mineralogical evolution in the Bivalvia (Mollusca). J Paleontol 72:991–1010

Checa AG, Harper EM (2010) Spikey bivalves: intra-periostracal crystal growth in anomalodesmatans. Biol Bull 219:231–248

Checa AG, Jiménez-López C, Rodríguez-Navarro A, Machado JP (2007) Precipitation of aragonite by calcitic bivalves in Mg-enriched marine waters. Mar Biol 150:819–827

Checa AG, Salas C, Harper EM, Bueno-Pérez J (2014) Early stage biomineralization in the periostracum of the 'living fossil' bivalve *Neotrigonia*. PLoS One 9(2):e90033

Cohen PA, Schopf JW, Butterfield NJ, Kudryavtsev AB, MacDonald FA (2011) Phosphate biomineralization in mid-Neoproterozoic protists. Geology 39:539–542

Conway Morris S (1977) Fossil priapulid worms. Spec Pap Palaeontol 20:1–95

Conway Morris S, Jenkins RJF (1985) Healed injuries in early Cambrian trilobites from South Australia. Alcheringa 9:167–177

Cook PJ, Shergold JH (1984) Phosphorus, phosphorites and skeletal evolution at the Precambrian–Cambrian boundary. Nature 308:231–236

Daley AC, Paterson JR, Edgecombe GD, García-Bellido DC, Jago JB (2013) New anatomical information on *Anomalocaris* from the Cambrian Emu Bay Shale of South Australia and a reassessment of it inferred predatory habits. Palaeontology 56:971–990

Daniel MJ, Boyden CR (1975) Diurnal variations in physico-chemical conditions within intertidal rockpools. Field Stud 4:161–176

De Paula SM, Huila MFG, Araki K, Toma HE (2010) Confocal Raman and electronic microscopy studies on the topotactic conversion of calcium carbonate from *Pomacea lineata* shells into hydroxyapatite bioceramic materials in phosphate media. Micron 41:983–989

DiMasi E, Gower LB (eds) (2014) Biomineralization sourcebook. CRC Press, Boca Raton, FL

Falini G, Albeck S, Weiner S, Addadi L (1996) Control of aragonite or calcite polymorphism by mollusk shell macromolecules. Science 271:67–69

Gál J, Horváth G, Clarkson EN, Haiman O (2000) Image formation by bifocal lenses in a trilobite eye? Vision Res 40:843–853

Harper EM (1997) The molluscan periostracum: an important constraint in bivalve evolution. Palaeontology 40:71–97

Harper EM (2000) Are calcitic layers an effective adaptation against shell dissolution in the Bivalvia? J Zool 251:179–186

Hasse B (2002) A crystallographic study of the love dart (Gypsobelum) of the land snail *Helix pomatia* (L.). J Molluscan Stud 68:249–254

Hyun B, Choi K-H, Jang P-G, Jang M-C, Lee W-J, Moon C-H, Shin K (2014) Effects of increased CO_2 and temperature on the growth of four diatom species (*Chaetoceros debilis*, *Chaetoceros didymus*, *Skeletonema costatum* and *Thalassiosira nordenskioeldii*) in laboratory experiments. J Environ Sci Int 23:1003–1012

Kaplan DL (1998) Molluscs shell structure: novel design strategies for synthetic materials. Curr Opin Solid State Mater Sci 3:232–236

Knoll AH (2003) Biomineralization and evolutionary history. In: Dove PM, De Yoro JJ, Weiner S (eds) Biomineralization: reviews in mineralogy and geochemistry, vol 54. Mineralogical Society of America, Chantilly, pp 329–356

Kroeker KJ, Kordas RL, Crim R, Hendriks IE, Ramajo L, Singh GS, Duarte CM, Gattuso J-P (2013) Impacts of ocean acidification on marine organisms: quantifying sensitivities and interaction with warming. Glob Chang Biol 19:1884–1896

Liao H, Mutvei H, Sjöström M, Hammarström L, Li J (2000) Tissue responses to natural aragonite (*Margaritifera* shell) implants in vivo. Biomaterials 21:457–468

Lipps J (1992) Proterozoic and Cambrian skeletonized protists. In: Schopf JW, Klein C (eds) The proterozoic biosphere: a multidisciplinary study. Cambridge University Press, Cambridge, UK, pp 237–240

Lowenstam HA (1954) Factors affecting the aragonite: calcite ratios in carbonate-secreting marine organisms. J Geol 62:284–322

Lowenstam HA, Weiner S (1989) On biomineralization. Oxford University Press, Oxford

Mackenzie FT, Bischoff WD, Bishop FC, Loijens M, Schoonmaker J, Wollast R (1983) Mg-calcites: low temperature occurrence, solubility and solid-solution behavior. In: Reeder RJ (ed) Reviews in mineralogy, carbonates: mineralogy and chemistry. Mineralogical Society of America, Washington, DC, pp 97–143

McIlroy D, Green OR, Brasier MD (2001) Palaeobiology and evolution of the earliest agglutinated foraminifera: *Platysolenites*, *Spirosolenites* and related forms. Lethaia 34:13–29

Nicol D (1966) Cope's rule and Precambrian and Cambrian invertebrates. J Palaeont 40:1397–1399

Palmer AR (1983) Relative cost of producing skeletal organic matrix versus calcification: evidence from marine gastropods. Marine Biol 57:287–292

Palmer AR (1992) Calcification in marine molluscs: how costly is it? Proc Natl Acad Sci U S A 89:1379–1382

Peck LS (2008) Brachiopods and climate change. Earth Environ Sci Trans R Soc Edinb 98:451–456

Peck LS, Brockington S, Brey T (1997) Growth and metabolism in the Antarctic brachiopod *Liothyrella uva*. Philos Trans R Soc 352:851–858

Porter SM (2007) Seawater chemistry and early carbonate biomineralization. Science 316 (5829):1301–1302

Porter S (2011) The rise of predators. Geology 39:607–608

Privat KL, O'Connell TC, Richards MP (2002) Stable isotope analysis of human and faunal remains from the Anglo-Saxon cemetery at Berinsfield, Oxfordshire: dietary and social implications. J Archaeol Sci 29:779–790

Richards MP, Hedges REM (1999) Stable isotope evidence for similarities in the types of marine foods used by Late Mesolithic humans at sites along the Atlantic coast of Europe. J Archaeol Sci 26:717–722

Riding R (1982) Cyanophyte calcification and changes in ocean chemistry. Nature 299:814–815
Ries JB, Cohen AL, McCorkle DC (2009) Marine calcifiers exhibit mixed responses to CO_2-induced ocean acidification. Geology 37:1131–1134
Rotjan RD, Lewis SM (2009) Predators selectively graze reproductive structures in a clonal marine organism. Marine Biol 156:569–577
Runnegar B (1985) Shell microstructures of Cambrian molluscs replicated by phosphate. Alcheringa 9:245–257
Sartori AF, Harper EM (2009) Sticky bivalves from the Mesozoic: clues to the origin of the anomalodesmatan arenophilic system. Lethaia 42:486–494
Shen C, Pratt BR, Zhang X (2014) Phosphatised coprolites from the middle Cambrian (Stage 5) Duyun fauna of China. Palaeogeogr Palaeoclimatol, Paleoecol 410:104–112
Siesser W (1993) Calcareous nannoplankton. In: Lipps J (ed) Fossil prokaryotes and protists. Blackwell Scientific, Oxford, pp 169–201
Simkiss K (1977) Biomineralization and detoxification. Calc Tissue Res 24:199–200
Sleight VA, Thorne MA, Peck LS, Clark MS (2015) Transcriptomic response to shell damage in the Antarctic clam, *Laternula elliptica*: time scales and spatial localization. Marine Genomics 20:45–55. doi:10.1016/j.margen.2015.01.009, Epub 2015 Feb 9
Spann N, Harper EM, Aldridge DC (2010) The unusual mineral vaterite in shells of the freshwater bivalve *Corbicula fluminea* from the UK. Naturwissenschaften 97:743–751
Stanley GD, Fautin DG (2001) The origins of modern corals. Science 291:1913–1914
Stanley SM, Hardie LA (1998) Secular oscillations in the carbonate mineralogy of reefbuilding and sediment-producing organisms driven by tectonically forced shifts in seawater chemistry. Palaeogeogr, Palaeoclimatol, Paleoecol 144:3–19
Stolarski J, Meibom A, Przeniosło M, Mazur M (2007) A Cretaceous scleractinian coral with a calcitic skeleton. Science 318:92–94
Taylor JD (1973) The structural evolution of the bivalve shell. Palaeontology 16:519–534
Taylor JD, Kennedy WJ (1969) The influence of the periostracum on the shell structure of bivalve molluscs. Calcif Tissue Res 3:274–283
Taylor JD, Reid DG (1990) Shell microstructure and mineralogy of the Littorinidae; ecological and evolutionary significance. Hydrobiologia 193:199–215
Taylor JD, Kennedy WJ, Hall A (1969) The shell structure and mineralogy of the Bivalvia. Introduction, Nuculacea–Trigonacea. Bull Brit Mus (Nat Hist) Zool 3:1–125
Taylor JD, Kennedy WJ, Hall A (1973) The shell structure and mineralogy of the Bivalvia. II. Lucinacea–Clavagellacea, conclusions. Bull Brit Mus (Nat Hist) Zool 22:253–284
Taylor JD, Glover EA, Braithwaite CJR (1999) Bivalves with 'concrete overcoats': *Granicorium* and *Samarangia*. Acta Zool 80:285–300
Taylor PD, Lombardi C, Concito S (2014) Biomineralization in bryozoans: past, present and future. Biol Rev – Online early
Thomas RDK, Reif WE (1993) The skeleton space: a finite set of organic designs. Evolution 47:341–360
Thomas RDK, Shearman RM, Stewart GW (2000) Evolutionary exploitation of design options by the first animals with hard skeletons. Science 288:1239–1242
Vendrasco MJ, Checa AG, Kouchinsky AV (2011) Shell microstructure of the early bivalve *Pojetaia* and the independent origin of nacre within the Mollusca. Palaeontology 54:825–850
Vermeij GJ (1983) Traces and trends in predation, with special reference to bivalved animals. Palaeontology 26:455–465
Vermeij GJ (1990) The origin of skeletons. Palaios 4:585–589
Warén A, Bengtson S, Goffredi SK, Van Dover CL (2003) A hot-vent gastropod with iron sulfide dermal sclerites. Science 302:1007
Weiner S, Addadi L (2011) Crystallization pathways in biomineralization. Annu Rev Mater Res 41:21–40
Wilkinson BH (1979) Biomineralization, palaeoceanography, and the evolution of calcareous marine organisms. Geology 7:524–527

Wood R (2011) Paleoecology of early skeletal metazoans: insights into biomineralization. Earth Sci Rev 106:184–190

Wood R, Zhuravlev AY (2012) Escalation and ecological selectively of mineralogy in the Cambrian Radiation of skeletons. Earth Sci Rev 115:249–261

Wood RA, Grotzinger JP, Dickson JAD (2002) Proterozoic modular biomineralized metazoan from the Nama Group, Namibia. Science 296:2383–2386

Zhang Z-F, Li G-X, Holmer LE, Brock GA, Balthasar U, Skovsted CB, Fu D-J, Zhang X-L, Wang H-Z, Butler A, Zhang Z-L, Cao C-Q, Han J, Liu J-N, Shu D-G (2014) An early Cambrian agglutinated tubular lophophorate with brachiopod characters. Sci Rep 4:4682

Zhuravlev AY, Wood RA (2008) Eve of biomineralization: controls on skeletal mineralogy. Geology 36:923–926

Part I
Cremations: Anthropology, Mineralogy, Radiocarbon Dating

Complexities of the Ancient Mortuary Rite of Cremation: An Osteoarchaeological Conundrum

Jacqueline I. McKinley

Introduction

Undoubtedly, there will have been geographic and temporal variations in practices and beliefs associated with the rite of cremation or parts thereof, but the central issues are the same across Europe and beyond—the deliberate use of fire as a medium of transformation, altering the corpse from one state to another, forming the primary part of a complex mortuary rite which involved various secondary procedures, predominantly that of burial of some or all of the cremated remains. Consequently, although the contents of this paper draw largely on the writer's observations and analyses of cremated remains and mortuary deposits from the British Isles [over 7000, encompassing a broad temporal range from Early Neolithic to Norse (fourth millennium BC to ninth century AD)], archaeologically the aims, interests, and challenges are shared irrespective of the origins of the material.

The analysis and interpretation of cremated remains covers a broad range of themes: those common to the study of all archaeological human bone, comprising the recovery of demographic data and evidence for pathological lesions/conditions, and those specific to cremation mortuary rites and pyre technology. Each area of study carries its own challenges and possibilities. It is beyond the scope of this chapter to cover all aspects associated with the study of such remains; so the intention is to focus on cremation itself and consider how the data recovered in analysis can be used to further our understanding of the overall mortuary rite including pyre technology.

There are two imperatives when working with cremated remains that were often overlooked in the past and occasionally still are now: an understanding of what happens when a body is cremated (i.e. burnt as part of the mortuary rite) or otherwise subject to the effects of fire is fundamental. A further essential ingredient

J.I. McKinley (✉)
Wessex Archaeology, Portway House, Old Sarum Park, Salisbury, SP4 6EB, UK
e-mail: j.mckinley@wessexarch.co.uk

G. Grupe, G.C. McGlynn (eds.), *Isotopic Landscapes in Bioarchaeology*,
DOI 10.1007/978-3-662-48339-8_2

of any analysis is the archaeological context in which the material was found. In this complex rite, the components within a deposit may be the same or similar, but the formation process(es) and location may differ and reflect different parts of the overall mortuary rite (e.g. the cleared or un-cleared (manipulated or intact) pyre site, the burial remains, or redeposited pyre debris; Fig. 1).

Other context details may reveal factors affecting the condition of the bone. These include the locality and the associated geology and soils. Although cremated bone often survives in soils where unburnt bone does not (the organic components of the bone being removed or at least substantially depleted during cremation), it

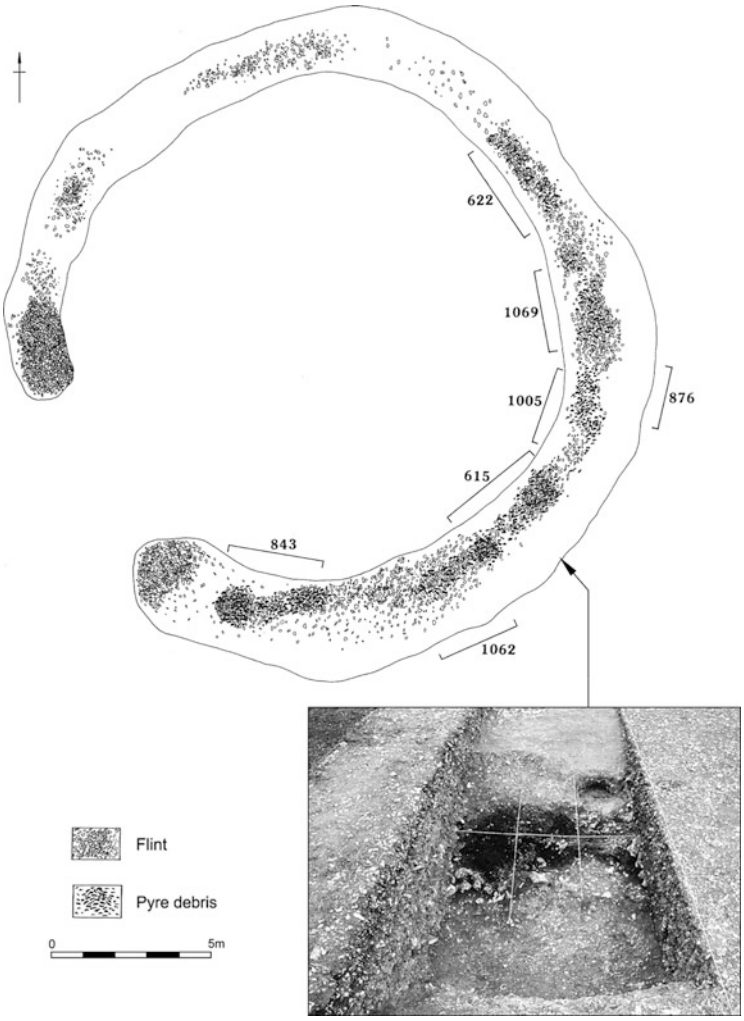

Fig. 1 Bronze age ring ditch, Twyford Down, Winchester, Hampshire, showing location of dumps of pyre debris within ditch fill and inset detail of deposit 615 (McKinley 2000c)

still suffers detrimental effects within some burial environments. Acid soils, such as free-draining sandy gravels and the alluvial silty clays commonly known as 'brickearth' in the British Isles, for example, frequently have damaging effects on cremated bone resulting in preferential destruction of the trabecular components. Cremated bone found in peaty soils is generally devoid of trabecular elements whilst the compact bone has a worn and 'chalky' appearance (Fig. 2a). Post-depositional disturbance of the remains (accidental/deliberate human activity or bioturbation) can affect the quantity of the bone recovered due to either removal of material and/or physical breakdown of the bone (which is very brittle and more susceptible to damage than unburnt bone). Some types of deposit afford greater protection than others, for example, an urned burial compared with an unurned one, the presence of an intact lid in association with the former and absence of soil around the bone being a major influence on preservation (Fig. 2b–c).

Finally, the excavation procedures and post-excavation processes employed can affect both the quantity and condition of the material available for analysis. Advised excavation procedures (McKinley 2000a, 2013a, forthcoming a) aim to ensure full recovery of all that survives and the maintenance, as far as possible, of the physical integrity of the material collected (which requires careful handling and storage due to its brittle nature).

The Cremation Process

Modern Cremation

Various mechanisms have been used to enhance and expand our understanding of the cremation process, but modern crematoria offer the most useful starting place. Here the process is undertaken in a controlled environment, with a regulated heat source (gas in many countries, but electric in others (Davies 2005)) and air flows (to provide oxygen and heat circulation), within a heat-retentive structure, creating optimum conditions for what is deemed the most effective mode of cremation (ibid. 147–151; McKinley 1994a: 72–6, Figs. 16 and 17; Schultz et al. 2008).

Details of the chemical changes effected during cremation/heating bone have been covered by other contributors of this volume (see Tropper, van Strydonck, Schmahl) and researchers elsewhere (e.g. Herrmann 1977; Hiller et al. 2003; Holden et al. 1995a, b) and will not be repeated here. In summary, the cremation process is one of dehydration and oxidation of both the soft tissues and the bone itself (*c*. 30 % organic), affecting the bone chemistry and resulting in alterations in the crystal size/structure of the bone mineral (*c*. 70 % mineral component; calcium phosphate changed to tri-calcium phosphate; Lange et al. 1987: 17–19). These changes are affected by a combination of time, temperature, and oxygen supply; the first and last of these requisites are often overlooked in favour of the role of

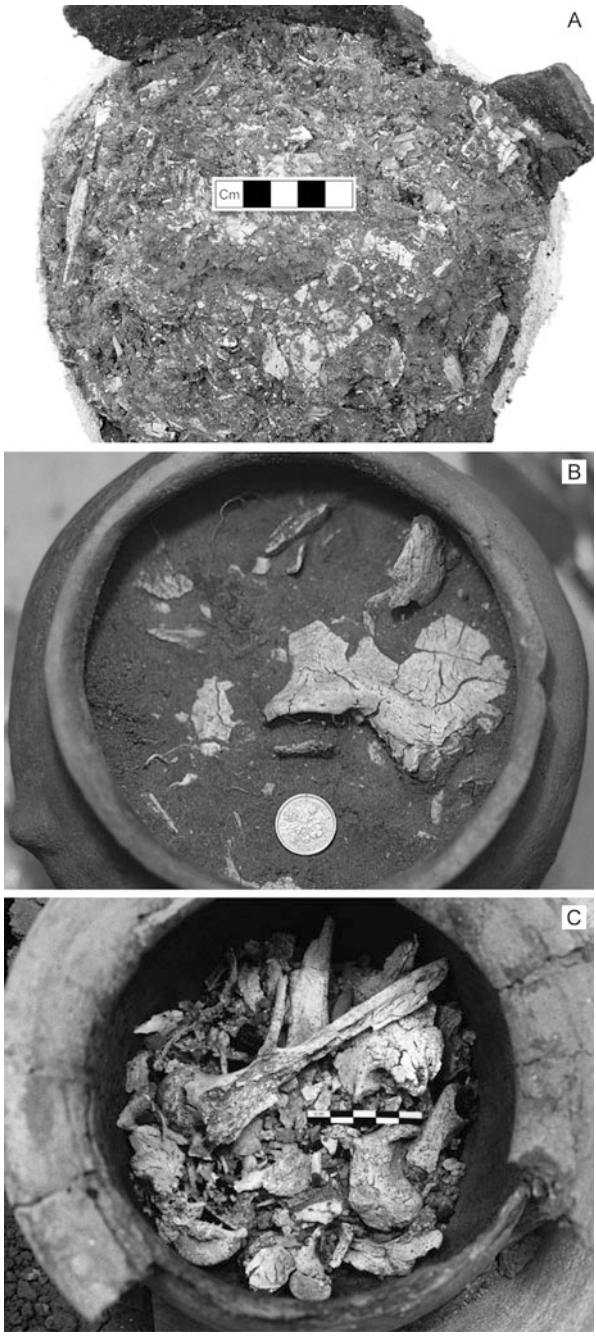

Fig. 2 Urned burials showing different levels of bone preservation: (**a**) degraded bone in acidic soils; (**b**) soil infiltration of dehydration fissures; (**c**) lidded vessel with no soil infiltration

temperature, but, without sufficient oxygen, for example, reducing conditions will prevail.

The operating temperatures within modern crematoria generally fall in the 800–1100 °C range, with an ignition temperature of around 500 °C. Overall duration of the process is variable but averages about 1½ h. The temperature fluctuates throughout cremation following a similar pattern in each case: a rapid rise as the soft tissues ignite and create heat as they burn, with a gradual fall once most of the organic material has gone (Fig. 3). Cremators cool over the weekend/night when not in use and may be preheated for the first charge of the day; following one or two cremations in a day, the ignition temperature is sufficient without the need to apply the external heat source. There are variables associated with body mass; those with little soft tissues to enhance the temperature (children, the elderly, and emaciated individuals) require more external heat to aid cremation; those with heavy fat deposits may cremate more rapidly due to an early boost in temperature; those with heavy muscle deposits (dense tissue) tend to take longest to cremate. Unknown variables may also have an influence; e.g. Charges 5a and 5b in Fig. 3a, males of similar age and build, were placed in adjacent cremators registering the same temperature at the same time. Charge 5b followed the standard oxidising pattern; however, charge 5a showed a drop in temperature and over the same period only charring occurred. The cause of the latter was undetected (no known medical or different funerary treatment); full cremation was eventually effected by allowing more time.

The variable extent of soft tissue coverage affects at what stage different parts of the skeleton will cremate/oxidise, e.g. the bones of the hand/feet, cranium, leg, and forearm will burn before those of the upper arm and thigh. Some dense soft tissues might fall away from the skeleton and continue to burn after the bone itself is oxidised, e.g. the large muscle mass around the buttock area and the brain tissues—the cranium needs to be open to allow oxygen access (NB. These materials will remain in the cremator until they have oxidised: in the lower hearth with refreshed oxygen supply following collection of the bone if necessary; McKinley 1994a: Figs. 16 and 17). Once freed from the insulating effects of the overlying soft tissues (oxygen cut-off) the bone itself oxidises from the exposed surfaces (outside or medullary cavity) through towards the centre, potentially creating a 'sandwich' effect where oxidation is incomplete (McKinley 2008: Fig. 10.2). The degree of oxidation is evident in the colour of the bone, progressing from the black of charred bone through hues of blue and grey to the white of fully oxidised (Devlin and Herrmann 2008; Holden et al. 1995a; Shipman et al. 1984). Consequently, the heat-induced microscopic changes to the bone mineral seen in individual bones from a cremation will not necessarily all reflect the same temperature, or that of the cremator (or pyre) itself (ibid.; Rogers and Daniels 2002; Thompson et al. 2013). Potentially, different bones will reflect different temperatures dependent on the depth of the overlying soft tissue insulation, and the stage at which that is removed relative to the heat of the cremator.

Cremated bones maintain their original basic morphological appearance (Fig. 4a). The visual effects, other than colour, are largely related to dehydration.

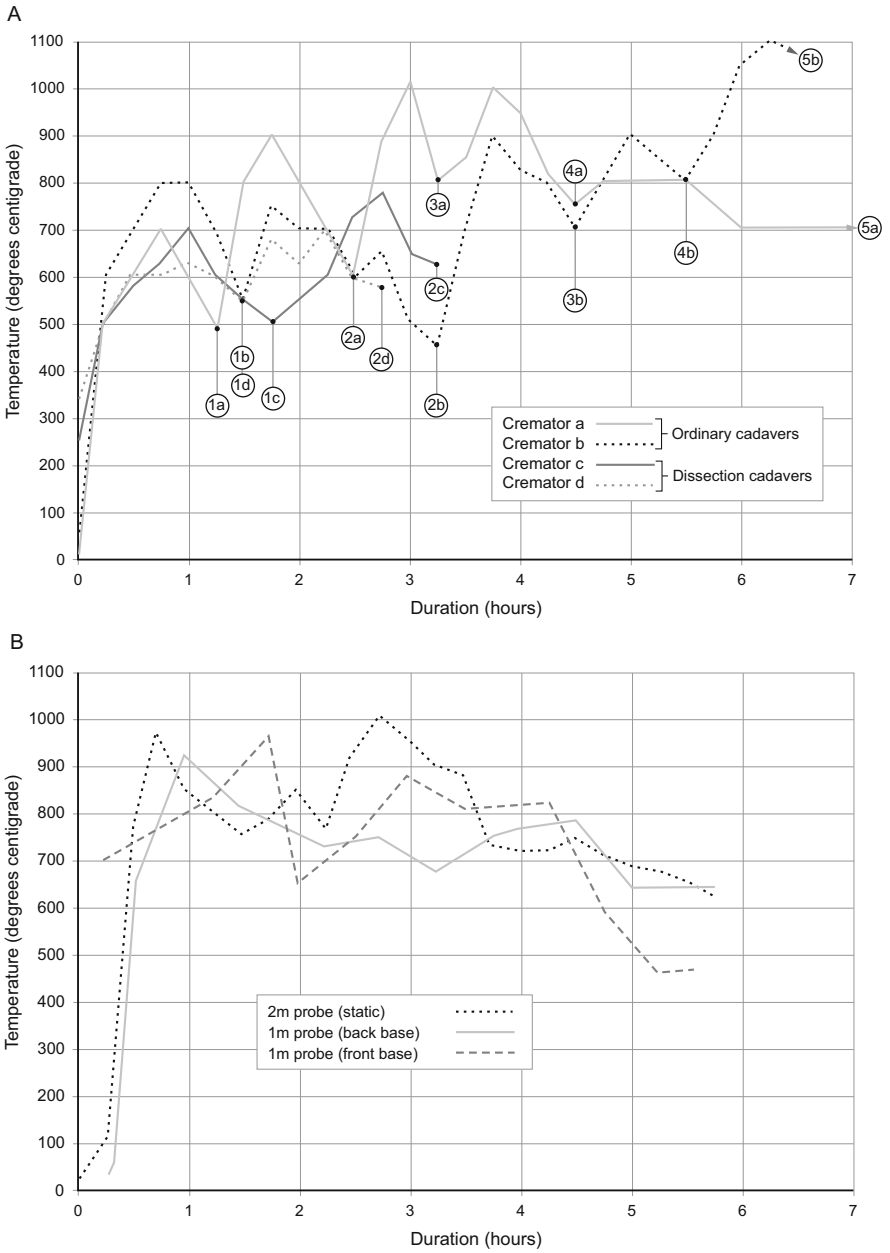

Fig. 3 Temperature readings: (**a**) from four modern cremators (**a**–**d**), showing between two and five separate charges for each cremator, (**b**) from three probes located in different parts of an experimental pyre cremation

Fig. 4 Modern cremated remains: (**a**) on main hearth towards end of cremation, (**b**) in collection box prior to cremulation

Variable levels of shrinkage may be evident (both amongst material from the same firing and between cremations), especially amongst the trabecular components; the smaller bones, such as carpals and tarsals, often survive complete (Fig. 4b). The bone fissures and fragments, sometimes with marked twisting. The points of breakage are commonly at junctions between different bone densities, e.g. that between the compact long bone shaft and the trabecular articular surface, and between the vertebral body and dorsal portion. Classic fragmentation patterns include 'U'-shaped fissuring along long bone shafts, concentric fissuring within humeral/femoral heads, and parting between the anterior and dorsal sides of the mandibular arch (Fig. 5; see Symes et al. 2008 for further details). Tooth enamel, having no organic components, does not have the flexibility of the rest of the skeleton and shatters into small fragments as it expands in the heat of cremation. Unerupted tooth crowns provide an exception; being insulated from the heat within the crown crypts, these elements commonly survive relatively unscathed.

The quantity of bone remaining at the end of cremation is largely dependent on the age and size/body mass of the living subject. There is inconsistency within the minimum, maximum, and mean values for adults recorded by different researchers, though there are understandable reasons for such variability. The writer's own observations (McKinley 1993), which gave a range of 1001.5–2422.5 g with a mean of 1625.9 g, were deliberately targeted at recovering data commensurate with that which might survive archaeologically. The bone from the collecting box was weighted pre-cremulation (i.e. before mechanical pulverisation) excluding the smallest 'dust' fraction (<2 mm) which would not be recovered in archaeological contexts (also serving to eliminate any coffin dust. NB. Including the dust fraction

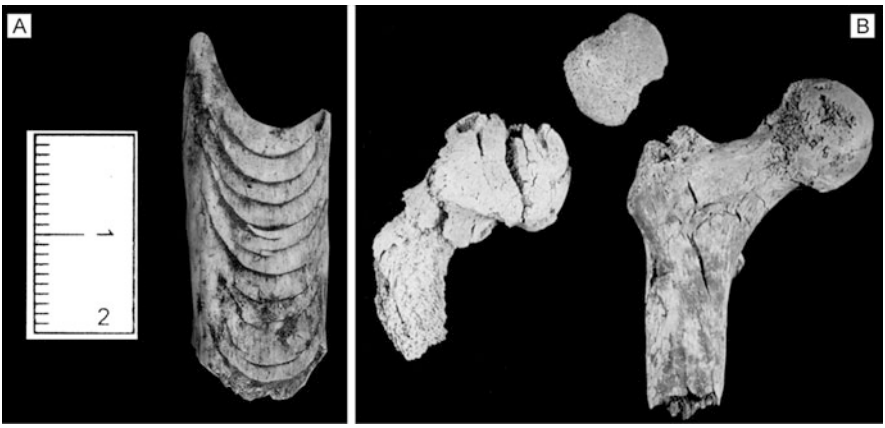

Fig. 5 Dehydration fissures: (**a**) 'U'-shaped fissuring in long bone shafts, (**b**) progressive levels of fissuring in proximal femora

the weights were about 20 % higher with an average of 2016.4 g). It was also observed that many of the subjects were elderly individuals (>70 year) who (particularly the females) had clearly suffered from some degree of osteoporosis resulting in much of the trabecular bone (particularly the vertebral bodies) crumbling extensively during cremation and recovery; NB. other pathological conditions may have a similar affect. Weights recorded elsewhere (mean values 2348–2893 g, maximum 5379 g; Bass and Jantz 2004; Gonçalves et al. 2015; Holck 1989: Table 9) appear to be inclusive of the 'dust' fraction and younger individuals with a more robust bone structure and potentially larger body mass. It should also be remembered, when comparing some of these weights with archaeological material, that average height has increased within the last five to six decades, the larger body mass associated with enhanced dietary intake for many undoubtedly also affecting bone weights.

Observations of the cremation of dissection-room cadavers, representative of defleshed corpses, showed speedier and consistently full oxidation of the bone due to the absence of overlying soft tissues. There tended to be more pronounced warping of bone due to the enhanced speed and generally higher temperature affecting the bone (it being earlier in the process). However, in an anonymous situation, the visual effects could not confidently be distinguished from those seen in some fleshed cadavers.

Dry bone is already dehydrated so the classic fissuring observed in 'green' bone is absent. Similarly, since much/most of the organic component of the bone has already been lost, the colour changes indicative of oxidation are less consistent (Baby 1954; Binford 1963; Thurman and Wilmore 1981).

Pyre Cremation

Whilst modern crematoria present the optimum conditions, archaeologists need to be familiar with cremation on an open pyre, generally using wood as a fuel, this being the mechanism by which the rite would most commonly have been undertaken in the past, and the operational similarities and potential differences that would have entailed.

Images and texts, from Bronze Age Greece to present-day India (Fig. 6), demonstrate a similar pyre construction (e.g. Holck 1989: Figs. 2 and 4; Lange et al. 1987, cover plate; Toynbee 1996: Figs. 15 and 16); an open lattice-work, rectangular form (layers of logs/poles set at right angles) of variable size, providing sufficient fuel to 'complete' cremation and a stable platform on which to lay the corpse and pyre goods, whilst allowing oxygen access. There may have been a shallow under-pyre draught pit to assist drawing air in, and corner poles (or further marginal uprights) may have been employed to help stabilise the structure (e.g. Fitzpatrick 1997: Figs. 11–20, Plates 10–11).

Placing the corpse towards or at the top of the pyre ensures the benefit of optimum heat and oxygen availability (lower down, most oxygen would be consumed by the burning fuel), and as the pyre collapses the body maintains its position relative to the fuel source. Experimental pyres have recorded temperatures similar

Fig. 6 Pyre under construction on an Indian cremation ghat

Fig. 7 Effects of strong wind on an experimental pyre cremation, Shetland (NB. Pyre comprised supportive wooden structure around a peat stack hence relative paucity of wood)

to modern crematoria, but obviously the heat is lost to the atmosphere rather than being circulated, and there are sometimes marked spatial variations, e.g. cooler margins (Fig. 3b). The potential effects of the weather, particularly in an often wet and windy British Isles, might have influenced the length of time between death and cremation (also potentially affected by other ritual and practical considerations) and rendered the presence of someone to manage/attend the pyre and deal with unanticipated problems, desirable. Strong, veering winds could cause uneven burning and collapse of the pyre, for example, with unwanted slippage of the corpse (Fig. 7), or heavy, persistent rain could douse the whole process.

In experiments conducted by or in corroboration with the writer, the pyres burnt down to an ash base over 3–4 h, at which stage a considerable amount of charred soft tissues remained together with some oxidised bone (Fig. 8). However, the wood ash remained hot (around 500 °C) for 6–7 h or more (depending on the weather; wind strength), and in cases where peat was used as the primary fuel source the base was still too hot to handle 12 h later. Left overnight, most of the soft tissues from a pyre lit in the early afternoon had oxidised (McKinley 1997a, 2008; Becker et al. 2005: Plates 5–6). Obviously, the speed of the burn is influenced by a number of factors, including the quantity and type of fuel (see Holck (1989: 27–45) for calorific values of different wood species).

Fig. 8 Experimental pyre cremation showing cremated bone and charred soft tissues (sheep) on wood ash base 4 h after lighting pyre

Laboratory Experiments

With regular applied controls, laboratory experiments have given valuable insights into aspects of the cremation process, particularly into microscopic details and bone chemistry (see Lange et al. 1987; Schmidt and Symes 2008; Thompson 2015), not readily accessible by other means. Such analyses do have limitations, however. Principally, researchers tend to use body parts or individual skeletal elements, often defleshed, that do not mimic the cremation of intact fleshed bodies. Ideally, the approaches covered in this section—observations at modern crematoria, experimental pyre cremations, laboratory experiments, and observations from forensic settings—will complement one another and combine to assist our understanding of ancient cremations.

General Osteological Analysis

As with most archaeological analyses, that of cremated bone needs to be methodical and replicable to facilitate comparisons between datasets. This is particularly important when looking at aspects of pyre technology and cremation ritual. The level of detail and magnitude of recoverable data is dependent on the quantity and condition of the surviving bone, which for a variety of reasons (see above) can be highly variable. Figure 9, for example, shows a large collection of bone from the

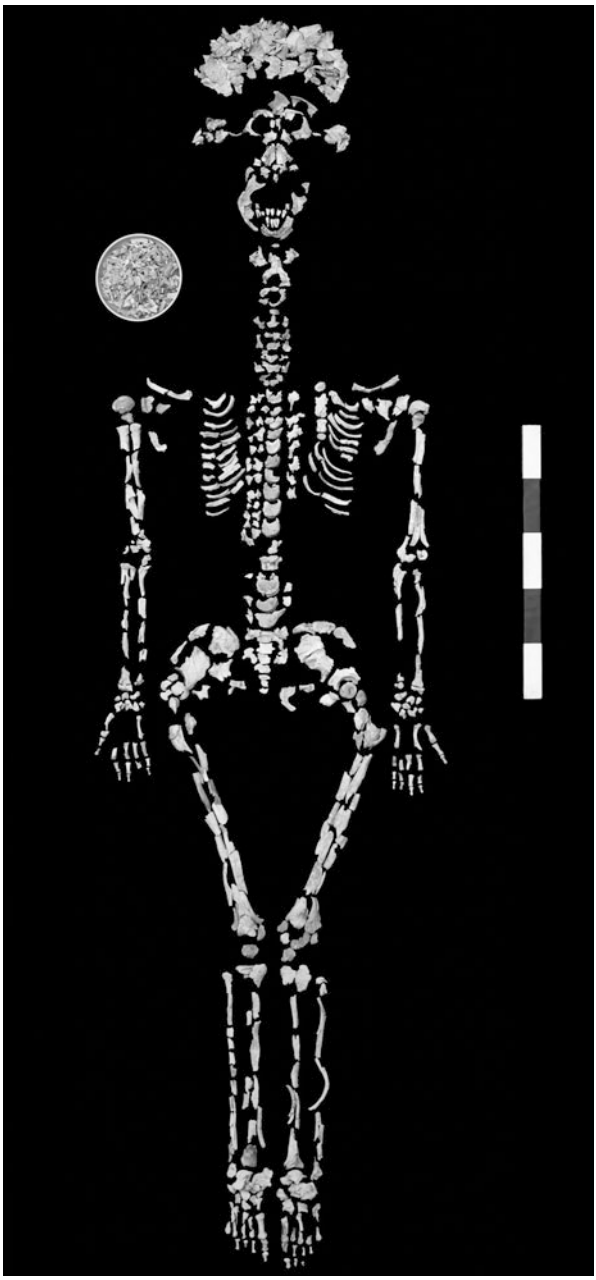

Fig. 9 Amesbury barrow 1/52; Early Bronze Age subadult female, remains laid in anatomical order

remains of an Early Bronze Age urned burial (1758.9 g; female, *c*. 15–17 years.) where an unusually high proportion of the bone (78 % by weight; laid out in anatomical order) could be identified to skeletal element; more commonly,

substantially lower weights of bone are recovered, *c*. 500–800 g, and about 30–50 % is identifiable to element. Knowledge of the archaeological context is important for all areas of interpretation: the osteologist must distinguish levels of disturbance and the type of deposit, and consider locational and archaeological criteria; one cannot, for example, make direct comparisons between material from heavily disturbed unurned burials with that from intact, lidded urned burials; unsurprisingly, it will not look the same.

The recovery of demographic and pathological data is not within the primary remit of this paper, but both have their challenges and limitations. The most frequently encountered deposit types are burial remains, deriving from a secondary event within the overall mortuary rite (and one which may not always have occurred). The primary act of cremation represented the main focus of the mortuary rite, and the burial remains rarely comprise all that would have survived at the end of cremation. Inevitably, those collecting bone for burial did not always recover the fragments of most use to future osteoarchaeologist for ageing and sexing individuals, or those which would enable them to record and diagnose someone's pathological conditions. In brief, some of the challenges specific to cremated remains comprise:

The *minimum number of individuals (MNI)*, primarily determined by duplication of specific skeletal elements (predominantly singular or paired cranial features such as the petrous temporals, malar bones or neural crests) or major age-related variations, is not always readily apparent. In addition to a deposit potentially including the remains of more than one individual (e.g. an Early Bronze Age cist grave at Trelowthas Barrow, Cornwall was found to contain the remains of a minimum of 19 individuals (bone weight 9584.8 g; McKinley 1996 unpublished) and a spread of redeposited pyre debris from the Romano-British cemeteries of East London (Plot 28) from which a MNI of 18 was recovered (McKinley 2000b: 64–66), the remains of one individual could be represented within more than one type of deposit within a cemetery/group of mortuary related features. Examples of the latter include single burial deposits made in more than one vessel or combined urned and unurned burial deposits such as those in the Early Anglo-Saxon cemetery (fourth-early fifth century AD) at Spong Hill, Norfolk (McKinley 1994a: 93–4, Fig. 28). Singular or small numbers of duplicate skeletal elements may be the product of contamination (disturbance/re-used pyre sites) or represent 'token'/memento mori deposits (see below).

Ageing and sexing can be rendered difficult, with only partial recovery of remains for burial exacerbated by small fragment sizes and incomplete skeletal elements. Sternal rib ends have been found in less than 0.1 % of deposits examined by the writer, for example; it is generally not possible to discern the wear patterns in fragments of erupted tooth crowns, even in the exceptional cases where they are found; and some of the classic pelvic elements used in sexing are rarely recovered in useful numbers, with only about 4 % of the deposits examined by the writer containing fragments of the pubic symphysis with a decipherable sub-pubic angle. The common survival of unerupted tooth crowns is, however, useful for ageing infants and juveniles.

Pathological lesions do survive, including some fairly unusual forms e.g. calcified lymph nodes indicative of tuberculosis (McKinley 1994a: Plate 33); benign osteoma in the mandibular fossa (McKinley 1994a: Plates 34–5); and diffuse idiopathic skeletal hyperostosis (DISH; McKinley 2013b: Plate 2), but incomplete skeletal recovery often limits diagnosis.

Cremation Ritual

The interpretation of pyre technology and cremation ritual considers features of the bone's appearance and the composition of individual and potentially related deposits.

Efficiency of Oxidation

The efficiency of oxidation is reflected in the colour of the bone (see above). Variations in colour, affecting specific areas of the skeleton or individual skeletal elements, may indicate shortfalls in the levels of oxidation.

General shortfalls may be related to insufficient time or temperature. A review of cremated remains from 1720 Romano-British burials collated from 60 sites in England indicated body mass was the main factor affecting level of oxidation, with the remains of adult males showing the most frequent and extensive lack of oxidation (McKinley 2008). The results suggest a lack of adjustment in pyre size to suit the size of the individual being cremated. Unlike in most other periods when the rite was practised, Roman cremation (certainly in towns) was probably undertaken by professionals (*ustores*) with clients paying for the quantity of wood used. This is also the only period in which the writer has observed evidence for incomplete cremation ('trunk' area of corpse unburnt, charring to mid-distal shafts of humerus and femur, the hands/feet, forearm, and leg bones, and parts of skull vault fully cremated; McKinley 1991 unpublished report on the Area 15 cemetery Baldock, Hertfordshire), a likely explanation being that heavy rain curtailed the process leaving most of the corpse only charred.

Incomplete oxidation of the hand/foot bones and the cranium might reflect the peripheral location of these elements on a slightly undersized pyre, with a related reduction in the temperature in these areas. Skeletal elements could also fall off the pyre once a breakdown of the integrity of the corpse had occurred. This was observed in several experimental pyres, involving limb extremities being thrown up to a metre out of the pyre during a shift of the structure as it collapsed down, and without an attendant to return the elements to the pyre the degree of oxidation could be affected.

More specific patterns of incomplete oxidation, such as that to only one upper limb or the cranium, might indicate the insulating effect of items under/around the corpse, e.g. a leather/fur hat/cape or a pillow under the head. This would cut off the oxygen supply and heat to this area delaying the onset of cremation (NB. newspapers placed on a fire will only burnt around the edges unless the individual sheets are separated to allow oxygen between them).

Whilst full oxidation of the all the organic components of the bone is a requisite of modern Western cremation, such is not necessarily the case globally or in the past. Where the 'magic' of a visual transformation from one state to another was what was required, the degree of oxidation attained by individual skeletal components may have been of little or no consequence.

Fragmentation

Much of the fragmentation of the bone occurs during cremation (see above). Very brittle, especially when hot, further breakage would have ensued during management to re-oxygenate the pyre during cremation, and in the course of recovery for burial and other forms of deposition, which might have involved trampling across the pyre site rather than raking or hand collection of bone from the margins, and could have included recurrent transference of the remains from one receptacle to another. Deliberate cooling of the hot bone—using water, wine, or other liquids for practical and/or ritual purposes, for which there is written evidence (e.g. *Iliad* Book 23, Lines 239–240; Toynbee 1996: 50 and 63; Downes 1999: 23; Noy 2005)—would cause the bone to fragment further, generally along the lines of pre-existing dehydration fissures. Were the bone raked off the pyre *en masse* and winnowed (via deposition in water or using a basket and the wind) to remove the fuel ash (cremation burials, certainly in the UK, are generally devoid of this material even if the rest of the grave fill is not), this would also result in further fragmentation.

It is also clear that the bone breaks up further within the burial environment. Over time, soil infiltrates the cracks/fissures, breaking the bone down via wet/dry/freeze/thaw action and chemical degradation in adverse soil conditions (Fig. 2), particularly where the bone is afforded no barrier between it and the soil matrix, and disturbance has caused additional stress either directly (physical damage) or indirectly (by altering the burial environment).

None of these mechanisms represent deliberate fragmentation. Arguments have been made for intentional fragmentation in cases of the use of narrow-necked ceramic vessels as burial containers, the bone presumed to have been broken to fit. There is, however, clear evidence that either the vessels themselves were manipulated or that large bone fragments were 'fed in' at an appropriate angle. Figure 10a, b shows a Dressel 20 amphora which functioned as a burial urn. Recognising that the internal diameter of the neck (30 mm) was too narrow to allow the bone to be inserted, those undertaking the burial had knocked off the neck, creating a 61 × 49 mm opening through which the large bone fragments could be fed (maximum fragment 111 mm), replacing the broken neck before burial (McKinley 2015a). Another urned burial from the same site (Fig. 10c) represents one of numerous examples of bone fragments of substantial length (170 mm; commensurate in size with those from modern crematoria prior to cremulation) being added to the vessel length-ways and maintaining position in burial.

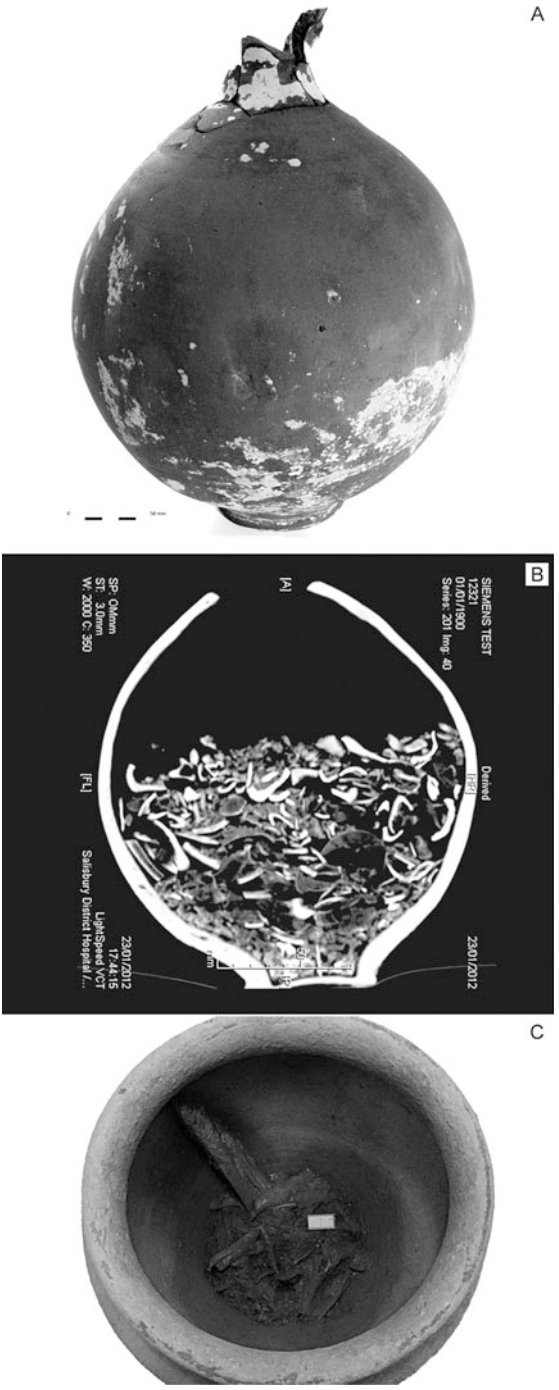

Fig. 10 (**a**) Dressel 20 vessel used as a cremation urn, showing in situ deliberately broken neck and (**b**) CT scan of vessel contents prior to removal; (**c**) In situ large bone fragments set upright within a vessel

An average maximum fragment size of 128 mm and an overall maximum of 195 mm were recorded from modern British crematoria where no deliberate fragmentation occurs prior to cremulation (Fig. 4); the majority of the bone (average 55 % by weight) being recovered from the 10 mm fraction (from a series of 10, 5, and 2 mm sieves; McKinley 1993). Similarly, the majority of the bone (>50 %) in archaeological burials from the UK is generally recovered from the larger sieve fraction with mean maximum fragment sizes of 40–70 mm, though up to 215 mm has been recorded (remains from unurned burials, disturbed deposits, those with overlying flint cairns (exerting pressure), and those of immature individuals tend to be more extensively fragmented; e.g. McKinley 1994b, 2004: Table 6.7, 2015b). Taking into consideration the potential contributory mechanisms on individual sites, in the majority of cases there is no convincing evidence for deliberate fragmentation of bone from burials from the British Isles, though incidental breakage due to differences in tending/collection procedures has been suggested (e.g. McKinley 2015a). There are, however, rare exceptions where the consistently small size of fragments (e.g. 78 % 5 mm or less; maximum 35 mm) within undisturbed adult burial deposits where the bone is well preserved suggest a more methodical attempt at fragmentation (e.g. the Mid-Late Bronze Age burial from Hartshill Copse, Berkshire; McKinley 2003 unpublished). NB. No evidence for percussive breaks has been observed to date.

Bone Weights

The weights of bone recovered from cremation burials are immensely variable. Most adult burials fall into the 500–800 g range, though in some periods and localities the averages can be lower (around 300–500 g), with a relatively small proportion (about 5–10 %) weighing over 1000 g (e.g. McKinley 1997a, 2004: Table 6.6). Of the three largest single adult burials examined by the writer (1900–2000 g), two were Bronze Age and one Romano-British; all were male and from different regions in England.

Although some bone loss occurs due to taphonomic factors, it is clear that it was rare for all the bone remaining at the end of cremation to be included in the burial (see above); though experiments have demonstrated that even very small bones would survive the process and, with sufficient expenditure of time, could all be collected (Fig. 11).

This poses the questions: Why there was this variation and what happened to the rest of the bone? The only consistent patterns the writer has detected to date are that the 'primary' Early and Middle Bronze Age barrow burials seem to consistently include high weights of bone (e.g. Fig. 9), and that in the Late, pre-Roman Iron Age there seems to be consistently lower weights of bone than in other periods in some areas (e.g. McKinley 1997b: 68–9, 2015a; Wahl 2008, a Danish colleague recently

Fig. 11 Survival of small bones: vertebrae (**a**) and distal bones of the front and rear limb (**b**) of a small elderly cat afforded pyre cremation

confirmed this was also the case there). The variation may have reflected the status of the individual (not necessarily related to power or wealth) reflected in the time/effort expended in the secondary rites, the personal preference of those undertaking the cremation, or in a requirement for deliberate separation of the remains.

Cremated bone is recovered from a variety of deposit types and it is likely that much of the bone remained amongst the pyre debris, which was then disposed of in a variety of ways (McKinley 1997a, forthcoming a; Polfer 1993, 2000), with only a random selection of elements from various parts of the skeleton required for the mortuary act of burial. Other uses or modes of disposal for this highly divisible and portable material are likely, some of which have been recognised archaeologically. Selected bones might have been distributed to relatives or friends (Hiatt 1969: 105; see memento mori), some might have been scattered on the land/water as in some contemporary cultures (Metcalf and Huntington 1991: 102; Downes 1999: 23), and in certain cases some or most might have been dispatched for burial elsewhere (Oestigaard 1999). There is evidence, for example, that members of the Roman military who died away from home were cremated where they died and their remains transported back for burial, as in the case of the Emperor Septimius Severus (died and cremated in York, cremated remains returned to Rome; Noy 2005; Toynbee 1996: 59). Some cremation-related features can have all the outward appearance of a cremation grave but include little or no bone; several examples of such cenotaph/memorial deposits have been found in a few of the Romano-British Northern Frontier Forts, some taking the form of *bustum*-style pyre sites (Cool 2004: 457–460; McKinley 2004: 306–7, forthcoming a; Toynbee 1996: 54; Wheeler 1985).

There is also growing evidence for the existence of memento mori/'tokens', small quantities or even single bones apparently dispensed to relatives/friends, at

least some of which were later buried together with someone else. Striking examples of the latter were recovered from Early Anglo-Saxon (late fifth-early seventh century AD) inhumation graves in a cemetery in southern England. Here small packets of cremated bone (9 g and 48 g) were placed directly over the inhumed corpse in two graves (Fig. 12: McKinley forthcoming b). Elsewhere, smaller (single bones or <10 g) 'token' quantities of bone are believed to have been added to cremation graves, predominantly of prehistoric date, at or potentially shortly after burial (McKinley 2013a, 2006, 2015b).

Pyre goods and Grave Goods

The recovery of pyre goods demonstrates the significance of the primary part of the mortuary rite: the corpse laid out on the pyre, dressed and adorned, often with other items arrayed about them (e.g. Sjösvärd et al. 1983). Not all pyre goods were

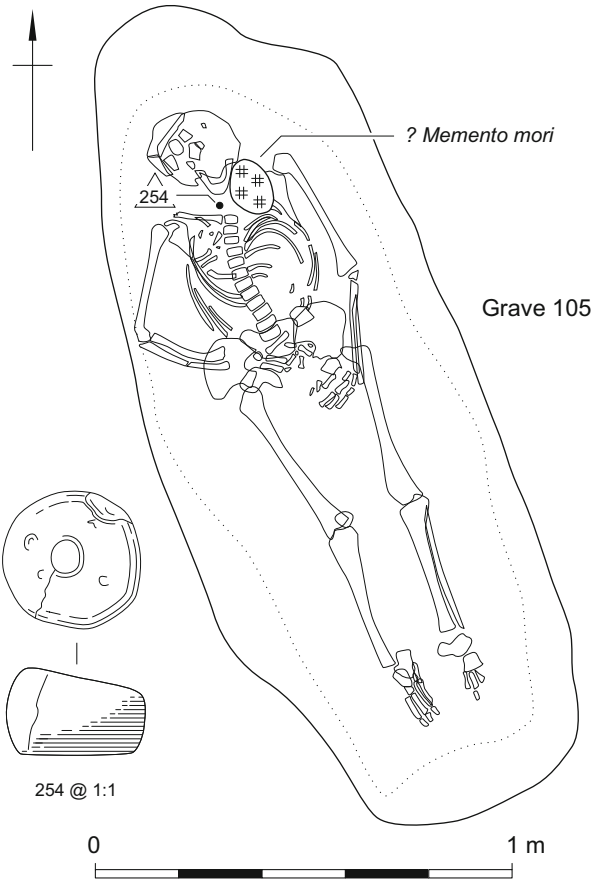

Fig. 12 Anglo-Saxon inhumation grave showing location of memento mori deposit of cremated bone

Table 1 Pyre goods; frequency and range of animal species commonly observed in British cremation burials (from a multi-period sample examined by the writer)

Period	Frequency (variations between cemeteries)	Quantities	Number of species	Common species
Mid-late Neolithic	c. 4 % burials	Few grams	Single	Sheep/sheep sized
Bronze Age	c. 16 % burials	Few grams	Single	Immature sheep/pig, bird
Late Iron Age (first century BC–early first century AD)	c. 22 % burials	Few grams	1–2	Piglet, chicken
Romano-British	10–80 % burials	Few grams (generally)	1–2	Immature pig/ sheep, bird
Early Anglo-Saxon (earliest cemeteries only)	23–44 % burials	Often several 100 g	1–5	Horse, cattle, pig, dog

incorporated in the grave (Cool 2004; Polfer 1993, 2000), but the recovered materials indicate status, temperatures attained in parts of the pyre (melted glass and copper alloy), and where they may have laid in relation to the corpse (cooled material fusing to bones; e.g. McKinley 1994a: 86–92; Northover and Montague 1997). The inclusion of animal remains on the pyre was a common feature, quantities and species varying with time (Table 1); most seem to have represented food offerings, but status animals, pets, and those with ritual/amuletic qualities have also been found and studies have shown that specific species may be linked to the age and/or sex of the individual (McKinley 1994a: 92–100; Sigvallius 1994; Wahl 2008).

The presence of grave goods (unburnt items added only at the time of burial) in some periods raises interesting questions about why distinctions were made between these items and pyre goods, and what their purpose may have been. Such materials that survive are most common in the UK in the Romano-British period, and were generally ceramics (e.g. Cool 2004), perhaps connected with the grave-side commemorative feasting for which there is literary evidence (Hope 2007: 66, 115–6, 154–5; Toynbee 1996: 62, 95). In some recent excavations of both Romano-British and Anglo-Saxon burials, however, items more commonly used as pyre goods (personal adornment/equipment) have been recovered placed (unburnt) on top of the bone within the urns (Fig. 13). Were these items accidentally excluded from the pyre? did they represent mourner's gifts rather than personal items of the deceased's?, or are they linked with differing soul beliefs as discussed by Gräslund (1994).

Fig. 13 Romano-British urned cremation burial from Kent showing unburnt grave goods (copper alloy bracelets and a ring) placed on top of the cremated bone

Concluding Remarks

Fire is a powerful element combining opposites, being both destructive and life-giving. It has transformative powers, possessing the ability to render something that is potentially dangerous and frightening (i.e. the corpse) into something inert and 'clean'. The end product of cremation is fragmentary and transportable, offering myriad possible uses. Most appears to have been subject to immediate burial, but not of all the remains; some or all was occasionally kept above ground; there is evidence for movement of remains with populations, perhaps helping to reinforce land claims in some cases (e.g. migrant Anglo-Saxons) or simply as tokens of personal affection, forming tangible and accessible memento mori of a loved one. The 'living' flame, with its varying colours, movement, and heat, is fascinating to watch (Fig. 14), the ever upward transmission potentially offering greater comfort and appeal than deposition in the cold, dark ground.

The Romans appear to have viewed cremation (at least theoretically) in a very modern light, as a neat hygienic way of disposing of the corpse, the end product forming a convenient 'package' for final disposal, whilst at the same time providing the opportunity for a 'good show' (Noy 2005). At other times cremation was viewed as a mechanism by which the spirit of the deceased was released (see *Beowulf* '...Heaven swallowed the smoke ...' (Line 3154); Brøndsted 1960: 304; Downes 1999: 28; Homer's *Odyssey* Book XI, Lines 221–2) or prevented from returning (Barber 1990: 385–7). Unlocking these beliefs from the archaeological remains continues to present a fascinating archaeologically challenge.

Fig. 14 Living flame; pyre cremation (much loved pet cat)

Acknowledgements Thanks to Rob Gollar of Wessex Archaeology for preparation of the figures. Figures 1, 9, and 12 are with kind permission of Wessex Archaeology, Figs. 10 and 13 Oxford Wessex Archaeology, and Fig. 2a CotswoldWessex Archaeology. Thanks to Charlotte Roberts for providing the author with Fig. 6.

References

Baby RS (1954) Hopewell cremation practices. Papers in archaeology 1–7. Ohio Historical Society, Columbus, OH

Barber PT (1990) Cremation. JIES 18(3–4):379–388

Bass WM, Jantz RL (2004) Cremation weights in East Tennessee. J For Sci 49(5):901–904

Becker VM, Döhle HJ, Hellmund M, Leineweber R, Schafberg R (2005) Nach dem großen Brand Verbrennung auf dem Scheiterhaufen – ein interdisziplinärer Ansatz. Ber Röm-Germ Komm 86:61–195
Binford LR (1963) An analysis of cremations from three Michigan sites. Wis Archaeol 44:98–110
Bröndsted J (1960) The Vikings. Penguin, Harmondsworth
Cool HEM (2004) The Roman cemetery at Brougham Cumbria: excavations 1966–67, Britannia monograph 21, Roman Society, London
Davies DJ (ed) (2005) Encyclopaedia of cremation. Ashgate, Aldershot
Devlin JB, Herrmann NP (2008) Bone color as an interpretative tool of the depositional history of archaeological cremains. In: Schmidt CA, Symes S (eds) Beyond recognition: the analysis of burned human remains. Levier, Oxford, pp 109–135
Downes J (1999) Cremation: a spectacle and a journey. In: Downes J, Pollard T (eds) The loved body's corruption. Cruithne Press, Glasgow, pp 19–29
Fitzpatrick AP (1997) Archaeological excavations on the route of the A27 Westhampnett Bypass, West Sussex, 1992, vol 2. Wessex Archaeology Report No 12, Salisbury
Gonçalves D, Campanacho V, Thompson T, Mataloto R (2015) The weight of the matter: examining the potential of skeletal weight for the bioarchaeological analysis of cremation at the Iron Age necropolis of Tera (Portugal). In: Thompson T (ed) The archaeology of cremation: burned human remains in funerary studies. Oxbow Books, Oxford, pp 63–96
Gräslund B (1994) Prehistoric soul beliefs in Northern Europe. Proc Prehist Soc 60:15–26
Herrmann B (1977) On histological investigations of cremated human remains. J Hum Evol 6:101–103
Hiatt B (1969) Cremation in aboriginal Australia. Mankind 7(2):104–120
Hiller JC, Thompson TJU, Evison MP, Chamberlain AT, Wess TJ (2003) Bone mineral changes during experimental heating: an X-ray scattering investigation. Biomaterials 24:5091–5097
Holck P (1989) Cremated bones: a medical-anthropological study of an archaeological material on cremation burials Anatomisk institutt. University of Oslo, Oslo
Holden JL, Phakley PP, Clement JG (1995a) Scanning electron microscope observations of incinerated human femoral bone: a case study. Forensic Sci Int 74:17–28
Holden JL, Phakley PP, Clement JG (1995b) Scanning electron microscope observations of heat-treated human bone. Forensic Sci Int 74:29–45
Hope VM (2007) Death in ancient Rome. Routledge, Abingdon
Lange M, Schutkowski H, Hummel S, Herrmann B (1987) A bibliography on cremations. PACT 19. University of Göttingen, Göttingen
McKinley JI (1993) Bone fragment size and weights of bone from modern British cremations and its implications for the interpretation of archaeological cremations. Int J Osteoarchaeol 3:283–287
McKinley JI (1994a) The Anglo-Saxon cemetery at Spong Hill, North Elmham Part VIII: the Cremations. East Anglian Archaeology 69
McKinley JI (1994b) Bone fragment size in British cremation burials and its implications for pyre technology and ritual. J Archaeol Sci 21:339–342
McKinley JI (1997a) Bronze Age 'barrows' and the funerary rites and rituals of cremation. Proc Prehist Soc 63:129–145
McKinley JI (1997b) The cremated human bone from [Iron Age] burial and cremation-related contexts. In: Fitzpatrick AE Archaeological excavations on the route of the A27 Westhampnett Bypass, West Sussex, 1992, vol 2. Wessex Archaeology Report 12, pp 55–72
McKinley JI (2000a) Putting cremated human remains in context. In: Roskams S (ed) Interpreting stratigraphy; site evaluation, recording procedures and stratigraphic analysis, vol 910, BAR International Series. Archaeopress, Oxford, pp 135–140
McKinley JI (2000b) Cremated human remains; Cremation burials; and Cremated remains. In: Barber B, Bowsher D The Eastern cemetery of Roman London. MoLAS monograph 5. Museum of London Archaeology Service, London, pp 61–67, 264–277, 360–265

McKinley JI (2000c) Human bone and funerary deposits. In: Walker KE, Farwell DE Twyford Down, Hampshire: Archaeological investigations on the M3 motorway from Bar End to Compton, 1990–93, Hampshire Fieldclub Monograph 9, Hampshire Field Club and Archaeological Society, Winchester, pp 85–117

McKinley JI (2004) The human remains and aspects of pyre technology and cremation rituals. In: Cool HEM The Roman cemetery at Brougham Cumbria: excavations 1966–67, Britannia monograph 21, Society for the Promotion of Roman Studies, London, pp 283–309

McKinley JI (2006) Human bone. In: Chadwick AM Bronze Age burials and settlement and an Anglo-Saxon settlement at Clay Pit Lane, Westhampnett, West Sussex, Sussex Archaeological Collections 144. Sussex Archaeological Society, Lewes, pp 7–50

McKinley JI (2008) In the heat of the pyre: efficiency of oxidation in Romano-British cremations – did it really matter? In: Schmidt CA, Symes S (eds) Beyond recognition: the analysis of burned human remains. Levier, Oxford, pp 163–184

McKinley JI (2013a) Cremation: excavation, analysis and interpretation of material from cremation-related contexts. In: Nilsson Stutz L, Tarlow S (eds) Handbook on the archaeology of death and burial. Oxford University Press, Oxford, pp 147–171

McKinley JI (2013b) Mersea Island barrow: the cremated bone and aspects of the mortuary rite. Essex Soc Archaeol Hist 4:74–80

McKinley JI (2015a) Cremated bone. In: Andrews P, Booth P, Fitzpatrick AP, Welsh K (eds) Digging at the gateway, archaeology landscapes of south Thanet: the archaeology of East Kent access Phase II. The finds and environmental reports, vol 2. Oxford Wessex archaeology monograph 8, Salisbury

McKinley JI (2015b) The cremated human bone. In: Powell AB Archaeological discoveries along the Farningham to Hadlow Gas Pipeline, Kent, Kent Archaeological Society eArchaeology report

McKinley JI How did it go? Putting the process back into cremation. In: Pearce J, Weekes J (eds) Death as a process. Oxbow monograph. Oxford (forthcoming a)

McKinley JI Cremated bone and aspects of the mortuary rite. In: Egging Dinwiddy K, Stoodley N (eds) The Anglo-Saxon cemetery at Collingbourne Ducis, Wiltshire. Wessex archaeology monograph (forthcoming b)

Metcalf P, Huntington R (1991) Celebrations of death, 2nd edn. Cambridge University Press, Cambridge

Northover P, Montague R (1997) Heat-altered metal. In: Fitzpatrick AP Archaeological excavations on the route of the A27 Westhampnett Bypass, West Sussex, 1992, vol 2. Wessex Archaeology Report 12. Salisbury, pp 90–91

Noy D (2005) Romans. In: Davies D (ed) Encyclopaedia of cremation. Ashgate, Aldershot, pp 366–369

Oestigaard T (1999) Cremations as transformations: when the dual cultural hypothesis was cremated and carried away in urns. Eur J Archaeol 2(3):345–364

Polfer M (1993) La nécropole gallo-romaine de Septfontaines-Deckt (Grand-Duché de Luxembourg) et son ustrinum central: analyse comparative du matériel archéologique. In: Ferdière A (ed) Monde des Morts, Monde des Vivants en Gaule Rurale Actes des colloque AGER/ ARCHEA (Tours), pp 173–176

Polfer M (2000) Reconstructing funerary rituals: the evidence of *ustrina* and related archaeological structures. In: Millett M, Pearce J, Struck M (eds) Burial, society and context in the Roman world. Oxbow Books, Oxford, pp 30–37

Rogers KD, Daniels P (2002) An X-ray diffraction study of the effects of heat treatment on bone mineral microstructure. Biomaterials 23:2577–2585

Schmidt CA, Symes S (eds) (2008) Beyond recognition: the analysis of burned human remains. Levier, Oxford

Schultz JJ, Warren MW, Krigbaum JS (2008) Analysis of human cremains: gross and chemical methods. In: Schmidt CA, Symes S (eds) Beyond recognition: the analysis of burned human remains. Levier, Oxford, pp 75–94

Shipman P, Forster G, Schoeninger M (1984) Burnt bones and teeth: an experimental study of colour, morphology, crystal structure and shrinkage. J Archaeol Sci 11:307–325

Sigvallius B (1994) Funeral pyres: Iron Age cremations in North Spånga. Osteological Research Laboratory, Stockholm University, Stockholm

Sjösvärd L, Vertemark M, Gustavson H (1983) Vendel warrior from Vallentuna. The grave, human remains and animal offerings. Vendel Period Studies 2 Transactions of the boat grave symposium in Stockholm. National Antiquities, Stockholm, pp 133–150

Symes SA, Rainwater CW, Chapman EN, Gipson DR, Piper AL (2008) Patterned thermal destruction of human remains in a forensic setting. In: Schmidt CA, Symes S (eds) Beyond recognition: the analysis of burned human remains. Levier, Oxford, pp 15–54

Thompson T (ed) (2015) The archaeology of cremation: burned human remains in funerary studies. Oxbow Books, Oxford

Thompson TJU, Islam M, Bonniere M (2013) A new statistical approach for determining the crystallinity of heat-altered bone mineral from FTIR spectra. J Archaeol Sci 40:416–422

Thurman MD, Wilmore LJ (1981) A replicative cremation experiment. North Am Archaeol 2:275–283

Toynbee JMC (1996) Death and burial in the Roman world. Johns Hopkins University Press, London

Wahl J (2008) Investigations on pre-Roman and Roman cremation remains from southwestern Germany: results, potentialities and limits. In: Schmidt CA, Symes S (eds) Beyond recognition: the analysis of burned human remains. Levier, Oxford, pp 145–161

Wheeler H (1985) The Racecourse cemetery. In: Dool J, Wheeler H, et al. Roman Derby: excavations 1968–1983. Derbyshire Archaeol J 105:222–280

Bones, Rocks, and Flames: Mineralogy and Petrology of Slags and Cremated Bones from Ritual Immolation Sites in Tyrol

Peter Tropper

Introduction

Prehistoric ritual immolation sites in the Alpine area have been investigated for the past 40 years. Research on ritual immolation sites in the Alps started in 1966 by a paper by Werner Krämer. He describes: *. . . where masses of calcinated bones allow the interpretation of ritual immolation. . .. . . .as well as the occurrence of large masses of ceramic fragments which can also be interpreted as sacrificial offerings. . ..* For the first time these sites were considered from an archaeological standpoint as a group of their own. Fire is considered to have cleansing properties. The so "cleansed" sacrifice is transferred to the gods via smoke. Weiss (1997) showed that due to the lack of surface characteristics, ritual burning sites are very hard to identify and indeed their identification is mainly accidental. Weiss (1997) mentions about 120 ritual immolation sites from an area extending between the Alps and the Danube, which probably represents a lower limiting number of the actual sites. A more recent study by Gleirscher et al. (2002) extended the number of ritual immolation sites to 201 in the Alps. In the last few years, investigations concerning alpine ritual immolation sites intensified by the extensive studies of Steiner (2010) on the ritual immolation site of St. Walburg/Ulten in South-Tyrol and a proceedings volume (Stadler et al. 2013) following a conference on Alpine ritual immolation sites in Nenzing 2012. The study by Steiner represents a comprehensive investigation involving not only archaeological but also archaeobotanical and archaeozoological aspects.

Based on literature consensus, ritual immolation of offerings started roughly in the Early Bronze Age (ca. 1800 BC) and occasionally lasted until the Roman period. It was mostly carried out by farming populations asking the gods for good harvests

P. Tropper (✉)
Institute of Mineralogy and Petrography, University of Innsbruck, Innrain 52f, 6020 Innsbruck, Austria
e-mail: peter.tropper@uibk.ac.at

G. Grupe, G.C. McGlynn (eds.), *Isotopic Landscapes in Bioarchaeology*,
DOI 10.1007/978-3-662-48339-8_3

and herds. In the mountains the sacrifices were goats and sheep and in the valleys cows, pigs, deer, etc. Usually skulls and extremities of the animals were sacrificed. Besides animals the offerings also contained grains, tools, pottery, jewelry, and coins. In the Bronze Age, these activities took place in isolated sites whereas in the Iron Age they took place in the vicinity of dwellings. Increasing ritual immolation activities from the Middle Bronze Age onward coincide with increasing populations and hence increasing farming.

What are the characteristics of alpine ritual immolation sites? According to Steiner (2010) a unique definition of what clearly defines a ritual immolation site is not an easy task. The most important criterion is the presence of calcinated bones. It has been shown that the following features are also typical for a ritual immolation site: exposed position, ash layers, the presence of stone altars, ceramic fragments, and other sacrificed libations, the occurrence of pyrometamorphic slags, and the presence of adjacent bone deposits. Therefore, most sites were identified based on the presence of pottery sherds, metal artifacts, and bone fragments. However, until 2004 none of the sites had ever been investigated from a mineralogical point of view, since characteristic P-bearing minerals can form due to the interaction between bone material and rocks in the course of the immolation process (Tropper et al. 2004, 2006; Spielmann 2013). Two prehistoric immolation sites in Tyrol associated with slags were chosen for mineralogical/petrological investigations, the Goldbichl in Igls near Innsbruck (Schneider et al. 2013) and a site outside of Oetz in the Ötz Valley approximately 50 km W of Innsbruck (Tropper et al. 2004). In both areas, the site is always on top of a hill. Ritual sites have been known in Tyrol for a long time, but Von Chlingensperg (1904) was the first to interpret these sites as localities where ritual immolations took place, based in part on the abundant presence of bone fragments of domestic animals such as cows, sheep, goats, and pigs (Weiss 1997; Tomedi and Nicolussi Castellan 2000). Tropper et al. (2004) investigated slags from the ritual immolation site near Oetz and concluded, based on experiments using natural animal bones (Tropper et al. 2006), that mineralogical observations such as the assemblage phosphorus-rich olivine + whitlockite can indeed provide possible evidence for the burning of bone material and thus be very helpful in the identification of prehistoric immolation sites in cases where clear archaeological evidence is lacking. Schneider et al. (2013) investigated the Goldbichl immolation site and found the highly unusual mineral assemblage P-bearing olivine + stanfieldite. They concluded that the formation of phosphoran olivine and stanfieldite is not due to the interaction between bone material and rocks but can form locally due to the pyrometamorphic breakdown of a P-rich accessory precursor phase such as detrital apatite.

Scope of This Contribution

As stated previously, although prehistoric sacrificial burning sites have been studied in the Alpine region for the past 40 years, these investigations only focused on the

pottery, metal, and bone fragments and only two of these sites have ever been investigated from a mineralogical point of view, namely the Goldbichl site (Schneider et al. 2013) and the site in Oetz (Tropper et al. 2004). The scope of this contribution is a summary of the mineralogical and petrological characterization of slags from the two ritual immolation places: Oetz and Goldbichl. These petrographic observations are then compared to experimental investigations concerning the T-fO_2 conditions of the pyrometamorphic overprint. The experiments presented in this article were done using either whole-rock samples tempered at different temperatures with or without the presence of bones or mineral separates of sheet silicates (chlorite). These were investigated separately with several methods (high-temperature diffractometry under oxidizing conditions, HT-XRD; differential thermal analyses and thermogravimetry under reducing conditions, DTA-TG). Finally the archaeological implications of the petrological and experimental results will be discussed.

Archaeological Setting

Goldbichl/Igls: This ritual immolation site is on top of the Goldbichl, a small hill a few kilometers to the south of Innsbruck near the village of Igls (Fig. 1). The Goldbichl has been used as a prehistoric cult site since the Neolithic Age (Tomedi and Nicolussi Castellan 2000). In the Early Bronze Age (1900–1650 BC) it gained importance as a ritual immolation place. In the process of these ritual immolations, cattle, goats, and sheep were sacrificed on a stepped altar made of loam and local rocks (quartzphyllites). Due to the presence of a natural air draft, huge fires were made so that the flames could be easily seen from far away (Tomedi and Nicolussi Castellan 2000). The immolation fires were set on a circular place on the loamy ground. It was only at a later point in time that stone altars were built. Archaeological excavations yielded fragments of ceramic vessels that contained libations representing offerings of liquids and vessels sacrificed during these rituals. After every ritual immolation the place was cleaned and the precious sacrificial offerings were carried to a secret depot. According to Tomedi and Nicolussi Castellan (2000) immolation activity started again at this site during the Iron Age (ca. 450–15 BC) following a long period of neglect. At the end of this period the site was ritually "closed down" with a huge fire that completely destroyed the site leaving behind large amounts of slags.

Oetz: The presumably La-Tène (450–15 BC) age ritual immolation site is situated south of Oetz at the entrance to the Ötz Valley (Fig. 1) and is located on the back of a small ridge composed of biotite–plagioclase gneisses. Archaeological evidence for a prehistoric ritual immolation site is provided by the presence of bone fragments, broken pieces of clay vessels, and the occurrence of foamy patches of dark glassy material at the surface of gneiss boulders (Tropper et al. 2004).

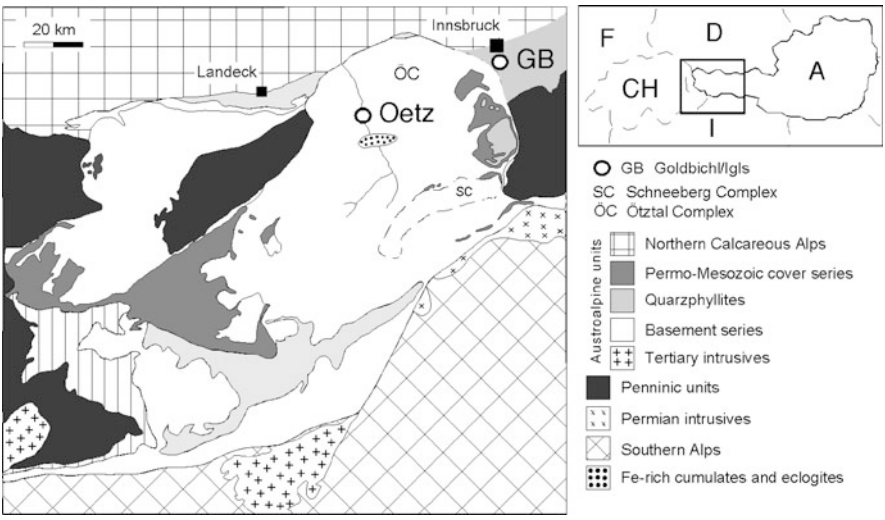

Fig. 1 Geological overview of the lower Inn Valley from Tropper et al. (2004). The locations of the Goldbichl/Igls (GB) and Oetz are shown. The Goldbichl site is geologically located in the Innsbruck quartzphyllite complex and the site in Oetz is in the Ötztal Complex (ÖC)

Geological Setting

Goldbichl/Igls: The stones for the altar are local and stem from the area around the Goldbichl. Geologically this site is situated in the westernmost part of the Innsbruck Quartzphyllite complex, which is part of the Austroalpine basement nappes north of the Tauern Window (Fig. 1). In the vicinity of Innsbruck the polymetamorphic Austroalpine basement consists of lower Ordovician porphyroid gneisses (Kellerjochgneiss or Schwazer Augengneiss), micaschists (Patscherkofel and Glungezer Crystalline Complex), and Palaeozoic schists (Innsbruck Quartzphyllite complex and Wildschönau Schists) with intercalated carbonates (Piber 2005).

Oetz: According to Hoinkes et al. (1997), the gneisses are part of the polymetamorphic Ötztal–Stubai Complex (ÖSC) and were metamorphosed during the Variscan metamorphic event under amphibolite-facies conditions (500–600 °C, 5–7 kbar).

Petrography and Textural Relations

Goldbichl/Igls: The westernmost part of the Innsbruck Quartzphyllite complex consists of metapsammites and metapelites. The mineral assemblage of the protolith quartzphyllites consists of muscovite + chlorite + plagioclase + quartz ± apatite ± biotite ± garnet ± clinozoisite ± ilmenite ± rutile ± titanite

Fig. 2 Hand specimen of *s* slag sample from the Goldbichl site. The slag is characterized by a multitude of vesicles indicating a high amount of sheet silicates in the protolith rock. Relict patches of quartzphyllite can still be seen on the *left side*

(Schneider et al. 2013). Titanite is the most abundant Ti-mineral and quartz and feldspar contents are highly variable and chlorite, muscovite, and if present biotite form the penetrative foliation. The rocks of the immolation place show signs of a strong thermal overprint, which often differs on a centimeter scale. The samples show foamy textures as well as thin (<0.5 cm) layers of glass. The foamy patches show a diameter of <3 cm and contain many vesicles which clearly indicate a high-temperature overprint while other less reactive domains still show the primary foliation (Fig. 2). Most of the slags show bloated structures. The minerals in the foamy patches were exposed to the highest temperatures, which resulted in the formation of high-*T* minerals (olivine, spinel) and melt (Fig. 3a). The pyrometamorphic rocks mostly contain the mineral assemblage olivine + orthopyroxene + plagioclase + spinel + glass. During the investigation an apatite-rich domain was found in which P-rich phases occur. Elongated crystals of plagioclase dominate the texture of the microdomain and between these laths the highly unusual mineral assemblage stanfieldite $[Ca_4(Mg, Fe^{2+}, Mn^{2+})_5(PO_4)_6]$ + phosphoran olivine occurs (Fig. 3b). Relict detrital apatite grains still occur in this domain.

Oetz: The rock samples still retain their gneissose texture showing an alternation of light and dark bands (Fig. 4). Unmelted gneiss samples show the assemblage

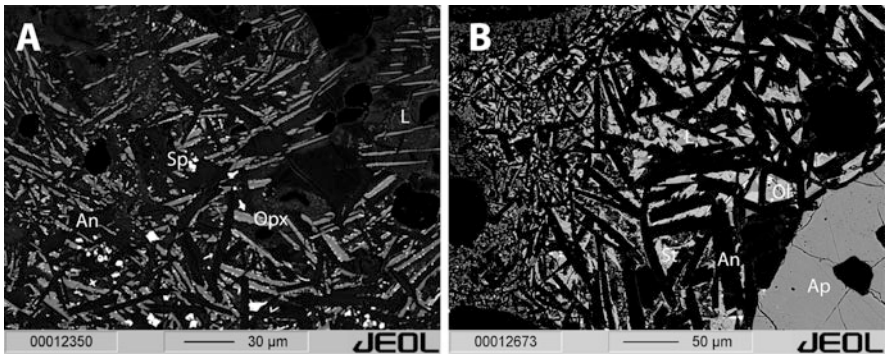

Fig. 3 (**a**) BSE (backscattered electron) image of a chlorite-rich domain in a slag sample of the Goldbichl. The high-temperature assemblage is orthopyroxene (Opx) + spinel (Sp) + anorthite (An) + glass (L). (**b**) BSE close-up of the phosphorous domain in the slag. Stanfieldite (St) and phosphoran olivine (Ol) crystallized as interstitial phases between An-rich plagioclase (An) laths. In the *right corner* relict detrital apatite (Ap) still can be seen

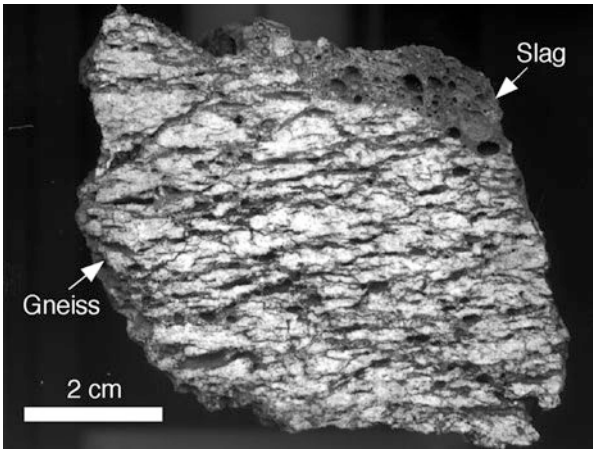

Fig. 4 Cut hand specimen of a paragneiss sample from the immolation site. The metapelitic gneiss contains a *dark*, porous layer of glassy material (slag) on the surface as well as *dark layers* within but still retains its texture. The *white* areas consist mostly of quartz

biotite + plagioclase + quartz + accessories (apatite + zircon). During partial melting, foamy patches of dark glassy material formed at the surface of the rocks and also as layers within the rocks (Fig. 4). In this glassy crust the assemblage clinopyroxene + plagioclase + quartz + anorthite + glass was observed (Fig. 5a). Plagioclase mostly forms lath-shaped crystals overgrowing the mineral assemblage. Clinopyroxene tends to form dendritic crystals, whereas olivine always occurs as angular grains. In a few small areas, melt is still preserved and quenched to glass, whereas in the majority of cases, melt recrystallized to form very small dendritic crystals which could not be analyzed properly. Toward the contact between the dark

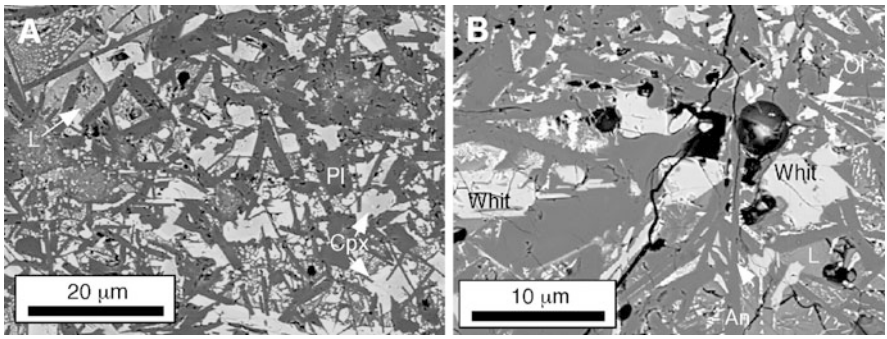

Fig. 5 Backscatter electron (BSE) images from the vicinity of the contact between rock and glass layer. (**a**) Overview over a clinopyroxene (Cpx)- and olivine (Ol)-rich domain. Interstitial glass pockets (L) and Ti-bearing magnetite also occur. Abundant plagioclase (An) laths grow within the glass and the minerals. (**b**) The assemblage olivine (Ol) + whitlockite (Whit) + plagioclase (An) + interstitial glass (L)

glassy layers and the protolith, rock whitlockite [$Ca_9(Mg,Fe)(PO_4)_6(PO_3OH)$] occurs in the assemblage olivine + clinopyroxene + plagioclase + whitlockite + glass (Fig. 5b).

Analytical Methods

Electron Microprobe Analysis (EMPA)

A JEOL 8100 SUPERPROBE electron microprobe was used at the Institute of Mineralogy and Petrography at the University of Innsbruck. For a preliminary identification of minerals the energy-dispersive spectrometer (Thermo Noran EDS system) was applied. The measurements were made using five wavelength-dispersive spectrometers (TAB, PETJ, PETH, LIF, and LIFH). Measurement conditions were 15 kV acceleration voltage and a sample current of 10 nA. The measurement time was 20 s for the peak and 10 s for each side of the background positions. The beam size was 1 µm and for corrections the Phi-Rho-Z method was used. Standardization was done using natural and synthetic standards. In order to minimize the loss of volatile elements such as K and Na, a defocused beam with a diameter of 5 µm was used for mica and feldspar analysis.

High-T Powder XRD (HT-XRD)

The HT-XRD measurements were done using an AXS-Bruker D-8 powder X-ray diffractometer. The radiation used is $CuKa_{1,2}$ with a wavelength of 0.15406 nm. The measurements occur under parallel beam optics, and an energy-dispersive

counter was used. The detector and the beam optic were theta/theta coupled and the standard operating conditions were 40 kV and 40 mA with a continuous scan ranging from 2 to 70° in theta/2theta configuration. The measurement was done with a step size of 0.01 steps and a counting time of 2 s at room conditions. Experiments were done by heating up the chlorite mineral separate with a heating rate of 0.3 °C/s. At every 20 °C step a diffractogram was measured. A 2-theta range of 5–70° was scanned with a step size of 0.02°. Each step was measured for 4 s. The measurement started at 300 °C and ended at 1200 °C. All measurements were conducted under oxidizing conditions and took place over the course of several days. The advantage of this method is the in situ observation of mineral reactions as a function of temperature.

Differential Thermal Analysis–Thermogravimetry (DTA–TG)

The principle of the differential thermo analyses/thermogravimetry is that during heating, temperature changes and changes in the mass of a sample are recorded. Endothermal or exothermal effects in a sample can be observed as well as effects of dihydroxylation. As such, mineral reactions associated with these energetic effects can be monitored as a function of temperature. DTA-TG was used to investigate the breakdown of chlorite under reducing helium atmosphere. An empty crucible of corundum was used as a standard and was held at $T = 25$ °C. The heating rate was 3 °C/s, and the temperature range was from 25 to 1200 °C. The device was the Setsys Evolution 2400 by Setaram and corund crucibles with 100 µl were used. Helium was the flushing gas with a flow rate of 20 ml/min.

Mineral Chemistry of the Slags

Goldbichl/Igls

Olivines show X_{Fe} [Fe/(Fe + Mg)] contents ranging from 0.44 to 0.84. Olivines also contain an extraordinary high amount of P of up to 23 wt% P_2O_5. The P content strongly varies but reaches a maximum of 0.536 apfu (atoms per formula unit). Figure 6 shows that not only the Si content decreases with increasing P contents (Fig. 6a), but also the sum of cations on the $M_{1,2}$ positions decreases down to 1.655 apfu (Fig. 6b). The formula of olivine illustrates the strong compositional variations: $Mg_{0.584–0.978}Fe_{0.768–1.116}Mn_{0.011–0.022}Ca_{0.004–0.014}P_{0.289–0.536}Si_{0.480–0.777}O_4$. No chemical zoning was observed in olivine. Boesenberg and Hewins (2010) postulated the following charge balancing scheme for P incorporation in olivine:

$$2^{IV}Si^{+4} + 4^{VI}M^{+2} \leftrightarrow 3^{VI}M^{+2} + 2^{IV}P^{+5} + {}^{VI}\square$$

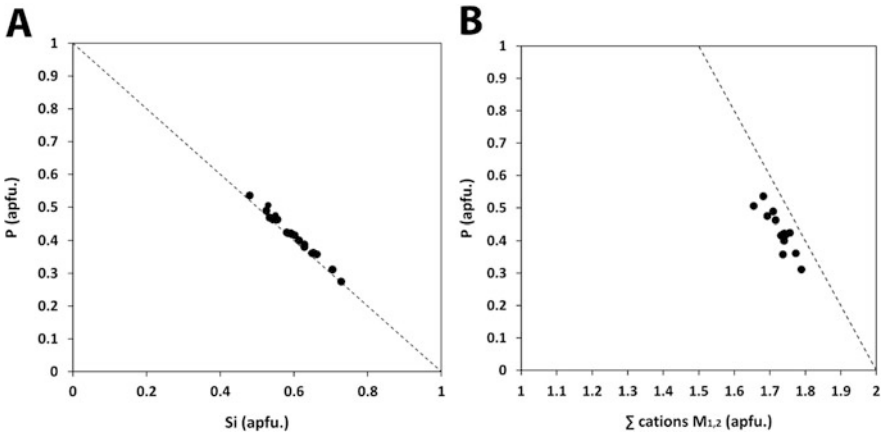

Fig. 6 (**a**) Linear correlation between Si and P (apfu) in the phosphoran olivines of the samples from the Goldbichl immolation place. The dashed line represents the 1:1 P substitution for Si according to the charge balance scheme $2Si^{4+} + {}^{VI}M^{2+} \leftrightarrow 2P^{5+} + {}^{VI}\square$. (**b**) Correlation between P and the sum of $M_{1,2}$ cations in the phosphoran olivines. The *dashed line* represents the correlation between the vacancies in $M_{1,2}$ and the P content according to the charge balance scheme $2Si^{4+} + {}^{VI}M^{2+} \leftrightarrow 2P^{5+} + {}^{VI}\square$

Rearrangement of their charge-balancing scheme leads to the more simplified charge balance scheme according to Tropper et al. (2004):

$$2Si^{4+} + {}^{VI}M^{2+} \leftrightarrow 2P^{5+} + {}^{VI}\square$$

In the course of this investigation, a tri-calcium phosphate phase (TCP) was found. Chemically, its composition fits several Ca-phosphates, namely graftonite (Ca, Mg, Fe^{2+}, $Mn^{2+})_3(PO_4)_2$, beusite $(Mn^{2+}, Fe^{2+}, Ca, Mg)_3(PO_4)_2$, and stanfieldite $Ca_4(Mg, Fe^{2+}, Mn^{2+})_5(PO_4)_6$. Stanfieldite has been described from stony-iron meteorites (Fuchs 1967), as well as pallasites (Buseck and Holdsworth 1977). The TCP from the P-rich domain has a high content of Fe, Ca, and especially Mg, which is in good agreement with the chemical composition of stanfieldite as reported by Fuchs (1967). The Ca contents of 3.41–3.83 apfu are lower than in the ideal stanfieldite formula by Fuchs (1967) but similar to the analysis by Buseck and Holdsworth (1977) who report Ca contents down to 3.69 apfu. Therefore based on the observed chemical composition the TCP is most likely stanfieldite. Spinel is a solid solution between spinel–magnetite–hercynite–magnesioferrite and ulvöspinel. The feldspar laths are plagioclase and also contain up to 0.6 wt% P_2O_5. Melt compositions outside the P-rich domains are peraluminous and also vary strongly in composition due to its formation in different microdomains. Minor orthopyroxene can be found in the slags as well as in the P-rich domain. The P-bearing orthopyroxenes vary strongly in their composition and all show a high Al component of 3–6 wt% Al_2O_3. Al is incorporated on the tetrahedral position due to the Tschermaks substitution ($2Al^{3+} \leftrightarrow Si^{4+} + M^{2+}$). The P_2O_5 content is around 0.5 wt% except for one

orthopyroxene which contains 5.0 wt% P_2O_5 which represents 0.16 apfu P. This amount of P can only be accommodated by the substitution of P and Al instead of Si on the tetrahedral site according to the following vector (Boesenberg and Hewins 2010):

$$P^{5+} + Al^{3+} \leftrightarrow 2\ Si^{4+}$$

Oetz

Olivine is characterized by highly variable X_{Fe} ranging from 0.26 to 0.52 and P_2O_5 contents from below the detection limit up to 8.8 wt% P_2O_5, respectively. Again all analyzed olivines show a linear negative correlation between P and Si with a slope close to −1, which is consistent with data from the literature (Goodrich 1984; Buseck and Clark 1984; Agrell et al. 1998). Moreover, a significant decrease in total cation sums with increasing P contents can be observed with ∑cat as low as 2.90 for the highest P content of 0.20 apfu. Clinopyroxenes are mostly augitic in composition with limited Ca-Tschermak ($Al^{IV} = 0.02–0.10$ apfu) component. Clinopyroxenes may contain significant enstatite and ferrosilite solid solution with (Mg + Fe) contents on the M(2) site, ranging from 0.08 to 0.43 apfu. Plagioclase laths coexisting with olivine and clinopyroxene show anorthite contents in the range 40–65 mol%. In contrast to the chemical composition of apatite [$Ca_5(PO_4)_3(OH,F,Cl)$], whitlockite [$Ca_9(Mg,Fe)(PO_4)_6(PO_3OH)$] contains significant amounts of MgO (3.29–3.69 wt%), FeO (0.70–1.33 wt%), and Na_2O (1.46–1.85 wt%). All interstitial glasses are quartz-normative and show a granitic composition with SiO_2 ranging from 62.52 to 69.06 wt%. FeO contents of the glass are highly variable and range from 4.97 to 16.11 wt%. The P_2O_5 contents are very low and are <0.99 wt%.

The chemical variability of the phases formed in the slags during the ritual immolation process and the occurrence of extensive P-substitution in olivine both strongly indicate disequilibrium growth in relatively SiO_2-rich domains due to rapid quenching. This is consistent with the implications associated with phosphoran olivine growth in natural occurrences (Buseck and Clark 1984; Agrell et al. 1998; Goodrich 1984; Brunet and Chazot 2000) and in a ritual immolation site (Tropper et al. 2004), as well as in experimental investigations (Bousenberg et al. 2004; Boesenberg and Hewins 2010; Tropper et al. 2006).

Experimental Investigations

Very few experimental investigations simulating pyrometamorphic processes are available and are mainly concerned with the formation and development of disequilibrium textures due to the breakdown of hydrous phases (e.g., Cultrone et al. 2001; Brearley and Rubie 1990). Tropper et al. (2006) performed firing

experiments at 1 bar to investigate the formation of phosphorus olivines and thus compare the results with the observations of Tropper et al. (2004) from the ritual immolation site near Oetz in Tyrol. Schneider (2009) and Spielmann (2013) conducted additional experiments using natural quartzphyllite samples in order to place temperature constraints on the firing process in the samples from the Goldbichl. So far the experimental investigations can be placed in three groups: (1) whole-rock experiments without the presence of bones, (2) bone-rock experiments, and (3) high-*T* experiments (HT-XRD, DTA–TG) investigating the thermal evolution of a chlorite sample with intermediate Fe-content ($X_{Fe} = 0.46$).

Whole-Rock Experiments

To place constraints on the temperature of formation of the Oetz slags melting experiments at 1 bar and 900–1300 °C were conducted in a box furnace (Tropper et al. 2006). To investigate the role of crucible material during firing, two experiments at 1000 °C were conducted: one in a graphite crucible and the other in a Pt crucible. Secondary electron (SE) images of the rock cubes from the experiment in the Pt-crucible at 1000 °C showed almost no melting textures on the surface (Fig. 7a) and therefore the experiments in the Pt crucible were not pursued any further. In contrast in the experiments with the graphite crucible visible melting took place at the surface of the rock cube (Fig. 7b) indicating that more reducing fO_2 conditions facilitate a higher degree of partial melting. In the experiments without the addition of bones biotite is stable up to 900 °C and its breakdown yielded the mineral assemblage olivine + Ti-bearing magnetite + melt from 1000 °C on. In order to put preliminary temperature constraints on the pyrometamorphic formation of the slags from the Goldbichl site Schneider (2009) conducted an experiment using a quartzphyllite sample at 1100 °C and obtained the same mineral assemblage orthopyroxene + olivine + spinel + melt as observed in the slag samples from the Goldbichl site.

Bone–Whole-Rock Experiments

For this study Tropper et al. (2006) used samples of unmelted biotite-plagioclase-gneisses from the burning site near Oetz, which were cut into cubes of approximately 1 cm edge length. To be as close as possible to the observations simple experiments were designed where fO_2 was only approximated to the CCO (graphite C/carbon monoxide CO) buffer but not fixed. Most experiments were performed with the rock cube placed on top of a layer of crushed chicken bones. These rock–bone aggregates were then subjected to temperatures between 900 and 1300 °C with run durations from 90 to 480 min. In addition, the presence of bone material to the rock cubes led to complete melting of the rock cubes at temperatures of 1300 °C as

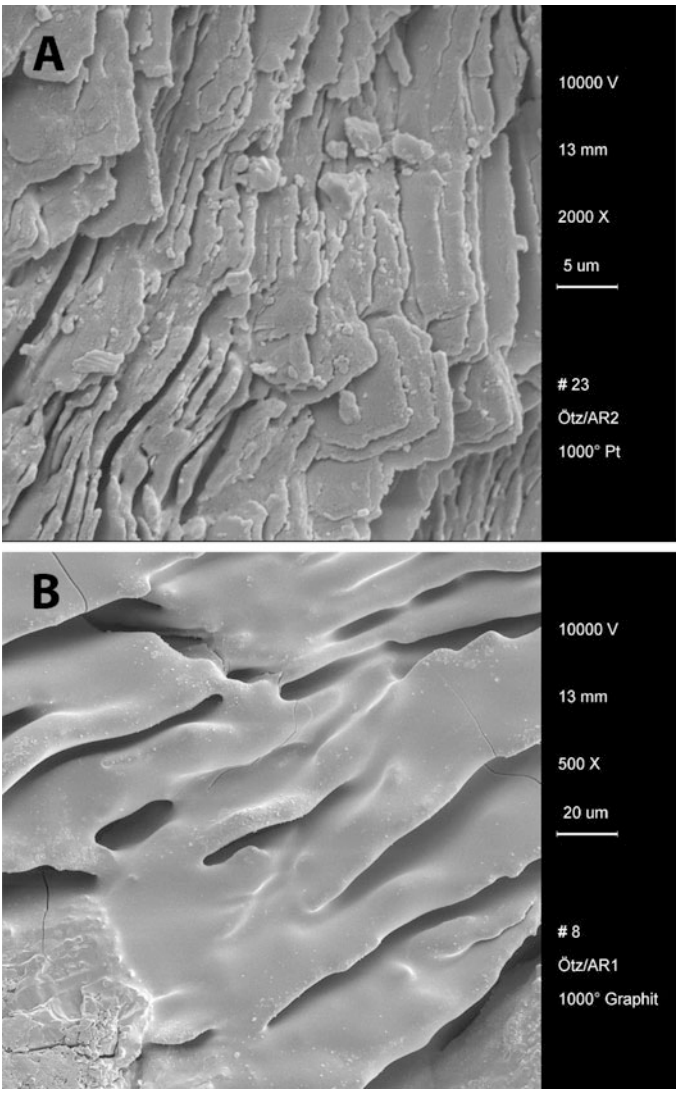

Fig. 7 Secondary electron (SE) image of the surface of rock cubes from experiments at 1000 °C. (**a**) Experiment in a Pt crucible. The *sharp edges* of the biotites do not indicate a significant degree of melting. (**b**) Experiment in a graphite crucible. The *rounded edges* and *open spaces* indicate a considerable degree of melting

shown in Fig. 8a. Most experiments were quenched by quickly removing the crucible from the furnace. Although olivine occasionally formed, quenching and the presence of bone material on only one side of the rock cube did not lead to sufficient mineral reactions at the interface between the rock and the bone layer and thus experiments were conducted where bone material was sandwiched between

rock cubes. Therefore, in order to allow a more intimate contact between bone and rock and thus to enable a stronger reaction, bone material was sandwiched between two rock slabs in two experiments (Fig. 8b). Instead of quenching, these experiments were cooled slowly from 1100 and 1200 °C down to 500 and 700 °C with cooling rates of 60 and 120 °C/h to allow slow crystallization from the melt. After the experiment the cubes were embedded in epoxy resin and polished for electron microprobe and scanning electron microscope analysis (Fig. 9a, b). The former

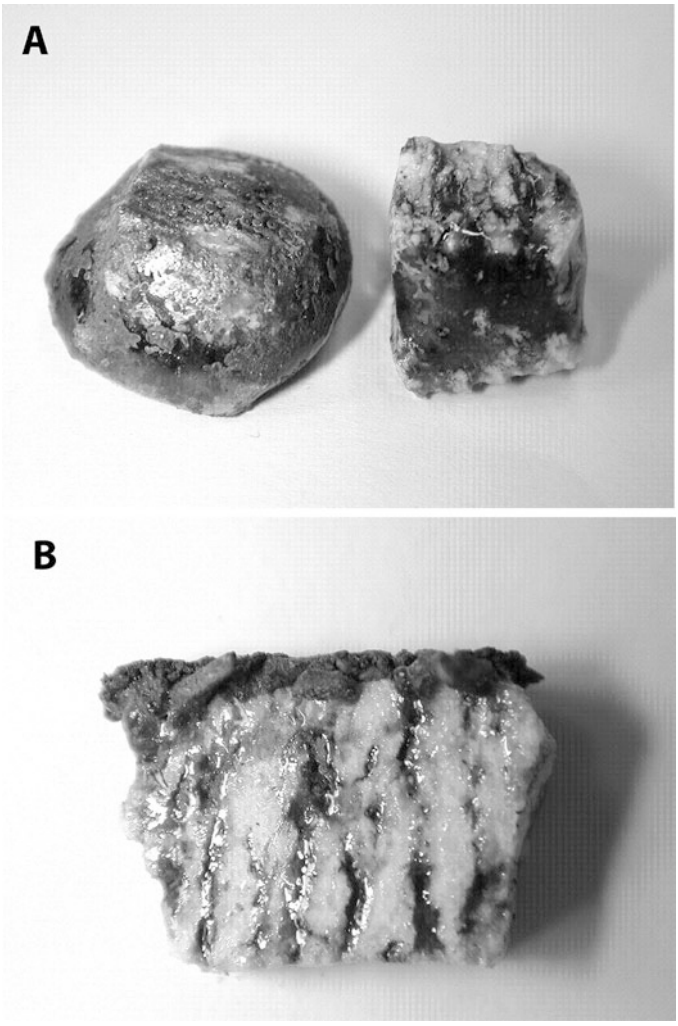

Fig. 8 (**a**) Comparison between two experiments at 1300 °C from an experiment in a graphite crucible with bone material added (*left*) and without bone material (*right*). The addition of bone material to the experiments leads to a strong increase in melting during the experiments. The diameter of the cube on the *right* is 1 cm

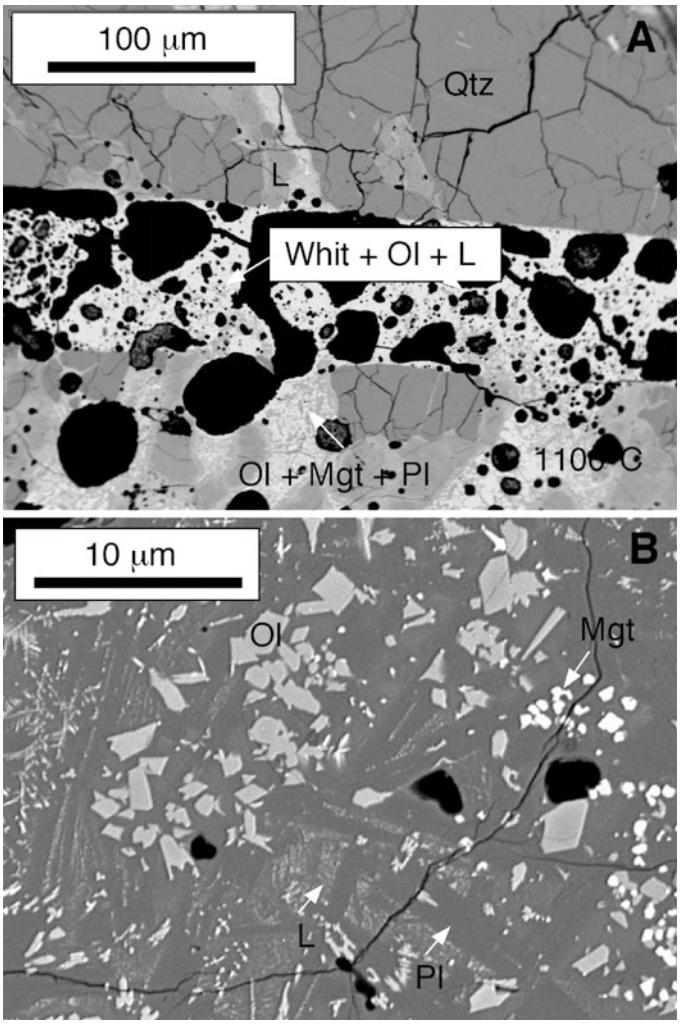

Fig. 9 Backscatter electron (BSE) images of a slowly cooled bone-paragneiss experiment in a graphite crucible at 1100 °C from Tropper et al. (2006). (**a**) The layering of the former bone layer is still visible and contains the assemblage whitlockite (Whit) + olivine (Ol) + melt (L). Small injections of melt veins into the adjacent rock cubes are also visible. (**b**) Within the melt pockets the assemblage olivine (Ol) + magnetite (Mgt) + plagioclase (Pl) + melt (L) occurs

bone domain now contains the assemblage whitlockite (Whit) + olivine (Ol) + melt (L). Olivines from the experiment at 1100 °C show a wide range in P_2O_5-concentrations from 0.18 to 1.19 wt% along with significant variations in their Fe/Mg-ratios ($Fo_{30}Fa_{70}$–$Fo_{50}Fa_{50}$). Compared to olivines from the immolation site in Oetz site the experimentally produced olivines extend to more Fe-rich compositions but do not contain as much P_2O_5. Similar to the olivines from the immolation site the experimentally grown olivines also show a negative correlation between

P and Si apfu and also between P and total cation sums. Both correlations, however, are not as pronounced as those observed for olivines from the immolation site. The chemical analyses of whitlockites from the slowly cooled experiments at 1100 and 1200 °C are very similar to whitlockites reported by Tropper et al. (2004) and contain 3–4 wt% MgO and <1 wt% FeO. Na_2O varies between 0.7 and 2.4 wt%.

Spielmann (2013) carried out high-temperature investigations at 1200 °C by using typical rocks (paragneiss, quartzphyllite, granite, garnet-amphibolite) of the eastern Alps together with bone material. The paragneiss-bone experiment yielded the mineral assemblage whitlockite + clinopyroxene + anorthite + Fe-Ti-spinel + Fe metal + melt in the bone–rock contact area (Fig. 10a). The obtained textures and the mineral assemblage only lack olivine in the contact area between bone and rock when compared to the slags from Oetz. Olivine does form in this experiment slightly further away from the direct contact in former biotite domains. The granite-bone experiment yielded in the contact area the mineral assemblage whitlockite + wollastonite + anorthite + melt. The quartzphyllite-bone experiment yielded the mineral assemblage whitlockite + P-bearing olivine + spinel + Fe metal + melt (Fig. 10b). The most complex mineral assemblage was obtained in the garnet-amphibolite-bone experiment where the assemblage whitlockite + clinopyroxene + perovskite + Fe-Ti-spinel + anorthite + Fe metal + melt formed in the bone–rock contact zone. The chemical composition of whitlockite in the experiments strongly depends on the composition of the protolith rocks and shows MgO and FeO contents of 1–2 wt% and 0–3 wt%. In the quartzphyllite-bone experiments P-bearing olivine with P_2O_5 contents up to 4.5 wt% occurs. P-incorporation follows the similar coupled substitution as observed in the slags from the two immolation sites. In addition to olivine clinopyroxenes from the paragneiss-bone and garnet-amphibolite-bone experiments, contain significant

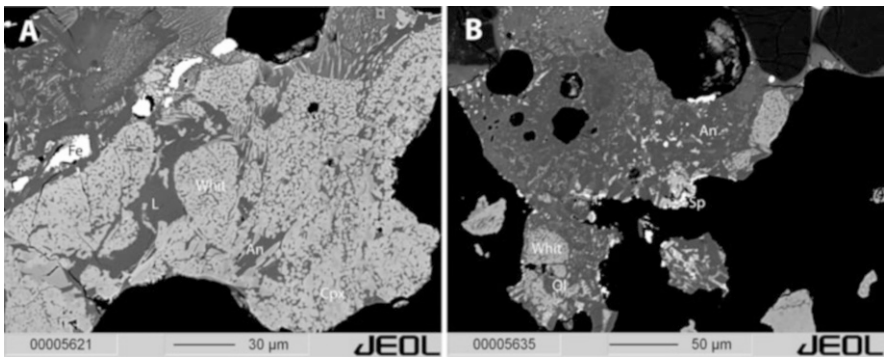

Fig. 10 Close-up backscatter electron (BSE) images of the contact zones in the bone-paragneiss (**a**) and bone-quartzphyllite (**b**) experiments in a graphite crucible at 1200 °C from Spielmann (2013). (**a**) In the contact zone between paragneiss and bone the assemblage whitlockite (Whit) + clinopyroxene (Cpx) + anorthite (An) + Fe metal (Fe) occurs. (**b**) In the contact zone between quartzphyllite and bone the assemblage whitlockite (Whit) + olivine (Ol) + spinel (Sp) + anorthite (An) + melt (L) occurs

P_2O_5 contents of up to 15 wt%. This amount of P can only be accommodated by the substitution of P and Al instead of Si on the tetrahedral site according to the following vector $P^{5+} + Al^{3+} = 2Si^{4+}$. The occurrence of metallic Fe in the experiments indicates that fO_2 conditions were too reducing when compared to the Goldbichl and Oetz slags where Fe occurs as Fe^{2+} in olivines and the QFM assemblage (quartz-olivine-spinel) is still stable.

High-T XRD Experiments of Chlorite Under Oxidizing Conditions

For this experiment a chlorite with an intermediate Fe content ($X_{Fe} = 0.46$) similar to the composition from the protolith quartzphyllites from the Goldbichl site was used. With increasing temperature the chlorite lattice shrinks in c-direction (Schneider 2009). This is a consequence of the high water loss during heating. With rising temperature the (002)-peak disappears finally at 550 °C and the (001)-peak rises which was also reported by Villieras et al. (1994). This structure is known as the chlorite "modified structure" (Brindley and Chang 1974; Villieras et al. 1994; Guggenheim and Zhan 1999) and is stable until 760 °C. Above this temperature chlorite-like structure can no longer be observed. The shrinking of the lattice at higher temperatures due to dehydroxylation of the brucite-like layers to lower spacings for the (001)-peak is also reported by Villieras et al. (1994). At 800 °C the sample is completely decomposed and at 900 °C spinel forms. At 1120 °C sapphirine and at 1140 °C cristobalite appear.

DTA–TG Experiments of Chlorite Under Reducing Conditions

The $X_{Fe} = 0.46$ chlorite shows a two-step dehydroxylation starting with a drastic weight loss at 507 °C. It is remarkable that no loss of adhesively bound water was observed, which usually occurs between a temperature range of 50–200 °C. Then at a temperature of 740 °C the second dehydroxylation step occurs until 812 °C where a mass gain starts again (Schneider 2009). This phenomenon of gaining mass is still unexplained and might be attributed due to oxidations due to the presence of small concentrations of oxygen in the flushing helium gas. XRD of the products of the DTA/TG measurement yielded the mineral assemblage spinel + orthopyroxene + cristoballite/β-quartz.

Discussion

Textural Evolution of the Slags from the Goldbichl Site

At atmospheric pressure the sheet silicates start changing their shape due to the rising temperatures with intensified bloating and microcracking due to dehydration of adhesive and structurally bound water (Grapes 2006). Until the α–β transition of quartz at 575 °C the dilation occurs moderately and continuously (Grapes 2006). Vitrification occurs at a temperature of ca. 900 °C while degasification channels and bloating structures are produced at temperatures ca. 1200 °C (Grapes 2006). During firing of the quartzphyllites the micas break down along a continuous process beginning with substantial water loss. The original textures of muscovite and chlorite are preserved only as relicts and at higher firing temperatures small cubic crystals of spinel form within the chlorite layers. Depending on the distance to the fire different temperatures and oxygen conditions affected the rocks. The highest temperature was at the contact area between the rock and the fire where the most obvious melting processes took place. In these areas high temperature led to the breakdown of the initial assemblage muscovite + chlorite + plagioclase + quartz ± biotite ± clinozoisite ± ilmenite to the formation of the new pyrometamorphic assemblage: plagioclase (an-rich) + olivine + spinel + melt ± orthopyroxene due to the following model reactions involving the breakdown of chlorite (Schneider et al. 2013):

$$\text{Chlorite} = \text{Olivine} + \text{Spinel} + \text{Quartz} + \text{H}_2\text{O}$$
$$\text{Chlorite} = \text{Olivine} + \text{Spinel} + \text{Orthopyroxene} + \text{H}_2\text{O}$$

Orthopyroxene can also form due to a reaction between olivine and quartz and occurs therefore in an advanced stage of pyrometamorphism (Grapes 2006). Adjacent to olivine, large blades of plagioclase crystallized.

Textural Evolution of the Slags from the Oetz Site

Unmelted gneiss samples from the immolation site show the mineral assemblage biotite + plagioclase + K-feldspar + quartz with feldspars showing strong retrograde alteration to clinozoisite + albite + muscovite (sericite). Based on the petrographic observation, dark bands within the partially molten rock samples are therefore interpreted as former layers rich in biotite where partial melting was initiated. The breakdown of biotite at high temperatures and very low pressures has been reported so far from partially fused metapelites and granites (Maury and Bizouard 1974; Le Maitre 1974; Grapes 1986; Brearley 1987). Textural observations revealed that olivine and Ti-bearing magnetite form within the former biotite domains according to the reaction (Tropper et al. 2004):

$$\text{Biotite} + \text{Quartz} = \text{Olivine} + \text{Ti-bearing Magnetite} + \text{K-rich melt}$$

The presence of clinopyroxene in the partially molten rocks could be ascribed to a reaction involving clinozoisite, the latter being a product of plagioclase alteration:

$$\text{Clinozoisite} + \text{Phlogopite} + \text{Quartz} = \text{Anorthite} + \text{Diopside} + \text{K-feldspar} + H_2O$$

which would lead to the formation of K-rich melt at high temperatures. The high enstatite and ferrosilite components in the clinopyroxene indicate the simultaneous proceeding of the biotite breakdown reaction:

$$\text{Biotite} + \text{Quartz} = \text{Orthopyroxene} + \text{K-feldspar} + H_2O$$

Derived Chlorite Breakdown Reactions from the Experimental Results

DTA-TG experiments: The decomposition of chlorite is a complex process strongly dependent of its Fe content and fO_2 conditions (Schneider 2009). Chlorite with a low Fe content ($X_{Fe} = 0.11$) forms under vacuum (DTA-TG) as well as under air atmosphere (HT-XRD) the assemblage forsterite + spinel + enstatite + water. Under helium atmosphere chlorites with even a higher X_{Fe} produce the assemblage spinel + enstatite (for $X_{Fe} = 0.46$ and 0.62). Chlorite with $X_{Fe} = 0.62$ formed cordierite in addition and chlorite with $X_{Fe} = 0.89$ formed hercynite + melt. The derived mineral reactions that occur in helium atmosphere are:

$$\text{Chlorite}\ (X_{Fe} = 0.11) = \text{Forsterite} + \text{Spinel} + \text{Enstatite} + H_2O$$
$$\text{Chlorite}\ (X_{Fe} = 0.46) = \text{Spinel} + \text{Enstatite} + \text{Quartz} + H_2O$$
$$\text{Chlorite}\ (X_{Fe} = 0.62) = \text{Spinel} + \text{Enstatite} + \text{Cordierite} + \text{Quartz} + H_2O$$
$$\text{Chlorite}\ (X_{Fe} = 0.89) = \text{Hercynite} + \text{Melt}$$

High-T XRD experiments: Under strongly oxidizing conditions and with high X_{Fe}, phases with Fe^{3+} appear. Chlorite with the medium Fe-content ($X_{Fe} = 0.46$) decomposes to pleonaste (spinel soild solution), while the Fe-rich chlorite ($X_{Fe} = 0.89$) forms hematite and mullite. Sapphirine occurs in both cases only in minor concentrations. The reactions that occur in oxidizing air atmosphere (Schneider 2009) are:

$$\text{Chlorite}\ (X_{Fe} = 0.11) + O_2 = \text{Forsterite} + \text{Spinel} + \text{Enstatite} + H_2O$$
$$\text{Chlorite}\ (X_{Fe} = 0.46) + O_2 = \text{Pleonaste} + \text{Sapphirine} + \text{Quartz} + H_2O$$
$$\text{Chlorite}\ (X_{Fe} = 0.89) + O_2 = \text{Hematite} + \text{Mullite} + \text{Sapphirine} + \text{Quartz} + H_2O$$

Comparison of these experimental results to the slags from the Goldbichl site clearly indicates that the firing process must have taken place under very reducing conditions (most likely QFM) since the mineral assemblage spinel + orthopyroxene

+ quartz from the $X_{Fe} = 0.46$ DTA-TG experiment closely reproduced the observed mineral assemblage in the former chlorite domains of the Innsbruck quartzphyllite.

Bone–rock experiments: The experimental investigations by Tropper et al. (2006) have shown that the interaction of bone material and metapelitic gneisses during partial melting led to the formation of P-rich olivines + whitlockite + plagioclase + K-rich glass. The experimental investigations indicate that the temperature of olivine formation due to the reaction biotite + quartz = olivine + Ti-bearing magnetite + K-rich melt must have exceeded 1000 °C at fO_2 conditions near the CCO buffer and are in agreement with temperature estimates from pallasite meteorites (1143–1359 °C). The occurrence of phosphoran olivine and whitlockite in meteorites with compositions similar to those encountered in the experiments and the rocks at the firing site (Goodrich 1984; Buseck and Clark 1984; Agrell et al. 1998) further indicates a similarity with the experimental conditions. The chemical and experimental data strongly indicate olivine growth under disequilibrium conditions. Although phosphoran olivine did form in the experiments the extent of P-incorporation into olivine is much smaller compared to the olivines from the burning site at Oetz. Olivines with P_2O_5 contents similar to those found in the experiments do occur in Oetz but are restricted to microdomains more distant to the rock/bone interface. Clearly, local variations in firing temperature, oxygen fugacity, bulk phosphorus, and the geometry of the bone–rock aggregates must have controlled the P-incorporation in olivine. The experimental study of Spielmann (2013) extended the investigations of Tropper et al. (2006) by using four different rock types: paragneiss, quartzphyllite, granite, and garnet-amphibolite in the experiments. Whitlockite formed in all experiments and P-bearing olivine formed in some (quartzphyllite-bone) of the experiments. The occurrence of P-rich olivine and whitlockite in the quartzphyllite experiments is therefore also diagnostic for bone–rock interaction at high temperatures similar to the results from Tropper et al. (2006).

Temperature Constraints on Firing Temperatures During Pyrometamorphism

Temperature Estimates Based on Mineral Reactions in the Slags

Schneider (2009) has shown by using high-*T* XRD that the breakdown reactions of chlorites with different X_{Fe} strongly differ. Fe-rich chlorite also dehdroxylates 140 °C earlier than clinochlore. DTA-TG experiments using a chlorite sample with intermediate Fe-contents yielded at 1100 °C the product assemblage of enstatite + spinell + quartz which forms from 740 to 810 °C according to the reaction chlorite ($X_{Fe} = 0.46$) = spinel + enstatite + quartz + H_2O. The slags from the immolation place contain the minerals: olivine + spinel + orthopyroxene + anorthite + glass. Thus, the occurrence of the assemblage spinel + orthopyroxene + olivine leads to the conclusion that temperatures of at least

800 °C were reached during the firing. The experimental investigations of Tropper et al. (2006) and Schneider (2009) using rock samples without the addition of bones also reproduced the mineral assemblages of the pyrometamorphic slags olivine + spinel + melt (Oetz) and olivine + orthopyroxene + spinel + melt (Goldbichl) over a temperature range of 900–1100 °C.

Temperature Constraints Based on Coexisting Feldspars

Schneider (2009) analyzed coexisting feldspars in the pyrometamorph slags from the Goldbichl site. The texture of the feldspars indicates that they were the first crystals that crystallized from the melt. The feldspars are plagioclases with low K contents. The temperature dependence of the miscibility gap between plagioclase and K-feldspar can be used to estimate temperatures present during the immolation process (Fuhrmann and Lindsley 1988). Coexisting feldspar composition yielded temperatures ranging from 900 °C to 1200 °C. The spread in the data is probably due to the lack of equilibrium but consistent with the experimental results.

Temperature Constraints Based on Phase Diagrams

Phase equilibria in the system $FeO–Al_2O_3–SiO_2$ by Osborn and Muan (1960 written comm., NIST 2004) show that fayalite and hercynite coexist along a cotectic line over a temperature range of 1100–1200 °C. These temperature constraints should only be viewed as lower constraints since the observed phase compositions deviate significantly from this end-member system due to the incorporation of a significant MgO (forsterite) component.

Temperature Constraints Based on XRD of Cremated Bones from Immolation Sites

Calcination of bones is a thermal process leading to thermal decomposition and hence removal of the volatile fraction of bone material. During this process organic matter (collagen) burns off and minerals such as hydroxyl-apatite remain. During heating, the color of the bones changes from yellow to white. Due to heating shrinkage and extensive fragmentation of bones also occur. HAT-XRD studies of bone material show that at ca. 350 °C organic matter burns off and hydroxylapatite recrystallizes with increasing temperature (Haberko et al. 2006). This is indicated by XRD patterns which become sharper with increasing temperature due to better crystallization of apatite. At $T > 700$ °C CaO forms (Haberko et al. 2006). The size of the crystallites also strongly increases and Piga et al. (2008) conducted a calibration of apatite crystallite size as a function of temperature based on cremated human remains. It turns out that not only temperature is important but the duration of firing is important as well. Crystallite sizes of bone apatite from two ritual

immolation sites namely the Scheibenstuhl near Nenzing in Vorarlberg and from the calcinated bone deposit of the ritual immolation site at Weer in the lower Inn Valley yielded apatite crystallite sizes of 300–380 nm which corresponds to temperatures of 650–750 °C according to Piga et al. (2008). It is interesting to note that the calcinated bones show much lower temperatures (>650 °C) than the slags (1000–1100 °C).

Mineralogical Implications

The investigated sites (Goldbichl/Igls and Oetz) contain pyrometamorphic slags (Goldbichl shows massive amounts and Oetz only small amounts) and temperatures derived from these slags are >1000–1100 °C under highly reducing conditions (QFM). Tropper et al. (2004) pointed out the possible importance of P-bearing phases such as whitlockite and P-bearing olivines in pyrometamorphic slags as diagnostic phases for bone–rock interaction at very high temperatures. The subsequent experimental investigations by Tropper et al. (2006) and Spielmann (2013) confirmed this suggestion since whitlockite + P-bearing olivine indeed did form in the bone–rock experiments. The formation of whitlockite in a quartzphyllite precursor rock can be explained by using a model reaction such as:

$$\text{Apatite} + \text{Chamosite} + \text{Quartz} + O_2 = \text{Whitlockite} + \text{Anorthite} + \text{Fayalite} + H_2O$$

On the other hand, Schneider et al. (2013) investigated the pyrometamorphic slags from the Goldbichl site and found in a former apatite micro-domain P-rich olivine coexisting with stanfieldite instead of whitlockite. Therefore, Schneider (2009) concluded that the occurrence of phosphoran olivine + stanfieldite is restricted to extremely P-rich domains in the rocks and thus is only related to the breakdown of accessory detrital apatite in the slag. The formation of P-rich olivine from accessory apatite is thus in contrast to the investigations by Tropper et al. (2004) who proposed that bone–rock interactions alone are responsible for the formation of phosphoran olivines and phosphates. This fact might also be reflected by the presence of a different phosphate phase in the slag samples from the Goldbichl. In this investigation a TCP phase (stanfieldite) instead of whitlockite was found. Therefore, caution is advised concerning archaeological implications based on the occurrence of phosphoran phases in slags from ritual immolation sites since they can also form without the presence of bone material. Based on the mineralogical observations, P-rich minerals, which indicate the presence of a P-source in the fire, are as follows: whitlockite, P-rich olivine, P-rich clinopyroxene, and stanfieldite. The following mineral assemblage is experimentally shown to be associated with bone–rock interactions: P-rich olivine ± P-rich clinopyroxene, yet only when coexisting with whitlockite. P-rich olivine, P-rich clinopyroxene, and stanfieldite

form by decomposition of detrital apatite in the slags of the Goldbichl and no bone material is involved in their formation. P-rich olivine and whitlockite have been found in the slags from Oetz and based upon the experimental results bone material might be involved in their formation.

The pyrometamorphic slags as well as the experimental investigations show P-bearing olivines as a diagnostic phase. The occurrence of phosphoran olivine with significant phosphorus contents (>2 wt% P_2O_5) has been reported from only a few unusual places of the world (see Tropper et al. 2004). The terrestrial phosphoran olivines commonly occur together with farringtonite and/or stanfieldite (Agrell et al. 1998). In contrast, experimental investigations by Boesenberg and Hewins (2010) yielded phosphoran olivines with up to 27 wt% P_2O_5. Synthetic olivines with slightly elevated phosphorus contents (<1 wt% P_2O_5) are known from blast furnace slags from modern, prehistoric, and medieval smelting operations (Müller et al. 1988; Heimann et al. 1998) and phosphoran olivines with up to 10.5 wt% P_2O_5 were reported from wrought iron from the USS Monitor (Boesenberg 2006).

Because of the similarity of crystal chemical properties of P and Si (low cation radius, highly charged) both occupy preferentially the tetrahedral site. Previous descriptions of the occurrence of phosphoran olivines indicate that they grew under strongly disequilibrium conditions and P substitution for Si in olivine is not surprising since several phosphates with olivine-like structures exist (e.g., Langer et al. 2006, 2007). Therefore, with respect to the nature of the olivine–phosphate phase solid solution several possibilities for olivine-phosphate solid solutions exist. The structure of farringtonite $Mg_3(PO_4)_2$ is closely related to the structure of forsterite, but shows monoclinic instead of orthorhombic symmetry. Similar to olivine, the three-dimensional framework of farringtonite is composed of PO_4-tetrahedra that are linked together by metal-oxide polyhedra. There are also two sites M_1 and M_2, which are five and sixfold coordinated (MgO_5, i.e., MgO_6) according to Nord and Kierkegaard (1968). But even more closely related to the olivine structure are the phosphate minerals sarcopside ($Fe_3(PO_4)_2$, Moore 1972) and its Mg-rich counterpart chopinite ($Mg_3(PO_4)_2$, Grew et al. 2010) which also have an olivine-type structure with hexagonal closest oxygen package. Therefore, phosphoran olivines can form due to the breakdown of detrital apatite by model reactions such as:

$$\text{Chamosite} + \text{Apatite} + \text{Quartz} = \text{Sarcopside} + \text{Anorthite} + \text{Fayalite} + H_2O$$
$$\text{Chamosite} + \text{Apatite} = \text{Sarcopside} + \text{Anorthite} + \text{Hercynite} + \text{Fayalite} + H_2O$$

Archaeological Implications

Contrary to the slags bone apatite crystallinity of calcinated bones yields much lower temperatures. This might be due to their position in "cooler" spots of the fire (e.g., at or very close to the surface). The high temperatures deduced from the slags (1000–1100 °C) are compatible with core temperatures of large bone fires with a

possible wind-driven air circulation. Concerning the source of phosphorus in the slags one also has to bear in mind that bone material might not be the only source of P since meat and wood also contain P and if the samples were found in cultivated soil post-ritual immolation activities over the centuries such as fertilization of soil also alter the P contents of the samples. The archaeological implications for the Goldbichl site point toward the implication that the massive amounts of slags probably represent the last firing event of the immolation site most likely the ritual "closing" of the site by an enormous fire and hence they are most likely not associated with ritual immolation activities. The archaeological implications for the Oetz site imply that bone–rock interactions at very high temperatures might indeed have occurred although clear archaeological evidence (e.g., bone–slag sample) is lacking. High-temperature bone–rock interaction could occur when small bone fragments migrate into deeper and hence hotter portions of the fire since usually bones crack and defragment and no flesh is attached to the bones anymore.

The experiments have shown that the occurrence of the phosphate mineral whitlockite in pyrometamorphic slags from ritual immolation sites could indeed be mineralogically diagnostic for bone–rock interactions but only when archaeological data are considered.

Acknowledgments Financial support through the FWF special research program HiMAT (F3110-G02 to P.T.) is gratefully acknowledged. Thanks to Philipp Schneider and Magdalena Spielmann for the data, Daniela Schmidmair for her help with high-*T* XRD, and Waltraud Wertl for her help with DTA-TG. Gerhard Tomedi is thanked for helpful discussions concerning the archaeology of ritual immolation sites. Harald Stadler, Gerhard Tomedi, and Ulrike Töchterle are thanked for providing calcinated bone samples from immolation sites.

References

Agrell SO, Charnley NR, Chinner A (1998) Phosphoran olivine from Pine Canyon, Piute Co., Utah. Mineral Mag 62:265–269

Boesenberg JS (2006) Wrought iron from the USS monitor: mineralogy, petrology and metallography. Archaeometry 48:613–631

Boesenberg JS, Hewins RH (2010) An experimental investigation into the metastable formation of phosphoran olivine and pyroxene. Geochim Cosmochim Acta 74:1923–1941

Bousenberg JS, Ebel RH, Hewins RH (2004) An experimental study of phosphoran olivine and its significance in main group pallasites. In: Lunar and Planetary Science Conference XXXV, Lunar Planet Institute, Houston:#1368 (abstract)

Brearley AJ (1987) An experimental and kinetic study of the breakdown of aluminous biotite at 800 °C: reaction microstructures and mineral chemistry. Bull Mineral 110:513–532

Brearley AJ, Rubie DC (1990) Effects of H_2O on the disequilibrium breakdown of muscovite + quartz. J Petrol 31:925–956

Brindley GW, Chang T (1974) Development of long basal spacings in chlorites by thermal treatment. Am Mineral 59:152–158

Brunet F, Chazot G (2000) Partitioning of phosphorus between olivine, clinopyroxene and silicate glass in a spinel lherzolite xenolith from Yemen. Chem Geol 176:51–72

Buseck PR, Clark J (1984) Zaisho – a pallasite containing pyroxene and phosphoran olivine. Mineral Mag 48:229–235

Buseck PR, Holdsworth E (1977) Phosphate minerals in pallasite meteorites. Mineral Mag 41:91–102

Chlingensperg MV (1904) Der Knochenhügel am Langacker und die vorgeschichtliche Herdstelle am Eisenbichl bei Reichenhall in Oberbayern. Mitt Anthrop Ges Wien 34:53–70

Cultrone G, Rodriguez-Navarro C, Sebastian E, Cazalla O, De La Torre MJ (2001) Carbonate and silicate phase reactions during ceramic firing. Eur J Mineral 13:621–634

Fuchs LH (1967) Stanfieldite: a new phosphate mineral from stony-iron meteorites. Science 158:910–911

Fuhrmann ML, Lindsley DL (1988) Ternary feldspar modelling and thermometry. Am Mineral 73:201–215

Gleirscher P, Nothdurfter H, Schubert E (2002) Das Rungger Egg. Röm-German Forsch, Verlag Philipp von Zabern, Mainz, 61, 264 pp

Goodrich CA (1984) Phosphoran pyroxene and olivine in silicate inclusions in natural iron-carbon alloy, Disko Island, Greenland. Geochim Cosmochim Acta 48:2769–2771

Grapes RH (1986) Melting and thermal reconstitution of pelitic xenoliths, Wehr Volcano, East Eifel, West Germany. J Petrol 27:343–396

Grapes RH (2006) Pyrometamorphism. Springer, New York, 275 pp

Grew ES, Yates MG, Beane RJ, Floss C, Gerbi C (2010) Chopinite-sarcopside solid solution, $[(Mg, Fe)_3\square](PO_4)_2$, in GRA95209, a transitional acapulcoite: implications for phosphate genesis in meteorites. Am Mineral 95:260–272

Guggenheim S, Zhan WD (1999) Crystal structures of two partially dehydrated chlorites: the modified chlorite structure. Am Mineral 84:1415–1421

Haberko K, Bućko MM, Brzezińska-Miecznik J, Haberko M, Mozgawa W, Panz T, Pyda A, Zarębski J (2006) Natural hydroxyapatite—its behaviour during heat treatment. J Eur Ceram Soc 26:537–542

Heimann R, Kreher U, Oexele J, Hirsekom V, Ullrich O, Janke D, Ullrich B, Lindner H, Wagenbreth B (1998) Archaeometallurgical investigations into the iron production technology in Upper Lusatia, Saxony, from the early Iron Age (Billendorf period) to the 12th century A.D. Eur J Mineral 10:1015–1035

Hoinkes G, Thöni M, Bernhard F, Kaindl R, Lichem C, Schweigl J, Tropper P, Cosca M (1997) Metagranitoids and associated metasediments as indicators for the pre-Alpine magmatic and metamorphic evolution of the Western Austroalpine Ötztal Basement (Kaunertal, Tirol). Schweiz Mineral Petrogr Mitt 77:299–314

Krämer W (1966) Prähistorische Brandopferplätze. Helv Antiqua Festschr Emil Vogt 111–122

Langer K, Taran MN, Fransolet AM (2006) Electronic absorption spectra of phosphate minerals with olivine-type structures: I. Members of the triphylite-lithiophilite series, $^{M1[6]}Li^{M2[6]}(Fe_{x2+}Mn_{1-x}{}^{2+})[PO_4]$. Eur J Mineral 18:337–344

Langer K, Taran MN, Fransolet AM (2007) Electronic absorption spectra of phosphate minerals with olivine-type structures: II. The oxidized minerals ferrisicklerite, $^{M1[6]}(\square_{1-x}Li_x)^{M2[6]}(Fe^{3+}{}_{1-x}Mn^{2+}{}_x)[PO_4]$, and heterosite, $^{M1[6]}(\square_{1.00})^{M2[6]}(Fe^{3+}{}_{1-x}Mn^{3+}{}_x)[PO_4]$, with $x \leq 0.5$. Eur J Mineral 19:589–592

Le Maitre RW (1974) Partially fused granite blocks from Mt. Elephant, Victoria, Australia. J Petrol 15:403–412

Maury RC, Bizouard H (1974) Melting of acid xenoliths into a basanite: an approach to the possible mechanisms of crustal contamination. Contrib Mineral Petrol 48:275–286

Moore PB (1972) Sarcopside: its atomic arrangement. Am Mineral 57:24–35

Müller G, Schuster AK, Zippert Y (1988) Spinifex textures and texture zoning in fayalite-rich slags of medieval iron-works near Schieder Village, NW-Germany. N Jb Mineral Monatsh 3:111–120

NIST (2004) Phase Equilibria Database Version 3.0

Nord AG, Kierkegaard P (1968) The crystal structure of $Mg_3(PO_4)_2$. Acta Chem Scand 22:1466–1474

Piber A (2005) The metamorphic evolution of the Austro-Alpine nappes north of the Tauern window (Innsbruck Quartzphyllite Complex – Patscherkofel Complex – Kellerjochgneiss and Wildschönau Schist). Unpublished Ph.D. Thesis, University of Innsbruck, 261 pp

Piga G, Malgosa A, Thompson TJU, Enzo S (2008) A new calibration of the XRD technique for the study of archaeological burned human remains. J Archaeol Sci 35:2171–2178

Schneider P (2009) Mineralogisch-petrologische Untersuchungen der Pyrometamorphose in Brandopferplätzen. Institut für Mineralogie und Petrographie. Unpubl MSc Thesis, University of Innsbruck, 124 pp

Schneider P, Tropper P, Kaindl R, Tomedi G (2013) The formation of P-rich olivine and stanfieldite from the pyrometamorphic breakdown of apatite in slags of a prehistoric ritual immolation site (Goldbichl, Igls, Tyrol, Austria). Mineral Petrol 107:327–340

Spielmann M (2013) Experimentelle Untersuchungen zu Knochen-Gesteinswechselwirkungen in Brandopferplätzen. Unpublished Bsc Thesis. University of Innsbruck, 59 pp

Stadler H, Leib S, Gamon T (2013) Brandopferplätze in den Alpen. Der Scheibenstuhl in Nenzing. Prearchos 3, 136 pp

Steiner H (2010) Alpine Brandopferplätze: archäologische und naturwissenschaftliche Untersuchungen. Forsch Denkmal Südtirol V, 907 pp

Tomedi G, Nicolussi Castellan S (2000) Ein bronze- und eisenzeitlicher Brandopferplatz am Goldbichl bei Igls (Bez. Innsbruck-Stadt). ArchaeoTirol Kl Schrift 2:122–123

Tropper P, Recheis A, Konzett J (2004) Experimental investigations on the pyrometamorphic formation of phosphorous-bearing olivines in partially molten metapelitic gneisses. Eur J Mineral 16:631–640

Tropper P, Konzett J, Recheis A (2006) Experimental investigations on the pyrometamorphic formation of phosphorus-bearing olivines in partially molten metapelitic gneisses. Mitt Österr Mineral Ges 152:47–56

Villieras F, Yvon J, Cases JM, De Donato P, Lhote F, Baeza R (1994) Development of microporosity in clinochlore upon heating. Clays Clay Mineral 42:679–688

Weiss RM (1997) Prähistorische Brandopferplätze in Bayern. Intern Archäologie 35, 203 pp

Radiocarbon Dating of Cremated Bones: An Overview

Mark Van Strydonck

Introduction: Radiocarbon Dating of Bones

Bones

Bones consist of an organic and an inorganic fraction. The organic fraction of a dry bone, about 30 % by weight, consists mainly of collagen fibres. These fibres are made of amino acids forming a triple helix structure and originating from the proteins in the food. It is the collagen fibres that give the bone some elasticity. Although collagen tends to deteriorate after death due to biological and chemical alteration, most archaeological bones still contain some collagen. There are different techniques to extract and purify the collagen from the bone in order to date it with the ^{14}C-method. Most of these are based on the so-called Longin method (1971). In fact, bone collagen is one of the most frequently dated sample types in archaeology. Since the carbon in the collagen derives from the proteins in the food, the ^{14}C as well as the stable isotope data (δ^{13}C) reflect those of the food protein.

The inorganic bone fraction is comprised mainly of a bone mineral composed of very small crystals of a special type of hydroxy apatite or bioapatite, a calcium phosphate with the formula $Ca_{10}(PO_4)_6(OH)_2$. An important property of the bioapatite is the possibility to occur in non-stoichiometric forms (Sillen 1989; Pate and Hutton 1988; Neuman and Neuman 1958: 41). This makes it possible for different ions present in the blood, such as CO_3^{2-}, to become incorporated in the apatite structure (Fig. 1) (Neuman and Neuman 1958: 63–64; Neuman 1980: 90; Molleson 1990: 343; Kibby and Hall 1972). This carbonate is also called structural carbonate.

The source of this carbon is the carbon dioxide dissolved in the bloodstream. The ^{14}C as well as the stable isotope data (δ^{13}C) from the bioapatite reflect the total diet

M. Van Strydonck (✉)
Royal Institute for Cultural Heritage (KIK-IRPA), Jubelpark 1, 1000 Brussels, Belgium
e-mail: mark.vanstrydonck@kikirpa.be

G. Grupe, G.C. McGlynn (eds.), *Isotopic Landscapes in Bioarchaeology*,
DOI 10.1007/978-3-662-48339-8_4

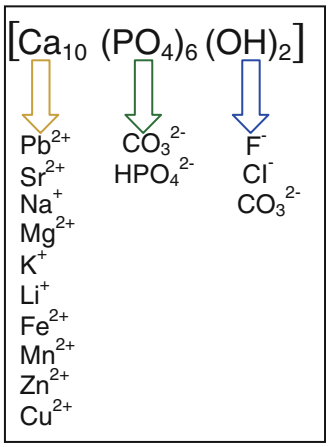

Fig. 1 Bioapatite

(proteins, hydrocarbons) of the person. Theoretically both the bioapatite carbon and the collagen carbon can be used to date a bone. Before Accelerated Mass Spectrometry (AMS) it was, however, extremely difficult to extract carbon from bioapatite because the carbon concentration is very low. Bioapatite contains about 2–4 % of carbonate by weight (McKinley 1997). The old β-counting machines used about 1 g of carbon, while the new AMS machines routinely work with about 1 mg of carbon. As a result, large amounts of bone material had to be destroyed for one measurement.

^{14}C-Dating of Bones Without Collagen

In the early days of radiocarbon dating many laboratories tried to date the bioapatite of bones without collagen. The results were, however, very disappointing (Table 1). Under burial conditions, the carbonate (CO_3^{2-}) in the bioapatite exchanges with the dissolved carbonate in groundwater over time. As such the carbon content of the bioapatite does not reflect the original radiocarbon signal anymore. Hence, apatite dating was almost completely abandoned. Between 1959 and 2009 less than 6 % of all the bone dates published in Radiocarbon were performed on purified bioapatite (Zazzo and Saliège 2011).

However, in the 1990s Saliège et al. (1995) reported successful dating of bones without collagen found in Saharan tombs. It was said that the original ^{14}C signal in the bones was preserved due to the absence of water. These results were corroborated by dates from the Cova des Pas burial cave in Menorca, Spain. Although wood and hair survived in the cave, the human skeletons no longer contained any collagen. When the necessary precautions in sample preparation were taken into consideration, valid results were obtained from the bioapatite (Van Strydonck et al. 2010a). Since then there is a somewhat renewed interest in bioapatite dating.

Table 1 Bioapatite dates performed with proportional gas counting in the 1960s at the KIK-IRPA

Site	Lab code	Dated material	^{14}C date (BP)	Archaeological date
Spy	IRPA-201	Bone apatite	23460 ± 500	Aurignacian
Spy	IRPA-202	Bone apatite	20675 ± 455	Perigordian
Spy	IRPA-203	Bone apatite	25300 ± 510	Old Aurignacian
Spiennes	IRPA-196	Bone apatite	2680 ± 150	Palaeolithic

Table 2 Some of the first results obtained by the Dutch team

Site		Lab code	^{14}C date on bioapatite (BP)	^{14}C date on associated charcoal (BP)
Anlo-Molenes		GrA-11256	2970 ± 40	2945 ± 35
Wapse 58	S	GrA-11669	2540 ± 40	2580 ± 40
	F	GrA-11671	2530 ± 40	
Eext 1967	S	GrA-11676	2230 ± 40	2345 ± 35
	F	GrA-11677	2210 ± 40	
Hijkeres		GrA-11259	1760 ± 50	1720 ± 30
Doetinchem-Dichteren 8		GrA-13387	10880 ± 50	10870 ± 50

The analyses were performed on solid bones (S) as well as on fragments (F)

The First Cremated Bone Dates

Inspired by the work of Saliège, a Dutch team made the first attempt to date cremated bones (Table 2) (Lanting and Brindley 1998; Lanting et al. 2001).

The Dutch team also stated that the dating was successful, even on bones buried in acid soils. This important remark will be discussed later. Some charcoal dates were, however, somewhat older than the cremated dates. They ascribed this to an old wood effect, another topic that will be discussed later.

The dates were corroborated by cremated dates on Urnfield sites in Belgium (De Mulder et al. 2004, 2007). Table 3 lists some results from Velzeke (Provinciebaan and Paddestraat sites) and Blicquy. One charcoal sample from the Provinciebaan was remarkably younger than the cremated bones. It was in fact Roman. The charcoal was considered to be a younger intrusion because the site was also used intensively during the Roman period. Cremated bone is indeed often a more reliable archaeological material for dating than the associated charcoal because it is the object of interest itself and not an associated find. Or phrased otherwise: 'the relation between the human event of interest and the radiocarbon event' (Van Strydonck et al. 1999) is much more direct in the case of cremated bones than in the case of charcoal.

In spite of the good results it was unclear why the bioapatite of cremated bones gave good results, while that of unburnt bones in most cases gave erroneous dates. This could only be explained by changes taking place in the bone during

Table 3 Charcoal and bone carbonate dates from the same grave

Grave no.	Charcoal (BP)	Carbonate (BP)
Paddestraat		
2	KIA-15733: 2870 ± 30	KIA-20075: 2870 ± 25
6	KIA-15703: 2790 ± 30	KIA-20200: 2785 ± 25
18	KIA-15734: 2900 ± 30	KIA-20064: 2920 ± 30
20	KIA-15735: 2780 ± 30	KIA-20201: 2825 ± 25
32	KIA-15736: 2875 ± 30	KIA-20076: 2880 ± 25
Provinciebaan		
1	KIA-15737: 1960 ± 30	KIA-20058: 2595 ± 25
6	KIA-15723: 2600 ± 30	KIA-20070: 2565 ± 25
Blicquy		
F68	KIA-23746: 3080 ± 30	KIA-23758: 3010 ± 30
F125	KIA-23745: 2945 ± 30	KIA-23757: 3110 ± 30
F127	KIA-23744: 3160 ± 40	KIA-23766: 2975 ± 30
F129	KIA-23747: 3075 ± 30	KIA-23752: 3185 ± 30

the cremation process that make them inert to carbon exchange with the environment.

Visible and Measurable Changes of the Bone Due to Heating

Visible Changes During Incineration

In the past many papers discussed the changes that take place when bones are subjected to heat. Most of them can be found in Hoefkens (2004) and references therein. What follows here is only a summary of what is important in the context of ^{14}C-dating of bones. First of all a differentiation has to be made between burnt, incinerated, and cremated bones. Burnt bones are bones that have been subject to a rather mild heat treatment, either because of the low heating temperature or a short heating time. Burnt bones are black and still contain some organic carbon originating from the partly burnt collagen and fat. Incinerated bones are white and do not contain organic carbon anymore. Grey bones must be situated in between the burnt and incinerated bones. Cremated bones are burnt or incinerated bones that have been subject to a ritual cremation. This difference in nomenclature is necessary to differentiate between for instance the animal bones found in a Mesolithic hearth and the human bones found in an Urnfield cemetery.

In the literature one can find different colour charts describing the relationship between temperature and colour. They all have their pros and cons, but in the context of radiocarbon dating it is only necessary to distinguish between burnt (black) and incinerated (white) bones as will be discussed further (Fig. 2).

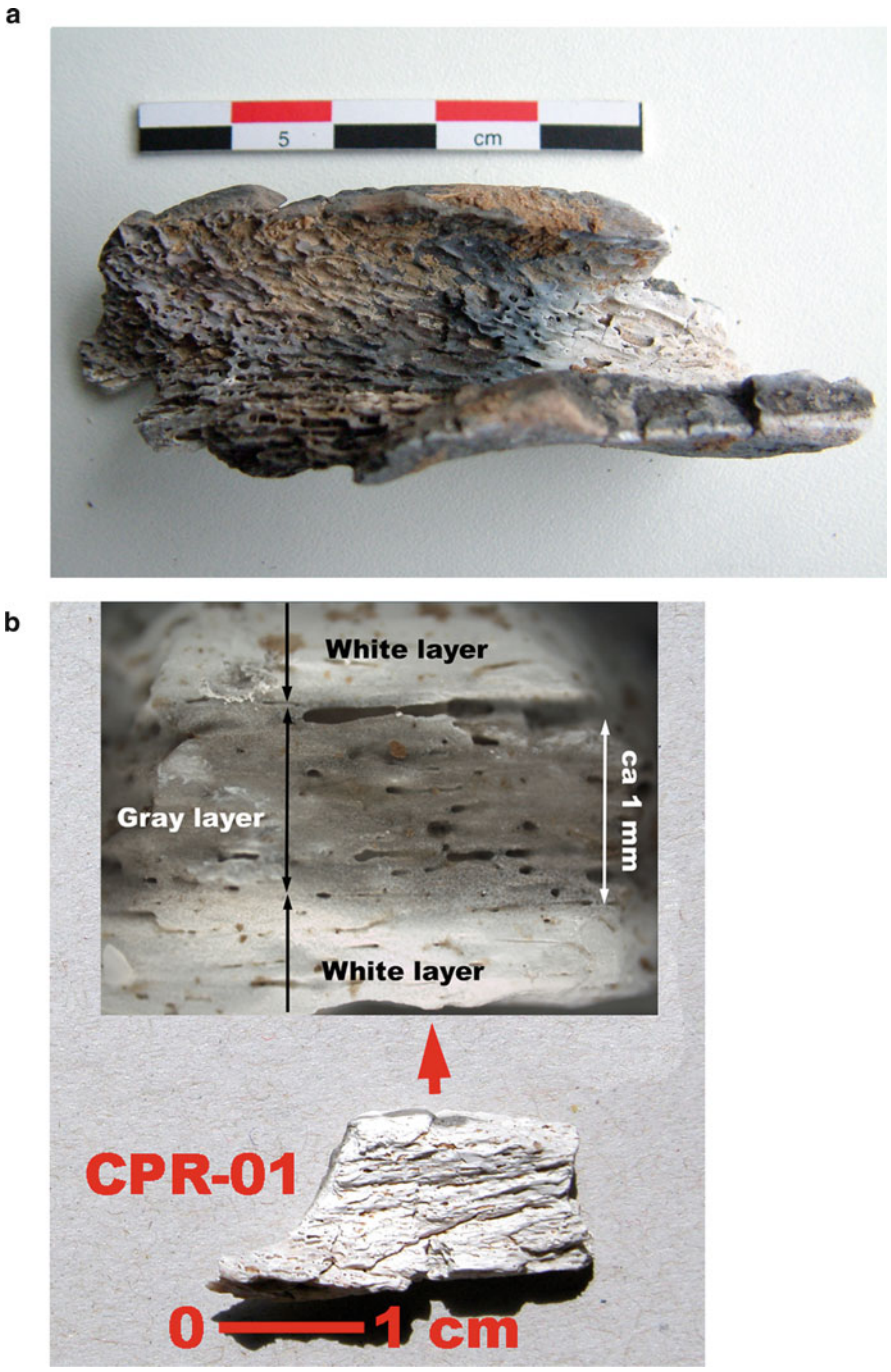

Fig. 2 (**a**) In some cases one bone shows the three stages of combustion: burnt (*black*), partly incinerated (*grey*), and incinerated (*white*). Bone from the necropolis of Can Missert (Spain). (**b**) Some bones are white on the outside, but are still *grey* on the inside because, although the

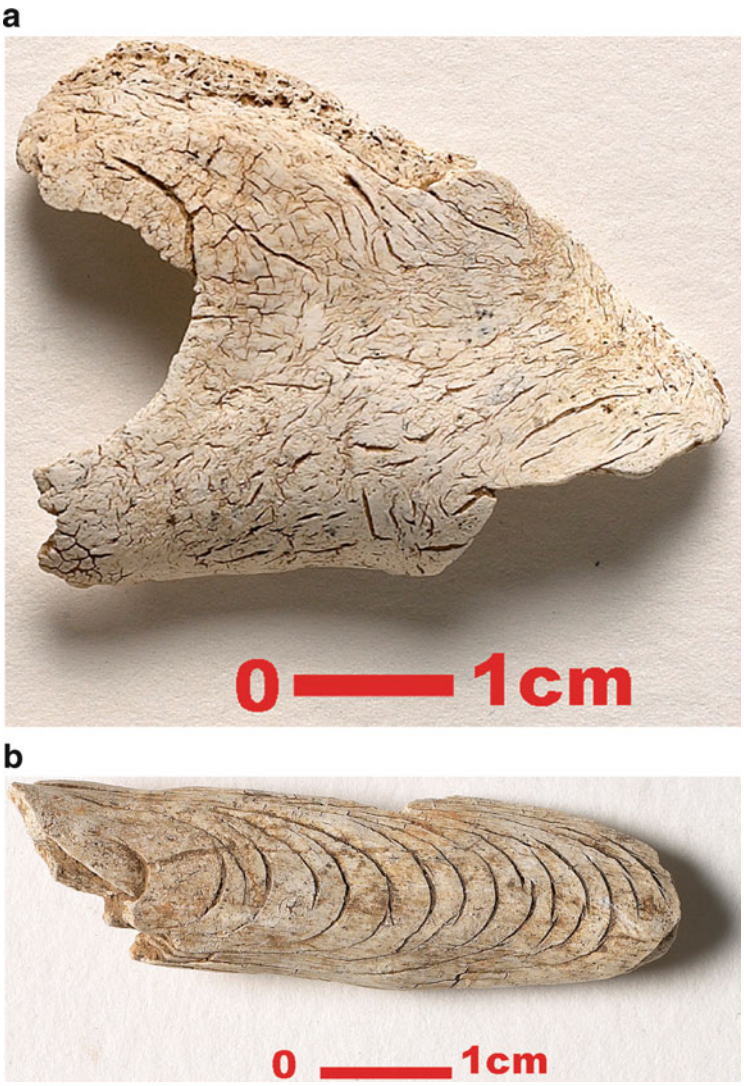

Fig. 3 The typical parched earth and U-shaped cracks (Urnfield of Velzeke, Belgium)

Typical of incinerated bones are warping, cracking, and compaction. This is due to the combustion of the organic material but also to the recrystallization of the bioapatite (Fig. 3).

Fig. 2 (continued) temperature was high enough for a complete incineration, the combustion time was too short to ensure a complete transformation of the bone (Urnfield site of Can Piteu-Can Roqueta (Sabadell, Spain)

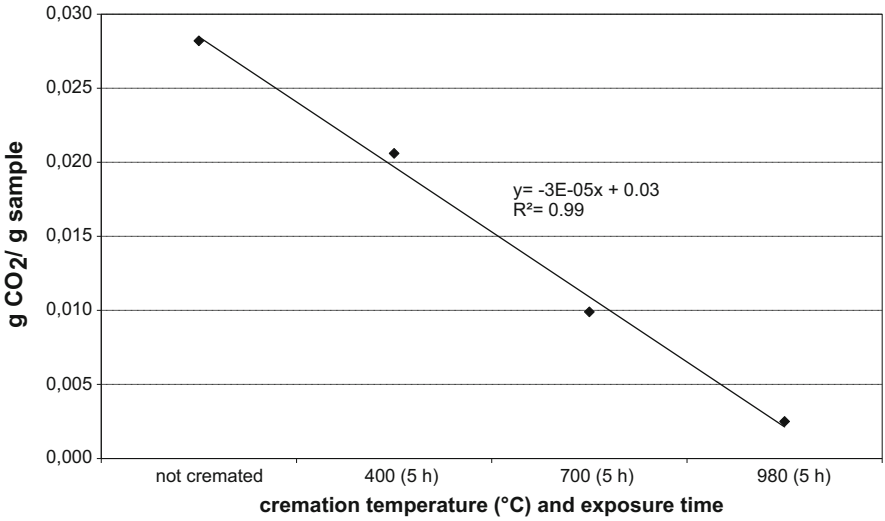

Fig. 4 The remaining carbon content of the bone is expressed as a weight ratio CO_2/bone (incinerated in an electric furnace)

Measurable Changes

Carbon Content of Incinerated Bones

Laboratory experiments have shown that the carbon content of bioapatite decreases during incineration (Van Strydonck et al. 2005) (Figs. 4 and 5). The longer the exposure time and the higher the temperature of cremation, the more the bioapatite loses its carbon. This implies that the carbon content of the cremated bones gives some information on the cremation ritual. It has been observed that even within a small geographic region there are important differences in the carbon content of cremated bones, hence showing local differences in cremation rituals (Table 4).

Stable Isotopes Measurements

The fact that the bones became depleted in ^{13}C during heating was an expected but misleading result, as will be demonstrated later.

CI and SF

In the past it was common to use the X-Ray Diffraction (XRD) Crystallinity Index (CI) to calculate and compare the degree of incineration (Shipman et al. 1984;

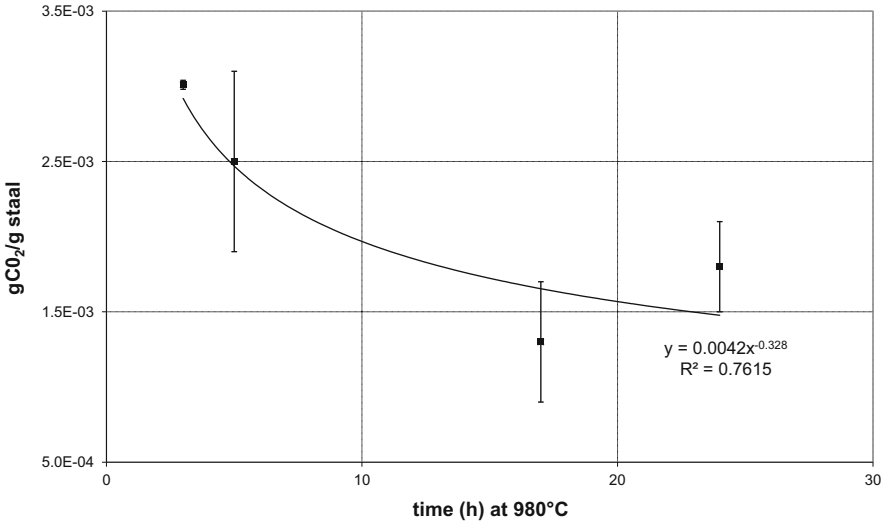

Fig. 5 The remaining carbon content of the bone is expressed as a weight ratio CO_2/bone (incinerated in an electric furnace)

Table 4 Amount of remaining structural carbonate in cremated bones from Urnfields in Belgium

Sample	C/total bone weight (‰)
Velzeke V74/C790/C5/gr12	1.72
Kontich 2006 Grave 1	1.98
Destelbergen DES67/82 Grave 35	0.3
TessenderloTE93 Grave 15	3.14

Person et al. 1995); however, it later became more common to use FT-IR (Fourier Transform Infrared Spectroscopy) Splitting Factor (SF) to obtain this information (Wright and Schwarcz 1996; Olsen et al. 2008) (Figs. 6 and 7).

According to different investigations summarized in Olsen et al. (2008), an SF of 2–2.9 represents an unburnt bone. Values between 3 and 4 represent a bone burnt at low temperature, values above four a partial recrystallization of the bone, and values above seven a complete recrystallization. Although the SF value is a good indication of the crystallinity, the information obtained is not very precise. The SF probably became more popular than the CI because other information could be

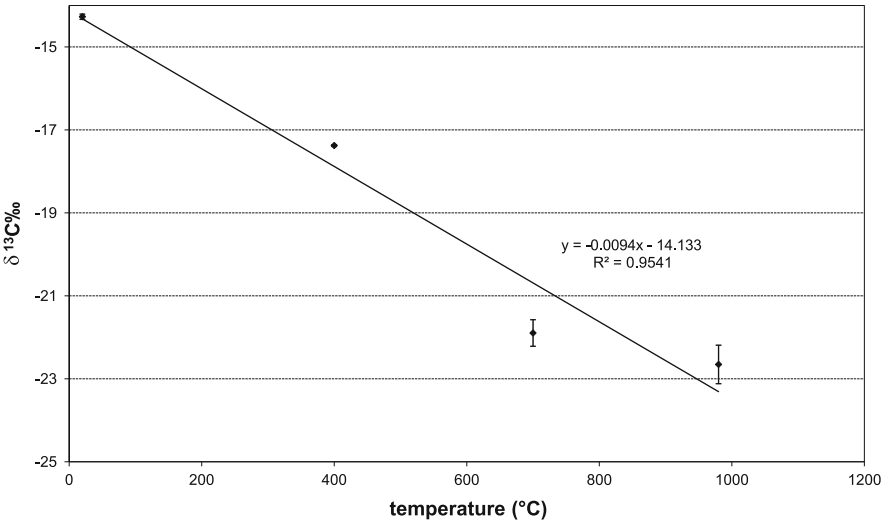

Fig. 6 Relationship between ^{13}C isotopic fractionation expressed as $\delta^{13}C$ (‰) and incineration temperature (incinerated in an electric furnace)

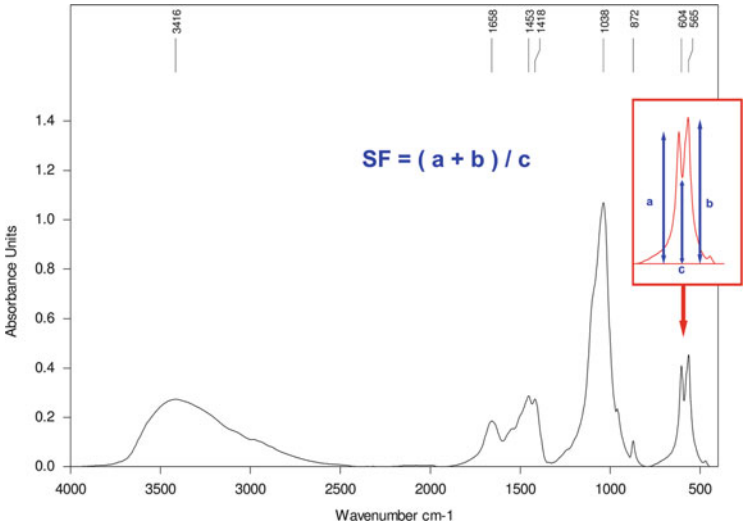

Fig. 7 The SF or Splitting Factor is defined as the sum of the peak heights $a + b$ divided by c. The higher this value the more crystalline the bone is

retrieved from this method as well (Fig. 8), such as the presence of collagen and secondary carbonate. A very distinctive small peak sometimes appears around 2013 cm^{-1}. This peak is not stable and can disappear when incineration continues past this point (Van Strydonck et al. 2013).

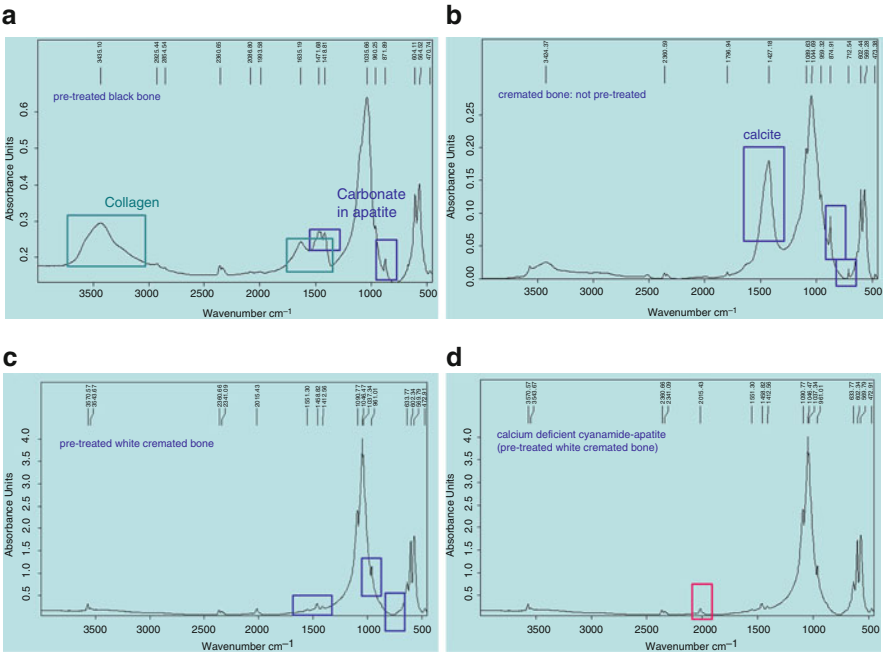

Fig. 8 (**a**) The collagen peak is still present in the burnt bone. (**b**) The calcite in the untreated bone is a secondary precipitation. (**c**) The pretreated *white* bone without secondary calcite or collagen. (**d**) The small peak probably indicates that the incinerated bone was a fresh one

Towards an Understanding of the Dating Method of Incinerated Bones

The Basic Assumption

In his early papers Lanting noted that the dating of cremated bones was also possible on bones buried in acidic soils. This was remarkable because bones normally don't survive for prolonged periods in that type of soil. So the idea was put forth that due to bone compaction and the very low concentration of carbonate remaining in the incinerated bone, it becomes very difficult for the reactive agents in the environment (soil) to reach the reactive part of the bone and to cause carbonate ion exchange. The enhanced crystallinity of the bone matrix forms a mechanical barrier and protects the remaining structural carbonate (Van Strydonck et al. 2005).

Testing the Basic Assumption

If compaction and a higher crystallinity are responsible for the protection of the structural carbonate against exchange, then (1) the surface of the bone is more vulnerable to apatite carbonate ion exchange than the inner parts of the cremated bone and (2) burnt bones are unsuitable for dating because they don't have the same compact and closed structure as incinerated bones.

In fact it could be demonstrated that in some cases the surface layer of the bone had a different apatite radiocarbon age than the inner part of the bone, showing an exchange at the surface that did not exist in deeper parts of the bone (Fig. 9).

This carbonate exchange must not be confused with a possible deposition of secondary carbonate on the bone (Fig. 8b). A secondary carbonate deposition does not react (exchange) with the apatite and can be easily removed with an acetic acid wash (Van Strydonck et al. 2009). Table 5 shows very clearly that the CO_2 released during the acetic acid wash of a well-cremated bone from Can Missert gave an erroneous and much more recent date for a Bronze Age cremation.

The assumption that burnt bones are not suitable for radiocarbon dating could be clearly proven on samples from the necropolis of Can Missert (Petit i Mendizàbal 1989). The material of the site consisted of bones that were not very well cremated (Fig. 2a). Table 6 shows that the dates on burnt bones are inconsistent with a Bronze Age burial site.

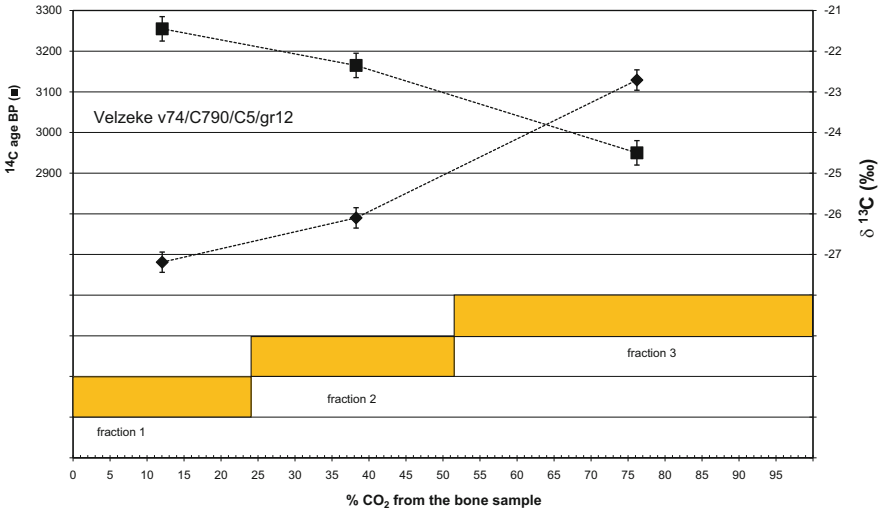

Fig. 9 Radiocarbon and stable isotope analysis of a cremated bone from the Urnfield site of Velzeke: fraction 1 is the surface (about 24.1 % of the sample); fraction 2 is the middle part (about 28.3 %); fraction 3 is the inner part of the bone (about 47.6 %)

Table 5 ^{14}C dates from CO_2 released during treatment with acetic acid and from CO_2 from the residue

Can Missert site sample MEV-3581	Lab code (KIA-)	^{14}C age (BP)	$\delta^{13}C$ (‰)
CO_2 released during acetic acid treatment (secondary carbonate deposit)	35577	960 ± 30	−9.25
CO_2 from residue (bioapatite)	35567	2815 ± 30	−17.19

Table 6 The two dates obtained on white bone material confirm each other

Sample	Degree of cremation	Lab code (KIA-)	^{14}C age (BP)
Mdt-2107	Incinerated	36268	2745 ± 25
	Burnt	36266	2330 ± 25
Mdt-2120	Incinerated	36269	2760 ± 25
	Burnt	36267	2675 ± 30
MEV-3579	Incinerated	No white parts	
	Burnt	36270	2535 ± 25

The dates on burnt bones are inconsistent with a Bronze Age burial site

Blind Testing and Inter-comparison

The good results obtained on paired samples of bone and charcoal led the radiocarbon community to organize an inter-comparative test. The aim was to prove that the dating of the same materials in different laboratories gave the same results, and they were therefore reliable (Naysmith et al. 2007). Individual laboratories also conducted blind tests (Olsen et al. 2008). All tests confirmed the reliability of the dating method, although not all of the existing problems were resolved.

The Impact of Cremation on Structural Carbonate

The previous paragraphs focused on the impact of post-depositional processes on the radiocarbon content of incinerated bones. But it is clear that the most important changes in the structure of bone do not take place after but during incineration (Munro et al. 2007). So the question was raised if carbon exchange during the incineration process could be possible. Two independent studies were set up simultaneously, one by Hüls et al. (2010) and one by Van Strydonck et al. (2010b). Both experiments were based on the same principle: fresh animal bones were incinerated in an atmosphere containing fossil CO_2 (free of ^{14}C). Should there be carbon exchange between the bioapatite and the CO_2 from the surrounding atmosphere, then the bone would show artificial ageing. The difference between both tests was primarily due to their set-up. Hüls chose a closed laboratory

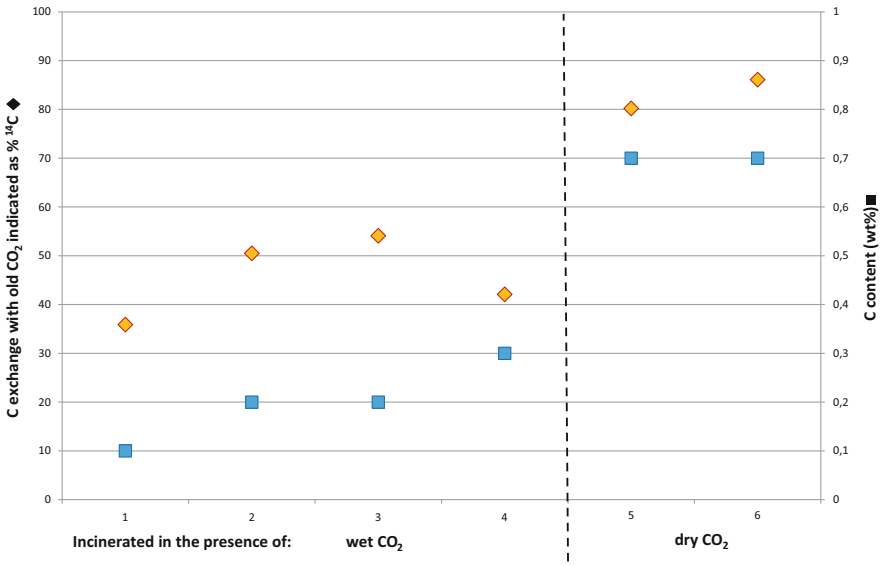

Fig. 10 Carbon content and ^{14}C signal of incinerated bones in a fossil CO_2 atmosphere (after Hüls et al. 2010)

set-up, while the author chose for a more open system that more realistically simulates a cremation pyre.

Both tests proved that during cremation there was a significant exchange of carbon between the bioapatite and the atmosphere surrounding the pyre. The closed laboratory test also showed the importance of water in the reactions. In a humid atmosphere, just like during a real cremation, a much larger depletion of carbon (ate) content could be observed (Fig. 10).

This implies that when the fuel of the pyre is composed of old wood (wood from long-living trees) or peat, the incinerated bones will suffer from a reservoir age. Unfortunately, most studies dealing with the wood used for pyres focus on the species of the wood that is used for making a pyre and not on the age of the wood. Nevertheless some authors mention that '*the gathering of wood was based rather on availability, which probably was derived from the least possible effort made during its collection. Also, this probably was a consequence of some cultural rules*' (Moskal-del Hoyo 2012). This implies that it is more probable that branch wood was used instead of trunk wood. Other people mention the use of old timber wood, branches, and even fresh wood (see Van Strydonck et al. 2010b and reference therein) to make a pyre. Ethnographic sources as well as some rare representations of ancient pyres indicate that old wood was probably not used to make a pyre (Fig. 11).

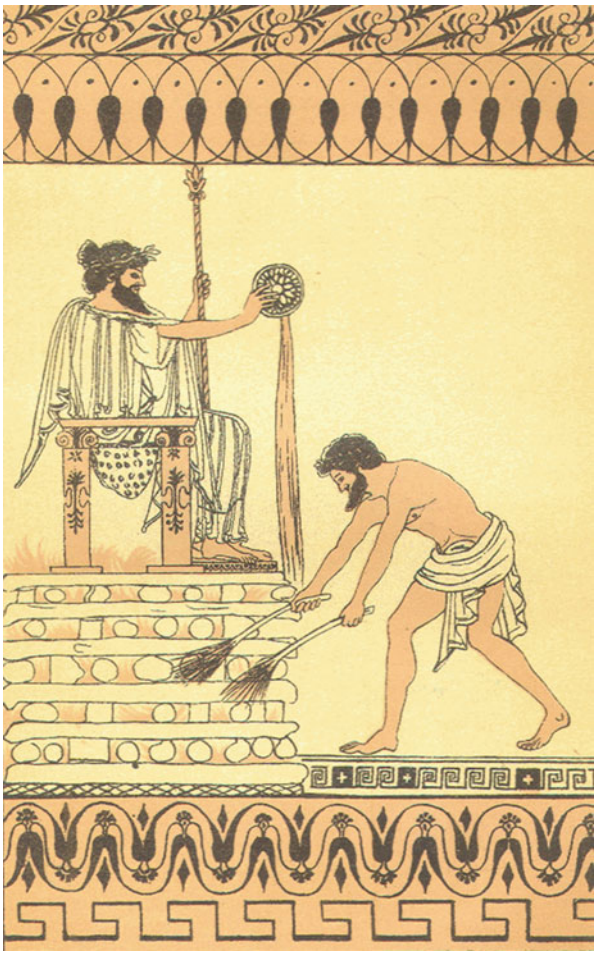

Fig. 11 King Croesus of Lydia on the funeral pyre, lit by his servant Euthymos. Attic red-figure amphora (500–490 BC) from Vulci, attributed to Myson (Louvre, Paris)

We assert that the effect of using old wood on the bone dates will not exceed the statistical uncertainty of the radiocarbon measurement and can therefore in most cases be neglected.

This is, however, not true for the stable isotope data ($\delta^{13}C$). The $\delta\ ^{13}C$ of the incinerated bone is distorted because (1) a supplementary isotopic fraction occurs when the apatite loses CO_2 and (2) the absorbed CO_2 from the pyre will have a different $\delta^{13}C$ signal than the original structural carbonate. So the $\delta^{13}C$ data of cremated bones cannot be used for dietary studies! It seems, however, that the strontium isotope signature remains intact after incineration (Harbeck et al. 2011).

Some Examples of Erroneous Results Due to Carbon Exchange During Incineration

Not All Is Wrong that Looks Wrong

The presence of aberrant radiocarbon results does not mean that they are necessarily wrong. Sometimes archaeological surprises do happen. At different Urnfield cemeteries in Belgium, for instance, Merovingian cremation remains were found. At the site of Borsbeek this could be proven by a set of radiocarbon dates (Table 7, Figs. 12 and 13) (De Mulder et al. 2012).

It seems that the Merovingian people were attracted by the Bronze Age burial sites.

This example shows that archaeologists must always keep in mind that a routine radiocarbon analysis does not exist and that every result must be evaluated taking into account the archaeological reality of the site. Environmental conditions as well as the physical and chemical changes are also important. This is demonstrated in the following two examples.

The Balearic (Spain) Quicklime Burials

In the Balearic Iron Age a very particular burial practice came in use. The bodies of the deceased were not simply cremated on a wooden pyre; rather prior to cremation they were covered (in an as yet unknown manner) with a layer of very finely crushed limestone powder (Van Strydonck 2014). During incineration the heat of the pyre transforms the limestone into quicklime. After the pyre was extinguished, the remaining charcoal was washed out and the incinerated bones and quicklime were deposited at the burial site. After some time the quicklime sets due to a

Table 7 ^{14}C results on cremated bones from the cremation graves at Borsbeek (Belgium)

Grave no.	Lab code	^{14}C age (BP)	Period
1	KIA-37896	2865 ± 35	Bronze Age
	KIA-38428	2855 ± 30	Bronze Age
2	KIA-37916	2670 ± 35	Late Bronze Age
3	KIA-37919	2805 ± 35	Bronze Age
4	KIA-37917	1460 ± 35	Merovingian
	KIA-40552	1465 ± 30	Merovingian
5	KIA-37897	2895 ± 40	Bronze Age
6	KIA-37898	2825 ± 30	Bronze Age
7	KIA-37920	2825 ± 40	Bronze Age
8	KIA-37903	2865 ± 35	Bronze Age
12	KIA-37904	1520 ± 30	Merovingian
14	KIA-37905	1580 ± 30	Merovingian
26	KIA-37921	2595 ± 40	Iron Age

Fig. 12 Urn with cremated bones from Borsbeek

reaction with atmospheric CO_2. This makes the lime burial look like a massive block of lime full of fragmented and disorderly deposited cremated bones (Fig. 14).

Due to the decomposition of the limestone powder by the heat of the pyre, fossil CO_2 is released into the pyre's atmosphere. This fossil and infinitely old CO_2 are partly incorporated into the bioapatite of the bone. This results in an artificial date of the bone. It was proven that the better the bones were incinerated (higher SF), the more the date deviated from the expected age because more fossil carbon was incorporated in the cremated bone (Fig. 15) (Van Strydonck et al. 2013).

Yuma Wash Cemetery

The archaeological site of Yuma Wash is located just above the floodplain of the Santa Cruz River in Marana, Arizona. The site dates from approximately AD 1100–1450 during the Hohokam Classic Period (Cerezo-Roman and McClelland 2009). The area where the site is located is suitable for farming, and Yuma Wash is one of several large sites in the area. At Yuma Wash a total of 37 burials from the Classic Period were recovered. Both cremation and inhumation were practised, and the interments were found in several clusters and as isolates on the site.

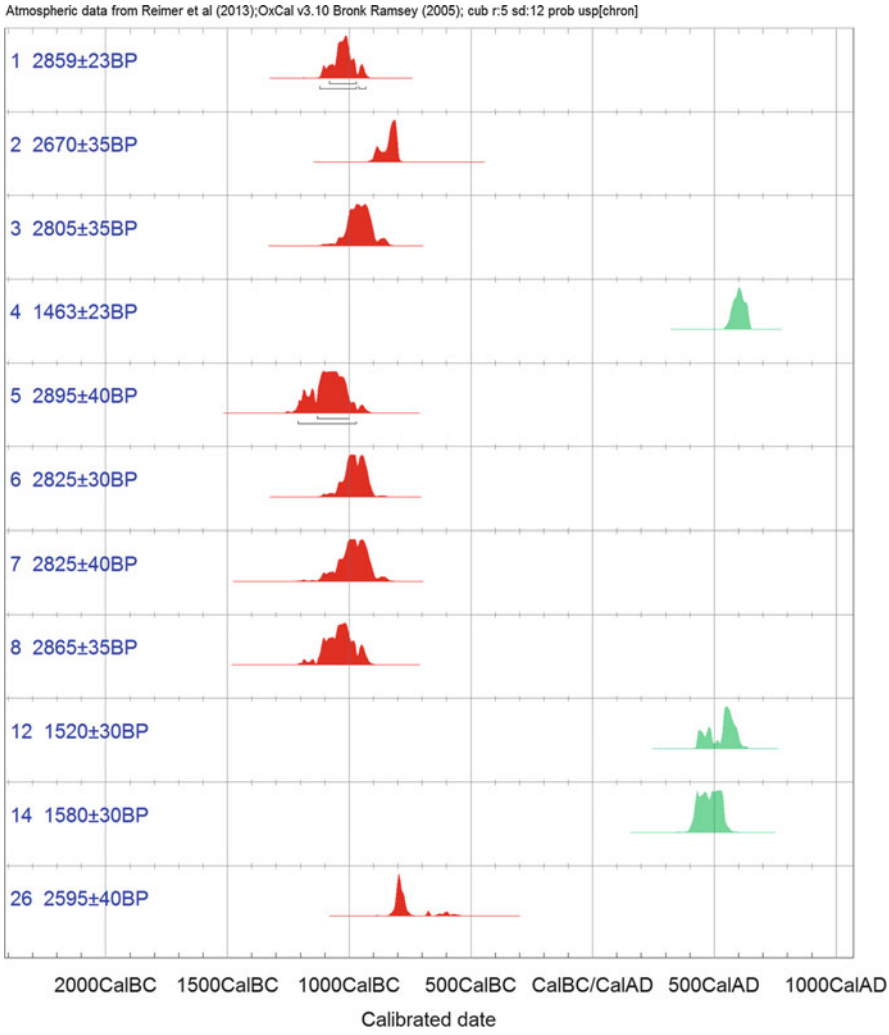

Fig. 13 Calibrated radiocarbon dates from Borsbeek

The differences in age between the cremated bones and the charcoal from the burials were enigmatic. Sometimes the cremated bones are older than the charcoal, sometimes the situation is reversed (Fig. 16 and Table 8). There is, however, a straightforward explanation.

Wood from the Sonoran Desert in Arizona such as ironwood (*Olneya tesota*) and mesquite (*Prosopis* spp.) is very hard and highly resistant to insect damage. Furthermore, fungal activity on dead wood is limited due to small amounts of precipitation and low humidity. As such, old wood is readily available in the Sonora Desert to build fires or construct pyres. Even the remains of the less resistant palo

Fig. 14 (**a**) Cova de Sa Prior (Binigaus, Es Migjorn Gran, Menorca, Spain). The lime burial is situated at the cave entrance. (**b**) A lime lump from the Cova de Sa Prior; the cremated bones are embedded in the lime

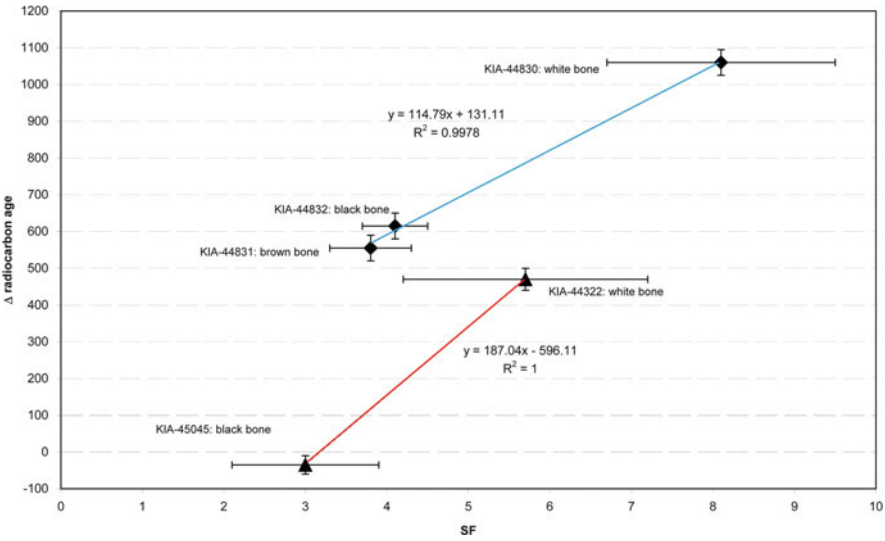

Fig. 15 The SF as a proxy for the degree of incineration in function of the difference between accepted radiocarbon age and the measured radiocarbon age of cremated bones from two locations within the Son Matge lime burial (Valldemossa, Mallorca, Spain)

verde tree (*Cercidium* spp.) can survive in the drier parts of the desert (Schiffer 1986).

The carbon in the cremated bones is composed of carbon from the bioapatite itself and of carbon from the pyre's surrounding atmosphere. The carbon in the pyre's atmosphere is a mixture of all carbon sources in the pyre and the carbon from the body. If the pyre is composed of a mixture of old wood from the desert floor and green wood harvested for the cremation ritual, then the ^{14}C content of the bioapatite

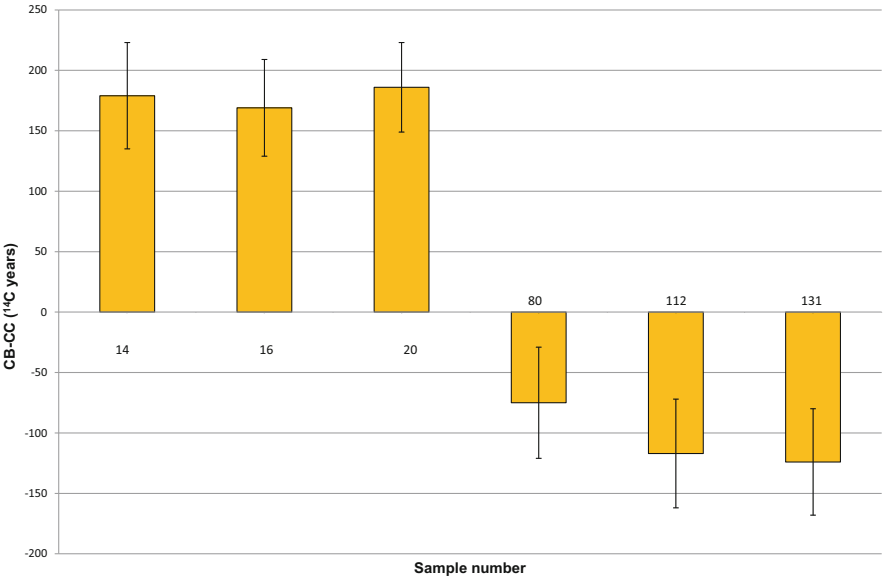

Fig. 16 The difference between the ^{14}C-age of cremated bone (CB) and of the charcoal (CC) from the same grave

Table 8 ^{14}C dates from charcoal and cremated bone from the same grave

Sample (grave)	Cremated bone date (BP)	Charcoal date (BP)	Difference
14	962 ± 35	1141 ± 26	179 ± 44
16	917 ± 28	1086 ± 28	169 ± 40
20	988 ± 25	1174 ± 27	186 ± 37
80	1045 ± 18	970 ± 42	-75 ± 46
112	1074 ± 35	957 ± 28	-117 ± 45
131	1099 ± 35	975 ± 26	-124 ± 44

will be in between the ^{14}C content of the old wood and the ^{14}C content of the green wood, in fact, a weighed mean of all sources. Only one piece of charcoal is needed for the radiocarbon analysis (single entity dating). The radiocarbon date of that piece either reflects the age of the freshly cut green wood or the age of the old wood from the desert.

Conclusions

Well-cremated bones are a valuable material for the radiocarbon dating method. Burnt bones on the other hand cannot be dated by radiocarbon because of carbon exchange between the bioapatite and the environment. In most cases it is better to

date the cremated bones than the charcoal found in their vicinity because there is a more direct relationship between the dated material and the archaeological event of interest. It is strongly suggested that a thorough evaluation of the sample's origin and taphonomy is made before submitting it for dating as is the case for all samples submitted for dating.

References

Cerezo-Roman JI, McClelland JA (2009) Mortuary practices at Yuma Wash and the Hohokam Classic World. In: MacWilliams C, Dart A (eds) Archaeological investigations at five sites west of the Santa Cruz River in Marana, Arizona, vol 1. Old Pueblo Archaeology Center, Tucson, pp 1–22

De Mulder G, Van Strydonck M, Boudin M (2004) ^{14}C-dateringen op gecremeerde menselijk botten uit de urnenvelden te Velzeke (O.-Vl.). Lunula 12:51–58

De Mulder G, Van Strydonck M, Boudin M, Leclercq W, Paridaens N, Warmenbol E (2007) Re-evaluation of the late bronze age and early iron age chronology of the Western Belgian Urnfields based on ^{14}C dating of cremated bones. Radiocarbon 49:499–514

De Mulder G, Van Strydonck M, Annaert R, Boudin M (2012) A Merovingian surprise: early medieval radiocarbon dates on cremated bone (Borsbeek, Belgium). Radiocarbon 54:581–588

Harbeck M, Schleuder R, Schneider J, Wiechmann I, Schmahl WW, Grupe G (2011) Research potential and limitations of trace analyses of cremated remains. Forensic Sci Int 204:191–200

Hoefkens M (2004) Onderzoek naar de dateerbaar-heid van gecremeerde botten met ^{14}C. Eindewerk voor het behalen van de graad en het diploma van Industrieel Ingenieur, De Nayer Instituut, St.-Katelijne Waver, p 92

Hüls CM, Erlenkeuser H, Grootes PM, Andersen N (2010) Experimental study on the origin of cremated bone apatite carbon. Radiocarbon 52:587–599

Kibby CL, Hall WK (1972) Surface properties of calcium phosphates. In: Hair ML (ed) The chemistry of biosurfaces, vol 2. Dekker, New York, pp 686–727

Lanting JN, Brindley AL (1998) Dating cremated bone: the dawn of a new era. J Irish Archaeol 9:1–7

Lanting JN, Aerts-Bijma AT, van der Plicht J (2001) Dating cremated bone. Radiocarbon 43:249–254

Longin R (1971) New method of collagen extraction for radiocarbon analysis. Nature 230:241–242

MCKinley JI (1997) The cremated human bone from burials and cremation-related contexts. In: Fitzpatrick AP (ed) The iron age, Romano-British and Anglo-Saxon cemeteries excavated in 1992, vol 12. Trust for Wessex Archaeology, Salisbury, pp 55–72

Molleson T (1990) The accumulation of trace metals during fossilization. In: Priest ND, Vandevyver FL (eds) Trace metals and fluoride in bones and teeth. CRC Press, Boca Raton, FL, pp 341–365

Moskal-del Hoyo M (2012) The use of wood in funerary pyres: random gathering or special selection of species? Case study of three necropolises from Poland. J Archaeol Sci 39:3386–3395

Munro LE, Longstaffe FJ, White CD (2007) Burning and boiling of modern deer bone: effects on crystallinity and oxygen isotope composition of bioapatite phosphate. Palaeogeogr Palaeoclimatol Palaeoecol 249:90–102

Naysmith P, Scott EM, Cook GT, Heinemeier J, van der Plicht J, Van Strydonck M, Bronk Ramsey C, Grootes PM, Freeman SPHT (2007) A cremated bone intercomparison study. Radiocarbon 49:403–408

Neuman WF (1980) Bone mineral and calcification mechanisms. In: Urist MR (ed) Fundamental and clinical bone physiology. JB Lippincott, Philadelphia, pp 83–107
Neuman WF, Neuman NW (1958) The chemical dynamics of bone mineral. University of Chicago Press, Chicago, p 209
Olsen J, Heinemeier J, Bennike P, Krause C, Hornstrup KM, Thrane H (2008) Characterisation and blind testing of radiocarbon dating of cremated bone. J Archaeol Sci 35:791–800
Pate FP, Hutton JT (1988) The use of soil chemistry data to address post-mortem diagenesis in bone mineral. J Archaeol Sci 15:729–739
Person A, Bocherens H, Saliège J-F, Paris F, Zeitoun V, Gérard M (1995) Early diagenetic evolution of bone phosphate: an X-ray diffractometry analysis. J Archaeol Sci 22:211–221
Petit i Mendizàbal ÀM (1989) Can Missert, una necropolis del Bronze Final al Vallès. Terme 4:7–11
Saliège J-F, Person A, Paris F (1995) Preservation of $^{13}C/^{12}C$ original ratio and ^{14}C dating of mineral fraction of human bones from Saharan tombs, Niger. J Archaeol Sci 22:301–312
Schiffer MB (1986) Radiocarbon dating and the "old wood" problem: the case of the Hohokam chronology. J Archaeol Sci 13:13–30
Shipman P, Foster GF, Schoeninger M (1984) Burnt bones and teeth: an experimental study of colour, morphology, crystal structure and shrinkage. J Archaeol Sci 11:307–325
Sillen A (1989) Diagenesis of the inorganic phase of cortical bone. In: Price TD (ed) The chemistry of prehistoric bone. Cambridge University Press, Cambridge, MA, pp 211–229
Van Strydonck M (2014) From Myotragus to Metellus, a journey through the pre- and early-history of Majorca and Minorca. Librum, Hochwald (Switzerland, p 160
Van Strydonck M, Nelson DE, Crombé P, Bronk Ramsey C, Scott E M, van der Plicht J, Hedges REM (1999) What's in a ^{14}C date. In: Evin J, Oberlin C, Daugas J-P, Salles J-F (eds) 3rd International symposium ^{14}C and archaeology, Mémoires de la Société Préhistorique Française 26, Supplément de la Revue d'Archéométrie, pp 433–448
Van Strydonck M, Boudin M, Hoefkens M, De Mulder G (2005) ^{14}C-dating of cremated bones, why does it work? Lunula 13:3–10
Van Strydonck M, Boudin M, De Mulder G (2009) ^{14}C dating of cremated bones: the issue of sample contamination. Radiocarbon 51:553–568
Van Strydonck M, Boudin M, Guerrero-Ayuso VM, Calvo M, Fullola JM, Àngeles Petit M (2010a) The necessity of sample quality assessment in ^{14}C AMS dating: the case of Cova des Pas (Menorca–Spain). Nucl Instr Meth Phys Res B 268:990–994
Van Strydonck M, Boudin M, De Mulder G (2010b) The origin of the carbon in bone apatite of cremated bones. Radiocarbon 52:578–586
Van Strydonck M, Decq L, Van den Brande T, Boudin M, Ramis D, Borms H, De Mulder G (2013) Int J Osteoarch. doi:10.1002/oa.2307
Wright LE, Schwarcz HP (1996) Infrared and isotopic evidence for diagenesis of bone apatite at Dos Pilas, Guatemala: palaeodietary implications. J Archaeol Sci 23:933–944
Zazzo A, Saliège J-F (2011) Radiocarbon dating of biological apatites: a review. Palaeogeogr Palaeoclimatol Palaeoecol 310:52–61

Mineralogic Characterisation of Archaeological Bone

Wolfgang W. Schmahl, Balazs Kocsis, Anita Toncala, and Gisela Grupe

Introduction

The interpretation of isotopic or microchemical data obtained from archaeological bone relies on the assumption that the analysed material is—at least chemically—the original, unaltered, and uncontaminated material that it was at the time of the death of the individual. Thus, the current *Forschergruppe* FOR1670 (www.for1650-transalpine.uni-muenchen.de) project on human transalpine mobility in the late Bronze Age to Early Roman times screens the archaeological bone finds selected for isotope studies by a mineralogical analysis based on X-ray diffraction (XRD).

The Bone Mineral

The mineral substance of mammal bone is a nanocrystalline carbonated hydroxyapatite with a composition which can be approximated as $Ca_{10}(PO_4, CO_3)_6$ (OH, $CO_3)_2$ (Lowenstam and Weiner 1989; Nielsen-Marsh et al. 2000). The total carbonate content substituted on the hydroxyl sites (type A substitution) and the phosphate sites (type B substitution) is in the order of 7 wt% in total. Pasteris et al. (2004) conclude from Raman spectroscopy that bone apatite is not hydroxylated and therefore not hydroxylapatite. The two different variants of $[CO_3]^{2-}$ substitution

W.W. Schmahl (✉) • B. Kocsis
Sektion Kristallographie, Ludwig-Maximilians-Universität München, Theresienstrasse 41, 80333 Munich, Germany
e-mail: Wolfgang.Schmahl@lrz.uni-muenchen.de

A. Toncala • G. Grupe
Ludwig-Maximilians-Universität München, Biozentrum, Grosshaderner Str.2, 82152 Martinsried, Germany

G. Grupe, G.C. McGlynn (eds.), *Isotopic Landscapes in Bioarchaeology*,
DOI 10.1007/978-3-662-48339-8_5

in the crystal structure (type A $[CO_3]^{2-} \leftrightarrow [PO_4]^{3-}$, type B $[CO_3]^{2-} \leftrightarrow [OH]^{-}$) can be distinguished by FTIR spectroscopy (Wopenka and Pasteris 2005). Numerous types of coupled exchange to maintain charge balance can be envisaged (Wopenka and Pasteris 2005; de Leeuw 2010). There are small amounts of F^{-} replacing OH^{-}, and on the cation position Na^{+} and Mg^{2+} can be substituted as well as traces of Sr^{2+} and Ba^{2+} (e.g. Elliot 2002; Turner-Walker 2008). Sponheimer et al. (2005) report that herbivore bones show higher levels of Sr^{2+} und Ba^{2+} than carnivores and omnivores. The bone mineral is sometimes addressed with the mineral name Dahllite as the F-content is less than 1 %. We refer to the material as bioapatite for brevity. Jäger et al. (2006) and Wang et al. (2013) interpret their nuclear magnetic resonance data as indicating an amorphous surface layer of water-bearing carbonated Ca-phosphate [amorphous calcium carbonate (ACC)] which coats a crystalline bioapatite nanoparticle core. The nanoscale mineral particles form—beginning right from the supramolecular scale—an intimate hierarchical hybrid composite with collagen and other organic/cellular components (Weiner et al. 1999). The nanoscale fabric of collagen and bioapatite stabilises each of these components against chemical decomposition or biochemical attack, as long as the composite structure is intact (Gernaey et al. 2001; Turner-Walker 2008). In the course of *post-mortem* bacterial decomposition of the organic components (amounting to about 30 wt% of the bone) a high porosity and internal surface is created in the remaining mineral substance. This structure promotes adsorption processes of ions and molecules from the surrounding soil. Furthermore, the high internal surface provides a substrate for heterogeneous nucleation of secondary minerals. Both the high surface/interface energy of the nanoparticles and the structural misfit of the carbonate substituted into the crystal structure provide an increase of free energy and thus an increased solubility of the bioapatite compared to inorganic hydroxyapatite (Hedges 2002; Berna et al. 2004; Wopenka and Pasteris 2005; de Leeuw 2010). In vivo this feature is of key importance in the continual physiologic reconstruction of the bone. During diagenesis the increased free energy provides a driving force for recrystallisation and formation of larger crystals. In the course of these diagenetic processes, the bone tends to incorporate secondary minerals (newly grown, secondary apatite and e.g. calcite, $CaCO_3$) and those incorporate ions such as Sr^{2+}, Pb^{2+}, etc., from the soil (Tütken et al. 2008), which change the original Sr^{2+} and Pb^{2+} signatures of the bone.

In their classic work Person et al. (1995) defined the "crystallinity index" (CI) to characterise the recrystallisation of apatite in early diagenesis on the basis of the width of XRD lines. This index number later achieved great popularity (Hedges 2002). Another popular alternative index number is the infrared splitting factor (IRSF) by Weiner et al. (1993); see also e.g. Surovell and Stiner (2001). Lebon et al. (2008) suggested procedures to make the IRSF more quantitative based on curve fitting of the relevant part of the infrared spectrum with a larger number of distinct peaks. Vandecandelaere et al. (2012) and Grunenwald et al. (2014) suggested improved curve-fitting methods. A more rigorous basis of spectroscopic properties of hydroxyapatite and carbonated hydroxyapatite was provided by Pedone et al. (2007) and Yi et al. (2014) on phosphate and carbonate vibrations, respectively. According to Shinomiyaa et al. (1998) chemical alterations were indicated by the IRSF already a

few years *post mortem* while Trueman et al. (2008) shed doubts on the quantitative use of this index. The assessment of this simplified index (IRSF) describing complex spectral features is debated in the literature (Sillen 1989; Shemesh 1990; Weiner and Bar-Yosef 1990; Wright and Schwarcz 1996; Trueman et al. 2008; Tütken et al. 2008). Sample preparation for XRD or FTIR measurement certainly has an influence on the CI/IRSF results (Surovell and Stiner 2001). The simplifying indices for a "crystallinity" of the bone mineral do not correlate with modifications of chemical composition and also not with stable isotope data of the structural carbonate (e.g. Lee-Thorp and Sponheimer 2003; Pucéat et al. 2004; Trueman et al. 2008; Tütken et al. 2008). Moreover, physiological differences in bioapatite characteristics between different species, different skeletal elements, and different age groups of the population can be expected and need to be considered in the future (Rey et al. 1991, 2009; Yerramshetty and Akkus 2008).

X-ray Diffraction

In modern materials science X-ray (or electron) diffraction—together with microscopy—are the obligatory methods to identify the structural state of a crystalline material. Crystals are objects with a spatially periodic arrangement of the constituting ions, atoms, or molecules. Their basic structural element is a unit cell (Fig. 1)

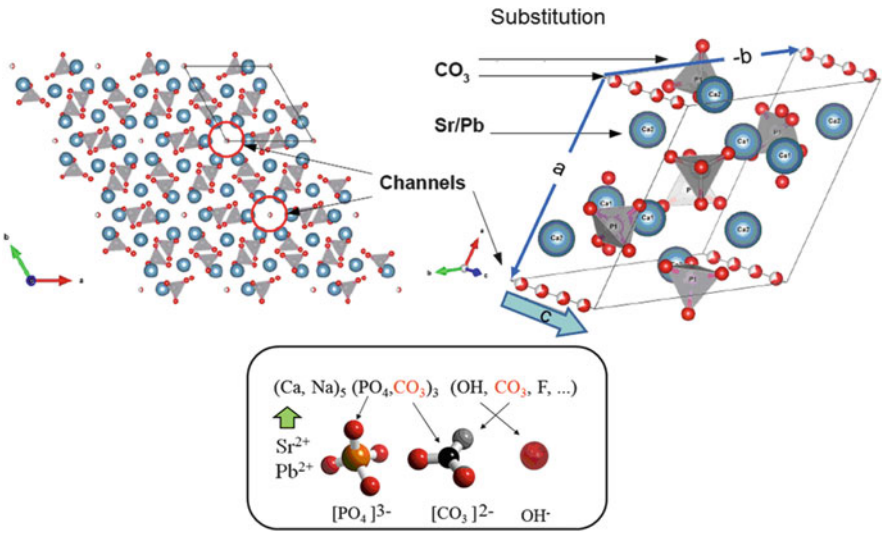

Fig. 1 *Left*: Projection of the crystal structure of apatite along the *c*-axis. The unit cell is outlined with a *thin black line*. *Blue*: Ca^{2+}-ions, *red*: O^{2-} ions, *purple*: tetrahedral coordination polyhedral of four oxygens around a central P^{5+} ion, OH^{-} is located in the channels. *Right*: perspective view of the contents of the unit cell. *Bottom*: Schematic indicating ionic substitutions in the bioapatite structure

which is periodically repeated to fill space. The XRD technique takes advantage of this periodic lattice-like structure. The interference of the electromagnetic X-ray waves scattered from a crystal gives rise to a pattern of sharp diffraction peaks. The positions of the peaks are defined by the distances between crystallographic lattice planes which are directly related to the unit cell dimensions. The peak intensities are related to the positions and electron densities of the atoms in the unit cell. Amorphous substances do not have a periodic structure; their diffraction pattern consists of diffuse halos with maxima related to the electron densities and average distances of the constituting atoms. In any case, amorphous, crystalline, or "in between", the diffraction signal is the Fourier transform of the electron density self-correlation function, which is straightforward to calculate:

$$I(\vec{H}) = S\ g\sum_{j=1}^{N}\sum_{l=1}^{N} f_j f_l \quad \exp\left[2\pi i\left(\vec{H}\times\left(\vec{x}_j - \vec{x}_l\right)\right)\right] \tag{1}$$

Here, $\vec{H}$ is the diffraction vector, the sums over j and l include all atoms contributing to the interference signal, $\vec{x}_j$ and $\vec{x}_l$ are the positions of two atoms which scatter the radiation with an amplitude f_j and f_l (Fourier transforms of the electron densities of the individual atoms), respectively, g is a geometric factor, and S is an overall scale factor. In the case of a crystal, for those diffraction vectors which match the periodicity of the lattice, there is constructive interference (high intensity) for the waves scattered from each unit cell, while for all other wave vectors the interfering waves have a more or less random phase difference and essentially cancel out. Thus, strong, sharp diffraction peaks occur for scattering vectors $\vec{H}$ corresponding to normal vectors of lattice planes with coordinates (Miller indices) hkl and with modulus $\left|\vec{H}\right| = 1/d_{\mathrm{hkl}}$, where d_{hkl} is the corresponding lattice plane spacing. Accordingly, the strong diffraction signal directly probes the long-range order of the periodic structure over about a micrometer, while a much weaker signal comes from deviations from this long-range order. For details the books of Pecharsky and Zavalij (2003) and Mittemeijer and Welzel (2012) provide a good basis. For the "in between" case there are two contributions which broaden the sharp maxima that a well-developed "ideal" crystal would have: the limited size of the crystal (the number of periodically repeated unit cells encountered) and the variation of the size or shape of the unit cell arising from an inhomogeneous distribution of chemical constituents or local mechanical strains. The latter effect is termed "microstrain".

A limited size $D(\vec{H})$ along $\vec{H}$ of a coherently diffracting crystal lattice broadens the XRD lines as a function of scattering angle (Bragg angle) θ with a Lorentzian peak shape contribution of width (integral breadth β; de Keijser et al. 1982):

$$\beta(2\theta) = \frac{\lambda}{D(\vec{H})} \frac{1}{\cos(\theta)} \tag{2}$$

The Lorentzian shape results from the Fourier transform of the limited number of lattice planes contributing to the interference. The lattice parameter variations of mean-square magnitude $\overline{\epsilon}(\vec{H})$ in the direction of $\vec{H}$ broaden the lines as

$$\beta(2\theta) = 4\overline{\epsilon}(\vec{H}) \tan(\theta) \tag{3}$$

If the random variation of the lattice parameters across the sample is assumed to be Gaussian, this peak broadening is of a Gaussian shape. Thus, the size effect and the strain effect can be separated due to the peak shape and the dependence on scattering angle. According to the dependence of D and $\overline{\epsilon}$ on the direction of $\vec{H}$, Rogers et al. (2010) pointed out that different diffraction peaks of bioapatite show different breadths according to the anisotropic, plate-like shape of the bioapatite crystallites.

Experimentally, the strain and size broadening effects are convoluted with the peak shape due to the instrumental resolution, which is also a function of θ. The instrumental resolution can be calculated from the geometry of the X-ray optical elements of the diffractometer, and/or confirmed with a suitable standard material of high crystalline quality, such as the National Institute of Standards and Technology (NIST) reference material LaB_6 660a.

For a polycrystalline material the peak shape function describing the measured intensity at diffraction angle 2θ due to an XRD peak at position $2\theta(\vec{H})$, $x = 2\theta - 2\theta(\vec{H})$ becomes

$$I_{\vec{H}}(x) = \{r(\theta) \otimes s(x) \otimes e(x)\} M(\theta) \left[F^*(\vec{H}) F(\vec{H})\right] \tag{4}$$

where $\otimes$ stands for convolution of the instrumental resolution $r(\theta)$, size $s(x)$, and microstrain $e(x)$ peak shape functions, $M(\theta)$ is a geometrical factor describing various characteristics of the experimental set-up, and $F(\vec{H})$ is the Fourier Transform of the electron density distribution in the unit cell as given by the average distribution of the atoms, the so-called structure factor.

The complete diffractogram is the superposition of a background signal B and all contributing peaks of all crystalline phases in the sample

$$I(2\theta) = B(2\theta) + S \sum_{\text{Phases}\ p} X_p \left[\sum_{\text{Reflections}\ H\,p} I_{\vec{H},\,p}(2\theta - 2\theta(\vec{H}_p)) \right] \tag{5}$$

where X_p is the fraction of phase p in the sample and S is an overall scale factor. Contributions of amorphous phases to a diffractogram are much weaker in signal than the diffraction peaks of the crystalline phases. However, they potentially show up in the difference between the measured and the calculated diffractogram (if care

is taken in the description of the background). Contributions of amorphous phase can be added as well, using essentially the Fourier transform of the electron density self-correlation function (Eq. 1).

In this way, modern XRD analysis is based on a rigorously calculated model with parameters which are adapted to the observed diffraction profile by a least-squared refinement algorithm (so-called Rietveld refinement method, Rodriguez-Carvajal 1993; Rodriguez-Carvajal and Roisnel 2004; Pecharsky and Zavalij 2003; Mittemeijer and Welzel 2012).

Modern development of quantitative XRD led to analyses of the diffraction profile to assess the crystallographic characteristics of archaeological and paleontological bone materials (Stathopoulou et al 2008; Piga et al. 2008, 2009a, b, 2013; Harbeck et al. 2011). The term "crystallinity" and therefore the classical CI are not rigorous, since the width of the diffraction peaks depends both on the coherence length of periodic lattice order along the diffraction vector (i.e. in the simplest case the crystallite size) and on the variance of the lattice parameters ("microstrain") in the sample. Microstrain results from inhomogeneities in chemical composition, lattice defects, and mechanical strains on the scale of the crystallite size. In the case of bone such mechanical stresses can result from the composite structure with collagen.

Stathopoulou et al. (2008) investigated Miocene and Pleistocene samples from the Aegean with the Rietveld method and concluded that "*Diagenetic trends, common to all these sites include a subtle but systematic decrease of the unit cell volume and a-axis of carbonate hydroxylapatite, as well as a parallel increase of the coherence length along the c-axis*". These authors also provide a valuable precise correlation of XRD data with IR data. Enzo et al. (2007) and Piga et al. (2008, 2009a, b, 2013) as well as Harbeck et al. (2011) demonstrate how modern full profile analysis of X-ray diffractograms can be applied to calibrate cremation temperatures. From about 500 °C a significant recrystallisation of the bioapatite and crystallite growth of hydroxyapatite sets in. According to our previous work (Harbeck et al. 2011) small changes are discernible already at low temperatures of 100 °C. Piga et al. (2008, 2009a) investigated cremation times at different temperatures and found that between 600 and 850 °C the recrystallisation is almost completed after 20 min.

Infrared spectroscopy (IR) probes the frequencies of molecular/atomic vibrations in the material. Infrared light is absorbed if a vibration in the sample matches the frequency of the light. The molecules/atoms vibrate independent of existing long-range order. For crystallographically well-ordered material, the vibrations in neighbouring unit cells are identical. In this case the IR absorption peaks are well developed and rather sharp. However, the method also works with perturbed order and with amorphous structures, where the IR absorption signal broadens as the molecular vibration frequencies become locally different due to different molecular environments in the structure. The XRD signal for amorphous materials, however, is very weak and diffuse compared to the signal from a crystalline structure. IR gives information on local molecular symmetry, where the XRD signal is an average over the periodically arranged unit cells. Accordingly, the two methods

give complementary information. IR probes crystallinity (periodic long-range order) only indirectly: by the variation of the vibration frequency and vibration amplitude of a molecule or atomic group, where the variations are induced by local distortions of the geometry and by vibrations of neighbouring molecules. So far, there is no straightforward general way to calculate this indirect influence.

Unit Cell Structure of Bioapatite

In the literature on the unit cell structure of hydroxyapatite, synthetic carbonated hydroxyapatite, and bioapatite, there is a substantial diversity of modifications of a basic scheme. It is beyond the scope of this article to compare this literature in full. A fundamental detail is the crystallographic symmetry of the apatite, which is hexagonal (space group $P6_3/m$) in the classical literature, and used e.g. in the work of Wilson et al. (1999) or Tonegawa et al. (2010). Some authors believe that monoclinic symmetry (space group $P2_1/c$) gives a more correct description (Ikoma et al. 1999; Tonegawa et al. 2010). This reduction of symmetry practically doubles the degrees of freedom in the description of the atomic positions, corresponding to the doubling the number of fitting parameters, which, of course, always provide a better fit to any observed data.

Materials and Methods

We investigated 63 random samples from the archaeological animal bone material selected for screening by XRD for isotope studies in the FOR1670. Fresh bovine bone and cremated medieval archaeological bone samples were obtained for comparison.

A piece of compact bone was cut from the skeletal element, and the endosteal and periosteal surfaces were mechanically removed. The sample was then ultrasonically washed in deionised H_2O (35 kHz), whereby the water was changed every 5 min. The washing procedure was repeated until the water remained clear. Thereafter the sample was air dried. The bone piece was defatted for 5 h with diethylether in a Soxhlet and air dried again. Finally, the sample was homogenised to a fine powder.

X-ray diffractograms were collected on a General Electric 3003 powder diffractometer in a Bragg–Bentano reflection geometry. Cu-Kα_1 radiation was selected with a focusing monochromator in the primary beam. An exposure time of 1000 s on a 1D-Meteor detector was used, resulting in a total collection time of 240 min for a complete diffractogram from 5 to 100° 2θ. The instrumental resolution function was determined empirically with a NIST LaB_6 standard. Data evaluation and Rietveld refinement were conducted with the FULLPROF code (Rodriguez-Carvajal 1993; Rodriguez-Carvajal and Roisnel 2004), where the Thompson–

Cox–Hastings method for convolution of instrumental resolution with anisotropic size and isotropic microstrain broadening (Thompson et al. 1987) was applied.

Infrared spectra were measured on a Bruker Equinox FTIR instrument with a resolution of 4 cm^{-1} with 128 scans resulting in a 2 min acquisition time per sample. The ground bone powder (as described above for XRD) was prepared for measurement by sieving through a 100 μm mesh; 1 mg of sample powder was manually mixed with 200 mg of KBr in a mortar and pressed to a pellet.

Results

The quantitative analysis of bioapatite diffractograms poses a challenge due to the peak broadening which results from the nanoscale crystallite size of the bioapatite. Further, due to the plate-like character of the mammal bioapatite, the peak width depends on the direction of the scattering vector in the crystal, i.e. the width depends on the lattice plane hkl.

The diffraction peaks related to the thin and to the broad dimension of the bioapatite platelets perpendicular to their *c*-axis are exactly superimposed; there is no information in the diffractogram to distinguish these two dimensions in a direct way. Thus, after numerous trials, the most practical solution for handling the anisotropic line broadening with a minimum of fit parameters was found to be a crystallite shape of a rotational ellipsoid elongated along the c-direction. An isotropic microstrain contribution clearly improved the fit result compared to a pure size-related broadening model. We attribute these fluctuations of the lattice parameter to an inhomogeneous substitution of carbonate across the sample, e.g. surface versus core of the nanoparticle or variation of the absolute $[CO_3]^{2-}$-content of the nanocrystals. Figure 2 shows the quality of the profile description which was achieved with the model.

We found no possibility to refine a specific location of carbonate in the unit cell since a multitude of models fitted the diffractograms equally well. We attribute this to the absence of ordering in the way in which the $[CO_3]^{2-}$-groups replace the $[PO_4]^{3-}$-groups and/or the OH^- groups (Wopenka and Pasteris 2005) due to geometrical and charge mismatch. To minimise the number of fit parameters we used only site occupancy parameters and mean-square displacement parameters (Debye–Waller factors) for the Ca- and P-sites, while considering the phosphate tetrahedral as rigid bodies (bond distance 1.54 Å).

Also, we found no evidence for a deviation from the hexagonal symmetry: neither was there any indication of the superlattice peaks which result from the monoclinic model, nor any significant deviation of the monoclinic unit cell angle from 120°, the value fixed by symmetry in the hexagonal case. Thus, we decided that any small improvement of the figures of merit for the monoclinic fit was spurious and simply due to the larger number of fit parameters, and we decided to stay with the hexagonal model of Wilson et al. (2005) as starting parameters for

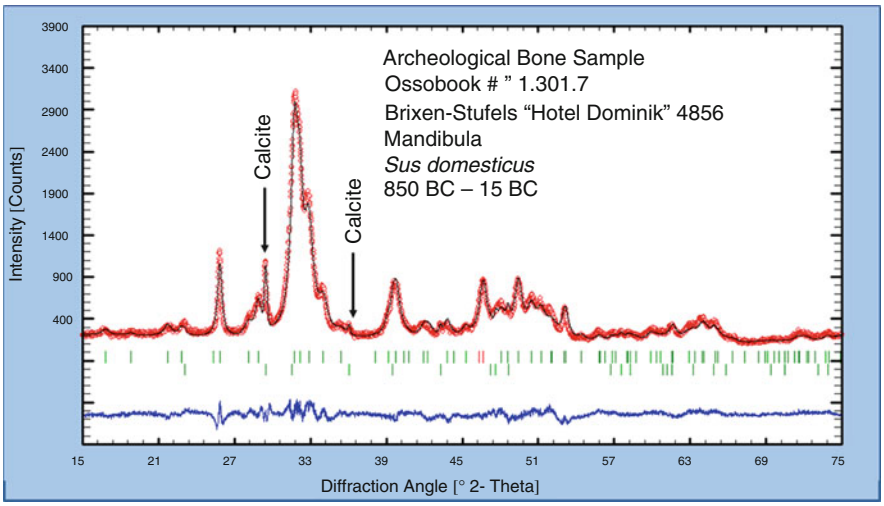

Fig. 2 Comparison of the observed X-ray diffraction profile (*red circles*) with the modelled profile (*black line*) after Rietveld analysis for an exemplary sample. The difference is shown as a *blue line* at the *bottom*. The small *vertical lines* in *green mark* the positions of the X-ray diffraction peaks of bioapatite (*top*) and calcite (*bottom*). The two most prominent calcite peaks are additionally marked with *arrows*. See Table 1 for key parameters

Table 1 Crystallographic parameters of archaeological bone for two sample materials

FOR1670 sample identifier	1.301.7	1.301.1
Cultural period	850 BC–15 BC	850 BC–15 BC
Find context	Brixen-Stufels "Hotel Dominik" 4856	
Species	*Sus domesticus*	*Cervus elaphus*
Skeletal element	Mandible	Metatarsal III + IV
Phase content bioapatite (wt%)	97.6(1)	95.3(1)
Phase content calcite (wt%)	2.4(1)	4.7(1)
Crystallite size *c*-direction (Å)	210.2(4)	593.4(3)
Crystallite size *a*–*b*-direction (Å)	91.0(8)	102.7(8)
c lattice parameter (Å)	6.8886(4)	6.8886(2)
a lattice parameter (Å)	9.4298(5)	9.4322(2)
Unit cell volume ($Å^3$)	530.5(6)	530.7(5)
Microstrain (%)	36.02(6)	24.77(4)
Calcite crystal size (Å)	360(1)	860(1)

refinement. Constraints were employed to keep the phosphate group in its tetrahedral geometry with appropriate P–O bond distances.

The Rietveld analysis revealed calcite as the only secondary phase. No contributions of other crystalline or amorphous phases were detected. Table 1 lists the most important parameters for two bone samples.

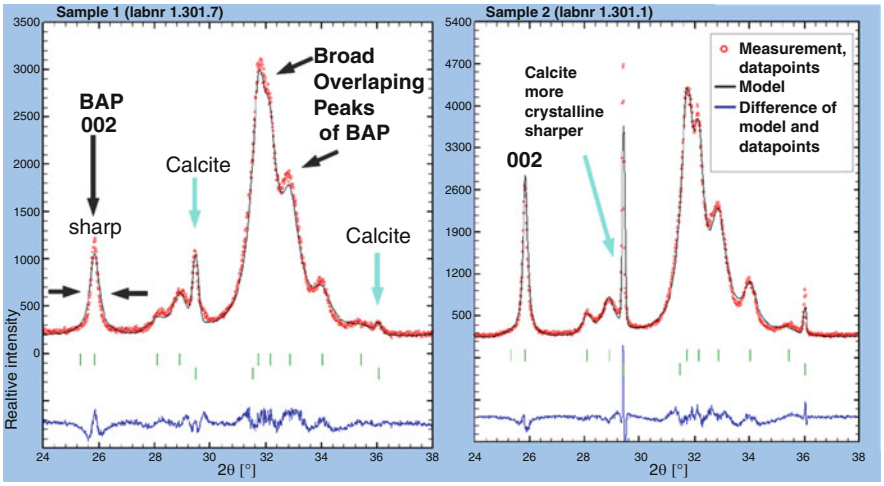

Fig. 3 Comparison of the diffractograms of the samples of Table 1. Note the satisfactory modelling of the anisotropic line broadening (the 002 peak of bioapatite (BAP) is sharp compared to the other peaks of BAP). Note also the breadth of the calcite peaks. Both samples are from the same archaeological site but from different animals and skeletal elements (*left*: *Sus domesticus*, *right*: *Cervus elaphus*)

The Rietveld fit quality is satisfactory and the anisotropy of the sharpness of the reflections is modelled adequately (cf. Figs. 2 and 3). The obtained crystallite sizes are in the range expected from the literature (Landis and Jacquet 2013). The remaining differences between observed and modelled diffraction profile are due to small remaining problems in modelling the peak shape even more precisely, and they do not indicate the presence of other phases such as e.g. octacalcium phosphate, amorphous calcium phosphate, or whitlockite in any measurable amount. At present we use a distinct (but anisotropic) crystallite size; in reality, a crystallite size distribution needs to be expected, and the effect of a crystallite size anisotropy in the plane perpendicular to c on the observed profile needs to be explored. With the least-squares fit procedure used in current Rietveld refinement programs, this is impossible due to strong parameter correlations resulting from the exact superposition of peaks which carry the relevant information. Figure 3 compares in detail the diffractograms of the two samples in Table 1. Interestingly, the small but significant difference in the bioapatite crystallite size of the two samples comes from the same archaeological site but from different animal species and skeletal elements. In addition, and even more significant, is the broadening of the calcite line, which indicates a crystallite size in the order of just some tens of nanometers. So far we interpret this fact in the way that the calcite has formed by diagenetic decomposition of the bone rather than by contamination with limestone or calcite crystallisation from the soil. Such inorganic calcite is never nanoscale. To compare the archaeological bone with fresh modern bone and with cremated bone material, we added Figs. 4 and 5. From Fig. 4 we see the small but significant increase in crystallite size (sharper

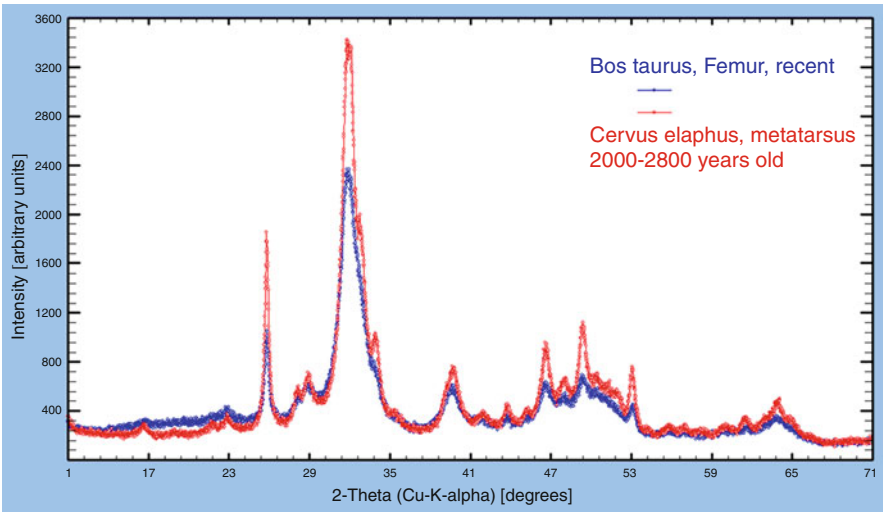

Fig. 4 Comparison of the X-ray diffractograms of modern bone (*Bos taurus*, femur) with 2000–2800 years old archaeological bone material (*Cervus elaphus*, metatarsus). The crystallite size of the archaeological bone is higher (it has sharper peaks)

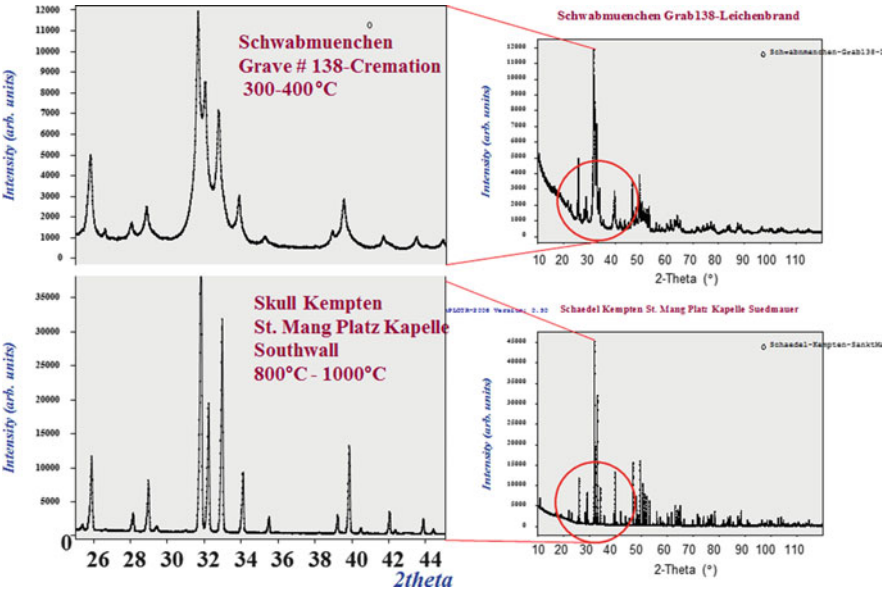

Fig. 5 Diffractograms of cremated bone with estimated cremation temperatures to indicate the significant growth in bioapatite crystallite size due to heating compared to the uncremated bones in Figs. 2, 3, and 4

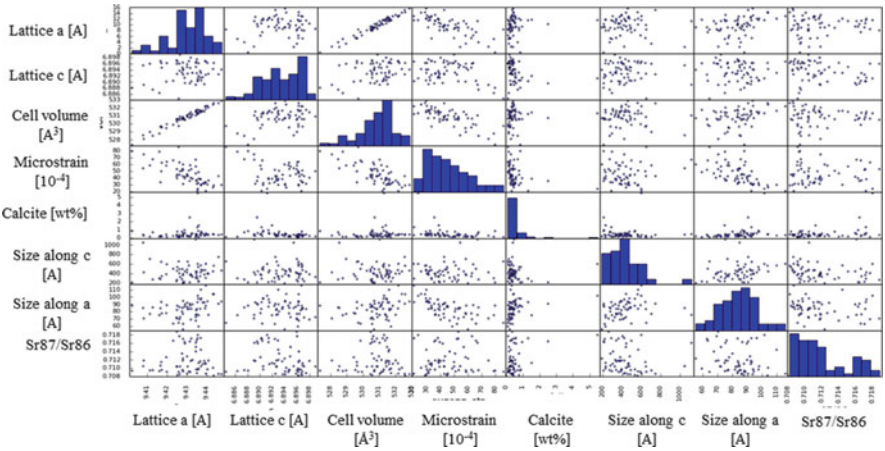

Fig. 6 Part of the cross-correlation diagram for statistical evaluation of the results obtained on the samples of FOR1670. Lattice a: a-lattice parameter [Å], Lattice c: c lattice parameter [Å], Cell Volume: unit cell volume [$Å^3$], isotropic microstrain, calcite content (wt%), size along c: crystallite size in *c*-direction [Å], size along a: mean size in *a*–*b*-directions [Å], $^{87/86}Sr$ isotope ratio. The fields in the diagonal show the frequency distribution histograms of the parameters; non-diagonal fields display the cross-correlation

peaks) of the 2000–2800 years old archaeological finds compared to fresh (bovine) material. To indicate the change in diffractogram line broadening as bone is cremated, Fig. 5 shows two examples of cremated bone of medieval age from archaeological sites outside the FOR1670 realm (the estimated cremation temperatures based on our calibration (Harbeck et al. 2011) are given in the figure).

Figure 6 shows a part of the cross-correlation diagram which we use to examine the obtained parameters and their potential relation to isotope or other data relevant in FOR1670. So far the results indicate that the selection principle of samples for isotope analysis was successful in avoiding degraded material and selecting a fairly homogeneous field of samples as far as the bone material is concerned. Only in a few samples is the calcite content larger than 1 wt. %. We can state that the *a* lattice parameter shows a stronger variation than the *c* lattice parameter, and we find a negative correlation between unit cell volume and microstrain, which is depicted in Fig. 7, where the crystallite size along the c-axis and the calcite content are also displayed as the size of the "bubbles". Large calcite contents tend to be associated with large unit cell volumes. The crystallite size does not appear to correlate with unit cell volume and microstrain. It becomes apparent that the data for the wild animal (*Cervus*) scatter significantly more around the trend line for this species, than it is the case for domesticated *Sus* and *Bos*.

The behaviour of some important crystallographic parameters versus archaeological age group of the find (corresponding to cultural periods determined by cultural artefacts) is shown in Fig. 8. It becomes apparent that for the investigated age range of bones selected for isotope analysis neither lattice parameters nor

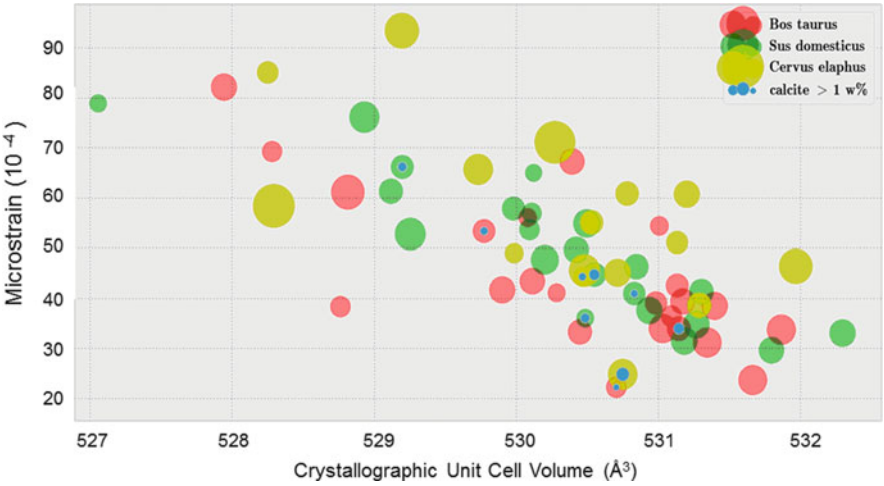

Fig. 7 Correlation diagram depicting the relation between microstrain and (hexagonal) crystallographic unit cell size. The size of the *blue bubbles* indicates calcite content for samples with more than 1 wt% calcite; the size of the other *bubbles* indicates the crystallite size in *c*-direction: *Red*: *Bos taurus* samples, *green*: *Sus domesticus* samples, *olive green*: *Cervus elaphus* samples

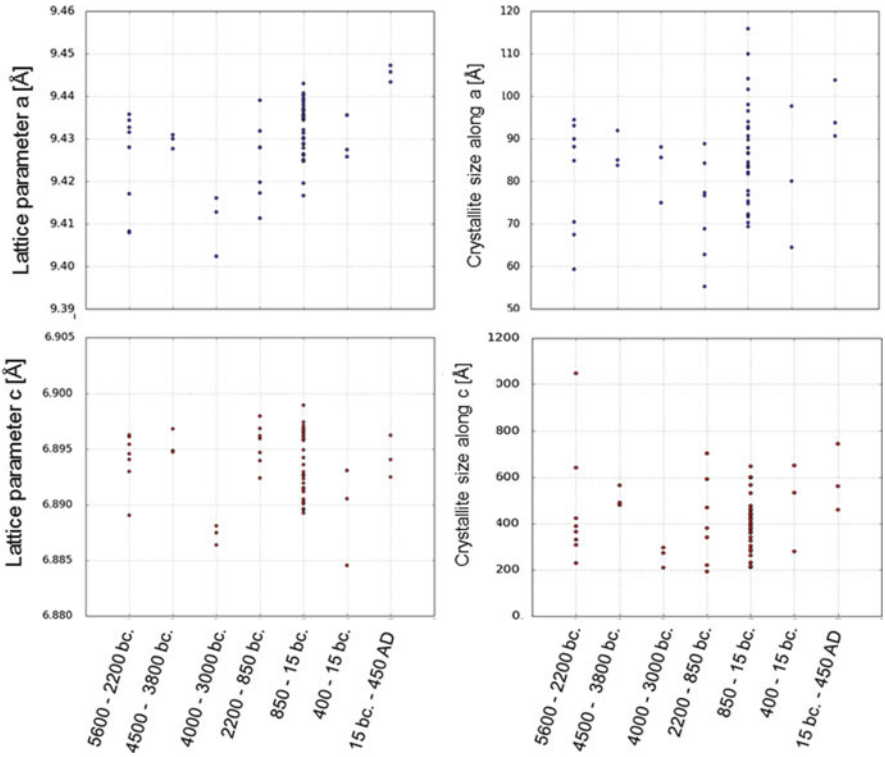

Fig. 8 Crystallographic parameters are plotted against archaeological time windows (corresponding to historical cultures) of FOR1670 samples. Windows are sorted from older to younger

crystallite sizes depend directly on age. This confirms the classical finding by Person et al. (1995).

FTIR results for several samples comparing fresh bone (*Bos taurus*, femur) with recrystallised bone (1000 °C, *Bos taurus*, femur) and archaeological bone (*Sus domesticus*, humerus, 5600–2200 BC, Griesstetten) are shown in Fig. 9. The stretching vibrations (ν_1 and ν_3) are less developed in fresh material and become defined in the sample recrystallised at 1000 °C. This sample also shows a well-defined vibration at 632 cm^{-1}, which is not separately visible in the fresh and the archaeological sample without curve fitting (see below). The bottom part of Fig. 9 compares the spectra in the spectral range which is relevant for calculation of the popular and empirical IRSF (Weiner et al. 1993). The IRSF is calculated from the region of the ν_4 bending vibrations of the phosphate group in the following way:

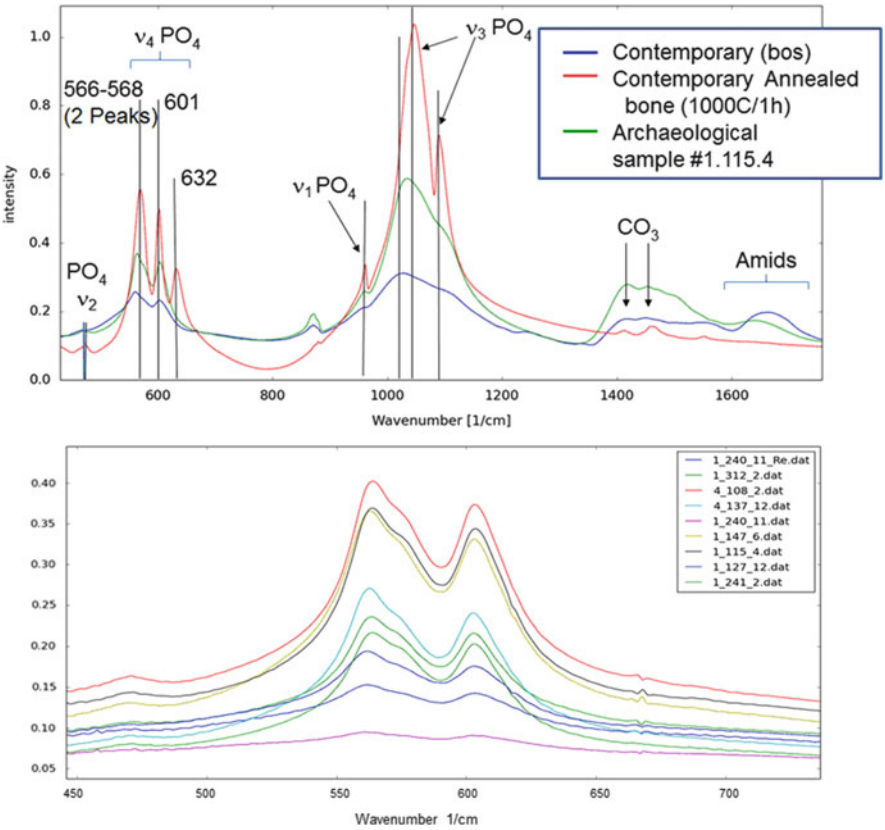

Fig. 9 Some examples of FTIR spectra of FOR1670. *Top*: Spectral range 400–1800 cm^{-1}. The major phosphate-, carbonate-, and collagen (amide) vibrational peaks are marked. *Bottom*: For the same weighed portion of 1 mg sample/200 mg KBr, we obtain significantly different absorbance curves even for the same material. We attribute this to problems in homogenisation of the KBr pellet as the ground bone material tends to agglomerate, and the agglomerate size distribution makes a difference

$$\mathrm{IRSF} = \left(A_{\mathrm{peak}}\left(567\mathrm{cm}^{-1}\right) + A_{\mathrm{peak}}\left(601\ \ \mathrm{cm}^{-1}\right)/A_{\mathrm{minimum}}\left(590\ \ \mathrm{cm}^{-1}\right)\right. \quad (6)$$

from the average peak height (absorbance) of the maxima located at 567 cm^{-1} and 601 cm^{-1}, respectively, divided by the absorbance value of the minimum in the valley around 590 cm^{-1} between the peaks. The IRSF correlates positively with increasing signal strength (peak height) and with increasing sharpness of the peaks, which makes the valley more pronounced (i.e. deeper) between the maxima.

We performed a spectral decomposition of the 400–800 cm^{-1} region separating the signal into eight components (i.e. peaks) as suggested by Vandecandelaere et al. (2012) and Grunenwald et al. (2014), which covers ν_4 bending vibrations and the $\nu_2[PO_4]$ peak near 467 cm^{-1}. This leads to the results shown in Fig. 10. The corresponding peak parameters are listed in Table 2. Note that the least-squares fit

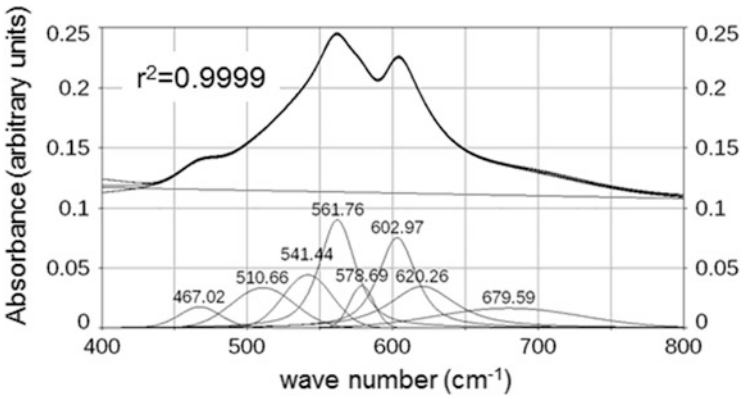

Fig. 10 Spectral decomposition of the 400–800 cm^{-1} infrared frequency range into eight peaks of pseudo-Voigt shape functions. See Table 2 and text for peak assignment. Sample: 1.1238.10, 1.238.20, 2200–850 BC, *Bos taurus*, tibia, from Radfeld-Mauken

Table 2 Results of spectral decomposition of the 400–800 cm^{-1} infrared frequency range into eight peaks of pseudo-Voigt shape functions

	Position (1/cm)	Amplitude (absorb.)	Width (FWHM) (1/cm)
$\nu_2(PO_4)$	467(2)	0.018(5)	34(4)
Non-apatitic HPO_4	510(41)	0.03(5)	50(48)
Apatitic HPO_4	541(11)	0.04(7)	40(27)
$\nu_4(PO_4)$	561.7(5)	0.09(6)	30(10)
$\nu_4(PO_4)$	578(1)	0.04(5)	20(7)
$\nu_4(PO_4)$	603.0(7)	0.08(6)	31(20)
$\nu_4(PO_4)$[a]	620(50)	0.04(6)	54(114)
Unknown origin[b]	680(115)	0.02(2)	118(119)

The peaks were assigned according to Vandecandelaere et al. (2012) except for the two last peaks
[a]Assigned according to Pedone et al. (2007)
[b]Vandecandelaere et al. (2012) proposed this peak to be due to apatite OH^-, which is not supported by ab initio theory (Pedone et al. 2007)

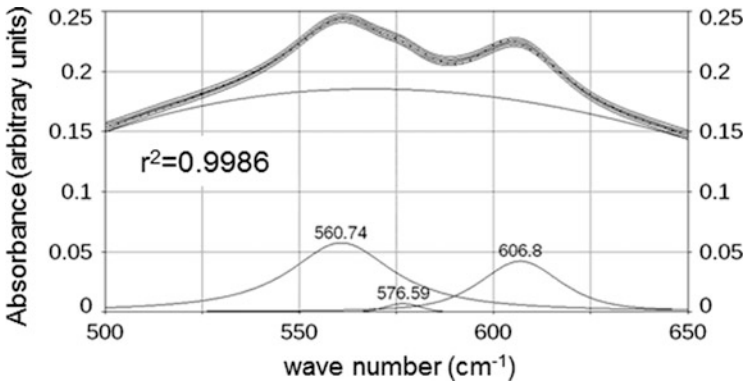

Fig. 11 Spectral decomposition of the 500–650 cm^{-1} part of the infrared spectrum of archaeological bone into three peaks of pseudo-Voigt shape functions. See Table 3 and text for peak assignment

Table 3 Results of spectral decomposition of the 500–650 cm^{-1} infrared frequency range into three peaks of pseudo-Voigt shape functions

	Position (1/cm)	Amplitude (absorb.)	Width(FWHM) (1/cm)
$\nu_4(PO_4)$	560.7(6)	0.058(7)	32(3)
$\nu_4(PO_4)$	576.7(9)	0.007(3)	10(3)
$\nu_4(PO_4)$	606.8(2)	0.042(6)	24(2)

standard deviations for the frequencies and peak widths become quite large. Attempting to fit the narrower region of 500–650 cm^{-1} with three peaks only, to get closer to the two-peak-and-valley approximation of the IRSF, we obtain the results shown in Fig. 11 and Table 3. Note that the standard deviations become smaller; however, the background needed to fit this description forms an implausible bulge located at 570 cm^{-1}. In summary we can say that there are definitely more than two peaks contributing to the spectral features in this range.

Discussion

A rigorous ab initio-based theoretical calculation of the vibrational modes of hydroxyapatite was presented by Pedone et al. (2007), and they show that in the spectral region relevant for the IRSF there are six (not two) infrared active ν_4 bending mode vibrations of the $[PO_4]$ group. On a rather empirical basis, Vandecandelaere et al. (2012) and Grunenwald et al. (2014) fitted the spectrum in this region in biomimetic apatite and bioapatite using seven peaks, three of which they assign to $\nu_4[PO_4]$ at the wavenumbers 560 cm^{-1}, 585 cm^{-1}, and 605 cm^{-1}, two more peaks are attributed to $[HPO_4]$, and a "non-apatitic $[PO_4]$", as well as an "apatitic OH^-". The latter is attributed to a peak near 631 cm^{-1}. Conversely, the

631 cm^{-1} peak is one of the six vibrational $\nu_4[PO_4]$ modes predicted by Pedone et al. (2007). This frequency is what we see emerging for annealed well-crystalline hydroxyapatite (Fig. 9). Hydroxyl vibrational modes must be expected to occur at much higher wavenumbers than 630 cm^{-1}, and the calculation of Pedone et al. in fact puts the hydroxyl stretching at 3604 cm^{-1}. We thus attribute the 630 cm^{-1} peak of the recrystallised sample to the $\nu_4[PO_4]$ predicted by Pedone et al. (2007).

At present, theory allows to predict the number of molecular vibrations of a certain character and to estimate the frequencies with a reasonable accuracy (which, however, is still not sufficient to pinpoint every theoretically predicted vibration exactly in the experimental spectrum of a complex substance). Peak widths and amplitudes cannot be predicted so far. Thus, the IRSF is an easy, convenient, and experimentally quick (minutes on a portable FTIR instrument in the field) way to obtain some number on the structural state of bone mineral. In contrast to XRD, which takes hours on a stationary laboratory instrument, however, it does not provide a clear scientific understanding of the features entering into this number, unless frequency, line width, and intensity of infrared spectral features can be theoretically predicted in the future. Moreover, great care must be taken in the preparation of the KBr pellets commonly used for FTIR. The bottom part of Fig. 9 shows a range of spectra for similar and some even identical bone materials, where the spectrum appears different because of different spatial distributions of sample within the KBr pellet, which can occur during sample preparation.

On the other hand, XRD provides a quite rigorous and quantitative characterisation of the observables in the case of crystalline and nanocrystalline materials. However, small amounts of amorphous material, such as the hydrated amorphous surface layer surrounding the bioapatite platelets in bone (Jäger et al. 2006; Wang et al. 2013), are practically undetectable. From our profile analyses we can say that in archaeological bone material employed for isotope analyses in FOR1670, due to selection and cleaning procedures (according to the description in the experimental section), there are only minor variations in crystallographic parameters. Only calcite was detected as a secondary mineral in amounts ranging <wt. 1 % in most samples to up to wt. 6 % (the calcite is removed by subsequent acid treatment prior to isotope analysis). The calcite shows an unexpected XRD line width broadening indicating a nanocrystalline microstructure, from which we assume that it formed from bone mineral alteration. We found no indications for phases such as octacalcium phosphate, amorphous calcium phosphate, or whitlockite, nor any other in any measurable amount. We can say that thus the sample selection procedures of FOR1670 were successful in producing a data base for reliable isotopic data. Also, there is very little to no intrinsic change in crystallite size of the bioapatite in the cleaned internal part of the bone material during the several thousands of years covered in our study. This confirms the classical finding by Person et al. (1995). As we did not investigate any bone material that was corroded according to visual inspection, the apparent intrinsic resilience of bone mineral against diagenetic alteration in the samples that we investigated does not mean that there is generally no bone diagenesis during several millennia (Nielsen-Marsh and Hedges 2000). In the XRD profiles of the investigated archaeological bones the

diffraction signal of collagen was not detectable, while it gives a prominent contribution to the XRD profile for fresh bones. Further, we clearly see a certain degree of bioapatite peak sharpening of the archaeological material compared to the fresh bone (Fig. 4). This diagenesis may well occur during just a few years after death.

Understanding of the cause of observed range of crystallographic parameters in the investigated 63 archaeological samples, which appear to show a random scatter in most cases, still needs extensive fundamental research on the natural variation of bone material (see also Piga et al. 2013) and short-term diagenesis. We note that the lattice parameter *a* shows the most significant variation of all parameters, which was also noted by Stathopoulou et al. (2008). We attribute the variability of the lattice constants and microstrain mainly to chemical aspects of the unit cell. Thermal recrystallisation and associated loss of carbonate is associated with a decrease in unit cell volume (Harbeck et al. 2011) and better crystallographic long-range order. Thus, our observed trend of increasing microstrain for smaller unit cell volume cannot simply be explained by crystallisation of a carbonate-free, well-ordered hydroxyapatite during diagenesis, unless we assume that after the burial times in question, the recrystallisation is incomplete and hydroxyapatites and bioapatites coexist with intermediates of various degrees of order.

Acknowledgement We thank the Deutsche Forschungsgemeinschaft, DFG, for financial support in Forschergruppe FOR1670, projects SCHM930/12-1 and GR959/21-1 and 20–1.

References

Berna F, Matthews A, Weiner S (2004) Solubilities of bone mineral from archaeological sites: the recrystallization window. J Archaeol Sci 31:867–882

de Keijser TH, Langford JI, Mittemeijer EJ, Vogels ABP (1982) Use of the Voigt function in a single-line method for the analysis of X-ray diffraction line broadening. J Appl Cryst 15:308–314

de Leeuw NH (2010) Computer simulations of structures and properties of the biomaterial hydroxyapatite. J Mater Chem 20:5376–5389

Elliot JC (2002) Calcium phosphate biominerals. In: Kohn MJ, Rakovan J, Hughes JM (eds) Phosphates: geochemical, geobiological and material importance. Reviews in mineralogy and geochemistry, vol 48. Mineralogical Society of America, Washington, DC, pp 631–672

Enzo S, Bazzoni M, Mazzarello V, Piga G, Bandiera P, Melis P (2007) A study by thermal treatment and X-ray powder diffraction on burnt fragmented bones from tombs II, IV and IX belonging to the hypogeic necropolis of “Sa Figu” near Ittiri, Sassari (Sardinia, Italy). J Archaeol Sci 34:1731–1737

Gernaey AM, Waite ER, Collins MJ, Craig OE, Sokol RJ (2001) Survival and interpretation of archaeological proteins. In: Brothwell DR, Pollard AM (eds) Handbook of archaeological science. Wiley, Chichester, pp 323–329

Grunenwald A, Keyser C, Sautereau AM, Crubézy E, Ludes B, Drouet C (2014) Novel contribution on the diagenetic physicochemical features of bone and teeth minerals, as substrates for ancient DNA typing. Anal Bioanal Chem 406:4691–4704

Harbeck M, Schleuder R, Schneider J, Wiechmann I, Schmahl WW, Grupe G (2011) Research potential and limitations of trace analyses of cremated remains. Forensic Sci Int 204:191–200
Hedges REM (2002) Bone diagenesis: an overview of processes. Archaeometry 44:319–328
Ikoma T, Yamazaki A, Nakamura S, Akao M (1999) Preparation and structure refinement of monoclinic hydroxyapatite. J Solid State Chem 144:272–276
Jäger C, Welzel T, Meyer-Zaika W, Epple M (2006) A solid-state NMR investigation of the structure of nanocrystalline hydroxyapatite. Magn Reson Chem 44:573–580
Landis WJ, Jacquet R (2013) Association of calcium and phosphate ions with collagen in the mineralization of vertebrate tissues. Calcif Tissue Int 93:329–337
Lebon M, Reiche I, Frohlich F, Bahain J, Falgueres C (2008) Characterization of archaeological burnt bones: contribution of a new analytical protocol based on derivative FTIR spectroscopy and curve fitting of the ν_1 and ν_3 PO_4. Anal Bioanal Chem 392:1479–1488
Lee-Thorp J, Sponheimer M (2003) Three case studies used to reassess the reliability of fossil bone and enamel isotope signals for paleodietary studies. J Anthropol Archaeol 23:208–216
Lowenstam HA, Weiner S (1989) On biomineralization. Oxford University Press, Oxford, 324 p
Mittemeijer EJ, Welzel U (eds) (2012) Modern diffraction methods. Wiley, Weinheim, 528 p
Nielsen-Marsh CM, Hedges REM (2000) Patterns of diagenesis in bone I: the effects of site environments. J Archaeol Sci 27:1139–1150
Nielsen-Marsh CM, Gernaey A, Turner-Walker G, Hedges REM, Pike A, Collins MJ (2000) The chemical degradation of bone. In: Cox M, Mays S (eds) Human osteology in archaeology and forensic science. Greenwich Medical Media, London, pp 439–454
Pasteris JD, Wopenka B, Freeman JJ, Rogers K, Valsami-Jones E, van der Houwen AM, Silva MJ (2004) Lack of OH in nanocrystalline apatite as a function of degree of atomic order: implications for bone and biomaterials. Biomaterials 25:229–238
Pecharsky VK, Zavalij PY (2003) Fundamentals of powder diffraction and structural characterization of materials. Springer, New York, NY, 741 p
Pedone A, Corno M, Civalleri B, Malavasi G, Menziani C, Segrea U, Ugliengo P (2007) An ab initio parameterized interatomic force field for hydroxyapatite. J Mater Chem 17:2061–2068
Person A, Bocherens H, Saliège J-F, Paris F, Zeitoun V, Geerard M (1995) Early diagenetic evolution of bone phosphate: an X-ray diffractometry analysis. J Archaeol Sci 22:211–221
Piga G, Malgosa A, Thompson TJU, Enzo S (2008) A new calibration of the XRD technique for the study of archaeological burned human remains. J Archaeol Sci 35:2171–2178
Piga G, Thompson TJU, Malgosa A, Enzo S (2009a) The potential of X-ray diffraction in the analysis of burned remains from forensic contexts. J For Sci 54:3534–3539
Piga G, Santos-Cubedo A, Moya Sola S, Brunetti A, Malgosa A, Enzo S (2009b) An X-ray diffraction (XRD) and X-ray fluorescence (XRF) investigation in human and animal fossil bones from Holocene to Middle Triassic. J Archaeol Sci 36:857–1868
Piga G, Solinas G, Thompson TJU, Brunetti A, Malgosa A, Enzo S (2013) Is X-ray diffraction able to distinguish between animal and human bones? J Archaeol Sci 40:778–785
Pucéat E, Reynard B, Lécuyer C (2004) Can crystallinity be used to determine the degree of chemical alteration of biogenic apatites? Chem Geol 205:83–97
Rey C, Renugopalakrishnan V, Collins B, Glimcher MJ (1991) Fourier transform infrared spectroscopic study of carbonate ions in bone mineral during aging. Calcif Tissue Int 49:251–258
Rey C, Combes C, Drouet C, Glimcher MJ (2009) Bone mineral: update on chemical composition and structure. Osteoporos Int 20:1013–1021
Rodriguez-Carvajal J (1993) Recent advances in magnetic structure determination by neutron powder diffraction. Phys B Condens Matter 192:55–69
Rodriguez-Carvajal J, Roisnel T (2004) Line broadening analysis using FullProf: determination of microstructural properties. Mater Sci Forum 443:123–126
Rogers K, Beckett S, Kuhn S, Chamberlain A, Clement J (2010) Contrasting the crystallinity indicators of heated and diagenetically altered bone mineral. Palaeogeog Palaeoclimatol Palaeoecol 296:125–129

Shemesh A (1990) Crystallinity and diagenesis of sedimentary apatites. Geochim Cosmochim Acta 54:2433–2438

Shinomiyaa T, Shinomiya K, Orimoto C, Minami T, Tohno Y, Yamada MO (1998) In- and out-flows of elements in bones embedded in reference soils. Forensic Sci Int 98:109–118

Sillen A (1989) Diagenesis of the inorganic phase of cortical bone. In: Price TD (ed) The chemistry of prehistoric human bone. Cambridge University Press, New York, pp 211–229

Sponheimer M, de Ruiter D, Lee-Thorp J, Späth A (2005) Sr/Ca and early hominin diets revisited: new data from modern and fossil tooth enamel. J Hum Evol 48:147–156

Stathopoulou ET, Psycharis V, Chryssikos GD, Gionis V, Theodorou G (2008) Bone diagenesis: new data from infrared spectroscopy and X-ray diffraction. Palaeogeog Palaeoclimatol Palaeoecol 266:168–174

Surovell TA, Stiner M (2001) Standardizing infra-red measures of bone mineral crystallinity: an experimental approach. J Archaeol Sci 28:633–642

Thompson P, Cox DE, Hastings JB (1987) Rietveld refinement of Debye-Scherrer Synchrotron X-ray data from Al_20_3. J Appl Cryst 20:79–83

Tonegawa T, Ikoma T, Yoshioka T, Hanagata N, Tanaka J (2010) Crystal structure refinement of A-type carbonate apatite by X-ray powder diffraction. J Mater Sci 45:2419–2426

Trueman CN, Privat K, Field J (2008) Why do crystallinity values fail to predict the extent of diagenetic alteration of bone mineral? Palaeogeog Palaeoclimatol Palaeoecol 266:160–167

Turner-Walker G (2008) The chemical and microbial degradation of bones and teeth. In: Pinhasi R, Mays S (eds) Advances in human paleopathology. Wiley, Chichester, pp 3–29

Tütken T, Vennemann TW, Pfretzschner H-U (2008) Early diagenesis of bone and tooth apatite in fluvial and marine settings: constraints from combined oxygen isotope, nitrogen and REE analysis. Palaeogeog Palaeoclimatol Palaeoecol 266:254–268

Vandecandelaere N, Rey C, Drouet C (2012) Biomimetic apatite-based biomaterials: on the critical impact of synthesis and post-synthesis parameters. J Mater Sci Mater Med 23:2593–2606

Wang Y, Von Euw S, Fernandes FM, Cassaignon S, Selmane M, Laurent G, Pehau-Arnaudet G, Coelho C, Bonhomme-Coury L, Giraud-Guille M-M, Babonneau F, Azaïs T, Nassif N (2013) Water-mediated structuring of bone apatite. Nat Mater 12:1144–1153

Weiner S, Bar-Yosef O (1990) State of preservation of bones from the prehistoric sites in the near East: a survey. J Archaeol Sci 17:187–196

Weiner S, Goldberg P, Bar-Yosef O (1993) Bone preservation in Kebara Cave, Israel using on-site Fourier-transform infrared spectroscopy. J Archaeol Sci 20:613–627

Weiner S, Traub W, Wagner HD (1999) Lamellar bone: structure-function relations. J Struct Biol 126:241–255

Wilson RM, Elliot JC, Dowker SEP (1999) Rietveld refinement of the crystallographic structure of human dental enamel apatites. Am Mineral 84:1406–1414

Wilson RM, Elliton JC, Dowker SEP, Rodriguez-Lorenzo LM (2005) Rietveld refinements and spectroscopic studies of the structure of Ca-deficient apatite. Biomaterials 26:1317–1327

Wopenka B, Pasteris JD (2005) A mineralogical perspective on the apatite in bone. Mater Sci Eng C 25:131–143

Wright LE, Schwarcz HP (1996) Infrared and isotopic evidence for diagenesis of bone apatite at Dos Pilas, Guatemala: palaeodietary implications. J Archaeol Sci 23:933–944

Yerramshetty JS, Akkus O (2008) The associations between mineral crystallinity and the mechanical properties of human cortical bone. Bone 42:476–482

Yi H, Balan E, Gervais C, Ségalen L, Blanchard M, Lazzeri M (2014)·Theoretical study of the local charge compensation and spectroscopic properties of B-type carbonate defects in apatite. Phys Chem Minerals 4:347–359

Part II
Geological Aspects of Isotopic Landscapes

Assessing the "Local" $^{87}Sr/^{86}Sr$ Ratio for Humans

James H. Burton and Rachel Hahn

Since the seminal paper of Ericson (1985), which proposed the measurement of $^{87}Sr/^{86}Sr$ in teeth to assess human mobility, decades of research have amply demonstrated the utility of the method in doing so. Nonetheless, the accumulated research also reveals some conceptual issues that should be more fully understood if we are to accurately apply the tool and avoid seriously misinterpreting the data. The purpose here is to present some of these issues so that we can avoid these errors and more fully, and appropriately, exploit the technique.

The determination of the geographic origins of humans using $^{87}Sr/^{86}Sr$ ratios in teeth is predicated upon two premises: that there is a geographic region that can be defined, typically geologically, by a specific $^{87}Sr/^{86}Sr$ ratio or a narrow range of $^{87}Sr/^{86}Sr$ ratios, i.e., an "isoscape," and that human dental enamel, which mineralizes during infancy, incorporates this geographic $^{87}Sr/^{86}Sr$ ratio essentially unmodified such that the region of origin can be identified. Although the utility of using $^{87}Sr/^{86}Sr$ ratios to identify obvious outliers—by implication immigrants—in burial populations has been repeatedly demonstrated, the two founding premises are for the general case quite problematic.

The major issue with the "isoscape" concept is the determination of a generally applicable "local" $^{87}Sr/^{86}Sr$ ratio for a specific location. The simplistic concept is that there is a geologic ratio that moves into the biosphere and through diet into human teeth unchanged. But, when we examine rocks and minerals on any scale from microns to kilometers, we find too much variability to allow the identification of locally born individuals. While we can assess a regional range in isotope values, it behooves us to compare such ranges with the precision required to infer geographic origins. A key metric here, one that mandates a better understanding, is the extremely narrow $^{87}Sr/^{86}Sr$ range in humans. In the comprehensive database of the

J.H. Burton (✉) • R. Hahn
Department of Anthropology, University of Wisconsin, 5240 W. H. Sewell Social Science Building, 1180 Observatory Drive, Madison, WI 53706, USA
e-mail: jhburton@wisc.edu

G. Grupe, G.C. McGlynn (eds.), *Isotopic Landscapes in Bioarchaeology*,
DOI 10.1007/978-3-662-48339-8_6

Laboratory for Archaeological Chemistry of 4885 samples of human dental enamel, spanning six continents, 95 % of the enamel $^{87}Sr/^{86}Sr$ ratios (i.e., ±2 S. Dev.) fall within *0.7047 to 0.7190*, a range less than 0.015, with a sharp mode at 0.7092 (Burton and Price 2013). For humans from a single location, the variation is much smaller, approximately ±0.00015. In contrast, minerals within the same rock can have ratios that vary from 0.7 to >10.0—one granite yielded minerals with ratios varying from 0.7 to 230 (Naylor et al. 1970). Even individual crystals can vary on micron scales; e.g., Davidson et al. (2005) found an $^{87}Sr/^{86}Sr$ range of 0.708–0.716 in a single crystal. In short, the variation of $^{87}Sr/^{86}Sr$ in geological materials from a single location can easily exceed the human variation by many orders of magnitude (Fig. 1).

One misconception in defining geographic $^{87}Sr/^{86}Sr$ regions is that $^{87}Sr/^{86}Sr$ is primarily the result of the age of the bedrock. Although the essential process for creating elevated $^{87}Sr/^{86}Sr$ ratios is the decay of radioactive ^{87}Rb (Faure 1986), the half-life of this process is on the order of 5×10^{10} years, greater than the age of the universe and an order of magnitude greater than the age of the earth. Not only are modest geological time differences of tens of millions of years insignificant, most rocks are mechanical or chemical remixtures of older rocks anyhow. Very old rocks, even those as old as the earth, can have $^{87}Sr/^{86}Sr$ much lower than the ratios of quite young volcanic rocks. Wetherill (1975), using Rb–Sr to determine the age of the earth as well as its primordial $^{87}Sr/^{86}Sr$, measured in meteorites $^{87}Sr/^{86}Sr$ ranging from approximately 0.7 to 1.0, high values not unexpected for rocks that are 4.5 billion years old. On the other hand, $^{87}Sr/^{86}Sr$ measurements of lunar highland anorthosites, of the same age, yield $^{87}Sr/^{86}Sr$ in the range from 0.70 to 0.71, at the very low end of the possible range—primordial $^{87}Sr/^{86}Sr$ being 0.699. Although the meteorites and anorthosites are essentially of the same age and from the same primordial starting ratio, their $^{87}Sr/^{86}Sr$ ratios vary between one extreme of the measurement scale and the other, entirely due to compositional differences in the

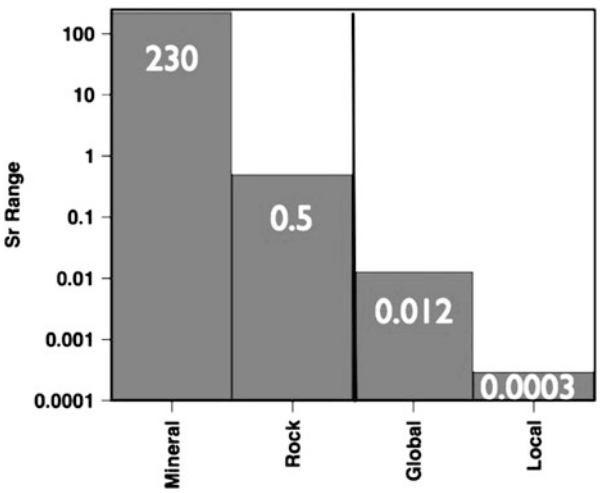

Fig. 1 Comparison of the range in $^{87}Sr/^{86}Sr$ in rocks and minerals from a single location (data from Naylor et al. 1970) to global and local ranges of humans (University of Wisconsin Laboratory for Archaeological Chemistry database). Note the scale is logarithmic

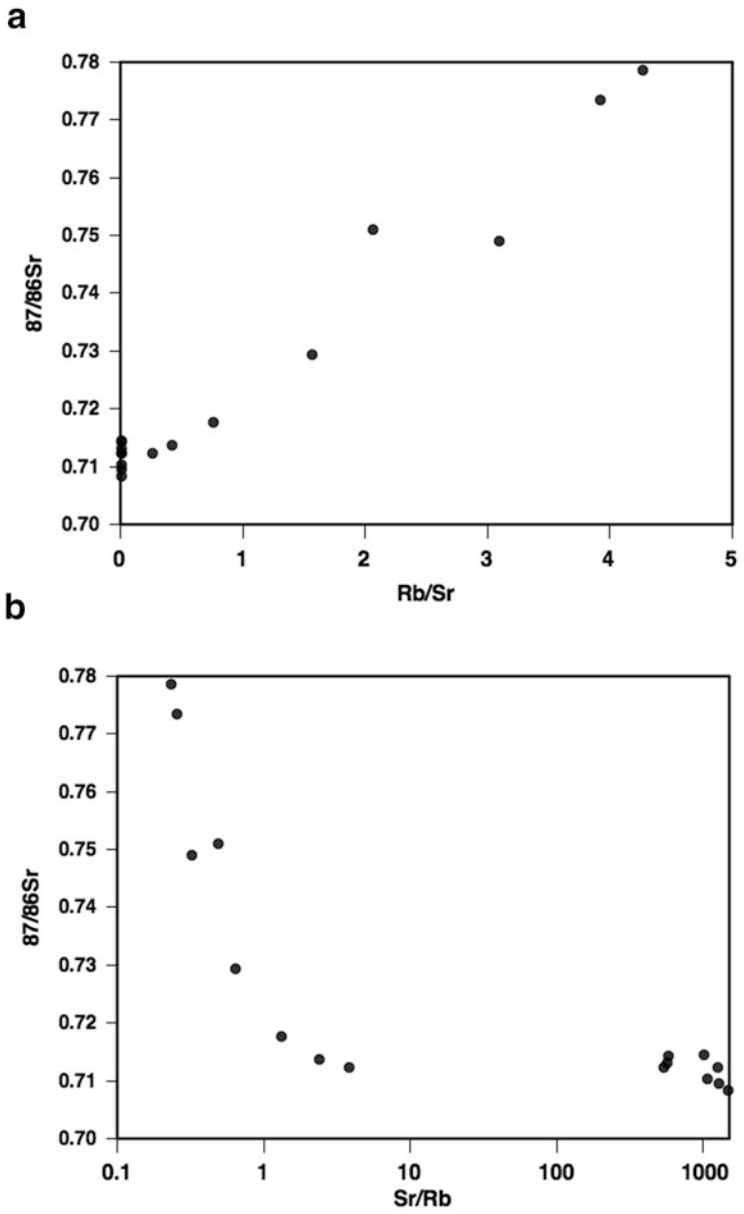

Fig. 2 (**a**) Graph of $^{87}Sr/^{86}Sr$ versus Rb/Sr for granites of Haeberlin (2002). (**b**) Graph of $^{87}Sr/^{86}Sr$ versus Sr/Rb for granites of Haeberlin (2002)

relative amounts of rubidium and strontium: the higher the Rb/Sr ratio, the higher the resulting $^{87}Sr/^{86}Sr$. Conversely rocks intrinsically high in strontium have the lowest $^{87}Sr/^{86}Sr$ ratios.

It is illuminating to examine a typical geological plot (Fig. 2a) of $^{87}Sr/^{86}Sr$ versus Rb/Sr—common among geologists to assess the age from which minerals separate from a homogeneous source—and to invert the abscissa into Sr/Rb (Fig. 2b). The data are chosen, arbitrarily, from the dissertation of Haeberlin (2002).

For a given amount of rubidium, the samples with the lowest $^{87}Sr/^{86}Sr$ have many orders of magnitude more strontium. Although individual mineral $^{87}Sr/^{86}Sr$ ratios can exceed 200, rocks containing those minerals have much lower whole-rock ratios, less than one, because the high ^{87}Sr minerals have too little strontium to affect the whole-rock ratios. Likewise, rocks with high $^{87}Sr/^{86}Sr$ (e.g., granite, shale) tend to be much lower in strontium than rocks that have lower whole-rock $^{87}Sr/^{86}Sr$ (e.g., limestone, basalt).

This compositional dependence is a clue to understanding the astonishing compression in the range of human ratios, compared to the geologic ratios, both in range and in actual values toward the low end of the $^{87}Sr/^{86}Sr$ scale: extremely high geologic $^{87}Sr/^{86}Sr$ ratios don't contribute to human (or biosphere) ratios because they don't contribute significantly to the total strontium.

A second problem with efforts to assess human $^{87}Sr/^{86}Sr$ from bedrock geology is a failure to appreciate how much biologically available strontium is derived not from bedrock but from airborne inputs such as sea salt, dust, smoke from fires, and sulfate salts from volcanic eruptions and from consumption of fossil fuels. The percentage of soil strontium contributed by atmospheric inputs can be astonishing. Miller et al. (2014) in the Wasatch Mountains of Utah found that, even over high-strontium limestone, half of the strontium was deposited from the atmosphere and over low-strontium quartzite more than 90 % of the strontium was atmospherically derived. These figures are in line with the 75 % atmospheric contribution found by Graustein and Armstrong (1983) in the Sangre de Cristo Mountains of New Mexico and the assessments of Van der Hoven and Quade (2002) near Grants, New Mexico, and Capo and Chadwick (1999) near Las Cruces, New Mexico, of essentially 100 %. While these levels seem quite high, they are not anomalous, but typical (e.g., Kennedy et al. 1998; Chiquet et al. 1999; Naiman et al. 2000; Kurtz et al. 2001; Stewart et al. 2001; Dart et al. 2004; Reynolds et al. 2012; Lawrence et al. 2013). Recent NASA aerosol simulations graphically illustrate the variety of inputs to atmospheric strontium as well as their global character (e.g., Colarco et al. 2009; Putman and da Silva 2013).

One such study that illustrates the relevance of atmospheric inputs to archaeological mobility studies is that of Whipkey et al. (2000) in Hawaii. Oceanic basalts, which constitute Hawaii's geology, are characterized by low $^{87}Sr/^{86}Sr$ ratios: ca. 0.704. Whipkey's study found that 48–83 % of the soil strontium (0.706–0.708), and more than 90 % of plant strontium, was derived from atmospheric deposition of marine salts (0.709). Price and Gestsdottir (2006) did a human mobility study in Iceland, which is also oceanic basalt with $^{87}Sr/^{86}Sr$ of 0.704. All fauna and flora (0.706–0.707) are far above this ratio. A simple geologic isoscape cannot explain this discrepancy, but consideration of aerosol deposition of 0.709, as in the Hawaiian case, places the fauna within the labile soil range of Whipkey et al.

Soil $^{87}Sr/^{86}Sr$ at one location will be a complex function of differential weathering of bedrock and atmospheric inputs and thus vary with the age of the soil, depth, and seasonal factors such as rainfall and streamflow (e.g., Bain and Bacon 1994; Blum and Erel 1997; Capo et al. 1998; Stewart et al. 2001; Poszwa et al. 2004). This variation, of course, is reflected in the variation of the biosphere. We recently analyzed 13 different vegetables—all locally produced on the same farm in Dane County, Wisconsin—the $^{87}Sr/^{86}Sr$ of which ranged from 0.709 to 0.725. The data nonetheless have a strong central tendency of 0.711 ± 0.004, with much less variation than in the geosphere.

A final factor in the compression of intrinsic local $^{87}Sr/^{86}Sr$ variation to the narrow spread seen in humans is that strontium in the biosphere is logarithmically distributed. That is to say, in a typical mixed diet, one or two foods are likely to have orders of magnitude more strontium than others. Like the case for highly radiogenic minerals, foods low in strontium will not greatly affect the composite dietary $^{87}Sr/^{86}Sr$ ratio, which will likely be dominated by the items highest in strontium and will not be dependent upon the amounts of other items. This is illustrated in Fig. 3, showing the mass balanced $^{87}Sr/^{86}Sr$ ratio of a composite diet ratio for a simple binary mix of two items both from the same abovementioned farm: Meat (chicken, 0.3 ppm Sr at 0.7085) and a leafy vegetable (kale, 30 ppm Sr at 0.7099). Even at 90 % meat, the leafy vegetable dominates the isotope ratio of the composite diet. Regardless of the relatively large isotopic difference between the two items, and regardless of the actual amounts of the items, the ratio is essentially that of the kale.

As a further caveat about dietary $^{87}Sr/^{86}Sr$ variation, strontium assimilation from the diet competes with that of calcium. In high calcium diets less strontium is absorbed. As a result, the assimilated $^{87}Sr/^{86}Sr$ depends upon the calcium content of the various foods—and also whether they are eaten together or separately. If together, then the total dietary calcium is the same for each item and the assimilated $^{87}Sr/^{86}Sr$ is a simple strontium mass balance of the sources, as illustrated above. If eaten separately, however, the assimilated $^{87}Sr/^{86}Sr$ will be weighted against the calcium content of each food separately. While this effect is likely to be small, it should be recognized. For example, the first molar largely reflects that of milk,

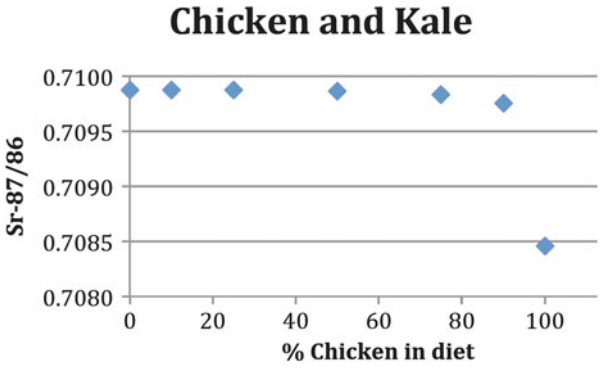

Fig. 3 Plot of dietary $^{87}Sr/^{86}Sr$ for a two-component kale/chicken diet as a function of the percentage of each in the diet

during nursing, but the third molar, reflecting the adult diet, can be biased by itemized Sr/Ca ratios. Thus, a small M1/M3 difference need not reflect mobility during youth, as some current studies presume.

Another difficulty in relating human $^{87}Sr/^{86}Sr$ to a specific locus is that, while human enamel $^{87}Sr/^{86}Sr$ is incontestably derived from diet, diet items need not be local. It's probably the rare exception, rather than the rule, for humans to obtain their food solely from a single geographic region. Mobile cultures seasonally exploited diverse ecological regions that include forest and grassland items, freshwater resources, and seafood as well as local vegetation (e.g., Kelly 1983). More sedentary people can obtain imported dietary items, if not through direct procurement, through trade and in markets.

An example of the influence of nonlocal dietary items on mobility studies is the investigation of Wright (2005) at Tikal, a Maya site in northern Belize. Wright estimated from the earlier geological measurements of Hodell et al. (2004) that local human values should be somewhere between 0.7078 and 0.7081, "assuming that they consumed only locally grown foods and were not highly mobile." Measurements of rodents (0.7079) and snails (0.7078) from Tikal yielded values consistent with this. Nonetheless, Tikal human samples, which represent many centuries, are significantly higher in $^{87}Sr/^{86}Sr$ (0.7081) than are the fauna, with a broad range 0.7077–0.7085, even after removing outliers and trimming the "locals" to a normal distribution. A strict interpretation based on the "biologically available" ratios represented by either the fauna or the geology would lead to the absurd interpretation that only a small minority of the population were born in the vicinity. It was clear to Wright that the normal distribution of the samples must represent the value of the local population. Wright then inferred that some extra-local item must have been elevating this above the faunal value. Wright postulated that sea salt, known to be imported from the north coast (Andrews 1983), was responsible and calculated that approximately 6 g of salt per day, even against high-strontium, cal-treated maize, would suffice to elevate the human ratios beyond the faunal values.

An analogous result was obtained in the aforementioned Iceland study of Price and Gestsdottir (2006), in which faunal and floral values (0.707) were far above geological values (0.704), and the majority of human data (0.709) were likewise far above the faunal and floral ratios. Paradigmatic use of the fauna for the "local" biological ratio would yield an absurd result that only a minority of the residents of Iceland were actually born there. Aware of the results of Wright, they concluded that the pronounced mode in the human data actually represented the true "local" value for the humans and proposed that this was elevated above the faunal/floral ratios due to the inclusion of seafood (0.709) in the diet.

Finally, while local foods can have considerable isotopic variation and humans need not have exclusively local diets, the $^{87}Sr/^{86}Sr$ variation in humans from a single location is nonetheless demonstrably extremely low, on the order of ± 0.0003 (Burton and Price 2013). And, clearly, measurement of dental $^{87}Sr/^{86}Sr$ ratios can be used to identify extra-local individuals and sometimes to identify origin locations. If geologic ratios are too variable and "bioavailable" measurements of fauna

and flora can have significantly offset ratios, how do we decide what is the ratio for locally born residents? This will necessarily depend on the situation case by case, but, in the absence of evidence that the majority of the people are extra-local, we can parsimoniously posit that the majority of the individuals in a collection are local, especially if there is some time depth to the collection. This is to say that the central tendency of the data, best represented by the most prominent mode, is, empirically, the local ratio for the humans. This seems to be the implicit, de facto approach in many studies anyhow: data are commonly plotted as a bar chart ranked from lowest to highest $^{87}Sr/^{86}Sr$ in the search for a flat plateau—i.e., a principal mode—in the data. In both the Iceland study of Price and Gestsdottir and the Tikal study of Wright, the discrepancies between human data and the faunal/geologic data were resolved by presuming that the major modes must be the values for local humans. Of course, there will also be situations such as mass migrations, major battlegrounds, or cemeteries with many reburials in which the majority of the individuals need not be local, but a modal approach might help resolve groups of different origins.

Conclusion

The use of strontium isotopes to determine geographic origins of humans is now a popular method that typically involves comparing isotope ratios in human dental enamel to "local" isotope ratios inferred from geological data or from the analysis of biological materials. While the utility of isotopes is beyond debate, we should consider exactly what human isotope ratios are measuring. Specifically, we should evaluate patterns or processes that might be involved in food procurement, the specific dietary sources of strontium, how and when they are incorporated into calcified tissues, and how human cultural practices might affect these factors. Without such consideration, the use of geological and "bioavailable" proxies for human isotope ratios can lead to demonstrably wrong, even absurd, inferences of locality and mobility. Because we are beginning to accumulate large sets of human data, we can also begin to make inferences about mobility and geographic origins directly, empirically, from the human data as prima facie data, without such proxy information.

References

Andrews AP (1983) Maya salt production and trade. The University of Arizona Press, Tucson

Bain DC, Bacon JR (1994) Strontium isotopes as indicators of mineral weathering in catchments. Catena 22:201–214

Blum JD, Erel Y (1997) Rb-Sr isotope systematics of a granitic soil chronosequence: the importance of biotite weathering. Geochim Cosmochim Acta 61:3193–3204

Burton JH, Price TD (2013) Seeking the local $^{87}Sr/^{86}Sr$ ratio to determine geographic origins of humans: no easy answers. In: Armitage RA, Burton JH (eds) Archaeological chemistry VIII. American Chemical Society, Washington, DC, pp 309–320

Capo RC, Chadwick OA (1999) Sources of strontium and calcium in desert soil and calcrete. Earth Planet Sci Lett 170:61–72

Capo RC, Stewart BW, Chadwick OA (1998) Strontium isotopes as tracers of ecosystem processes: theory and methods. Geoderma 82:197–225

Chiquet A, Michard A, Nahon D, Hamelin B (1999) Atmospheric input vs. in situ weathering in the genesis of calcretes: an Sr isotope study at Galvez (Central Spain). Geochim Cosmochim Acta 63:311–323

Colarco P, da Silva A, Chin M, Diehl T (2009) Online simulations of global aerosol distributions in the NASA GEOS-4 model and comparisons to satellite and ground-based aerosol optical depth. J Geophys Res 115:D14207

Dart RC, Wittwer PD, Barovich KM, Chittleborough DJ, Hill SM (2004) Strontium isotopes as an indicator of the source of calcium for regolith carbonates. In: Roach IC (ed) Regolith. CRC LEME, Adelaide, SA, pp 67–70

Davidson J, Charlier B, Hora JM, Perlroth R (2005) Mineral isochrons and isotopic fingerprinting: pitfalls and promises. Geology 33:29–32

Ericson JE (1985) Strontium isotope characterization in the study of prehistoric human ecology. J Hum Evol 14:503–514

Faure G (1986) Principles of isotope geology. Wiley, New York

Graustein WC, Armstrong RL (1983) The use of strontium-87/strontium-86 ratios to measure atmospheric transport into forested watersheds. Science 219:289–292

Haeberlin Y (2002) Geology and structural setting, age, and geochemistry of the orogenic gold deposits at the Pataz Province, Eastern Andean Cordillera, Peru. Thesis, University of Geneva, Earth Sciences Department of Mineralogy

Hodell DA, Brenner M, Kamenov G, Quinn R, Anton SC (2004) Spatial variation of strontium isotopes ($^{87}Sr/^{86}Sr$) in the Maya region: a tool for tracking ancient human migration. J Archaeol Sci 31:585–601

Kelly RL (1983) Hunter-gatherer mobility strategies. J Anthropol Res 39:277–306

Kennedy MJ, Chadwick OA, Vitousek PM, Derry LA, Hendricks DM (1998) Changing sources of base cations during ecosystem development, Hawaiian Islands. Geology 26:1015–1018

Kurtz AC, Derry LA, Chadwick OA (2001) Accretion of Asian dust to Hawaiian soils: Isotopic, elemental, and mineral mass balances. Geochim Cosmochim Acta 65:1971–1983

Lawrence CR, Reynolds RL, Ketterer ME, Neff JC (2013) Aeolian controls of soil geochemistry and weathering fluxes in high-elevation ecosystems of the Rocky Mountains, Colorado. Geochim Cosmochim Acta 107:27–46

Miller OL, Solomon DK, Fernandez DP, Cerling TE, Bowling DR (2014) Evaluating the use of strontium isotopes in tree rings to record the isotopic signal of dust deposited on the Wasatch Mountains. Appl Geochem 50:53–65

Naiman Z, Quade J, Patchett PJ (2000) Isotopic evidence for eolian recycling of pedogenic carbonate and variations in carbonate dust sources throughout the southwest United States. Geochim Cosmochim Acta 64:3099–3109

Naylor RS, Steger RH, Wasserburg GJ (1970) U-Th-Pb and Rb-Sr systematics in 2700 × 106-year old plutons from the southern Wind River Range, Wyoming. Geochim Cosmochim Acta 34:1133–1159

Poszwa A, Ferry B, Dambrine E, Pollier B, Wickman T, Loube M, Bishop K (2004) Variations of bioavailable Sr concentration and $^{87}Sr/^{86}Sr$ ratio in boreal forest ecosystems: role of biocycling, mineral weathering and depth of root uptake. Biogeochemistry 67:1–20

Price TD, Gestsdottir H (2006) The first settlers of Iceland: an isotopic approach to colonization. Antiquity 80:130–144

Putman W, da Silva A (2013) Simulating the transport of aerosols with GEOS-5 http://gmao.gsfc.nasa.gov/research/aerosol/modeling/nr1_movie/. Accessed Jan 2015

Reynolds AC, Quade J, Betancourt LL (2012) Strontium isotopes and nutrient sourcing in a semi-arid woodland. Geoderma 189–190:574–584

Stewart BW, Capo RC, Chadwick OA (2001) Effects of rainfall on weathering rate, base cation provenance, and Sr isotope composition of Hawaiian soils. Geochim Cosmochim Acta 65:1087–1099

Van der Hoven S, Quade J (2002) Tracing spatial and temporal variations in the sources of calcium in pedogenic carbonates in a semiarid environment. Geoderma 108:259–276

Wetherill GW (1975) Radiometric chronology of the early solar system. Ann Rev Nucl Sci 25:283–328

Whipkey CE, Capo RC, Chadwick OA, Stewart BW (2000) The contribution of sea spray aerosol to the soil cation budget in a Hawaiian coastal environment. Chem Geol 168:37–48

Wright LE (2005) Identifying immigrants to Tikal, Guatemala: defining local variability in strontium isotope ratios of human tooth enamel. J Arch Sci 32:555–566

Determination of Geo-dependent Bioavailable $^{87}Sr/^{86}Sr$ Isotopic Ratios for Archaeological Sites from the Inn Valley (Austria): A Model Calculation

Frank Söllner, Anita Toncala, Stefan Hölzl, and Gisela Grupe

Introduction

Numerous attempts have been made for an assessment of local bioavailable $^{87}Sr/^{86}Sr$ isotopic ratios, the knowledge of which is essential for the determination of local or primarily non-local bio-archaeological finds at a site. The majority of these investigations focus on the comparison of measured stable strontium isotopic ratios in archaeological bones and teeth with those of the regional geology (e.g. Grupe et al. 1997; Müller et al. 2003; Tütken 2010). It has only occasionally been attempted to introduce other factors such as water and vegetation into the discussion on local bioavailable $^{87}Sr/^{86}Sr$ isotopic ratios (see Drouet et al. 2005; Xin and Hanson 1994). Our study tries to integrate all relevant factors which mix in the consumer's tissues, be it man or animal. Vertebrates ingest strontium with their food and drinking water, whereby the strontium isotopic ratio of plants is influenced to a major degree by the respective ratio of the atmosphere and the soluble mineral soil components.

We undertook detailed re-investigations of several archaeological sites to establish a firm basis for model calculations of local bioavailable strontium isotopic signals, which are in turn based on mixing models integrating strontium isotopic ratios and strontium concentrations of the relevant parameters water, soil, and vegetation (Faure and Mensing 2005; Grupe et al. 2011). The first data sets, the results of which are presented in this chapter, concentrate on the Inn Valley, part of

F. Söllner (✉)
Department für Geo- und Umweltwissenschaften, Ludwig-Maximilians-Universität München, Munich, Germany, private:, Höhenstr. 12, 82229, Seefeld, Germany
e-mail: frank.soellner@hotmail.de

A. Toncala • G. Grupe
Ludwig-Maximilians-Universität München, Biozentrum, Grosshaderner Str.2, 82152 Martinsried, Germany

S. Hölzl
RiesKraterMuseum Nördlingen, Eugene-Shoemaker-Platz 1, 86720 Nördlingen, Germany

G. Grupe, G.C. McGlynn (eds.), *Isotopic Landscapes in Bioarchaeology*,
DOI 10.1007/978-3-662-48339-8_7

the archaeologically highly relevant transalpine Inn-Eisack-Etsch-Brenner passage (see www.for1670-transalpine.uni-muenchen.de). It was expected that the model calculation should lead to more reliable results with regard to the determination of place of origin of individual finds, which are hitherto frequently fraught with ambiguity.

It should be stressed, however, that model calculations alone do not permit the assessment of the reliability and correctness of this method. It is necessary to test and control the calculated data by analysis of $^{87}Sr/^{86}Sr$ isotopic ratios in archaeological vertebrate bone finds from the respective sites. Here, three species were chosen: domestic cattle (*Bos taurus*), domestic pig (*Sus domestica*), and red deer (*Cervus elaphus*). Taken all data together, a reliable image of the local, geo-dependent bioavailable $^{87}Sr/^{86}Sr$ isotopic ratio emerges. This is in turn indispensable for any attempt to quantify immigrant people or imported animals (or animal parts/raw material) at a site to firmly distinguish mobility from migration and trade.

Material: Samples and Site Description

Between 2013 and 2014, groundwater (naturally composed of atmospheric and soil conditioned components), "weathered soil" (comparable to acid leached soil), and vegetation from selected archaeological sites throughout the Inn Valley were sampled during several field excursions (Fig. 1). Soil samples were taken from the archaeological strata of the chosen sites to establish a baseline soil composition in order to correctly assess the growth of past and wild cultivated plants as closely as possible. Care was taken to exclude possible influences of modern fertilisers. Soil samples were subjected to a leaching step prior to analysis (see below; see also Drouet et al. 2005). Groundwater was taken from neighbouring springs or wells and therefore consists of both precipitation (rain water) and surface water, enriched with soil components. Unfortunately, no archaeological plant material was available for analysis. Modern vegetation samples were therefore taken directly from the location of the soil sample. To avoid species-specific peculiarities, hazelnut branches (*Corylus avellana*) were sampled because of their availability at nearly every site (Göhring 2014).

The following archaeological sites were chosen:

Fritzens Pirchboden *(Code Number 206)* The Pirchboden is a hill site located above the town of Fritzens, the type locality of the Fritzens-Sanzeno culture (sixth century BC; Lang 1998). The archaeological soil consists of argillaceous sand, light brown with crystalline components of boulder pavement of varying size, definitely of moraine origin ($^{87}Sr/^{86}Sr = 0.714$, profile depth = 100–110 cm). Branches of hazelnut were sampled, and spring water from a nearby well.

Innsbruck-Mühlau, Kalvarienberg *(Code Number 215)* The soil was taken from the sidecut of a road. It consists of brown rendzina with calcareous fragments and some crystalline pebbles ($^{87}Sr/^{86}Sr = 0.70876$, profile depth = 25–30 cm). It was

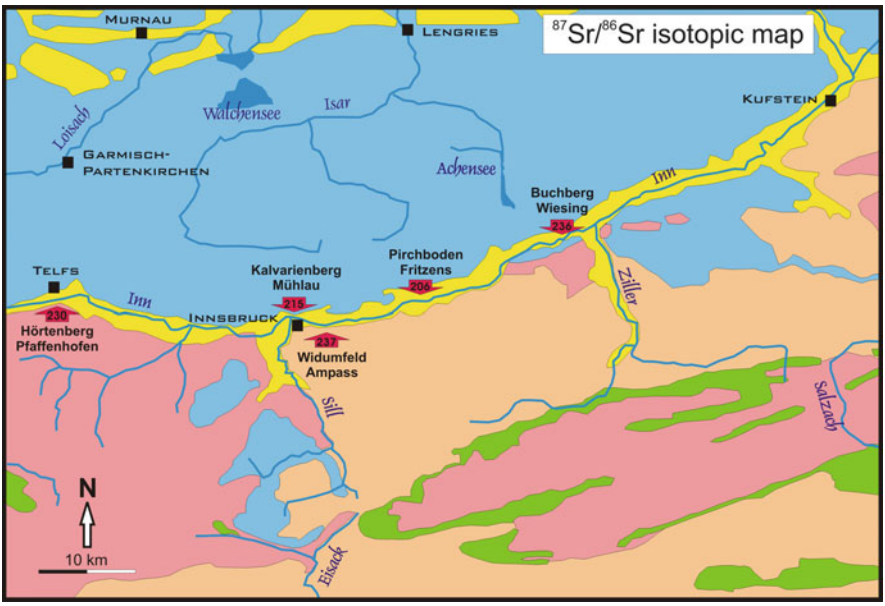

Fig. 1 $^{87}Sr/^{86}Sr$ isotopic map of the Inn Valley between the cities of Telfs and Kufstein. The investigated archaeological sites are marked with numbers. The Inn Valley is one of the largest East–west extending valleys of the Alps filled with glacial and fluviatile sediments (*yellow*), occasionally cut through by tertiary sandy outcrops. Moraine and fluviatile sediments of the Inn Valley prevalently enriched with crystalline rocks have mixed $^{87}Sr/^{86}Sr < 0.709$–0.7135. The Inn Valley forms the boundary between the Northern Calcareous Alps (*blue*, various types of calcareous rocks, $^{87}Sr/^{86}Sr = 0.707$–0.709) and the Central Alps which are made primarily of crust-dominated crystalline rocks (*pink*—of acid magmatic origin, and *beige*—of sedimentary and acid volcanic origin, $^{87}Sr/^{86}Sr > 0.71$). Lacustrine sediments, partly of tertiary age and often positioned on high Inn terraces underlain by crystalline rocks, have $^{87}Sr/^{86}Sr$ ratios > 0.7135. Mantle-dominated rocks are shown in *green* ($^{87}Sr/^{86}Sr < 0.707$)

covered by landslide material interspersed with carbonate fragments only. Vegetation (hazelnut branches) and water from a well were sampled next to church at the Kalvarienberg.

Pfaffenhofen/Ilm, Hörtenberg *(Code Number 230)* The Hörtenberg is a conspicuous hill near the town of Pfaffenhofen and is composed of quartz-phyllite. The Iron Age archaeological site (Fassbinder 2010) is located at the northern hill slope near the "Maierhof" farm. The soil sample was taken from a road sidecut, 100 cm below surface. It consists of grey soft clay ($^{87}Sr/^{86}Sr = 0.72533$, profile depth 100–130 cm), whereby the whole fine-grained loamy profile intercalated with chalk bands suggests a lacustrine sequence. The vegetation sample again consists of hazelnut branches; spring water originates from a well inside the "Maierhof" farm.

Wiesberg Buchberg *(Code Number 236)* The Buchberg is a conspicuous hill built by Triassic carbonate rocks overlain by glacial sediments loaded with rounded

crystalline components, and was once a Bronze Age settlement site (Pöll 2014). The archaeological soil sample consists of sandy silt ($^{87}Sr/^{86}Sr = 0.71081$, profile depth = 50–60 cm). The vegetation sample is hazelnut; spring water originates from a fountain in the nearby village of Jenbach.

Ampass Widumfeld *(Code Number 237)* The Widumfeld is located east of the town of Ampass and is of archaeological relevance from the Iron Age until Roman times (Tomedi et al. 2001; Castellan and Tomedi 2006). The soil sample ($^{87}Sr/^{86}Sr = 0.71736$, profile depth 50–60 cm) contains small pebbles of quartz-phyllite and probably relates to an argillaceous sandy valley or lake filling from post-Roman times. We assume that the sediment source has remained similar during post-glacial times and that no fundamental change in strontium isotopic ratios of the reservoir has taken place. Again, vegetation samples consist of hazelnut branches; spring water originates from the nearby forest.

Analytical Methods

Bone The surfaces of the bone samples were manually removed by grinding, and the remaining sample was washed ultrasonically in distilled water until the water remained clear. The air-dried sample was then defatted with diethylether for 5 h in a Soxhlet, air-dried and etched ultrasonically with HCOOH (98 %) for 5 min. Finally, the sample was washed in distilled water until the wash solution reached a pH of 5–6. The air-dried sample was then ashed for 12 h at 800 °C in a muffle furnace and homogenised to a fine powder. This bone meal was dissolved in 1 mL concentrated HNO_3 (65 %) on a hot plate at 100 °C and dried. For the column separation, the sample was dissolved in 1 mL 6 N HNO_3. This solution was used for the separation of the strontium fraction for the isotopic analysis by mass spectrometry, after a chromatographic column separation by use of Sr SPEC resin. All acids were of ultrapure quality. Distilled water was always of doubly distilled quality.

Water 1.5 L water was filtered through an MN 615 filter (if necessary). Ten millilitre of the sample was then evaporated to dryness and dissolved for 14 h in 65 % HNO_3 in a Teflon beaker on a hot plate at 100 °C, followed by a chromatographic column separation (see above).

Soil The soil samples were dried and sieved with a 500 μm sieve. Three hundred milligram of this sample was dissolved in a Teflon beaker in 2 mL 35 % HCl (suprapure) for 12 h at 120 °C, cooled to room temperature and centrifuged at 11,000 rpm for 10 min. The clear solution was separated and evaporated to dryness, followed by a chromatographic column separation (see above).

Wood From 150 mg of hazelnut wood each, only the annual rings were analysed; all other parts were removed mechanically. The wood was dried at 80 °C in an oven to constant weight, and then ashed for 12 h at 800 °C. Four hundred milligram of the ash was processed by chromatographic column separation (see above).

Mass Spectrometry $^{87}Sr/^{86}Sr$ was analysed with a Thermal Ionisation Mass Spectrometer Finnigan MAT 261.5 on single tungsten filaments. Significant extant Rb was evaporated from the loaded filament by controlled preheating before the isotopic Sr composition was measured. For quality control and to check for the proper operation of the mass spectrometer, a certified reference material was measured under the same conditions as the samples ($SrCO_3$, NIST SRM 987, $^{87}Sr/^{86}Sr$: 0.710210 ± 0.000056 STD, $n = 110$). Isotope mass fractionation during analysis was corrected by referencing to an invariant $^{88}Sr/^{86}Sr$ value of 8.37521. Total analytical uncertainty (precision + accuracy) for $^{87}Sr/^{86}Sr$ on natural samples is assumed to be <50 ppm. Standard Reference Material SRM 1400 "Bone ash" (NIBS, Washington DC) was used with regard to the wet ashing and Rb–Sr separation. Measurement precision was ± 0.00001.

Strontium Mixing Model for the Assessment of Local Geo-dependent Bioavailable $^{87}Sr/^{86}Sr$ Isotopic Ratios in Archaeological Fauna

Humans and animals ingest strontium with food and drinking water hence strontium from these sources with their source-specific isotopic ratio mixes in the consumer's body. The $^{87}Sr/^{86}Sr$ isotopic ratio in a consumer's tissue is therefore always a mixed isotopic ratio. In plants, $^{87}Sr/^{86}Sr$ is largely due to the atmospheric water and the solubilised mineral component in soil. It became obvious in the course of our research that local faunae and florae are not supplied with a uniform water composition, but that the mix of groundwater [groundwater X(wat) and ocean or rainwater X(atm)] could exhibit completely different values (see Fig. 2).

Chosen end members for the water composition are those of the North Atlantic ocean water ($^{87}Sr/^{86}Sr(atm) = 0.709024$, $Sr(atm) = 0.0013$ ppm; Veizer 1989) and of the locally sampled groundwater X(wat), respectively. Groundwater can be described as rainwater, the composition of which has been altered by solubilised mineral components in the soil. It is necessary to stress that no surface water has been sampled for this study, but rather water from shallow fountains (5–6 m maximum) or from springs near their bottom. Due to the residence time of the water in the soil, a measurable uptake of mineralogical components which are clearly related to the parent rock is evidenced (Table 1).

For an assessment of the other components contributing to the mixed isotopic ratio measured in the consumer's skeleton, soil and vegetation samples were taken and measured. Soil was sampled from the archaeological sites at a level equivalent to the surface at the time of the prehistoric settlement whenever possible. This way, the strontium isotopic ratio of such soil was measured that had once driven the prehistoric plant growth and was introduced into the prehistoric food chain. The soil samples were processed and leached to access a $^{87}Sr/^{86}Sr$ ratio comparable to the former bioavailable one. Since no archaeological plant material was available,

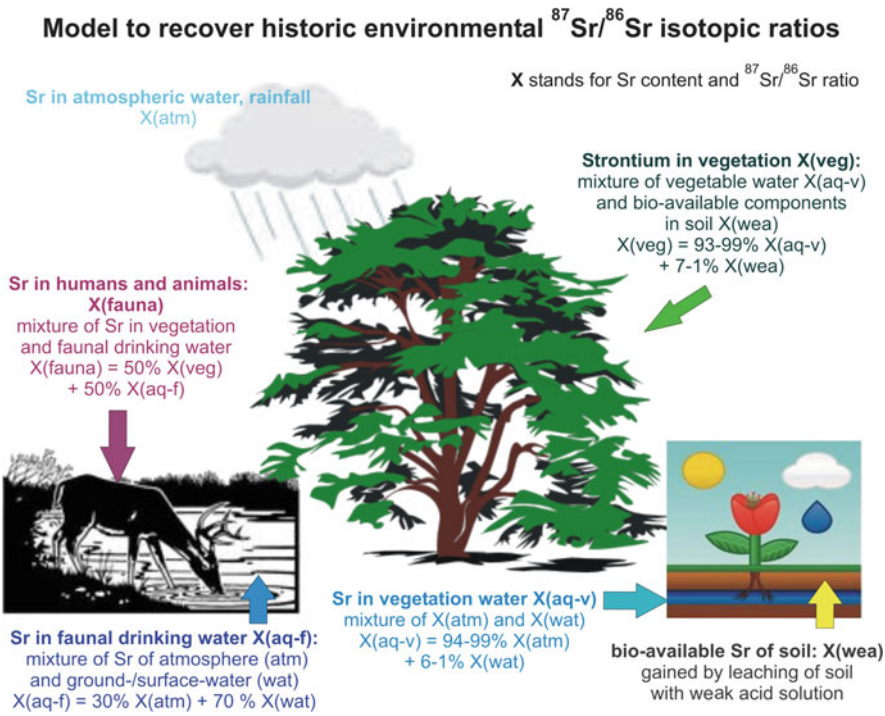

Fig. 2 Scheme for the recovery of local geo-dependent $^{87}Sr/^{86}Sr$ isotopic ratios. In this model, strontium from soil, vegetation, and water is analysed to evaluate the bioavailable $^{87}Sr/^{86}Sr$ isotopic ratio which characterises the place of residence in historical times (see text)

modern hazelnut was chosen not only because it was abundant at most of the former archaeological localities, but especially because the main roots reach into a depth of 30–40 cm and thus below the agricultural horizon.

For this pilot study, five archaeological sites from the Inn Valley were chosen, whereby the local geology is characterised by lacustrine-fluviatile sediments (sites nos 230 and 237), or by glacial sediments of the last glaciation period (sites nos 206 and 236). In contrast, the Innsbruck/Mühlau Kalvarienberg site (no 215) exhibits a soil composition which is best described as weathered soil on carbonate rock (rendzina). Archaeozoological remains of the three vertebrate species mentioned above were available from all five sites.

For the calculation of the local bioavailable $^{87}Sr/^{86}Sr$ isotopic ratio which should be reflected in the skeleton of residential animals (and also in humans; see Table 2 in the appendix), the following published data were used:

For the atmospheric water component *X*(atm), we took the $^{87}Sr/^{86}Sr$ ratio and the strontium content of modern ocean water (0.709024 ± 0.000032; Veizer 1989). Other values published by e.g. Graustein and Armstrong (1983) or Dupré et al. (1994) are influenced by aerosol and dust particle burdens (Xin and Hanson

Table 1 Measured $^{87}Sr/^{86}Sr$ isotopic ratios in archaeological animal bone finds, and calculated geo-dependent $^{87}Sr/^{86}Sr$ ratios, affected by local parameters of water, soil, and vegetation

Sample no.	Locality	Groundwater			Hazelnut			Soil leached	
		$^{87}Sr/^{86}Sr$(wat) measured	STDev	f(atm,aq-v)[a] in %	$^{87}Sr/^{86}Sr$(veg) measured	STDev	f(aq-v, veg)[b] in %	$^{87}Sr/^{86}Sr$(wea) measured	STDev
206	Pirchboden Fitzens	0.710884	0.0001	96	0.713703	0.000046	92.8	0.714[c]	0.000073
215	Kalvarienberg Mühlau/Innsbruck	0.70799	0.000142	99.5	0.708756	0.000043	99.9	0.708384	0.000139
230	Hörtenberg Pfaffenhofen/Inn	0.715413	0.000124	94	0.713103	0.000046	99.9	0.725331	0.000027
236	Buchberg Wiesing/Inn	0.710884[f]	0.0001[f]	96	0.71046	0.000059	99.9	0.716711	0.000068
237	Widumfeld Ampass	0.716387	0.000065	95	0.716514	0.000076	96.4	0.717355	0.0001

Sample no.	Localised						Local animal bone findings		
	$^{87}Sr/^{86}Sr$ (fauna) calculated	$^{87}Sr/^{86}Sr$ (fauna) STDev (mean)	+Cut-off calculated error	−Cut-off calculated error	+Cut-off adopted+ 0.001	−Cut-off adopted− 0.001	$^{87}Sr/^{86}Sr$ pig (bone)	$^{87}Sr/^{86}Sr$ cow (bone)	$^{87}Sr/^{86}Sr$ deer (bone)
206	**0.71254**	0.000781	0.715083	0.710398	**0.71354**	**0.71154**	0.710892[d] **0.713180**[e] 0.710987	0.714179, **0.711711**	
215	**0.708032**	0.000078	0.708368	0.7079	**0.709032**	**0.707032**	0.709437 0.710142 0.713157	0.709928 0.710964 0.709271	
230	**0.714913**	0.000604	0.716264	0.712638	**0.715913**	**0.713913**		**0.714405** **0.715243** 0.716443	

(continued)

Table 1 (continued)

Sample no.	Localised						Local animal bone findings		
	$^{87}Sr/^{86}Sr$ (fauna) calculated	$^{87}Sr/^{86}Sr$ (fauna) STDev (mean)	+Cut-off calculated error	−Cut-off calculated error	+Cut-off adopted+ 0.001	−Cut-off adopted− 0.001	$^{87}Sr/^{86}Sr$ pig (bone)	$^{87}Sr/^{86}Sr$ cow (bone)	$^{87}Sr/^{86}Sr$ deer (bone)
236	**0.710807**	0.000174	0.711254	0.710214	**0.711807**	**0.709807**	**0.711722** 0.712871 **0.711522**	0**.711136** 0.712383 **0.709828**	
237	**0.716342**	0.000043	0.716551	0.716294	**0.717342**	**0.715342**	**0.716362** **0.716544** **0.716576**	**0.716648** **0.716429** **0.716634**	**0.716071** **0.716724**

[a]Abundance of atmospheric water in vegetation water (water absorbed from vegetation, ca. 95 % is assumed)
[b]Abundance of vegetation water in vegetation (correlated with f(atm, aq-v), ≤100 % is precondition)
[c]Isotopic ratio is estimated, according to soil type
[d]Normal: isotopic ratio lies outside the cut-off range (sample is non-local)
[e]Bold: isotopic ratio lies inside the cut-off range (sample is local)
[f]Isotopic ratio is that of sample 206
For the cut-off values, a fixed value (±0.001) was used, see text

1994). Strontium concentrations in precipitation can be highly variable but usually do not exceed 1 ppb (Xin and Hanson 1994). For Central Belgium, Drouet et al. (2005) measured a mean concentration of 1.1 ± 0.3 ppb ($n = 9$). For our model calculation, we took an atmospheric strontium concentration Sr(atm) of 0.0013 ppm. This value correlates with that of sample BP1 determined from a post-glacial environment in Central Belgium (Drouet et al. 2005).

$^{87}Sr/^{86}Sr$ of groundwater *X*(wat) was measured; the strontium content was estimated. Both the stable strontium isotopic ratio and the strontium content of groundwater adjust to the respective local geological settings dependent on the residence time in the soil. Xin and Hanson (1994) published measurements of both soil and groundwater in the Peconic river watershed (New York) and found $^{87}Sr/^{86}Sr$ isotopic ratios between 0.71 and 0.7113 and strontium contents between 25 and 34 ppb. It is obvious that both the strontium concentration and the strontium isotopic ratio adjust to the geological conditions according to the residence time below ground (Voerkelius et al. 2010). For Denmark, Frei and Frei (2011) published decreasing mean strontium concentrations between 1 and 0.125 ppm for surface water with a $^{87}Sr/^{86}Sr$ variability between 0.708 and 0.711. Accordingly, we chose a strontium concentration of 0.06 ppm for carbonatic water with a $^{87}Sr/^{86}Sr$ isotopic ratio <0.709, 0.03 ppm Sr for soils with a $^{87}Sr/^{86}Sr$ isotopic ratio between 0.709 and 0.7135, and 0.02 ppm Sr for soils with a $^{87}Sr/^{86}Sr$ ratio >0.7135.

With these isotopic and concentration data, the stable strontium isotopic ratio of the water consumed by the fauna [drinking water *X*(aq-f)] can be calculated. We suggest that the proportion of atmospheric water f(atm,aq-f) in the drinking water averages 30 %. This percentage correlates with the one calculated from data of Xin and Hanson (1994) as a mixture of soil water (10–50 cm depth) and atmospheric (rain) water component.

With regard to the strontium concentrations in soil [Sr(wea)] and the frequency distribution of the water components in the atmosphere [f(atm, aq-f)], and the fauna [(aq-f, fauna)], variations of 50 % were assumed. Standard deviations (STDev) were taken into account with regard to the measurement error. To present an example, the complete model calculation is shown in Table 2 (see appendix) for sample no. 230 and visualised by the resulting mixing diagram (Fig. 3).

It is depicted from Fig. 3 that the data points for drinking water *X*(aq-f) and the sampled groundwater *X*(wat) plot closely together (*X* stands for both the isotopic ratio and the strontium concentration of the respective components). With regard to this position in the mixing diagram, drinking water cannot combine with the measured soil components *X*(wea) to the strontium mixing in the vegetation *X*(veg). Consequently, the water taken up by the vegetation must have a composition different from that of the drinking water of the fauna. The vegetation water *X*(aq-v) should rather plot at the intersection of the mixing lines groundwater *X*(wat)—atmospheric water *X*(atm) and soil *X*(wea)—vegetation *X*(veg) (Fig. 3). The calculated data for the vegetation water in Fig. 3 are $^{87}Sr/^{86}Sr(aq\text{-}v) = 0.712189$

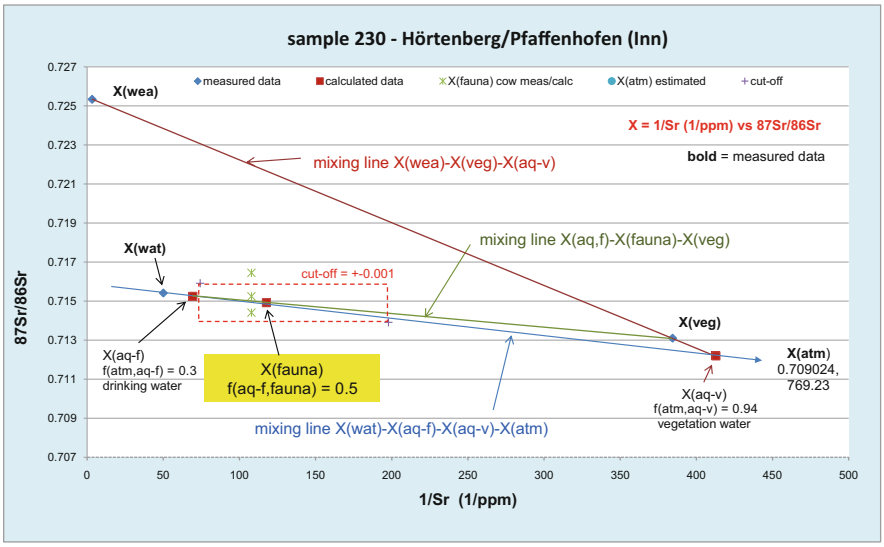

Fig. 3 The mixing diagram illustrates the mixing of three components with different strontium contents and different stable strontium isotopic ratios: groundwater *X*(wat), leached soil *X*(wea), and vegetation *X*(veg). *Straight lines* represent the non-linear mixing of the respective end members. *X*(aq-v) = vegetation water is a mixture of groundwater *X*(wat) and rain/atmospheric water *X*(atm) with a proportion f(atm, aq-v) of 94 %. *X*(aq-f) = drinking water is a mixture of the same components with a proportion f(atm, aq-f) of only 30 %. Strontium in vegetation [*X*(veg)] is made up of 99.9 % strontium from vegetation water *X*(aq-v) and only 0.1 % of strontium from soil water *X*(wea). The geo-dependent bioavailable strontium composition in faunal bone [*X*(fauna)] is a 1:1 mixture of strontium from drinking water *X*(aq-f) and from vegetation *X*(veg). All investigated samples reflect a far less abundance of strontium from soil than from the surrounding water component for the creation of the local bioavailable $^{87}Sr/^{86}Sr$ isotopic ratio than expected. Acronyms: see appendix

and Sr(aq-v) = 0.00242 ppm, whereby the atmospheric contribution to the vegetation water f(atm, aq-v) = 94 %. Note the nonlinear variation of f(atm, aq-v) along the straight mixing line in the diagram (see Faure and Mensing 2005). With a proportion f(aq-v, veg) of more than 99 %, the influence of the strontium component in vegetation water to the whole vegetation is remarkably high.

We would like to stress the dependencies between the proportion of rainwater in vegetation water [f(atm, aq-v)] and the proportion of vegetation water in the whole vegetation [f(aq-v, veg) = factor *K* (see Table 2). *K* is calculated by use of the strontium concentrations from vegetation, vegetation water, and leached soil. In the case of $K = 1$, data points *X*(veg) and *X*(aq-v) would plot in the same place, and a 100 % dependency of $^{87}Sr/^{86}Sr$ of the whole vegetation from $^{87}Sr/^{86}Sr$ in vegetation water would be the case. Since this is rather improbable, we chose an f(atm, aq-v) which renders $K < 1$ automatically. This way, f(atm, aq-v) declines to 0.94 (sample 230). But still, only 6 % of the $^{87}Sr/^{86}Sr$ ratio in the whole vegetation would be due to the soil component; 94 % would still stem from the water component.

While such a value seems to be very high, it is not unusual in nature (see e.g. Green et al. 2004; Grupe et al. 2011).

The strontium concentration of the leached soil Sr(wea), that of the vegetation water Sr(aq-v) and its abundance in the vegetation f(aq-v, veg) = 0.9994, permits the calculation of the strontium concentration in the vegetation Sr(veg) and results in 0.0026 ppm. This value, however, is far lower than some other published strontium concentrations in wood. Stem wood of different tree species had a mean concentration of about 5 ppm (Dijksta et al. 2003). Drouet et al. (2005) measured a mean concentration of 2.6 until 2.8 ppm for the genus *Fagus*, and Lambertz and Welling (2010) report a range of 1–10 ppm Sr in dry wood of various species. Just as in other tissues, Sr binds at Ca sites in plants which are mainly components of the cell wall (such as pectin acids, cellulose, and lignine; Torre et al. 1992), whereby the cellulose has a particularly low affinity to Ca and therefore also for Sr. Calculation of our model is performed under the assumption that in the course of mixing the components vegetation X(veg) and water X(aq-f) to form the Sr concentration in fauna X(fauna), the total Sr content of the vegetation is of no relevance but rather the bioavailable proportion of strontium only. We assume that it is only the strontium component which solubilised in the vegetation water is available to the consumer. This would in turn correspond to 0.05–0.1 % of the total strontium content of the plant.

Surprisingly, the calculated strontium concentration in animal bone [Sr(fauna)] is at first glance also very low (0.0085 ppm Sr according to the mixing diagram) and no longer comparable with the average total Sr content in bone (130–140 ppm; see Grupe et al. 1997). While the total Sr content in a bulk bone sample is the result of a long accumulation process lasting many years due to the long biological half-life of the apatite, the mixing diagram rather reflects the actual, time-dependent uptake in the course of the remodelling processes. Therefore, the resulting Sr content of 0.0085 ppm only is a function of the known slow remodelling of bone. Likewise, the low Sr content in vegetation which results from the mixing diagram is due to the time-dependent mineral uptake and precipitation into the plant tissue.

For an assessment of the local bioavailable and geo-dependent stable strontium isotopic ratio in vertebrate bone, possible strontium components provided by the diet are vegetation X(veg) and drinking water X(aq-f). Assuming that both components mix with the same proportion [f(aq-f, fauna) = 0.5], then the local $^{87}Sr/^{86}Sr$ isotopic ratio for the find with the code number 230 is 0.714913 (Table 2, appendix).

Table 2 also presents an error estimation for the data. For the measured $^{87}Sr/^{86}Sr$ ratios, the standard deviation of the measurement value was used, but no error estimation was carried out with regard to the Sr contents. Even a 100 % deviation only led to marginal changes. For the calculation of the proportion of the mixing components, a variation of 50 % was assumed with the exception of f(atm, aq-v), which varies between 0.1 and 2 %. A higher variation would be incompatible with the fact that K = f(aq-v, veg) must not exceed 1. For the sample no. 230, error estimation resulted in $^{87}Sr/^{86}Sr = 0.714913 \pm 0.000604$ (0.084 %, STDev, mean of errors).

Results

Table 1 presents the results obtained at all five sites chosen for this pilot study.

While it is highly plausible that the $^{87}Sr/^{86}Sr$ of the vegetation is largely due to the water that has been taken up by the plant, the low influence (1–6 %) of the bioavailable soil strontium component is surprising at first glance. This phenomenon is however particularly conspicuous when the $^{87}Sr/^{86}Sr$ isotopic ratios of groundwater and soil are significantly different from each other (see samples with the code numbers 230, 236). To relate the expected $^{87}Sr/^{86}Sr$ ratio in residential fauna to the bioavailable strontium isotopic ratio of the soil alone may therefore be totally misleading. Groundwater and vegetation indispensably need to be considered in addition.

The variability of local $^{87}Sr/^{86}Sr$ ratios in fauna defines the cut-off value which differentiates between local and non-local individuals. One possibility of defining this cut-off value is the traditional statistical way by use of the threefold error ($=3 \times STDev$). Other authors decided for a fixed value such as ± 0.001 (highly significant in terms of the measurement precision; see Grupe et al. 1997) which is also used in our study because on average, this value agrees well with the $3 \times STDev$ of the calculated $^{87}Sr/^{86}Sr$ ratios in fauna (Table 1; $3 \times STDev_{mean} = 0.00101$). By defining the cut-off values as $^{87}Sr/^{86}Sr(fauna) \pm 0.001$ this way, the variation of *calculated* $^{87}Sr/^{86}Sr$ of local vertebrates with the code number 230 would range from 0.713913 to 0.715913. The *measured* $^{87}Sr/^{86}Sr$ ratios in the three cattle bones from the site were 0.714405 ± 0.000135, 0.715243 ± 0.000264, and 0.716443 ± 0.000141 (± 2*STDev). The first two individuals should therefore have been of local origin; the third one can no longer be considered local.

Discussion

In sum, the analysis of archaeological animal bone finds and the modelled local, bioavailable $^{87}Sr/^{86}Sr$ isotopic ratios lead to the definition of three domains which correspond with the regional soil types (Fig. 4):

Domain 1: $^{87}Sr/^{86}Sr < 0.709$; brown calcareous soil, rendzina.
Domain 2: $0.709 \leq {}^{87}Sr/^{86}Sr \leq 0.7135$; moraine soil, often in hillside location, coarse detrital and mostly crystalline material.
Domain 3: $^{87}Sr/^{86}Sr \geq 0.7135$, fluvio-lacustrine sediments (silty alluvial deposits, fine sand and silt, lacustrine clay partly of tertiary origin).

The majority of the investigated animals exhibit $^{87}Sr/^{86}Sr$ isotopic ratios between 0.709 and 0.7135 and must have spent their lives on moraine soil. This was expected since the Inn Valley glacier had once been one of the largest glaciers in the whole alpine area, filling the Inn Valley to a depth of several hundred metres.

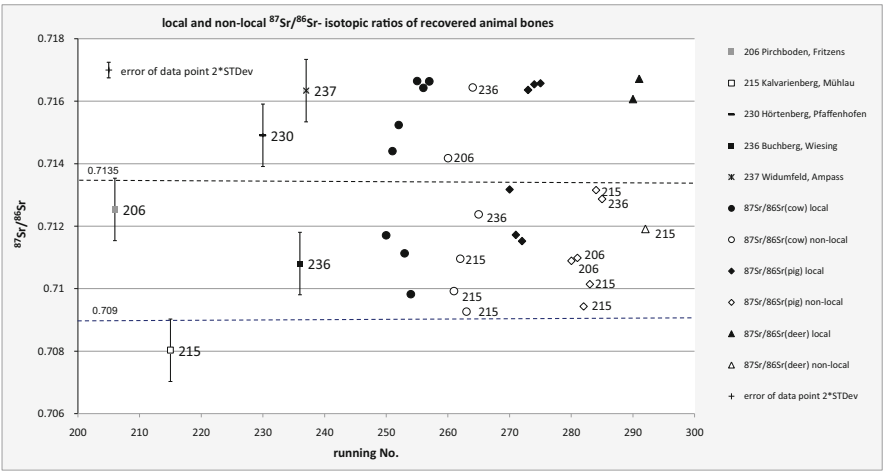

Fig. 4 Test of local or non-local origin of recovered animal bones from all five sites. Calculated local geo-dependent $^{87}Sr/^{86}Sr$ isotopic ratios are indicated by site code numbers with the corresponding cut-off error bar (±0.001). Marked domains of different isotopic ratios($^{87}Sr/^{86}Sr$ <0.709; 0.709–0.7135; >0.7135) correlate with local geological sediment/soil types (see text). Non-local animals according to the model calculation are numbered and marked in *white* and local animals in *black*

At other locations such as Pirchboden (code no. 206) and Buchberg (code no. 236), animals had been slaughtered which had obviously been raised elsewhere. A complete agreement of all data (calculated local $^{87}Sr/^{86}Sr$ isotopic ratio and measured ratios of cattle, pig, and red deer) was found at only one site (Widumfeld, Ampass, code no. 237), and no agreement at all was found between calculated and measured data for Innsbruck-Mühlau, code no. 215).

In sum, the model calculations permit for a much finer-scaled solution of isoscapes in the Inn Valley as the available geological map (Fig. 1). Furthermore, an association of single non-local bone finds to defined regions is possible beyond the mere detection of non-local finds by way of the exclusion principle.

Acknowledgements This study was financially supported by the Deutsche Forschungsgemeinschaft. Sample processing was performed by Anita Toncala and mass spectrometry was performed by Stefan Hölzl.

Appendix

Table 2 Model calculation of bioavailable geo-dependent Sr isotopic ratio

	Sr content in rainwater and atmospheric water	Sr content in groundwater (depends on soil type)	Abundance of rain water in drinking water	Sr content in drinking water, mixture of rain and groundwater (in ppm)	Sr isotopic ratio of atmospheric water	Groundwater	Groundwater error	Calculation parameter mixing line X(wat)−X (atm)		Sr isotopic ratio of drinking water, mixture of ground and rain water	Abundance of rain water in vegetable water	Sr content in vegetable water, mixture of rain and ground water (ppm)	Sr isotopic ratio in vegetable water	Sr isotopic ratio in vegetation (wood)	Vegetation error
	Input measured/estimated data						STDev				Normally about 0.95				STDev
	Sr(atm)	Sr(wat)	f(atm,aq-f)	Sr(aq-f)	$^{87}Sr/^{86}Sr$ (atm)	$^{87}Sr/^{86}Sr$ (wat)	$^{87}Sr/^{86}Sr$ (wat)			$^{87}Sr/^{86}Sr$ (aq-f)	f(atm,aq-v)	Sr(aq-v)	$^{87}Sr/^{86}Sr$ (aq-v)	$^{87}Sr/^{86}Sr$ (veg)	$^{87}Sr/^{86}Sr$ (veg)
	Estimated	Estimated	Estimated	Calculated	(Veizer 1989)	Measured	Measured	Slope	Intercept	Calculated	*Vary if K > 1*	Calculated	Calculated	Measured	Measured
Sample			Variation 50%			230–106	230–106				Variation 2 %			230–103	230–103
Two hundred and thirty mean Hörtenberg, Pfaffenhofen/Inn	0.0013	0.02	0.3	0.0144	0.709024	0.715413	0.000124	−8.883E-06	0.715857	0.715240	0.940	0.002422	0.712189	0.713103	0.000046
Estimated limit or calc./measured error			0.15	0.0172		0.715537		−9.056E-06	0.715990	0.715463	0.959	0.002070	0.711616	0.713149	
Estimated limit or calc./measured error			0.45	0.0116		0.715289		−8.711E-06	0.715725	0.714973	0.921	0.002774	0.712584	0.713057	

	Sr content in weathered (leached) soil in ppm	Sr isotopic ratio in weathered soil (acid-leachate), bioavailable component	Leached soil error	Calculation parameter mixing line X(wea)−X (veg)		Sr content in vegetation, time-dependent assimilated (ppm)	Abundance of vegetable water in the vegetation *K has to be ≤1*	Abundance of drinking water in the fauna	Calculation parameter mixing line X(veg)−X (aq-f)		Sr content in the fauna, time-dependent assimilated (ppm)	*Localised Sr isotopic ratio of the fauna (human and animal)*	Cut-off-value, calculated error	*Cut-off-value, estimated error*	
			STDev				*K*								
	Sr(wea)	$^{87}Sr/^{86}Sr$ (wea)	$^{87}Sr/^{86}Sr$ (wea)			Sr(veg)	f(aq-v,veg)	f(aq-f,fauna)			Sr(fauna)	$^{87}Sr/^{86}Sr$ *(fauna)*	Cut-off-value	*Cut-off-value*	
	Estimated	Measured	Measured	Slope	Intercept	Calculated	Calculated	Estimated	Slope	Intercept	Calculated	Calculated	Calculated	Estimated alternatively	
Sample	Variation 50 %	230–102	203–102					Variation 50 %							

Two hundred and thirty mean Hörtenberg, Pfaffenhofen/Inn	0.3	0.725331	0.000027	−3.209E-05	0.725438	0.00260	0.9994	0.5	−6.785E-06	0.715711	0.0085	**0.714913**	Cut-off=3x error	Cut-off= value±0.001	
Estimated limit or calc./measured error	0.45	0.725358		−2.858E-05	0.725422	0.00233		0.75	−6.234E-06	0.715826	0.0135	0.000450	0.716264	**0.715913**	
Estimated limit or calc./measured error	0.15	0.725304		−3.594E-05	0.725544	0.00288		0.25	−7.338E-06	0.715606	0.0051	0.000758	0.712638	**0.713913**	

f(atm,aq-f)—Abundance of atmospheric water (=rainwater) component in the drinking water
f(atm,aq-v)—Abundance of atmospheric water (=rainwater) component in the vegetable water
f(aq-v,veg)—Abundance of vegetable water component in the vegetation
f(aq-f,fauna)—Abundance of drinking water component in the fauna
$^{87}Sr/^{86}Sr$(atm)—Sr isotopic ratio in the atmosphere (ocean water, rainwater, taken from literature)
$^{87}Sr/^{86}Sr$(wat)—Sr isotopic ratio in the groundwater (sampled water from wells or groundwater horizon)
$^{87}Sr/^{86}Sr$(aq-f)—Sr isotopic composition of drinking water (mixture of rain and groundwater) incorporated into fauna
$^{87}Sr/^{86}Sr$(aq-v)—Sr isotopic composition of vegetable water (mixture of rain and groundwater) assimilated in vegetation
$^{87}Sr/^{86}Sr$(veg)—Sr isotopic ratio in the vegetation (wood, measured)
$^{87}Sr/^{86}Sr$(fauna)—Sr isotopic composition of the fauna (localised Sr isotopic ratio, human and animal, calculated)
$^{87}Sr/^{86}Sr$(wea)—Sr isotopic composition of weathered soil, bioavailable component (gained by leaching of sampled soil with 1 N HCl, details see “Analytical methods”)
Sr(atm) ppm—Sr content of the atmospheric or rainwater (taken from literature)
Sr(wat) ppm—Sr content of the groundwater (taken from literature)
Sr(aq-f) ppm—Sr content in drinking water, mixture of ground and rainwater
Sr(aq-v) ppm—Sr content in vegetable water, mixture of ground and rainwater
Sr(fauna) ppm—Sr content incorporated into the fauna, time-dependent assimilated (human and animal, calculated)
Sr(veg) ppm—Sr content of the vegetation (wood, time-dependent assimilated, calculated)
Sr(wea) ppm—Sr content of the weathered soil (taken from literature)

Abbreviations

f(atm, aq-f)	Abundance of the atmospheric water (=rainwater) component in the drinking water
f(atm, aq-v)	Abundance of the atmospheric water (=rainwater) component in the vegetation water
f(aq-v, veg)	Abundance of the vegetation water component in the vegetation
f(aq-f, fauna)	Abundance of the drinking water component in the fauna
$^{87}Sr/^{86}Sr$ (atm)	Sr isotopic ratio in the atmosphere (ocean water, rainwater, taken from the literature)
$^{87}Sr/^{86}Sr$ (wat)	Sr isotopic ratio in the groundwater (sampled water from wells or groundwater horizon)
$^{87}Sr/^{86}Sr$ (aq-f)	Sr isotopic composition of drinking water (mixture of rain and groundwater) incorporated into the fauna
$^{87}Sr/^{86}Sr$ (aq-v)	Sr isotopic composition of vegetable water (mixture of rain and groundwater)
$^{87}Sr/^{86}Sr$ (veg)	Sr isotopic ratio in the vegetation (wood, measured)
$^{87}Sr/^{86}Sr$ (fauna)	Sr isotopic composition of the fauna (localised Sr isotopic ratio, human and animal, calculated)
$^{87}Sr/^{86}Sr$ (wea)	Sr isotopic composition of weathered soil, bioavailable component (gained by leaching of sampled soil with 1 N HCl; for details see methods section)
Sr(atm) (ppm)	Sr content of the atmospheric or rainwater (taken from the literature)
Sr(wat) (ppm)	Sr content of the groundwater (taken from the literature)
Sr(aq-v) (ppm)	Sr content in vegetation water, mixture of ground and rainwater
Sr(aq-f) (ppm)	Sr content in drinking water, mixture of ground and rain water
Sr(veg) (ppm)	Sr content of the vegetation (wood, time-dependent assimilated, calculated)
Sr(fauna) (ppm)	Sr content incorporated into the fauna, time-dependent assimilated (human and animal, calculated)
Sr(wea) (ppm)	Sr content of the weathered soil (taken from literature)
$X(\ldots)$	correlation of $^{87}Sr/^{86}Sr$ and Sr content for the special case

Equation of the mixing hyperbola in coordinates of the $^{87}Sr/^{86}Sr$ ratio and the Sr concentration (Sr) (Faure and Mensing 2005)

$(^{87}Sr/^{86}Sr)_M = a/(Sr)_M + b$, with

$$a = \frac{Sr_A Sr_B \left(\frac{87Sr}{86Sr}\right)_B - Sr_B \left(\frac{87Sr}{86Sr}\right)_A}{Sr_A - Sr_B};$$

$$b = \frac{Sr_A \left(\frac{87Sr}{86Sr}\right)_A - Sr_B \left(\frac{87Sr}{86Sr}\right)_B}{Sr_A - Sr_B};$$

The numerical values of a and b entirely depend on the $^{87}Sr/^{86}Sr$ ratios and Sr concentrations of the components A and B in the mixture M.

$$Sr_M = Sr_A \times f_A + Sr_B \times (1 - f_A);$$

f_A is the abundance of A in the mixture M

References

Castellan SN, Tomedi G (2006) Archäologische Untersuchungen im Zuge der Renovierung des Ampasser Widums. Archaeo Tirol Kleine Schriften 5:221–223

Drouet T, Herbauats J, Gruber W, Demaiffe D (2005) Strontium isotope composition as a tracer of calcium sources in two forest ecosystems in Belgium. Geoderma 126:203–223

Dupré B, Négrel P, Seimbille F, Allegre CJ (1994) 87Sr/86Sr ratio variation during a rain event. Atmos Environ 28:617–620

Fassbinder JWE (2010) The Iron age settlement of Pfaffenhofen-Hörtenberg, Tirol (Austria): Akademie und BLfD zu Prospektion in Tirol. Denkmalpf Info 146:73–74

Faure G, Mensing TM (2005) Isotopes. Principles and applications. Wiley, Hoboken, NJ

Frei KM, Frei R (2011) The geographic distribution of strontium isotopes in Danish surface waters – a base for provenance studies in archaeology, hydrology and agriculture. Appl Geochem 26:326–340

Göhring AB (2014) Sauerstoff-Isotopiekartierung einer Alpenpassage anhand rezenter botanischer Proben. MSc Thesis, LMU München

Graustein WC, Armstrong RL (1983) The use of $^{87}Sr/^{86}Sr$ ratios to measure atmosphere transport into forest watersheds. Science 219:298–392

Green GP, Bestland EA, Walker GS (2004) Distinguishing sources of base cations in irrigated and natural soils: evidence from strontium isotopes. Biogeochemistry 68:199–225

Grupe G, Price TD, Schröter P, Söllner F, Johnson CM, Beard BL (1997) Mobility of Bell Beaker people revealed by strontium isotope ratios of tooth and bone: a study of southern Bavarian skeletal remains. Appl Geochem 12:517–525

Grupe G, von Carnap-Bornheim C, Söllner F (2011) Stable strontium isotope mapping for provenance studies in archaeology – different material, different signals? Bull Soc Suisse d'Anthrop 17:67–76

Lambertz G, Welling J (2010) Die chemische Zusammensetzung von naturbelassenem Holz. Expertise im Auftraf des Bundesverbandes Holzpackmittel, Paletten, Exportverpacing (HPE) e.V. Johann Heinrich von Thünen-Institut, Bundesforschungsinstitut für Ländliche Räume, Wald und Fischerei, Institut für Holztechnologie und Holzbiologie, Hamburg

Lang A (1998) Das Gräberfeld von Kundl im Tiroler Inntal. Studien zur vorrömischen Eisenzeit in den zentralen Alpen. Frühgeschichtliche und Provinzialrömische Archäologie. Materialien und Forschungen 2. Marie Leidorf, Rhaden/Westf

Müller W, Fricke H, Halliday AN, McCulloch MT, Wartho J-A (2003) Origin and migration of the alpine iceman. Science 302:862–866

Pöll J (2014) Der frühbronzezeitliche Vollgriffdolch vom Buchberg bei Wiesing. Conservatum est Schlern-Schriften 363:317–344

Tomedi G, Appler H, Castallen SN (2001) Vorbericht zu den Grabungen von ArchaeoTirol am Ampasser Widenfeld im Jahr 2000. ArchaeoTirol Kleine Schriften 3:91–98

Torre M, Rodriguez AR, Saura-Calixto F (1992) Study of the interactions of calcium ions with lignin, cellulose and pectine. J Agric Food Chem 40:1762–1766

Tütken T (2010) Die Isotopenanalyse fossiler Skelettreste – Bestimmung der Herkunft und Mobilität von Menschen und Tieren. Tagungen des Landesmuseums für Vorgeschichte Halle 3:33–51

Van Dijksta AD, Breemen N, Jongmans AG, Davies GR, Likens GE (2003) Calcium weathering in forested soils and the effect of different tree species. Biochemistry 62:253–275

Veizer J (1989) Strontium isotopes in seawater through time. Ann Rev Earth Planet Sci 17:141–167

Voerkelius S, Lorenz GD, Rummel S, Quétel CR, Heiss G, Baxter M, Brach-Papa C, Deters-Itzelberger P, Hölzl S, Hoogewerff J, Ponzevera E, VanBocxstaele M, Ueckermann H (2010) Strontium isotopic signatures of natural mineral waters, the reference to a simple geological map and its potential for authentication of food. Food Chem 118:933–940

Xin G, Hanson N (1994) Strontium isotope study of the Peconic river watershed, Long Island, New York. MSc thesis, State University of New York at Stony Brook

Provenancing Bronze: Exclusion, Inclusion, Uniqueness, and Occam's Razor

Igor M. Villa

Introduction

The question of the provenance of archaeological metal objects has become a very important theme in archaeometric studies. The present contribution will summarize, obviously not in a complete way, the present state of research, in the hope that additional developments and augmented databases will soon give the archaeological community an even more reliable tool.

When an ore is transformed into a metal object, the metallurgical processes that the source material undergoes are manifold: roasting, oxidation, reduction, fluxing, smelting, co-smelting, slagging, etc. All these operations have the precise aim to transform the source by removing most of the elements it contained and sometimes to add a few selected elements to obtain an alloy with improved properties. Contemporary metallurgy operates with electrolysis to reduce all "impurities" below the detection limit. In the case of prehistoric metal artefacts, fortunately for archaeometrists, the aim to remove most elements contained in the source is only imperfectly achieved, and trace elements remain detectable in the artefacts. However, the metallurgical operations effected an intentional modification of both element concentrations and ratios, and the artefact ends up bearing an extremely faint chemical resemblance to the ore it derives from. Amongst the elements that undergo metallurgical modification are those that exhibit volatile properties (including those with volatile oxides), such as As and to a lesser degree Sb (Tanahashi et al. 2005), which are depleted by the roasting of sulphate ores under oxidizing conditions and probable addition of slag refiners. Moreover, the presence of some elements (e.g. As, Sn, Pb), which may have been serendipitous during the

I.M. Villa (✉)
Centro Universitario Datazioni e Archeometria, Università di Milano Bicocca, piazza della Scienza 4, 20126 Milano, Italy

Institut für Geologie, Universität Bern, Baltzerstrasse 3, 3012 Bern, Switzerland
e-mail: igor@geo.unibe.ch

G. Grupe, G.C. McGlynn (eds.), *Isotopic Landscapes in Bioarchaeology*,
DOI 10.1007/978-3-662-48339-8_8

Chalcolithic, increasingly became an intentional addition during the Early Bronze Age (e.g. by co-smelting: Lechtman and Klein 1999). It is not always evident whether and when a particular local metallurgical tradition shifted from imperfect refinement to conscious alloying. Thus, it is not a straightforward archaeometric task to assign a source to an object after so many chemical modifications.

Since the 1960s, it became apparent that Early Bronze Age metal objects were compositionally varied (Friedman et al. 1966). Artefacts were divided into discrete groups on the basis of trace element concentrations (e.g. Junghans et al. 1968). After 50 years of analytical improvements, present-day chemical analyses have become more precise with lower detection limits. It is becoming increasingly clear that groupings based on very few (1–2) discriminating elements and encompassing very disparate upper and lower concentration limits do not adequately diagnose the true variability of bronze artefacts. Pb isotope analyses have further demonstrated that such large groups are not derived from a single source; a classification following Junghans et al. (1968) is not conducive to a recognition of sources.

One approach employed in the recent archaeometric literature has been the use of statistical techniques such as Principal Component Analysis (PCA). This technique examines the spatial distribution of data points in an N-dimensional space, whereby the dimensions are *N* quantitative attributes of the points, calculates the distances between all points, and identifies the combination of attributes that most accounts for the points' dispersion. While PCA is often used in statistical sciences, its application to geochemical problems is fraught with several difficulties. (1) The very question of what makes two data points "different" is a process-oriented one. Given an archaeological artefact, how did it come into existence, and how does the archaeometrist weigh the importance of the individual links of the chaîne opératoire? (2) The definition of the distance between two data points, i.e. "how different" two points are, is an example of the difficulty translating an abstract mathematical concept into a concrete definition. PCA algorithms resort to a logarithmic transformation of the data instead of true measured data. This compression of the natural variation is statistically legitimate when the data span a limited range; the rationale for the compression is avoiding overrepresentation of samples with high values of the investigated attributes. However, in the case of chemical compositions of archaeological objects, trace element concentrations span several orders of magnitude. Logarithmic compression simulates proximity of data and distorts and negates the large variations of measured objects. (3) PCA was never designed to take into account measurement uncertainties. These are an integral part of a measurement result (BIPM et al. 2012, entries 2.9 and 2.10). As the statistical significance of a distance between two data points is always a function of the respective relative uncertainties, neglecting this information always leads to unsubstantiated conclusions. (4) PCA assumes a Gaussian data distribution, which is practically never observed in natural rocks. (5) Related to this problem, an implicit assumption of PCA is unimodality, while heterogeneous sources are by definition multimodal. The variance of the points from the global, unimodal average, on which PCA algorithms are based, is meaningless if the data set consists of the sum of two or more distributions, each with its own average and variance.

(6) PCA is "unsupervised" (Lin et al. 2015), which means that the data are grouped and fitted without any a priori meta-information, whether the grouping is chemically or physically reasonable. Unsupervised application of PCA can produce groupings that are not robust with respect to the choice of trace elements being considered, or with respect to normalization (the so-called "dimensionless treatment" that transforms absolute element concentrations into dimensionless concentrations normalized to a chosen reference). Highly simplified, the groupings can be influenced by the user and do not always represent an objective datum that remains stable independent of the subjective user choices.

To better exemplify this, a simple, ad-hoc simulation is offered as follows. Consider three bronze objects: X containing 90 % Cu, 9 % Sb, and 1 % As; Y containing 90 % Cu, 5 % Sb, and 5 % As; Z containing 99 % Cu, 0.9 % Sb, and 0.1 % As. With these three concentrations as input data, the common PCA algorithms identify X and Y as closest. In fact, X and Z were constructed as deriving from the same tetrahedrite ore (see below) with different degrees of alloying and have the same Sb/As ratio, while Y derived from tennantite. Using a logarithmic compression instead of concentrations distorts the distances between the three points, but always leaves the X–Z proximity unrecognized.

In order to obtain accurate answers from the algorithms it is necessary to supervise a meaningful definition of "statistical distance". A correct approach first requires the quantitative evaluation of two kinds of physical processes: those that control the formation of an ore deposit (partition of trace elements into the fluid and into the ore minerals, following predictable chemical regularities) and those that occur during metallurgical transformation (loss of volatile elements during oxidation of sulphides, persistence of volatile elements under reducing conditions, mixing of ore charges, addition of fluxing agents and alloy solutes, recycling of old metal, etc.). This is followed by an estimation of the effects of these processes in the data.

An alternative approach to zero in on areas of provenance is the use of isotope analyses. Isotopic compositions are not modified by metallurgical operations (except those of O and S during roasting). Thus, all elements that show isotopic variations in nature always preserve the isotopic signature of the source and can be used to trace it. This pertains to metal objects, the focus of the present discussion, and also nonmetallic materials (marbles and alabasters; clay in earthenware; sometimes teeth). The isotopic systems most frequently used are those showing the largest natural variation, namely Pb in metallic objects (e.g. Grögler et al. 1966); Pb, Sr and O in marbles and alabasters (e.g. Lazzarini et al. 2012); Sr and Nd in clay, etc. Also, fingerprinting of obsidian by fission tracks (Bigazzi and Bonadonna 1973) can be viewed as a chemical/isotopic technique. Additional isotopic systems, such as Cu and Sn (Klein et al 2004; Haustein et al. 2010) have also been used for bronze objects, whereby it should be noted that success so far has been limited (Rehren and Pernicka 2008, p. 239).

The main ambiguity inherent in isotope tracing is that it rarely provides unique identifications amongst the very large number of possible ore sources. First of all, ore deposits are rarely monogenetic, and the different ore minerals are similar but not identical, as they were deposited at different times by different fluids with

different chemical and isotopic signatures (e.g. Mondillo et al. 2014). This ensures that ore deposits are usually represented by relatively wide fields in chemical and isotopic diagrams. Moreover, a rapid perusal of the growing database of Pb isotopic compositions of prehistoric ore deposits (e.g. Stos-Gale and Gale 2009, and references therein) shows that in most of the regions where early Bronze Age objects were discovered such as the peri-Mediterranean region and Central Europe, Pb isotope signatures overlap to a large extent.

Since radiogenic Pb isotopes 208, 207 and 206 are frozen in time during the formation of galena and other sulphides, their isotopic signature in ore districts is related to the age of ore formation. Conversely, knowing the age of an ore-forming mineralization event allows broad predictions of ore Pb isotopic composition. A more detailed discussion of the complications introduced in real-life ore deposits by host-rock isotope geochemistry (Kramers and Tolstikhin 1997; Cattin et al. 2011) and by multistage fluid circulation (Mondillo et al. 2014) exceeds the scope of the present review. In broad terms, one can note that the tectonic map of Central and Western Europe features four "age provinces" corresponding to discrete periods of tectonic (and, hence, minerogenetic) activity: the Cenozoic (Maghreb and southern Iberia, Apennines and partly Alps, Aegean and partly Balkans, partly Anatolia); the Late Paleozoic (most of Iberia, partly Sardinia, partly Pyrenees, Massif Central, Vosges/Black Forest, most of the Alps, German Mittelgebirge, Cornwall, Mendips, partly Balkans); the Early Paleozoic (most of the British Isles, Bohemia, most of Sardinia, partly Pyrenees); and the Precambrian (Bretagne, most of Scandinavia, Eastern European Platform). A consequence of the assemblage of the European continental crust is that most of Central Europe underwent local ore-forming events around the same time in the Late Paleozoic. Because Pb isotopic composition depends on the age of the ore, it is expected, and indeed observed, that ore deposits in the Alps, most of Central Europe, England, etc., have Pb isotope ratios of $^{206}Pb/^{204}Pb = 18.3–18.5$, $^{207}Pb/^{204}Pb = 15.6–15.7$, and $^{208}Pb/^{204}Pb = 38.3–38.7$ (cf. the cluster of points in Fig. 1). These same Pb isotopic ratios are observed wherever ores have the same approximate age—including Australia, China, and South America. The Pb isotopic composition of a Cu ore is essentially not unique.

For example, the isotopic signature of some bronze objects found near Sion (Switzerland) overlaps with that of ores deriving from all over Europe (Cattin et al. 2011). What Pb isotope analyses are excellently suited for is negative evidence: if an object and an ore, or two objects, have the same isotopic signature (within the full analytical uncertainty, as discussed by Villa (2009)), they may or may not be genetically related; but if the two isotopic signatures differ, then the object cannot derive from that ore deposit, nor can the two objects have the same source.

An apparently insurmountable difficulty is mixing metal lots obtained from different sources. It was expected that in Roman imperial times the industrial Pb production would blend heterogeneous ore sources. Indeed, the attempt (Boni et al. 2000) to determine the provenance of lead water pipes in Pompeii revealed no correspondence to any known individual mining district, because pipes were mixtures of Iberian, and/or Sardinian, and/or other lead ingots. Even before Roman industrial blends, mixing and/or recycling were probably very common, as Bray

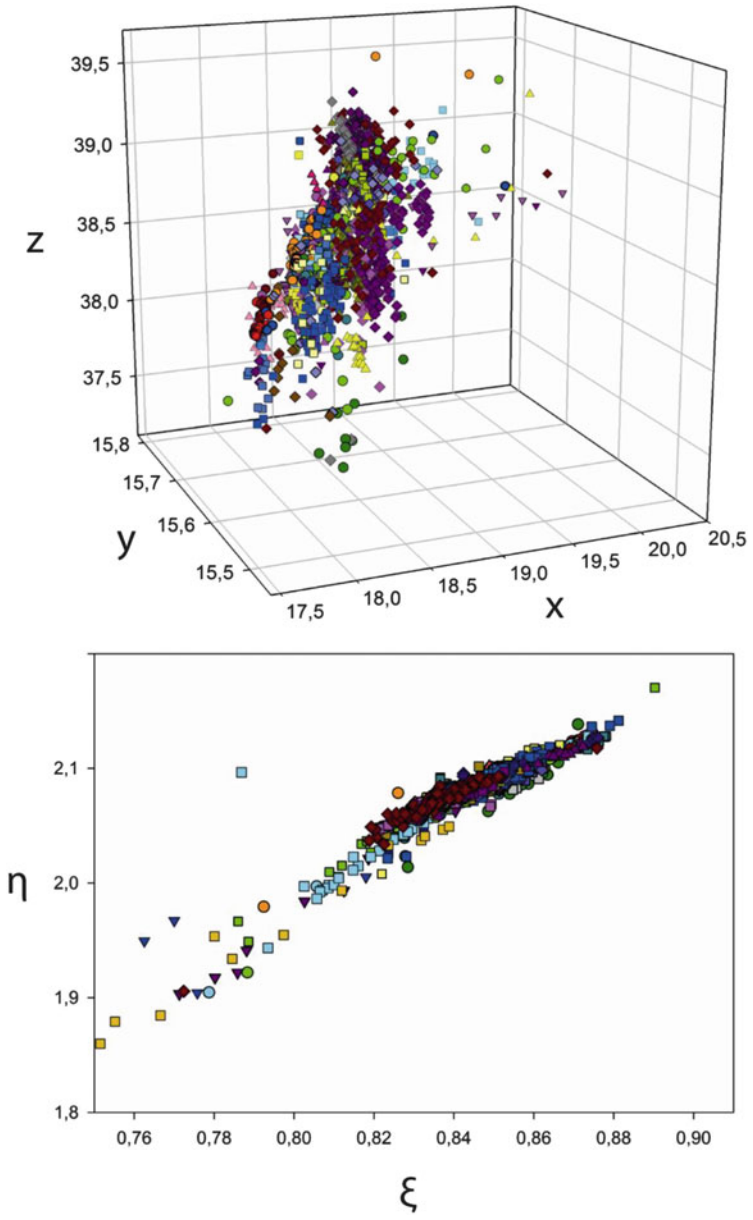

Fig. 1 Pb isotope ratio diagrams. (**a**) Three-dimensional presentation of ore and slag samples from different provenances (modified after Artioli et al. 2014). The coordinate axes are $x = {}^{206}\mathrm{Pb}/{}^{204}\mathrm{Pb}$, $y = {}^{207}\mathrm{Pb}/{}^{204}\mathrm{Pb}$, and $z = {}^{208}\mathrm{Pb}/{}^{204}\mathrm{Pb}$. (**b**) Two-dimensional projection, with $\xi = y/x$ and $\eta = z/x$. The loss of information and the blurring of differences are evident

and Pollard (2012) argued for British finds of Irish provenance. The discussion below will attempt to find possible diagnostic tools to recognize the occurrence of mixing and ideally constrain its end-members.

Isotope Discrimination

Thanks to its four long-lived isotopes (208, 207, 206, and 204), three of which are associated with a different decay system (Kramers and Tolstikhin 1997), Pb is excellently suited to provide high-resolution fingerprinting. It needs to be emphasized that in order to exploit the full diagnostic potential of Pb isotope analysis it is necessary to use all four Pb isotopes (see Villa 2009). A realistic example of how information is inherently lost when isotope 204 is left out is illustrated in Fig. 1a, which shows a three-dimensional correlation diagram that clearly displays differences between different samples, while Fig. 1b (a two-dimensional projection) confuses and merges heterogeneous samples, possibly leading the archaeologist to formulate inaccurate conclusions.

The three primary independent observables are the three measured Pb isotope ratios. Albarède et al. (2012) proposed to substitute the primary information by a derived, model-dependent coordinate transformation (their so-called μ–κ–T diagrams). Since the transformation is based on the three primary observables, it cannot generate new, additional information. While at first sight it could appear that it does not destroy information (thus being information-wise neutral), the model used to derive μ and T from the measured ratios, which assumes a single-stage differentiation of the Earth and a single-stage ore formation, is in fact geochemically flawed (see the discussion by Kramers and Tolstikhin (1997). This paper was not cited by Albarède et al. (2012). Documentation of multistage Pb-bearing fluid circulation by Mondillo et al. (2014) should also be considered here. Thus the μ–κ–T diagram introduces inaccuracy, while adding no further insight relative to the three-dimensional data representation as seen in Fig. 1a.

The choice of the coordinate axes in Fig. 1 is arbitrary to the extent that any set of three independent ratios serves the purpose of plotting coincident and heterogeneous samples respectively in proximity and at a distance to each other. A frequent problem confronting archaeometry is that ancient metal supplies were mixed during their history. A very convenient choice to help solve this problem is using three ratios that have a common denominator. Any common-denominator isotope correlation diagram has the algebraic property that mixtures always lie on the straight segment between the two end-members that are mixed (see, e.g. Villa 2001). This allows a reduction of the number of possible sources.

In one example presented by Artioli et al. (2014) and Addis (2013), the slags found near the very small smelting centre of Transacqua (Trento, Italy) have the Pb isotope ratios $^{206}Pb/^{204}Pb = 18.3–18.5$, $^{207}Pb/^{204}Pb = 15.6–15.7$, and $^{208}Pb/^{204}Pb = 38.5–38.7$. As mentioned above, there are hundreds of ores stemming from across Europe and non-European continents that possess matching isotope signatures. Bronze artefacts

from Alpine valleys near Trento, in a 10 km radius from Transacqua, show indistinguishable Pb signatures. These artefacts could, purely from the restricted isotopic point of view, derive from Peru, Britain, or other remote areas, and one may be tempted to declare the problem as unsolvable. However, one should instead be using Occam's Razor: given a measurement result, what explanation makes the smallest number of unreasonable assumptions? The case of Transacqua strongly suggests considering the cost efficiency of distance travelled: the least distance between ore source and artefacts is associated with the smallest transportation expense. Therefore, the most reasonable archaeological hypothesis is that bronze artefacts having a Transacqua-like Pb isotope signature were indeed derived from Transacqua and not from expensive providers in far-off exotic places.

A completely different situation is that of the "Singen copper" objects. On the basis of their Pb isotope signature, ores used to manufacture the bronze objects found in Singen could derive from anywhere within a 500 km radius (Austrian Alps, Swiss Alps, Harz, German Erzgebirge, Eifel, Massif Central...). Occam's Razor cannot be used because no ore deposit occurs within 10 km from the finds, and long-distance transport was unavoidable. Any further assumption on trade routes is subjective. Since a Pb isotope signature alone is not unique, additional discrimination criteria are required.

Geochemical Regularities in Trace Element Behaviour

As mentioned in the introduction, the usefulness of statistical software is limited by the capability to derive robust results relative to small variations in the input data: the decisive question is whether data points that are genetically close are indeed recognized by the software as being related. Robustness tests have not yet been reported for bronze objects (one epistemological reason is that there is no universally agreed independent assessment of what constitutes a family of "related" samples). For rock samples, there are established geological criteria that permit testing of software accuracy. Such a test was performed on magmatic rocks from the Himalayan region (Heri 2013; Heri et al. 2014) using Multidimensional Scaling and Hierarchical Clustering with various input formats (measured element concentrations; normalized concentrations; element ratios; Sr and Nd isotope ratios). The result was sobering: coarse clustering of the magmatic rocks was reproducible and reflected independent geological grouping, but the detailed family structure and the relatedness of the samples with each other was modified by the subjective choice of input format. One mathematical reason for this lack of reproducibility is likely to be that both inter-sample and intra-sample variability of the concentration of a given element can vary by one or more orders of magnitude (a factor of 10 is in itself a very large range!).

Starting from this overall failure of unsupervised statistical software, an alternative approach is needed. The first choice is to take into account the principles of chemistry and geochemistry. Elements have chemical and geochemical properties that follow well-understood regularities, as displayed in the periodic table. During

ore-forming mineralization processes, it is likely that the absolute concentration of most elements will show very large modifications. However, the modifications of the concentration of a given element will be paralleled by those of its close chemical relatives. For example, Co, Ni, and Fe are chemically extremely similar. It is expected that in a geological process, such as the formation of ore deposits, the absolute concentration of Ni (which can substitute for Fe in minerals, e.g. in pyrite) will show very large modifications, as will the absolute concentration of other elements. However, the modifications of the Ni concentration will be most closely matched by those of its close chemical relative Co. The Co/Ni ratio is predicted to show very little variation in a given ore deposit, but is expected to vary considerably among unrelated ore deposits that record vast genetic differences (Brill 1989). Examples are shown in Fig. 2a, summarizing Ni and Co concentrations in sulphide minerals from several deposits from the literature. The data by Oberthür et al. (1997) show that within one very large ore-bearing area (Great Dyke, Zimbabwe) the Co/Ni ratio in pentlandite, $(Fe,Ni)_9S_8$, is remarkably constant (0.017 ± 0.005) and well distinct from pyrrhotite, $Fe_{1-x}S$ (0.058 ± 0.009), and from pyrite, FeS_2 (between 4.7 and 12.6) from the same area. Very different Co/Ni ratios were measured in pyrite samples from Canada (Co/Ni = 0.03, Chenery et al. 1995) and Australia (Co/Ni = 1.1–4.2, Brill 1989). The Co/Ni element ratios are shown as diagonal lines through the origin in Fig. 2a.

A similar behaviour is shown by Group 15 metalloids (As, Sb, Bi). Each mineral in a given ore deposit is expected to have a relatively small range of variation for As/Sb and Bi/Sb element ratios. An example is presented in Fig. 2b, a common-denominator diagram showing the range of variation in the ratios of Group 15 elements in minerals from the Brixlegg ore deposit (a Cu source exploited during the early Bronze Age). Cu in Brixlegg was mainly hosted by fahlore, a group of sulphide minerals, which allow a continuous substitution between As and Sb; its end-members are tetrahedrite ($Cu_{12}Sb_4S_{13}$) and tennantite ($Cu_{12}As_4S_{13}$). As anticipated, Fahlore samples from Brixlegg show a comparatively narrow range of variation in both As/Sb and Bi/Sb ratios. Another Cu mineral occurring in Brixlegg, enargite (Cu_3AsS_4), has no Sb in its theoretical stoichiometry (but allows Sb–As substitution). Consequently, As/Sb and Bi/Sb ratios are both higher and less constant than those of fahlore.

The number of possible trace element ratio diagrams is very high, but the useful ones amongst them are quite few and also depend on the question asked. Diagrams without a common denominator can be used to diagnose heterogeneity of provenance, but do not make it possible to evidence two-component and even less so multicomponent mixing trends (the mixing trajectories depend, algebraically, on the mass balance between the denominators in the two end-members being mixed). The element ratios chosen for the coordinate axes should be uniform in cogenetic ore samples and variable amongst heterogenetic samples. This requirement is a "supervised" argument, in the sense that it is based on chemical/geochemical principles and is *not* automatically recognized by statistical software.

Even with a judicious axis choice based on a priori chemical knowledge, the questions that can be answered by such diagrams need creative thinking. For example, the recycling of Irish ores (Bray and Pollard 2012; Pollard et al. 2014)

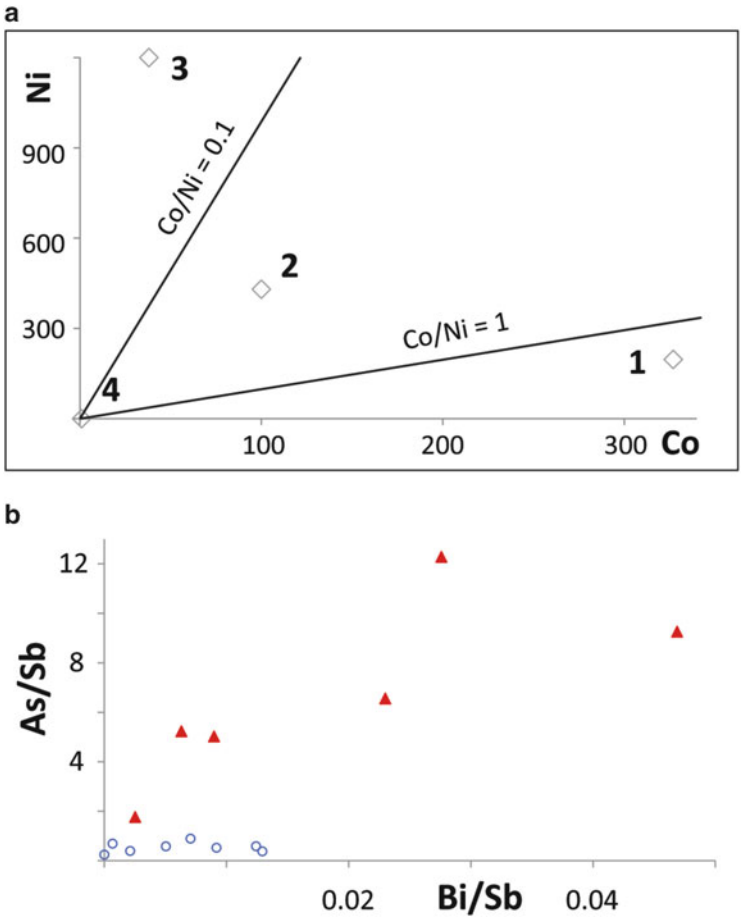

Fig. 2 Trace element patterns in pyrite samples from the literature. (**a**) Ni and Co concentrations in μg/g, and Co/Ni element ratio. Numbers refer to analyses from the following ore deposits: (1) CSA, Australia (Brill 1989); (2) Agincourt, Australia (Huston et al. 1995); (3) Hemlo, Canada (Chenery et al. 1995); (4) Great Dyke, Zimbabwe (Oberthür et al. 1997). Different ores plot in different areas of the diagram. (**b**) As/Sb and Bi/Sb ratios from the Brixlegg mining region, Austria. Fahlore samples (*open circles*) show remarkably uniform As/Sb and Bi/Sb ratios; enargite (*filled triangles*) scatters more, but still within one order of magnitude

is most clearly recognized by comparing contrasting common-denominator ratios: one having as the numerator an element that is modified by metallurgy (e.g. As), with one featuring an element that is not modified (e.g. Ag). On the other hand, selective use of fahlore over other Cu minerals (possibly due in part to mythical-religious influences: Budd and Taylor 2010) can be diagnosed if monogenetic slags are analysed for those elements that show the greatest variability spectrum amongst ore minerals. Incidentally, this recommends an overabundant, redundant data acquisition strategy: if workers had started reporting chemical analyses of all

possible trace elements in individual minerals since the 1980s, we would today have a much more useful database at our disposal and could infer much more about archaeometallurgy.

The metallurgical chaîne opératoire can introduce much larger variation in trace elements. Figure 3 illustrates two examples: Cu refinement with oxidative loss of volatile elements (Fig. 3a) and mixing (Fig. 3b). Mixing can occur in different stages of the chaîne opératoire: joint treatment of ore charges of different provenance, selective addition of other elements (hosted by different ores) to produce special alloys, and recycling of degraded implements.

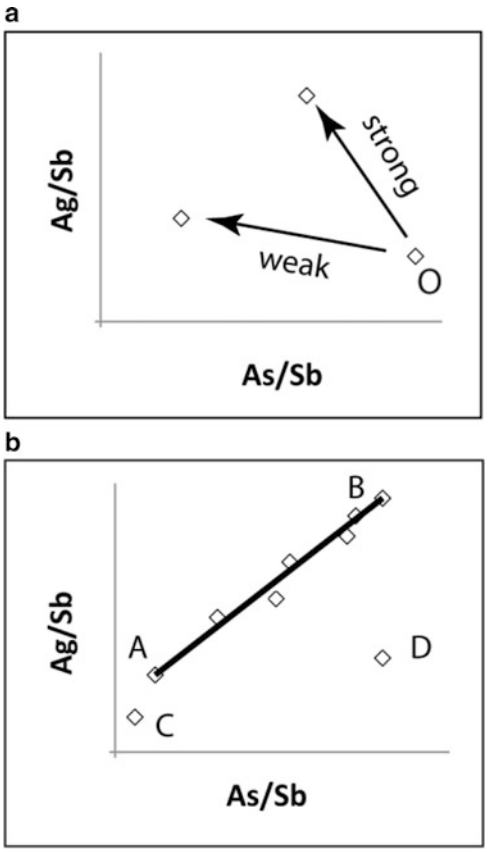

Fig. 3 The effect of metallurgical operations. The ratios on the axes are chosen to include highly volatile (As), moderately volatile (Sb) and comparatively refractory (Ag) elements. (**a**) Schematic representation of trends expected when samples of one ore (marked as O) are roasted under oxidizing conditions: while Ag remains in the metal phase, As is strongly depleted, and Sb is moderately depleted. Depending on the temperature and the availability of free oxygen, Sb can be weakly or strongly depleted relative to Ag, as indicated by the two diverging arrows. (**b**) Mixing trend. Because the *x* and *y* axes have a common denominator, any binary mixing between ore A and ore B gives rise to a linear trajectory. Conversely, if data points deviate from the straight line segment AB, admixture of additional component(s) is required (points C and D)

Figure 4 shows an application of these principles to bronze artefacts from the Singen graves (Germany). Cattin et al. (2015) analysed 12 objects from Singen and found that six of them have mutually discordant Pb isotopic signatures, meaning that certainly half of the analysed samples have heterogeneous provenances. The remaining six samples, which all belong to Group 1 (Sb–Ni-rich "Singen copper") following Krause (1988), have overlapping Pb isotopic signatures. The question

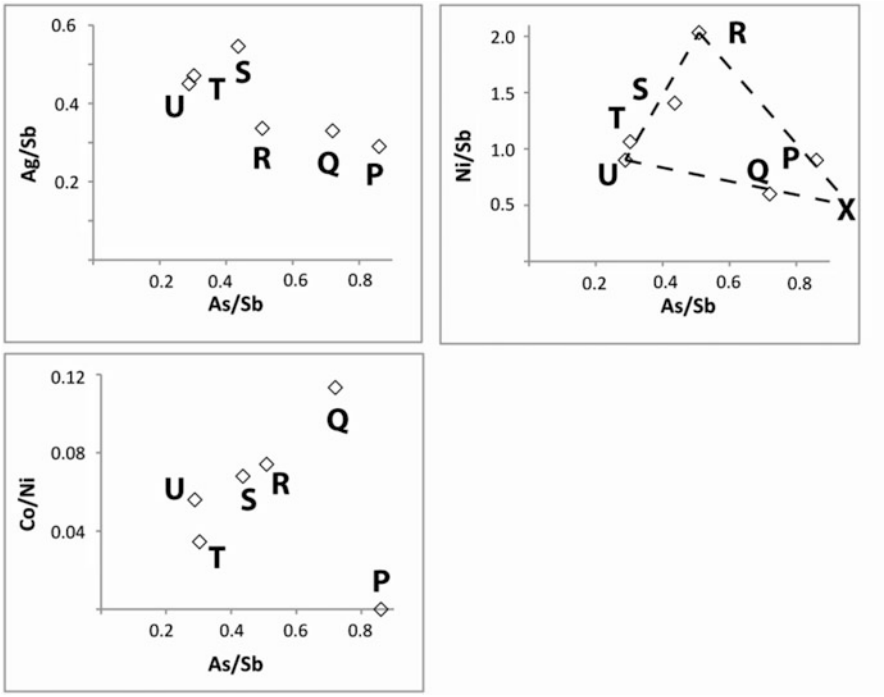

Fig. 4 Chemical signature of "Singen Copper" artefacts from Singen (Germany), from data in Cattin et al. (2015). Points are relabelled for ease of reference: P (Sn50/37:22), Q (Sn70 Beil2), R (Sn50/11:12), S (Sn58/10:4), T (Sn50/256:52), and U (Sn52/125:29). (**a**) Sb is moderately depleted relative to Ag; As is heavily depleted relative to Sb. This trend is ambiguous when taken alone, as it is compatible either with a monogenetic origin followed by differential loss of volatiles during metallurgical treatment or with a polygenetic origin due to mixing. (**b**) Mixing diagram. The minimum number of end-members (Villa 2001), as illustrated by the dashed triangle, is three, plausible candidate end-members being R, U, and X, an ore not directly observed, but having a Ni–As–Sb signature close to that of both P and Q. This means that the samples lying in the interior of the triangle RUX can be, at least in principle, produced by mixing suitable amounts of metal R with metal U and metal X. (**c**) Additional discrimination diagram. The *x* and *y* axes do not have a common denominator, therefore linear point arrays cannot be viewed as mixing trends; however, this graph allows a clear recognition of heterogeneous provenance. In particular, points P and Q are very different from each other. If both were derived from the same ore, X, they should have similar Co/Ni ratios. The data prove that the assumption of a common end-member X for both P and Q is incorrect. Thus, the number of resolvably different sources that need to be mixed to account for the variation of the six objects in (**b**) increases to at least four (but could be as high as six, each object deriving from a different source)

that Fig. 4 seeks to address is whether the trace element signature of these latter, potentially cogenetic six samples from Group 1, supports the classification in homogeneous groups.

The answer from the trace element discrimination diagrams is negative. The trace element variations of the six Group I objects in Fig. 4, whose Pb isotope signature (when taken alone) could be compatible with a single ore source, actually require at least 4 distinct sources. The sources of the "Singen copper" were numerous, heterogeneous ore deposits (Cattin et al. 2015). The context provided by a judicious, "supervised" choice of trace element signatures that exploits a priori chemical knowledge is able to improve the identification by exclusion.

Perspectives

The unique identification of provenance at the present time is a matter of luck. A much more frequent result is the narrowing down of possible sources by exclusion. Exclusion has already changed the archaeological paradigm that, ever since the beginning of metallurgy, bronze was the monopoly of just a few "industrial" production centres, controlled by an elite, which marketed a homogeneous product along long-distance trade routes. Exclusion can be based on Pb isotope analyses or on trace element patterns.

Inclusion on the basis of Pb isotopic compositions is mostly underconstrained. Inclusion on the basis of trace element concentrations, such as it was sometimes reported in the past, is even more questionable. Black box software that performs unsupervised statistical elaborations entails a very high risk of neglecting the chemical and geological reality and therefore of producing inaccurate results.

Trace element ratios can be a robust tool, as a judicious selection of element triplets in common-denominator diagrams can distinguish source signatures from subsequent anthropogenic modifications (depletion of impurities, doping with selected elements, mixing, and recycling). The synergic context of isotope and trace element correlation diagrams can result in increased reliability of exclusions and inclusions.

The charting of trace element patterns will require a massive analytical effort to create a database covering all possible ore values exhibited across all of the areas accessible to metal-using civilizations. Until that goal is achieved, archaeometrists will have to accept the incompleteness of knowledge and use Occam's razor: the nearest ore source, as small as it may be, is the most likely choice of origin.

The attempt to explain the Pb isotopic composition of bronze objects from the Swiss and Venetian Alpine realms by postulating that early Bronze Age metallurgists tried to minimize the logistical effort of ore transport has one potentially far-reaching implication: mining, smelting, and metallurgical operations occurred in hundreds of local, small-scale workshops, with a trade network that extended over a few km. Long-distance trade was also documented, and it is tantalizing to note that Tuscan metal was transported to the Valais about 1500 years before the

bloom of Etruscan city states. Clearly, more studies and large databases will have an influence on many of our present archaeological beliefs.

Acknowledgements Thanks are due to Prof. Gisela Grupe for organizing the workshop in Munich and to all colleagues there for stimulating discussions. Long discussions with A. R. Heri on the applications of PCA to geochemical problems are gratefully acknowledged; any remaining misunderstandings are solely my responsibility.

References

Addis A (2013) Late bronze age metallurgy in the Italian Eastern Alps: copper smelting slags and mine exploitation. PhD thesis, Università di Padova, 222 p

Albarède F, Blichert-Toft J, Desaulty A-M (2012) A geological perspective on the use of Pb isotopes in archaeometry. Archaeometry 54:853–867

Artioli G, Angelini I, Nimis P, Addis A, Villa IM (2014) Prehistoric copper metallurgy in the Italian Eastern Alps: recent results. Hist Metall 47:51–59

Bigazzi G, Bonadonna FP (1973) Fission track dating of the obsidian on Lipari Island (Italy). Nature 242:322–323

BIPM, IEC, IFCC, ILAC, IUPAC, IUPAP, ISO, OIML, JCGM (2012) The international vocabulary of metrology – basic and general concepts and associated terms, 3rd edn, JCGM 200:2012. http://www.iso.org/sites/JCGM/VIM-introduction.htm. Retrieved on 21 Dec 2014

Boni M, Di Maio G, Frei R, Villa IM (2000) Lead isotopic evidence for a mixed provenance of Roman water pipes from Pompeii. Archaeometry 42:201–208

Bray PJ, Pollard AM (2012) A new interpretative approach to the chemistry of copper-alloy objects: source, recycling and technology. Antiquity 86:853–867

Brill BA (1989) Trace-element contents and partitioning of elements in ore minerals from the CSA Cu-Pb-Zn deposit, Australia. Can Mineral 27:263–274

Budd P, Taylor T (2010) The faerie smith meets the bronze industry: magic versus science in the interpretation of prehistoric metal-making. World Archeol 27:133–143

Cattin F, Guénette-Beck B, Curdy P, Meisser N, Ansermet S, Hofmann B, Kündig R, Hubert V, Wörle M, Hametner K, Günther D, Wichser A, Ulrich A, Villa IM, Besse M (2011) Provenance of early Bronze age metal artefacts in Western Switzerland using elemental and lead isotopic compositions and their possible relation with copper minerals of the nearby Valais. J Archaeol Sci 38:1221–1233

Cattin F, Merkl MB, Strahm C, Villa IM (2015) Elemental and lead isotopic data of copper finds from the Singen cemetery, Germany – a methodological approach of investigating Early Bronze Age networks. In: Hauptmann A, Modarressi-Tehrani D (eds) Archaeometallurgy in Europe, III, pp 81–94

Chenery S, Cook JM, Stylus M, Cameron EM (1995) Determination of the 3-dimensional distributions of precious metals in sulfide minerals by laser-ablation microprobe inductively coupled plasma-mass spectrometry (LAMP-ICP-MS). Chem Geol 124:55–65

Friedman AM, Conway M, Kastner M, Milsted J, Metta D, Fields PR, Olsen E (1966) Copper artifacts: correlation with some types of copper ores. Science 152:1504–1506

Grögler N, Geiss J, Grünenfelder M, Houtermans FC (1966) Isotopenuntersuchungen zur Bestimmung der Herkunft römischer Bleirohre und Bleibarren. Z Naturforsch 21:1167–1172

Haustein M, Gillis C, Pernicka E (2010) Tin-isotopy – a new method for solving old questions. Archaeometry 52:816–832

Heri AR (2013) Geochemistry, geochronology and isotope geochemistry of Eocene dykes intruding the Ladakh Batholith. PhD thesis, University of Hong Kong, 317 p

Heri AR, King JA, Rolfo F, Aitchison JC, Bahl J, Villa IM (2014) Geochemistry and geobarometry of Eocene dykes intruding the Ladakh batholith. Abstract, 29th Himalaya Karakorum Tibet International Workshop

Huston DL, Sie SH, Suter GF, Cooke DR, Both RA (1995) Trace elements in sulfide minerals from Eastern Australian volcanic-hosted massive sulfide deposits. Econ Geol 90:1167–1196

Junghans S, Sangmeister E, Schröder M (1968) Kupfer und Bronze in der frühen Metallzeit Europas (Studien zu den Anfängen der Metallurgie 2). Gebr. Mann, Berlin

Klein S, Lahaye Y, Brey GP, von Kaenel H-M (2004) The early Roman imperial AES coinage II: tracing the copper sources by analysis of lead and copper isotopes—copper coins of Augustus and Tiberius. Archaeometry 46:469–480

Kramers JD, Tolstikhin IN (1997) Two terrestrial lead isotope paradoxes, forward transport modelling, core formation and the history of the continental crust. Chem Geol 139:75–110

Krause R (1988) Die endneolithischen und frühbronzeitlichen Grabfunde auf der Nordstadt-terrasse von Singen am Hohentwiel. Forsch Ber Vor- und Frühgesch Baden-Württemberg 32, Stuttgart

Lazzarini L, Visonà D, Giamello M, Villa IM (2012) Archaeometric characterisation of one Tunisian and two Italian calcareous alabasters used in antiquity. In: Proceedings, IX ASMOSIA conference, Tarragona, pp 436–444

Lechtman H, Klein S (1999) The production of copper-arsenic alloys (arsenic bronze) by cosmelting: modern experiment, ancient practice. J Archaeol Sci 26:497–526

Lin M, Zhao YG, Zhao LF, Li LL, Wang F, Zhu LC, Hu XN, Ning W (2015) Tracing origins of uranium ore concentrates (UOCs) by multidimensional statistics analysis of rare-earth impurities. J Anal Atom Spectrom 30:396–402

Mondillo N, Boni M, Balassone G, Villa IM (2014) The Yanque prospect (Peru): from polymetallic Zn-Pb mineralization to a nonsulfide deposit. Econ Geol 109:1735–1762

Oberthür T, Cabri LJ, Weiser TW, McMahon G, Muller P (1997) Pt, Pd and other trace elements in sulfides of the main sulfide zone, Great Dyke, Zimbabwe: a reconnaissance study. Can Mineral 35:597–609

Pollard AM, Bray PJ, Gosden C (2014) Is there something missing in scientific provenance studies of prehistoric artefacts? Antiquity 88:625–631

Rehren T, Pernicka E (2008) Coins, artefacts and isotopes – archaeometallurgy and archaeometry. Archaeometry 50:232–248

Stos-Gale ZA, Gale NH (2009) Metal provenancing using isotopes and the Oxford archaeological lead isotope database (OXALID). Anthropol Archaeol Sci 1:195–213

Tanahashi M, Fujinaga T, Su Z, Takeda K, Sohn HY, Yamauchi C (2005) Effects of coexisting oxygen and antimony in molten copper on rate of arsenic elimination from the copper phase by the use of Na_2CO_3 slag. Mater Trans 46:2180–2189

Villa IM (2001) Radiogenic isotopes in fluid inclusions. Lithos 55:115–124

Villa IM (2009) Lead isotopic measurements in archeological objects. Archaeol Anthropol Sci 1:149–153

Part III
Ecological Aspects of Isotopic Landscapes

Linking Oxygen Isotopes of Animal-Bone Phosphate with Altimetry: Results from Archaeological Finds from a Transect in the Alps

Christoph Mayr, Gisela Grupe, Anita Toncala, and Christina M. Lihl

Abstract Oxygen isotope ratios of organisms are closely linked to the hydrological environment in which they grow up. This is especially the case for mammals. Mammal-bone phosphate is formed at a constant body temperature and, thus, relatively insensitive to temperature-dependent isotope fractionation. The applicability of oxygen isotopes from mammal-bone phosphate for environmental reconstructions is tested here using bones of deer, domestic pig, and domestic cattle from 16 archaeological sites situated along a north–south transect crossing the Alps. Bones of 118 specimens in total were analysed, which covered an age span from the Late Neolithic to the Roman period. The main control on oxygen isotope ratios was site altitude. Significant negative correlations between phosphate isotope values and altitude were registered especially for cattle and pig. Pig bones from one site were deviating from this altitudinal pattern and were excluded from further correlations. Modern equations for translating oxygen isotope ratios of the three species to those of source water were applied. The reconstructed source water isotopic composition showed a similar altitudinal relation as modern Alpine precipitation. As a consequence, our study confirms the utility of oxygen isotope ratios of mammal-bone phosphate for source water and palaeoaltitudinal reconstructions.

C. Mayr (✉)
Institut für Geographie, Friedrich-Alexander Universität Erlangen-Nürnberg, Wetterkreuz 15, 91058 Erlangen, Germany

Paläontologie und Geobiologie, Ludwig-Maximilians-Universität München, Richard-Wagner-Str. 10, 80333 Munich, Germany
e-mails: christoph.mayr@fau.de; c.mayr@lrz.uni-muenchen.de

G. Grupe • A. Toncala
Ludwig-Maximilians-Universität München, Biozentrum, Grosshaderner Str. 2, 82152 Martinsried, Germany

C.M. Lihl
Institut für Grundwasserökologie, Helmholtz-Zentrum München, Ingolstädter Landstr. 1, 85764 Neuherberg, Germany

G. Grupe, G.C. McGlynn (eds.), *Isotopic Landscapes in Bioarchaeology*,
DOI 10.1007/978-3-662-48339-8_9

Introduction

The oxygen isotopic composition of biologically produced skeletal compounds and tissues from continental and marine archives is frequently used for the reconstruction of palaeoclimate and palaeoenvironments. Stable isotope records in continental areas are composed of tree-rings (Mayr et al. 2003), aquatic plant remains (Zhu et al. 2014), biogenic silica from lacustrine microfossils (Heyng et al. 2015), or carbonate from lacustrine shells (Schöll-Barna et al. 2012). In archaeological and palaeontological studies, the isotopic investigations of vertebrate bones and teeth additionally provide a wealth of information about animal and human living conditions and environments (Schoeninger and Moore 1992; Iacumin et al. 1996a; Grupe et al. 1997; Bentley and Knipper 2005), but also of palaeoclimatic variations (D'Angela and Longinelli 1993; Drucker et al. 2011). Besides an accurate dating, a profound understanding of the underlying processes determining each of the named isotope proxies is crucial for the interpretation of isotope records. Here, results of oxygen isotope analyses from mammalian bones from the Late Neolithic to Roman Times are presented and interpreted in terms of their geospatial variability. Before this, a short outline of the basics of applying oxygen isotopes from terrestrial archives in general, and of stable oxygen isotope ratios in bone phosphate in particular, for environmental research is given.

Oxygen Stable Isotopes and Hydrological Processes

The relationship between oxygen isotope ratios and climate is due to different behaviour of the water isotopologues in physical processes and chemical reactions. The associated changes in the ratio of $^{18}O/^{16}O$ (R) between a substrate and a product often occur in a predictable and measurable manner and are expressed as isotope fractionation factors. The isotope fractionation factor (α) of such a process commonly describes the change in the isotope ratio of a reactant relative to a product according to the following formula:

$$\alpha = R_{\text{reactant}}/R_{\text{product}} \quad (1)$$

Isotope fractionations are often strongly dependent on ambient temperature and can be accurately quantified. For instance, the most abundant oxygen isotope isotopologues $H_2{}^{16}O$ and $H_2{}^{18}O$ in natural water are partitioned differently during condensation and evaporation processes in the vapour and liquid phase. In the hydrological cycle, oxygen isotope fractionations occur, e.g., during evaporation of seawater and subsequent condensation processes during precipitation formation. Since the isotopic composition of precipitation is strongly dependent on the condensation temperature (Horita and Wesolowski 1994), the strong correlation

between air temperature and $\delta^{18}O$ of precipitation (Dansgaard 1964; Rozanski et al. 1993) is explained.

Other isotope effects in the hydrological cycle are linked to the history of an air mass from its source area to the area where condensation takes place. The further a moisture-bearing air mass moves away from its oceanic source region, the more its remaining vapour is enriched in the light isotope ^{16}O relative to ^{18}O due to successive cooling and rainout of the air mass (Gat 1996). Such effects are enhanced by orographic mountain barriers, large continents to be crossed by air masses, and latitudinal pathways of air masses coming from the atmospheric "heat engine" in the low latitudes. These effects are denominated as altitude, continental, and latitude effects, respectively (Dansgaard 1964).

Both temperature-dependent isotopic fractionation and air mass-related isotope effects reflect climatic and geospatial processes which are reflected in geo-biological archives. Thus, oxygen isotopes of biomaterials, such as bones and tooth enamel, in principle provide a valuable tool for archaeological studies by detecting origins and migration of animal and human populations (Dupras and Schwarcz 2001; Drucker et al. 2011) or palaeoclimatic changes (D'Angela and Longinelli 1993). Various tissues and compounds were investigated for such studies, e.g. collagen, phosphate, and carbonate in bones and—if preserved—hair, skin, and meat (e.g. Iacumin et al. 1996a). Here, we focus on oxygen isotopes of mammalian bones, in particular on bone phosphate, which is biogenic apatite with the generalized formula $Ca_5(PO_4,CO_3,F)_3(OH,F,Cl,CO_3)$ (Vennemann et al. 2002). This component is considered less prone to diagenetic alteration as bone carbonate (Iacumin et al. 1996b). The main advantage of using mammal remains for palaeoenvironmental reconstructions, compared to, e.g., carbonate shells of invertebrates, is that they are formed at a constant temperature of about 37 °C in mammals heavier than about 1 kg (Bryant and Froelich 1995). Thus, the isotopic composition of ingested water can directly be derived from bone phosphate and need not to be disentangled from temperature-dependent isotopic fractionation effects as is the case for most other biological oxygen isotope recorders (Luz and Kolodny 1989).

Oxygen Isotope Fractionations in Mammals

To fully understand the factors which are of influence on bone phosphate oxygen isotopes the oxygen sources and partitioning of their isotopes need to be evaluated as suggested in the fundamental study of Luz and Kolodny (1985). Sources of oxygen influx into the mammal body are mainly drinking water, organically bound oxygen in ingested food, and inhaled atmospheric oxygen. Oxygen is lost from a mammal body in the form of urine, transpired and exhaled water vapour, or as respired CO_2. In a mammal body, in which the oxygen balance is in steady state, the entering fluxes should equal those leaving the body. The associated fractionations of each of these fluxes can be estimated and permit the modelling of the isotopic

composition of body water (Luz and Kolodny 1985). Further model approaches integrated a nonlinear relation of oxygen fluxes with body mass, explaining the considerably differing oxygen isotopic relation between body water and ingested water of mammal species of varying size (Bryant and Froelich 1995). Accordingly, the body water of mammals with a large body size reflect the meteoric water isotopic composition better than those of small mammals, mainly because of higher proportions of drinking water relative to other oxygen influxes (Bryant and Froelich 1995).

Objectives of This Study

In this study, the relation between oxygen isotope composition of bone phosphate and geospatial data (latitude and altitude) was explored. Bone phosphate was purified from three different mammal taxa excavated at archaeological sites along a transect crossing the Alps. The data were obtained in the frame of the research project "Transalpine mobility and culture transfer" (research unit of the Deutsche Forschungsgemeinschaft DFG, FOR 1670) and represent a first database that will be completed with further isotopic investigations on animal and human remains from this area.

Material and Methods

Sites and Material

In this project, mammal bones from 16 archaeological sites in Germany, Austria, and Italy were investigated isotopically. The sites are located along a transect from 49.1°N (Berching–Pollanten) to 46.2°N (Zambana, northern Italy) at longitudes between 10.9°E and 11.8°E (Table 1). The sites along this transect reach from the Franconian Alb in southern Germany to South Tyrol (Trentino–Alto Adige) in northern Italy and thus cross the Alps from North to South. The altitude of the sites covers a range from 194 m a.s.l. (Zambana, Italy) to 792 m a.s.l. (Mieming, Austria). Mammal bones of three species were selected from archaeological collections. The selected bones belonged to three taxa: red deer (*Cervus elaphus*), domestic pigs (*Sus domesticus*), and domestic cattle (*Bos taurus*). Three different individuals per taxon were intended for isotopic analyses. However, six sites did not provide any deer bones. Although pig and cattle bones existed from all sites, not always three replicates were available (Table 1). In total, 26 deer, 47 cattle, and 45 pig bones were selected. The bones stem from different parts of the skeleton including cranium, mandibula, costa, coxa, scapula, and limb bones.

Table 1 Sites, number of investigated bone material, and geographical data

Site	Site no.	Cultural period	Latitude °S	Longitude °E	Altitude (m a.s.l.)	*N Cervus*	*N Bos*	*N Sus*
Berching–Pollanten, Germany	106	Iron Age (Latène)	49.1434	11.4477	400	3	3	3
Griesstetten, Germany	115	Late Neolithic	49.0290	11.6006	391	3	3	3
Manching, Germany	127	Iron Age (Latène)	48.7152	11.5258	379	3	3	3
Freising, Germany	114	Bronze Age (urnfield period) and Iron Age	48.3986	11.7473	459	3	3	3
Eching, Germany	108	Middle Bronze Age	48.2204	11.5323	483	0	2	2
Pestenacker, Germany	131	Late Neolithic	48.1459	10.9488	572	3	3	3
München–Unterhaching, Germany	137	Roman period	48.0605	11.6257	561	3	3	3
München–Grünwald, Germany	116	Iron Age	48.0373	11.5305	599	0	3	3
Wiesing, Austria	236	Bronze Age	47.3954	11.7914	614	0	3	3
Mieming, Austria	229	Iron Age	47.2820	10.9626	792	3	3	3
Ampass–Widumfeld, Austria	237	Iron Age, Roman period	47.2590	11.4580	636	1	3	3
Bergisel, Austria	201	Iron Age	47.2469	11.4000	725	0	3	3
Brixen–Stufels (Villa Kranebitt), Italy	314	Iron Age	46.7189	11.6598	553	1	3	1
Brixen–Stufels (Hotel Dominik), Italy	301	Iron Age	46.7167	11.6617	572	3	3	3
Sanzeno, Italy	310	Iron Age	46.3702	11.0802	683	0	3	3
Zambana–El Vato, Italy	311	Iron Age	46.1670	11.0812	194	0	3	3
Total number						26	47	45

The site number represents the internal code of the project

The archaeological sites are dated into the Late Neolithic (Griesstetten, Pestenacker), the Bronze Age (Freising, Eching, Wiesing), the Iron Age (Berching–Pollanten, Freising, Manching, München–Grünwald, Mieming, Ampass-Widumfeld, Bergisel, Brixen Stufels, Sanzeno, Zambana) and the Roman period (München–Unterhaching, Ampass-Widumfeld), thus covering approximately 4000 years.

Bone Phosphate Preparation

The isolation of phosphate from bone material is necessary to avoid analytical bias caused by contaminants with different isotopic composition such as collagen and carbonate. In a first step the bone sample was homogenized. For the removal of organic compounds, 5 ml of 4 % NaOCl solution was added to 100 mg of bone powder each and thoroughly mixed. The solution was replaced after the second day and continued until no reaction, indicated by bubble formation, was observed anymore. This was the case after 2.5–3 days. Thereafter, each sample was rinsed 5–6 times with distilled water and centrifuged (2100 g, 5 min) until the suspension was of neutral pH. Subsequently, the pellets were stirred in 5 ml 1 M calcium acetate–acetic acid buffer for half a day to remove absorbed carbonate. After four times rinsing with distilled water, the pellets were lyophilized.

For precipitation of bone phosphate as silver phosphate, a method similar to the one published by Joachimski et al (2009) was applied. Three milligram of the lyophilized sample was dissolved in 115 µl 2 M HF for 6 h in an Eppendorf® tube to precipitate calcium from the solution. Thereafter, 115 µl of 2 M KOH were added to neutralize the solution. After this step, the solution was centrifuged (3000 rpm, 15 min) and the supernatant pipetted off. Thereafter, silver phosphate was precipitated by adding 1500 µl of $AgNO_3$ solution (pH = 10–11). Then the samples were placed in a heated water bath (60 °C) for 12 h to ensure complete silver phosphate precipitation. The supernatant $AgNO_3$ solution was pipetted off (pH < 7) and the silver phosphate crystals were rinsed with distilled water. The crystals were removed from the wall of the reaction tube in an ultrasonic bath for 3 min. Rinsing with distilled water and ultrasonic treatment were repeated until all crystals accumulated at the tube bottom. Then the water was pipetted off and the samples dried in an oven at 60 °C for 3–4 h until all water was evaporated. The crystals were crushed in the Eppendorf® tube and the resulting powder was used for isotope analyses.

Stable Isotope Analyses

For isotope analyses, 0.92–0.94 mg of silver phosphate was weighed with a microbalance and wrapped into silver capsules. Prior to analyses, the samples

were stored in a vacuum drying cabinet at 60 °C for 48 h to remove any water vapour from the samples. After thorough drying, the samples were immediately filled in an autosampler flushed with helium. The samples were successively pyrolysed in a HEKAtech HT Oxygen Analyser. Pyrolysis took place quantitatively in a SiC-reaction tube at 1490 °C in the presence of glassy carbon covered with a thin layer of granulated carbon. The resulting gas carbon monoxide was transferred in a continuous helium flow via a trap filled with Carbosorb and $MgClO_4$ (both HEKAtech) and a gas chromatography column (GC, temperature 70 °C) to an isotope-ratio-mass spectrometer (Delta V Advantage, Thermo Fisher Scientific). Oxygen isotope ratios ($R = {}^{18}O/{}^{16}O$) of bone phosphate are reported in the common delta notation in ‰ deviation from the standard VSMOW as

$$\delta^{18}O = \left(R_{sample}/R_{VSMOW} - 1\right) \times 1000 \quad (2)$$

The $\delta^{18}O$ values were calculated from the *m/z* ratios 30 and 28 recorded in the mass spectrometer and were calculated using the international benzoic acid standards IAEA 601 ($\delta^{18}O = 23.3$ ‰) and IAEA 602 ($\delta^{18}O = 71.4$ ‰). Additionally, a laboratory α-cellulose standard ($\delta^{18}O = 31.4$ ‰; Sigma-Aldrich) was used for the verification and quality control of isotope values. A phosphorite rock standard (NBS 120c; National Institute of Standards and Technology NIST, USA) and bone ash (SRM 1400; NIST, USA) were processed in the same way as the bone samples and revealed $\delta^{18}O$ values of 22.6 ‰ ($N = 21$) and 17.1 ‰ ($N = 23$), respectively. Analytical precision derived from both standards was 0.2 ‰ (one standard deviation). The $\delta^{18}O$ value of NBS 120c is still debated. The value obtained in our study agrees with previously reported values of 22.6 ± 0.1 ‰ (Vennemann et al. (2002) and 22.4 ± 0.2 ‰ (Fischer et al. 2013), but disagrees with lower values reported in some other publications (Daux et al. 2008; Halas et al. 2011; see Fischer et al. 2013 for discussion). Such differences may arise from different calibration standards, phosphate extraction protocols or methods, and devices for isotope analyses (Vennemann et al. 2002). Triplicate analyses of 24 bone phosphate samples revealed an average standard deviation of 0.12 ‰. Oxygen concentrations of the samples were used to check the purity of the extracted phosphate. They were determined from sample peak areas related to weight of certified elemental standards, which were included regularly in each series of measurements.

Results

Inter-species Differences

Standard deviations of replicate analyses ($N = 3$ specimens per site) of bone phosphate ($\delta^{18}O_P$) ranged between 0.04 ‰ (pigs from Manching) and 1.14 ‰ (deer from Brixen-Stufels, Hotel Dominik). The correlation between mean $\delta^{18}O_P$

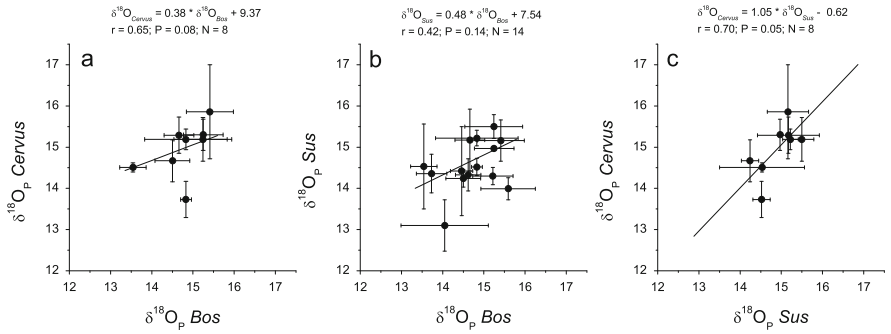

Fig. 1 Inter-species correlations between $\delta^{18}O_P$ values of (**a**) deer (*Cervus*), (**b**) cattle (*Bos*), and (**c**) pigs (*Sus*). Each *dot* represents the mean value of replicate samples from a site. The respective number of sites (N) and statistical parameters (*r*- and *P*-values, two-sided *t*-tests) are indicated below the correlation equation. *Bars* represent standard deviations of the mean of three replicates

values of different species was tested (Fig. 1). Only sites with three replicate analyses per species were used for this analysis reducing the number of sites for all correlations in which *Cervus* was involved (Fig. 1a, c). Inter-species correlations were weak except for correlations of *Cervus* versus *Sus* (Fig. 1c). A slope close to unity and an intercept close to 0 were observed for the correlation between these two species only.

Spatial Correlations

The relation of the bone phosphate $\delta^{18}O$ values with latitudinal position of the 16 archaeological sites is shown in Fig. 2. Higher $\delta^{18}O_P$ values occur more frequently in the northern and southern sites than in the central Alpine sites. A comparison between $\delta^{18}O$ values and altitude demonstrates that the driving force behind this pattern is the altitudinal position of the site rather than latitude (Fig. 2d).

All species exhibit a negative correlation with altitude (Fig. 3). Pig specimens from the site Zambana did not fit to the general correlation pattern and therefore were excluded. One deer specimen from Brixen-Stufels (Hotel Dominik) was not excluded from the correlation, although it had an extremely ^{18}O-enriched value of 17.1‰ and is the reason for a weak correlation and a relatively flat slope of the respective regression line. The slope of the line for deer changes from (-0.0020 ± 0.0011)‰ m^{-1} to (-0.0023 ± 0.0008)‰ m^{-1} and the correlation coefficient from -0.35 ($P = 0.07$) to -0.50 ($P = 0.01$), if this value is discarded. The $\delta^{18}O_P$—altitude relations for *Sus domesticus* (Zambana excluded) and *Cervus elaphus* were both significant at the 99.9 % level (Fig. 3) and had similar slopes (-0.0031 and -0.0028, respectively).

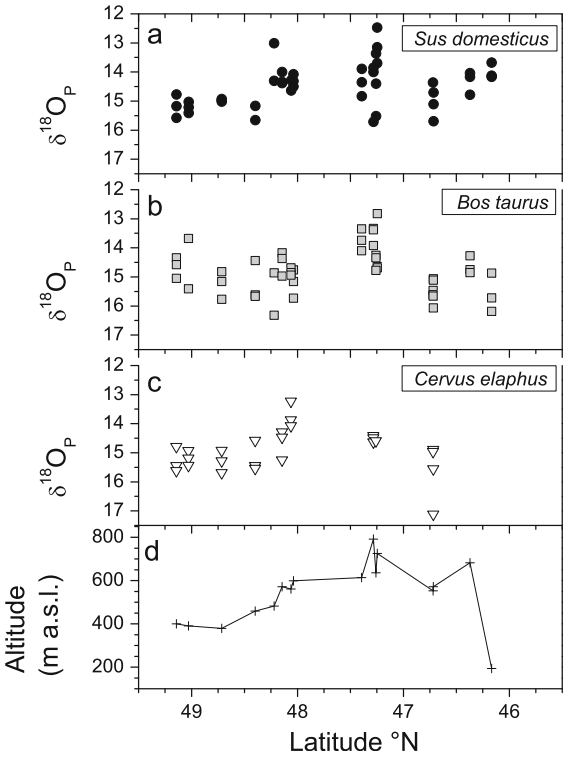

Fig. 2 (**a**–**c**) $\delta^{18}O_P$ values of the three investigated species versus latitudinal position of the respective sites. (**d**) Altitudinal range of the archaeological sites from which the bones come from. Note the inverse scale for $\delta^{18}O_P$ values for better comparison with altitude

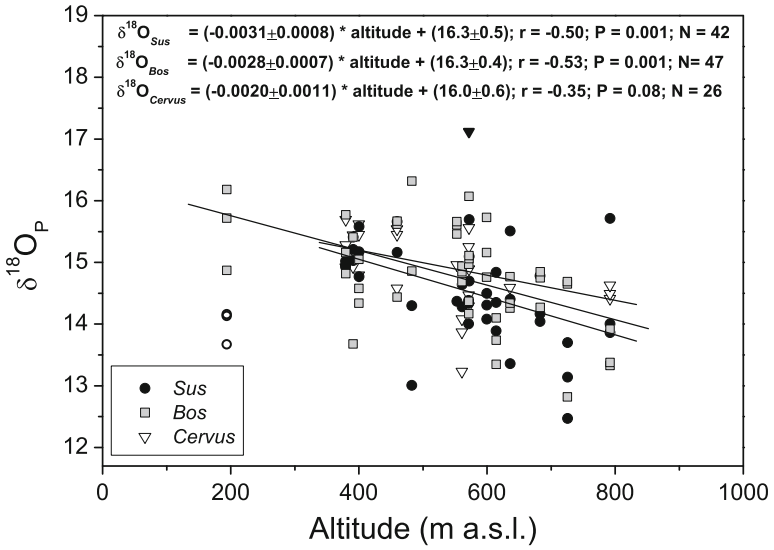

Fig. 3 Correlation between $\delta^{18}O_P$ values of single specimens versus altitude of the sites. Three specimens from the locality Zambana were excluded from the regression for *Sus domesticus* (*open circles*)

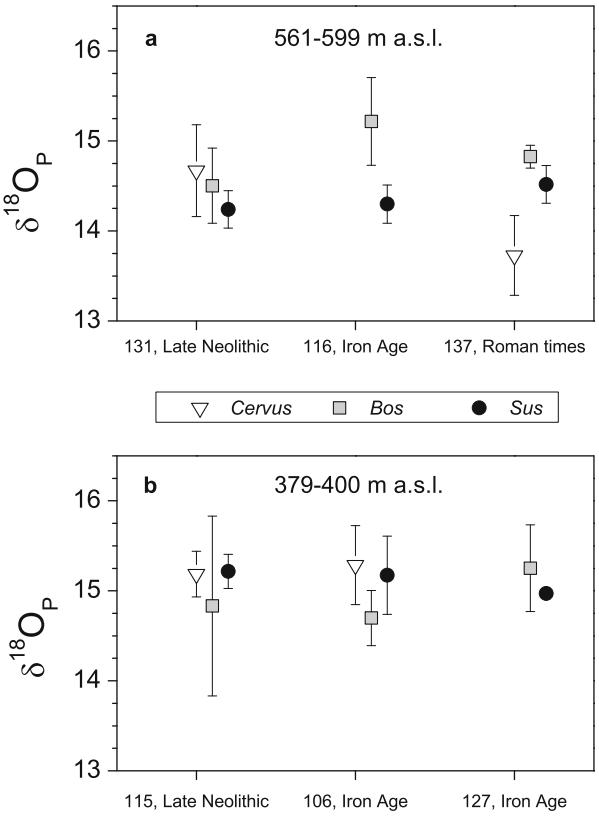

Fig. 4 Comparison of $\delta^{18}O_P$ values from sites with different age. The sites chosen are from the same region and similar in elevation. *Symbols* represent mean values from three specimens per taxon and bars one standard deviation from the mean. (**a**) sites at elevations between 561 and 599 m a.s.l. from southern Bavaria, Germany (Pestenacker, München–Grünwald, München–Unterhaching). Sites are attributed to the Late Neolithic, Iron Age and Roman Antiquity, respectively. (**b**) sites from the Franconian Alb and Danube valley in Germany (Griesstetten, Berching–Pollanten, Manching) at elevations between 379 and 400 m a.s.l. These sites belong to the Late Neolithic and Iron Age, respectively. Numbers next to the cultural period refer to site numbers in Table 1

Temporal Variability

The bone material covers a time period from Late Neolithic to Roman Times. To test potential temporal variability of the source water isotopic composition, different sites were compared with each other. The selection for this comparison took the altitude effect into account. Therefore, only sites from the same area and altitude were compared.

Two areas provided sufficient data for the test. The first region (Fig. 4a), located in southern Germany, comprises the sites Pestenacker, München–Grünwald, and

München–Unterhaching. These sites are located at elevations between 561 and 599 m a.s.l. and provide sufficient $\delta^{18}O_P$ values per species for comparison except of *Cervus* which is missing at München–Grünwald. The sites cover the Late Neolithic (Pestenacker), the Iron Age (München–Grünwald) and the Roman Times (München–Unterhaching). Taking all species together, no clear temporal trend is observed at these sites. However, *Bos* and *Sus* differ at the site München–Grünwald and *Cervus* deviates from the other taxa at München–Unterhaching (Fig. 4a).

The second region is at elevations between 379 and 400 m a.s.l. in southern Germany (Fig. 4b). The sites Griesstetten and Berching-Pollanten are located in the Franconian Alb, the third site, Manching, close to the Danube river. The bones from Griesstetten are from the Late Neolithic while the other finds are from the Iron Age. No consistent temporal trend was observed in this region as well, demonstrating that temporal changes of source water isotopic composition for the investigated time periods played a minor role compared to geospatial factors like site elevation.

Discussion

$\delta^{18}O_P$ and Source–Water Isotopic Composition

Similar to a study from ancient Egypt (Iacumin et al. 1996b), we found no significant temporal $\delta^{18}O_P$ variations pointing to a small signal-to-noise-ratio with regard to this effect. The geographical patterns, in particular altitude, had a much stronger imprint on $\delta^{18}O_P$ in our dataset. In particular, our $\delta^{18}O_P$ data from archaeological sites crossing the Alps from north to south demonstrate a significant correlation with site elevation. Such a relation is expected, if bone phosphate reflects the isotopic composition of local meteoric water, which should be the primary source of ingested water ($\delta^{18}O_W$) for most domesticated animals bred on site. However, fluxes and isotopic fractionations related to oxygen loss by respiration, transpiration, and excretion further shape body water isotopic composition, as outlined before. Thus, animal behaviour and physiology along with body mass can lead to significant differences in body water isotopic composition exemplified by differing equations for pigs and humans in the fundamental study by Longinelli (1984). The least squares fit for domestic pigs in this study provided the equation:

$$\delta^{18}O_{\text{blood, pig}} = (0.88 \pm 0.05) \times \delta^{18}O_W + 2.1 \quad (3)$$

In the same study the relation for humans was:

$$\delta^{18}O_{\text{blood, human}} = (0.60 \pm 0.03) \times \delta^{18}O_W + 0.68 \quad (4)$$

Since slopes between $\delta^{18}O_P$ and $\delta^{18}O_W$ were statistically indifferent from those of Eqs. (3) and (4), respectively, Longinelli (1984) concluded that the phosphate–water fractionation factor is constant. The equation for the $\delta^{18}O_P$–$\delta^{18}O_W$ relation for pigs found in this study was

$$\delta^{18}O_{P,\ \mathrm{pig}} = (0.86 \pm 0.05) \times \delta^{18}\ O_W + 22.71 \quad (5)$$

An oxygen isotope fractionation factor between bone phosphate and body water of 1.021 is commonly applied (Longinelli 1984; Meier-Augenstein 2010).

Different slopes of the regression lines in Fig. 3 between deer and the other taxa demonstrate that the mammals investigated in our study variably reflect the isotopic composition of the water they have taken up. Calibration studies by D'Angela and Longinelli (1990) yield the relations for the other two taxa investigated in our study. The following equation describes the respective relation for red deer (D'Angela and Longinelli 1990):

$$\delta^{18}O_{P,\ \mathrm{deer}} = (1.13 \pm 0.14) \times \delta^{18}O_W + 25.55 \quad (6)$$

The respective relationship for cattle (D'Angela and Longinelli 1990) is described by the equation:

$$\delta^{18}O_{P,\ \mathrm{cattle}} = (1.01 \pm 0.04) \times \delta^{18}O_W + 24.90 \quad (7)$$

The largely differing equations for the taxa partly explain the weak correlation between the taxa in our study (Fig. 1).

Reconstruction of Source Water Isotopic Composition

Rearranging Eqs. (5), (6), and (7) allows calculation of $\delta^{18}O_W$ for our dataset (Fig. 5). The slope of the regression lines between reconstructed $\delta^{18}O_W$ and altitude was different for the three taxa. The regression for pigs exhibited the highest (−0.0036) and for deer the lowest (−0.0018) slope. Given the overlapping errors, however, the slopes are indistinguishable. The varying number of individuals per taxa and obvious outliers weaken the statistical significance of these equations. Thus, all reconstructed $\delta^{18}O_W$ per site were averaged in the next step to minimize inter-site differences caused by varying specimen numbers. Although the degrees of freedom were reduced by this procedure, the overall slope in the correlation with altitudinal position appears to be better characterized (Fig. 6). Obviously, the specimens from the site Zambana, in particular the pigs, do not fit to the overall altitude relation. This site has the lowest altitude and is situated in the valley of the river Adige in northern Italy. It is possible that at this site some cattle and all pigs ingested river water that originated from higher altitudes. Such water is feeding the wells at the site until today. This would explain, why only at this site the values

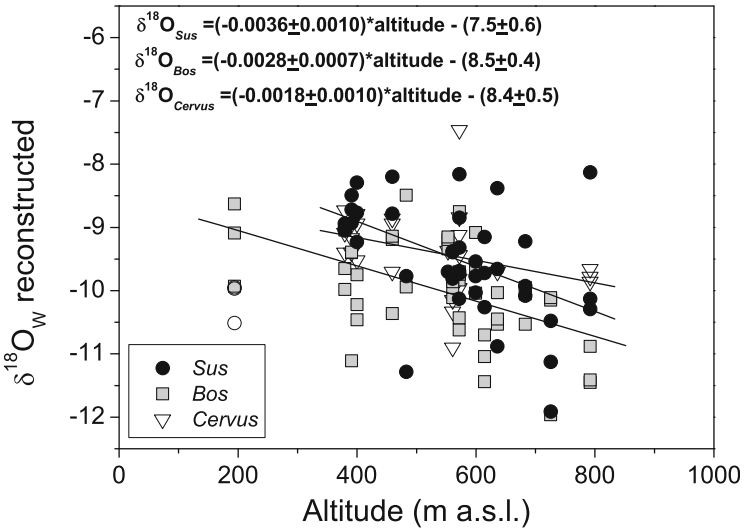

Fig. 5 Reconstruction of the oxygen isotope composition of ingested water for the three mammal taxa investigated versus altitude of the localities. *Dashed lines* represent regression lines. Note that pigs from the site Zambana (*open circles*) were not used for statistical correlations

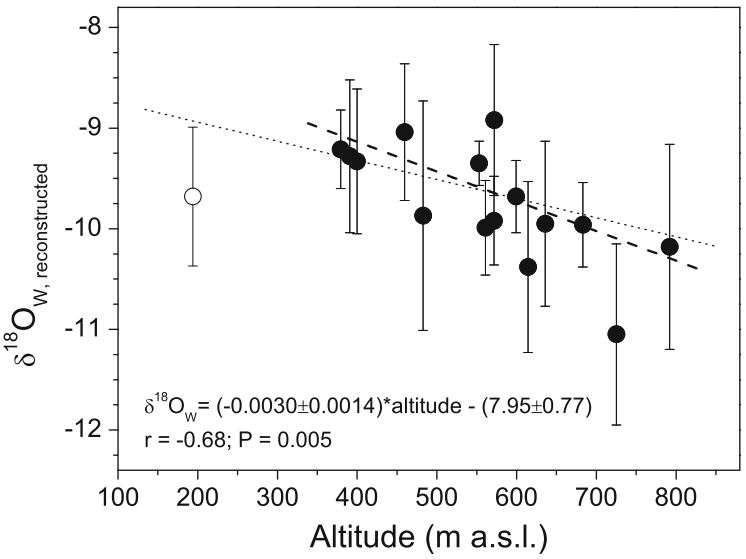

Fig. 6 Correlation between reconstructed mean water isotope values and altitude. Values from all specimens and taxa were averaged per site. *Bars* represent one standard deviation from each mean. *Dotted line* represents the regression line for all sites, *dashed line* for correlation with the site Zambana excluded. The regression equation is given for the latter selection

deviate strongly from the overall correlation. If the site Zambana is excluded, the relation between $\delta^{18}O_W$ and altitude is described by the equation:

$$\delta^{18}O_{W\ \text{reconstructed}} = (-0.0030 \pm 0.0014) \times \text{altitude} - (7.95 \pm 0.77) \quad (8)$$

The significant correlation of the remaining sites demonstrates that the altitude effect on the isotopic composition of meteoric water is reflected in the reconstructed $\delta^{18}O_W$ record. In a recent study, the isotopic composition of precipitation from 39 stations in Switzerland and adjacent regions for the period AD 1995–2000 was investigated by Kern et al. (2014). Their study demonstrated a strong linear relationship of annual precipitation with altitude at sites below 1200 m a.s.l., i.e. below the planetary boundary layer. At altitudes above the planetary boundary layer no significant correlation was found in the same study. The correlation of $\delta^{18}O$ for precipitation with altitude also varied with season and exhibited steeper slopes during winter compared to summer months (Kern et al. 2014). The study provided the following relation between altitude and annual amount-weighed $\delta^{18}O$ values of precipitation:

$$\delta^{18}O_{\text{meteoric water}} = -0.0034 \times \text{altitude} - 7.76 \ \text{(Kern et al. 2014)} \quad (9)$$

Within errors of slopes and intercepts, Eqs. (8) and (9) are indistinguishable from each other, demonstrating that the isotopic imprint of altitude is still preserved in the archaeological bone phosphate. Exceptions, like the material from the site Zambana or single outliers, however, also demonstrate that sufficient material has to be available to come to reliable conclusions and identify archaeological sites for which this relation is not valid due to diagenetic overprint, animal migration, or water sources of non-local origin. This apparent flaw of the method, however, bears also the potential to detect isotopic deviations caused by domestication, migration, and trade habits of ancient human populations that can be further substantiated by applying additional isotope systems such as strontium, nitrogen, sulphur, and carbon (Drucker et al. 2011).

Conclusions

The first results from oxygen isotope values of bone phosphate from trans-Alpine archaeological sites provided significant correlations with altitude. Thus, the bone isotope signature provides a promising proxy for palaeoaltitude reconstructions in the Alps, albeit some restrictions of the approach became evident. The reliability of altitudinal reconstructions increased substantially with the number of specimens per site. Potentially also the selected taxon plays a role. The altitude relation should be less significant for wild mammals seasonally migrating in different altitudes. Such behaviour could explain the less significant correlation with altitude for oxygen isotopes from deer in our study. Regression line slopes of reconstructed

water isotopic composition derived from domestic pigs and cattle bones versus altitude were similar to modern meteoric water in the Alps. Therefore, isotope values of these taxa can serve as reliable integrators of local isotopic composition of rainwater. However, pigs at the site Zambana illustrate the possibility that domestic mammals could have ingested water of non-local origin, such as river water, or that they were bred at locations other than where humans have deposited their remains. The latter option in turn, however, provides the potential to reconstruct prehistoric human behaviour, for instance, trade relations between populations. The comparison with other isotope techniques (e.g. $^{87}Sr/^{86}Sr$) in future studies will help to disentangle the potential causes for such outliers as the pig bones from the location Zambana.

Acknowledgements We are much indebted to Dr. Frank Söllner for help in the field and to Roswitha Höfner-Stich for assistance with stable isotope analyses. Prof. Dr. Joris Peters and Simon Trixl, M.A. are thanked for providing the mammalian bone material. This study was financially supported by the DFG Research Unit FOR 1670 "Transalpine mobility and culture transfer".

References

Bentley RA, Knipper C (2005) Geographical patterns in biologically available strontium, carbon and oxygen isotope signatures in prehistoric SW Germany. Archaeometry 47:629–644

Bryant JD, Froelich PN (1995) A model of oxygen isotope fractionation in body water of large mammals. Geochim Comsochim Acta 59:4523–4537

D'Angela D, Longinelli A (1990) Oxygen isotope in living mammal's bone phosphate: further results. Chem Geol 86:75–82

D'Angela D, Longinelli A (1993) Oxygen isotopic composition of fossil mammal bones of Holocene age: palaeoclimatological considerations. Chem Geol 103:171–179

Dansgaard W (1964) Stable isotopes in precipitation. Tellus 16:436–468

Daux V, Lécuyer C, Héran M-A, Amiot R, Simon L, Fourel F, Martineau F, Lynnerup N, Reychler H, Escarguel G (2008) Oxygen isotope fractionation between human phosphate and water revisited. J Hum Evol 55:1138–1147

Drucker DG, Bridault A, Cupillard C, Huijc A, Bocherens H (2011) Evolution of habitat and environment of red deer (Cervus elaphus) during the Late-glacial and early Holocene in eastern France (French Jura and the western Alps) using multi-isotope analysis ($\delta^{13}C$, $\delta^{15}N$, $\delta^{18}O$, $\delta^{34}S$) of archaeological remains. Q Int 245:268–278

Dupras TL, Schwarcz HP (2001) Strangers in a strange land: stable isotope evidence for human migration in the Dakhleh oasis, Egypt. J Archaeol Sci 28:1199–1208

Fischer J, Schneider JW, Voigt S, Joachimski MM, Tichomirowa M, Tütken T, Götze J, Berner U (2013) Oxygen and strontium isotopes from fossil shark teeth: environmental and ecological implication for Late Palaeozoic European basins. Chem Geol 342:44–62

Gat JR (1996) Oxygen and hydrogen isotopes in the hydrologic cycle. Annu Rev Earth Planet Sci 24:225–262

Grupe G, Price TD, Schröter P, Söllner F, Johnson CM, Beard BL (1997) Mobility of Bell Beaker people revealed by strontium isotope ratios of tooth and bone: a study of southern Bavarian skeletal remains. Appl Geochem 12:517–525

Halas S, Skrzypek G, Meier-Augenstein W, Pelc A, Kemp HF (2011) Inter-laboratory calibration of new silver orthophosphate comparison materials for the stable oxygen isotope analysis of phosphates. Rapid Commun Mass Spectrom 25:579–584

Heyng A, Mayr C, Lücke A, Moschen R, Wissel H, Striewski B, Bauersachs T (2015) Middle and Late Holocene paleotemperatures reconstructed from oxygen isotopes and GDGTs of sediments from Lake Pupuke, New Zealand. Q Int. doi:10.1016/j.quaint.2014.12.040

Horita J, Wesolowski DJ (1994) Liquid-vapor fractionation of oxygen and hydrogen isotopes of water from the freezing to the critical temperature. Geochim Cosmochim Acta 58:3425–3437

Iacumin P, Bocherens H, Mariotti A, Longinelli (1996a) An isotopic palaeoenvironmental study of human skeletal remains from the Nile Valley. Palaeogeogr Palaeoclimatol Palaeoecol 126:15–30

Iacumin P, Bocherens H, Mariotti A, Longinelli A (1996b) Oxygen analyses of co-existing carbonate and phosphate in biogenic apatite: a way to monitor diagenetic alteration of bone phosphate? Earth Planet Sci Lett 142:1–6

Joachimski MM, Breisig S, Buggisch W, Talent JA, Mawson R, Gereke M, Morrow JR, Day J, Weddige K (2009) Devonian climate and reef evolution: insights from oxygen isotopes in apatite. Earth Planet Sci Lett 284:599–609

Kern Z, Kohán B, Leuenberger M (2014) Precipitation isoscape of high reliefs: interpolation scheme designed and tested for monthly resolved precipitation oxygen isotope records of an Alpine domain. Atmos Chem Phys 14:1897–1907

Longinelli A (1984) Oxygen isotopes in mammal bone phosphate: a new tool for paleohydrological and paleoclimatological research? Geochim Cosmochim Acta 48:385–390

Luz B, Kolodny Y (1985) Oxygen isotope variations in phosphate of biogenic apatites, IV. Mammal teeth and bones. Earth Planet Sci Lett 75:29–36

Luz B, Kolodny Y (1989) Oxygen isotope variation in bone phosphate. Appl Geochem 4:317–323

Mayr C, Frenzel B, Friedrich M, Spurk M, Stichler W, Trimborn P (2003) Stable carbon- and hydrogen-isotope ratios of subfossil oaks in southern Germany: methodology and application to a composite record for the Holocene. The Holocene 13:393–402

Meier-Augenstein W (2010) Stable isotope forensics. Wiley-Blackwell, Chichester

Rozanski K, Araguás-Araguás L, Gonfiantini R (1993) Isotopic patterns in modern global precipitation. In: Swart PK, Lohmann KC, McKenzie J, Savin S (eds) Climate change in continental isotopic records, vol 78, Geophysical monograph. American Geophysical Union, Washington, pp 1–37

Schoeninger MJ, Moore K (1992) Bone stable isotope studies in archaeology. J World Prehist 6:247–296

Schöll-Barna G, Demény A, Serlegi G, Fábián S, Sümegi P, Fórisz I, Bajnóczi B (2012) Climatic variability in the late copper age: stable isotope fluctuation of prehistoric Unio pictorum (Unionidae) shells from Lake Balaton (Hungary). J Paleolimnol 47:87–100

Vennemann TW, Fricke HC, Blake RE, O'Neil JR, Colman A (2002) Oxygen isotope analysis of phosphates: a comparison of techniques for analysis of Ag_3PO_4. Chem Geol 185:321–336

Zhu J, Lücke A, Wissel H, Mayr C, Enters D, Ja Kim K, Ohlendorf C, Schäbitz F, Zolitschka B (2014) Climate history of the Southern Hemisphere Westerlies belt during the last glacial–interglacial transition revealed from lake water oxygen isotope reconstruction of Laguna Potrok Aike (52°S, Argentina). Clim Past 10:2153–2169

Oxygen and Hydrogen Stable Isotopes in Earth's Hydrologic Cycle

Robert van Geldern and Johannes A.C. Barth

Introduction

The foundations for the application of stable isotopes in geosciences were established in the 1940s and 1950s by the work of Harold Urey (1947) and the development of the first high precision gas source isotope ratio mass spectrometer (IRMS) (Nier 1947). Urey and coworkers discovered the oxygen isotope paleotemperature scale (Urey et al. 1951; Epstein et al. 1951) that marks the onset of quantitative paleoclimate reconstruction. Stable isotope analyses were soon applied in several pioneering survey studies that examined for example oxygen isotope variations in silicate rocks (Baertschi and Silverman 1951), variations in the carbon isotope ratio of various geological sources (Craig 1953), and in natural waters (Dansgaard 1954; Epstein and Mayeda 1953; Friedman 1953).

From these early beginnings, stable isotope research evolved into a powerful tool that has greatly influenced geoscientific research over the last 65 years. Stable isotopes are applied today in numerous scientific disciplines from geology over biology and medicine to planetary science.

The major elements of interest have been the so-called light stable isotopes of hydrogen (δ^2H), carbon (δ^{13}C), nitrogen (δ^{15}N), oxygen (δ^{18}O), and sulfur (δ^{34}S), also referred to as HCNOS. These elements form the *traditional* isotopes that provide the foundation for the field of stable isotope geochemistry. The investigation of variations in the isotopic composition of these elements provided important insights into today's geochemical cycles and the history of Earth.

The Earth can be divided into five different spheres: (1) biosphere, (2) atmosphere, (3) lithosphere, (4) hydrosphere, and (5) anthroposphere (Fig. 1). Spheres are not strictly separated but linked by physical and biogeochemical processes.

R. van Geldern (✉) • J.A.C. Barth
Department of Geography and Geosciences, GeoZentrum Nordbayern, Friedrich-Alexander University Erlangen-Nuremberg (FAU), Schlossgarten 5, 91054 Erlangen, Germany
e-mail: robert.van.geldern@fau.de

G. Grupe, G.C. McGlynn (eds.), *Isotopic Landscapes in Bioarchaeology*,
DOI 10.1007/978-3-662-48339-8_10

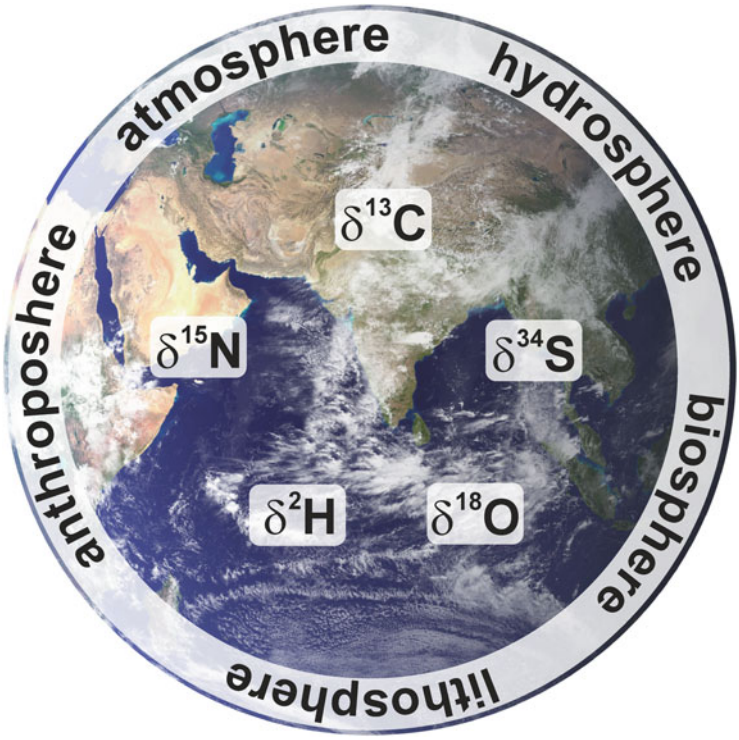

Fig. 1 Schematic representation of Earth's five spheres linked by the stable isotope systems of the elements H, C, N, O, and S

Stable isotope measurements play an important role in all these spheres and particularly across their boundaries. This work will highlight different aspects of stable isotope geochemistry with focus on water and its dissolved constituents.

The Earth's water cycle will be reviewed by means of oxygen and hydrogen stable isotopes. These isotope ratios serve as an ideal tool to trace the path of H_2O molecules from seawater evaporation over clouds in the atmosphere to precipitation that eventually returns to the sea.

Stable Isotopes in the Hydrologic Cycle

The Hydrologic Cycle

At its core, the hydrologic cycle describes the transition of water, liquid, or solid, from the Earth's surface into water vapor in the atmosphere and back again. During this continuous movement, water constantly changes states between liquid, vapor, and ice. Over 90 % of water that evaporated from the oceans goes directly back into

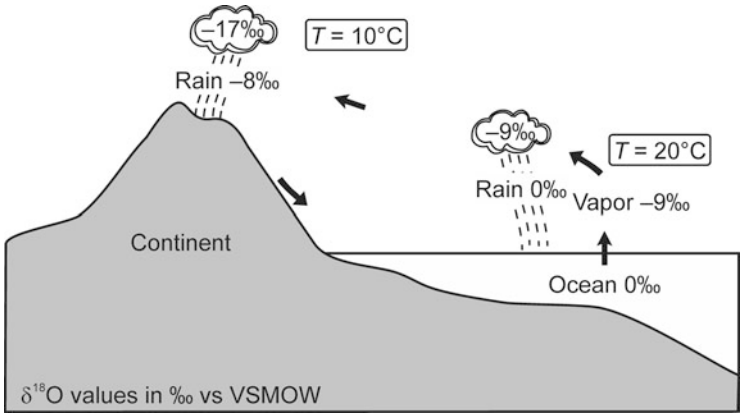

Fig. 2 Schematic representation of oxygen stable isotopes ($\delta^{18}O$) in the hydrologic cycle describing the continuous movement of water on the Earth. *VSMOW* Vienna Standard Mean Ocean Water (modified after Emerson and Hedges 2008)

the oceans as precipitation. The three major processes involved here are evaporation, condensation, and precipitation (Fig. 2). The hydrologic cycle becomes more complex for the about remaining 10 % of oceanic moisture that falls as precipitation over the continents. This water can travel along numerous pathways. When precipitation falls in the form of snow, it may be stored in frozen stage for thousands of years. Other water will return directly back to the ocean via surface runoff and rivers, while parts of precipitation infiltrate the surface from where water might be drawn up by plants to become vapor again through plant transpiration. Percolating water that bypasses this process recharges groundwater from where it can enter the anthroposphere and takes the way to human consumption and eventually reenters the water cycle in the form of sewage. Finally, almost all water returns to the oceans where the cycle continues.

Along its way, a water molecule will carry distinctive fingerprints in the form of heavy to light stable isotope ratios of oxygen ($^{18}O/^{16}O$) and hydrogen ($^{2}H/^{1}H$). The ratios are subject to change for example during phase transitions from liquid to vapor. This partial separation of isotopes is called isotope *fractionation* and can follow either equilibrium, kinetic, or non-mass-dependent processes. Measured by traditional IRMS or new laser-based techniques, this ratio carries information about the water vapor source and various other effects that influenced the stable isotope ratio during the various pathways in the hydrologic cycle.

All stable isotope values are expressed in the standard δ-notation (Coplen 2011; Brand et al. 2014) as deviations in per mil (‰) from the respective reference material according to

$$\delta = \left(\frac{R_{\text{sample}}}{R_{\text{reference}}} - 1 \right) \quad (1)$$

where R is the ratio of the numbers (n) of the heavy and light isotope of an element [e.g., $n(^{18}\text{O})/n(^{16}\text{O})$] in the sample and the reference (Coplen 2011). Oxygen and hydrogen isotope ratios are expressed relative to Vienna Standard Mean Ocean Water (VSMOW).

The key relationship for most of the abovementioned applications was published by Craig (1961) who detected the linear correlation between the $\delta^{18}\text{O}$ and $\delta^{2}\text{H}$ values of natural waters worldwide. This relation is called the global meteoric water line (GMWL) and was described by

$$\delta^{2}\text{H} = 8 \times \delta^{18}\text{O} + 10. \quad (2)$$

Local precipitation typically also defines a distinctive local meteoric water line (LMWL) that often differs from the above global correlation in slope and intercept.

The International Atomic Energy Agency (IAEA) in Vienna and the World Meteorological Organization (WMO) invest great efforts into the Global Network of Isotopes in Precipitation (GNIP) (IAEA/WMO 2006). This worldwide network operates since 1961 with the primary objective of collecting systematic data on the isotope content of precipitation on a global scale and to provide basic isotope data for the use on hydrological investigations (Schotterer et al. 1996).

More recently, this monitoring program was expanded to rivers by the Global Network of Isotopes in Rivers' (GNIR) initiative (IAEA 2012; new CRP program launched 2014). This new program plans to establish long-term records of river geochemistry that are crucial to understand the magnitude and direction of ongoing environmental changes.

From Precipitation to Groundwater

For most case studies in hydrology or hydrogeology it is essential to clearly define all participants, i.e., precipitation, groundwater, and surface water, with respect to their stable isotopic composition. Stable isotope values of local precipitation in temperate regions typically exhibit a sinusoidal shape with lower, more negative values in winter and higher values during summer. This defines the LMWL of a region. The annual mean value of precipitation, weighed by precipitation amount, often closely resembles the stable isotope value of close to surface and mostly unconfined aquifers, where groundwater is actively recharged by modern precipitation (Clark and Fritz 1997; Darling et al. 2006; Négrel and Petelet-Giraud 2011; Rozanski 1985; van Geldern et al. 2014a).

In many areas worldwide, the upper unconfined groundwater aquifers are influenced by anthropogenic use to various degrees with different contaminants,

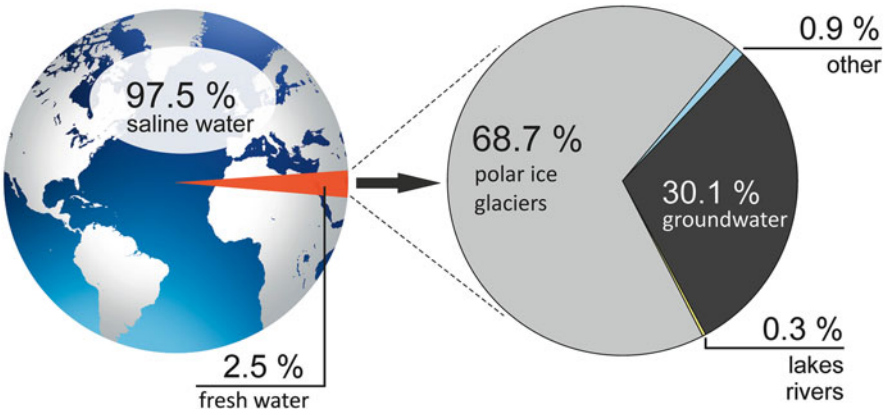

Fig. 3 Estimates of global water distribution. Freshwater represents only 2.5 % of the global water and from this fraction ~30 % is groundwater. Directly accessible lakes and rivers only represent 0.3 % of the global freshwater budget. The 0.9 % of remaining other water is mainly in the form of ground ice and permafrost. Numbers are after Gleick (1996)

whereas deeper confined aquifers hold potentially pristine water that often is hydraulically unconnected to shallow aquifers or surface water. In many cases, water from these deep aquifers is fossil paleo-water, a resource that is considered as nonrenewable on human timescale. These aquifers often provide valuable sources of good-quality drinking water, unaffected by impacts of the industrial era. They should therefore be treated as a strategic reserve (Edmunds 2001). Furthermore, groundwater is the world's largest usable freshwater resource (Fig. 3) and its accelerated depletion in many areas of the world is critically affecting food security and drinking water supply (Aeschbach-Hertig and Gleeson 2012).

A good example for the linkage between precipitation and groundwater are the aquifers of the Metropolitan Region Nuremberg that were investigated by van Geldern et al. (2014a). In their study, groundwater from two aquifers was analyzed for oxygen and hydrogen stable isotopes together with radiogenic isotopes to obtain absolute water ages. The groundwater samples from both aquifers were compared to the LMWL to investigate sources and conditions of groundwater recharge.

The confined groundwater stored in the Benkersandstein was identified as fossil Pleistocene paleo-groundwater by stable isotope and accompanying tritium and ^{14}C analyses. In contrast, the upper unconfined aquifer of the region mirrors the weighted average isotope value of local precipitation (Fig. 4). The significant shift to lower $\delta^{18}O$ and $\delta^{2}H$ values of the confined groundwater with respect to modern recharge indicates that groundwater recharge occurred during cooler conditions from isotopically depleted meltwater or precipitation during the Pleistocene ~20,000 year ago.

Clear identification of such nonrenewable paleo-waters by means of isotope geochemistry will help local water authorities to enact and justify measures for

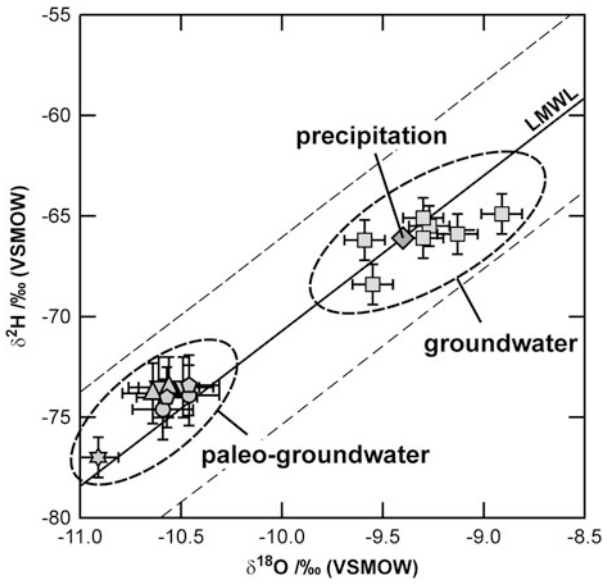

Fig. 4 Stable isotope compositions of precipitation, shallow, and deep groundwater. Paleo-groundwaters of the deep aquifer are characterized by lower stable isotope values that suggest cooler climatic conditions during recharge (modified from van Geldern et al. 2014a)

conservation of these valuable resources in the context of a sustainable water management.

Surface Water: Groundwater Interaction

Surface waters such as streams often receive pollutants including pharmaceuticals or personal care products that predominantly originate from discharges of sewage water treatment plants (Ternes 1998). Surface water exchanges with groundwater along rivers and streams and the pollutants can migrate to drinking water facilities that rely on bank filtration. Such wastewater-related pollutants can only be assessed properly by environmental tracers that truly mirror the migration of surface waters into the groundwater.

Stable isotopes provide such a tool for investigating and quantifying groundwater–surface water interaction under appropriate conditions. Provided that river water and groundwater show a pronounced difference in their $\delta^{18}O$ and $\delta^{2}H$ values, stable isotopes can be used to trace the fate and behavior of substances in the environment. Such conditions can occur after heavy precipitation events or during snowmelt. Besides the environmental tracers such as stable isotope also wastewater-related tracers such as for example the artificial sweetener acesulfame-K are often used to assess the hydrodynamic patterns along the riverbank.

A comparison of the stable isotopes $\delta^{2}H$ and $\delta^{18}O$ versus acesulfame-K, which are both assumed to behave conservatively in the environment, was published by

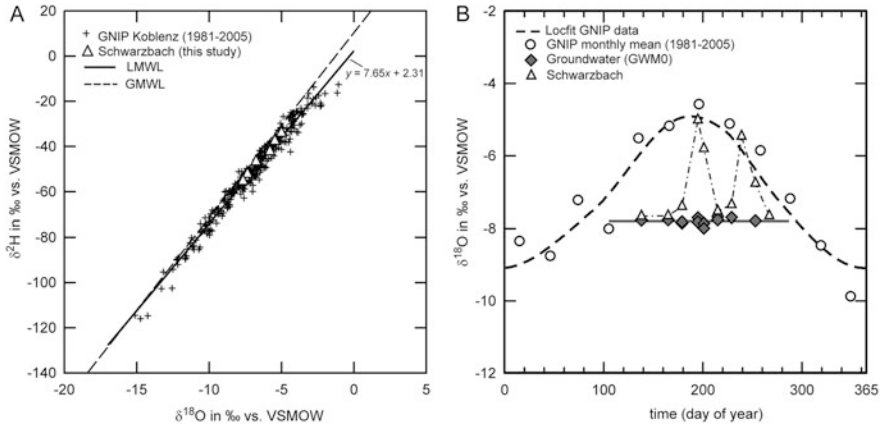

Fig. 5 (**a**) Precipitation isotope data with LMWL from GNIP station Koblenz (Germany) and stream data from the study site (Schwarzbach). (**b**) Locfit regression through weighted monthly mean precipitation data representing the seasonal sinusoidal function of local rainfall, groundwater isotope data, and stream water isotopic composition (from Engelhardt et al. 2014)

Engelhardt et al. (2014). During their 5-month study two flood events with very distinctive stable isotope compositions were detected (Fig. 5). Reduction of the river acesulfame-K concentrations due to dilution by surface runoff accompanied both isotope events. In contrast to stable isotopes, the event signal could not be traced properly in the groundwater observation wells (GWM) that were installed on both sides of the stream following the regional groundwater flow.

The results of the study point to limitations for the application of acesulfame to trace surface water–groundwater interactions. Acesulfame completely missed the wastewater-related surface water volumes that still remained in the hyporheic zone under stream-gaining conditions. On the other hand, stable isotopes proved to be valuable environmental tracers to identify surface water volumes within the hyporheic and riparian zones that work well also under stream-gaining and stream-losing conditions.

Stable Isotopes in Streams

Although GNIP stations are located worldwide, many areas still lack appropriate data coverage. Efforts were made to cover such areas by spatial data analyses of existing precipitation stable isotope data and to produce isotope distribution maps, so-called *isoscapes* (Bowen and Wilkinson 2002; Bowen 2010). However, such large-scale approaches will mostly not show specific regional details or the magnitude of isotope effects although recent efforts such as regionalized cluster-based water isotope prediction (RCWIP) maps might overcome these limitations (Terzer et al. 2013).

Kendall and Coplen (2001) demonstrated that the isotope composition of surface waters matches those of local precipitation and can be used to investigate spatial distributions of $\delta^{18}O$ and $\delta^{2}H$ of precipitation. Sampling surface water as a representative of local precipitation has the advantage that stream water often acts as a spatial and temporal integrator for the isotope composition of precipitation in a catchment and will also provide information on the isotope composition of groundwater that has been recharged by local precipitation (Kendall and Coplen 2001).

An example of the use of surface water instead of precipitation samples to characterize the isotope hydrological framework of an area with only little information about the isotopic composition of precipitation was recently published for the island of Corsica (van Geldern et al. 2014b). Corsica in the western Mediterranean is located in a region of intense climate change (Giorgi 2006). Because of its unique position, Corsica is ideal for recording climate variations through stable isotopes and has been selected for paleoclimate reconstructions based on stable isotope analyses of tree rings (Szymczak et al. 2012; Hetzer et al. 2014). For the evaluation and interpretation of such isotope paleoclimate proxies, it is essential to establish the isotope hydrology framework because the climatic character of a region is mainly determined by the water cycle (Lykoudis et al. 2010).

The study by van Geldern et al. (2014b) demonstrated that precipitation isotope effects can be traced in samples from streams and springs. Based on the analyses of these surface waters, it was possible to quantify isotope effects such as the altitude effect (Fig. 6) and to derive the mean isotope composition of the annual precipitation (δ_P). This value should be a good representative for the average isotope composition of the local groundwater at the island. The study can also help to better constrain the general hydrological framework for ongoing and future paleoclimate studies in this region that is highly sensitive to the global climate change.

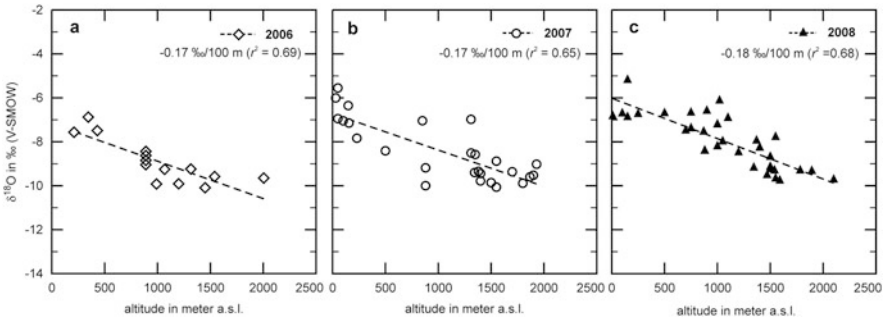

Fig. 6 Correlation between altitude of sampling location and oxygen isotope values for spring and stream samples taken in 2006, 2007, and 2008 at the island of Corsica. The slope of the linear regressions is similar in all years with a mean gradient of (-0.17 ± 0.02)‰/100 m elevation change for $\delta^{18}O$. Data after van Geldern et al. (2014b)

Other studies on rivers applied oxygen and hydrogen stable isotope analyses of water to evaluate the contribution of waters from the different compartments (groundwater, soil water, surface runoff) to streamflow generation in a karst river (van Geldern et al. 2015). Stable isotopes can also be used to detect anthropogenic influences caused by reservoir dams or the use of river water for power plant cooling purposes that can cause a relative enrichment in the heavy isotopes of the river water (Stögbauer et al. 2008).

Coastal Aquifers and Submarine Groundwater Discharge

At the end of its journey back to the ocean, freshwater will eventually mix with seawater. In contrast to meteoric water that is often characterized by more variable and rather negative isotope values, seawater shows much less spatial and temporal variations and typically exhibits values of (0 ± 1.5‰) for $\delta^{18}O$ (Bigg and Rohling 2000). Due to this distinct difference in their stable isotopic compositions, the amounts of freshwater and seawater in a mixed sample can be evaluated by mass balance calculations. When both end members are well defined with respect to their stable isotope values, it is possible to calculate the portion of each end member in a sample according to

$$a_{\mathrm{fw}} = \frac{\delta_{\mathrm{sample}} - \delta_{\mathrm{sw}}}{\delta_{\mathrm{fw}} - \delta_{\mathrm{sw}}} \tag{3}$$

$$b_{\mathrm{sw}} = \frac{\delta_{\mathrm{fw}} - \delta_{\mathrm{sample}}}{\delta_{\mathrm{fw}} - \delta_{\mathrm{sw}}} \tag{4}$$

where a_{fw} and b_{sw} are the portions of freshwater (fw) and seawater (sw) in the water sample, and δ are the corresponding isotope values ($\delta^{18}O$ or $\delta^{2}H$) according to their subscripts. Both end members define a linear mixing line in a $\delta^{18}O$ versus $\delta^{2}H$ diagram and any sample that represents a mixture of these end members plot along this line between these two sources.

This method was for instance used by Chandrajith et al. (2014) for the calculation of saltwater intrusion into a coastal freshwater aquifer in Sri Lanka. The local communities in this region depend entirely on groundwater, and one of the biggest threats to these fragile aquifers is seawater intrusion. Their study showed that salinization currently does not occur to a large extent but could be a potential threat due to predicted climate changes in the near future.

In another study, stable isotopes were also successfully used to identify the origin of the freshwater lens below the New Jersey shelf at the US East Coast (van Geldern et al. 2013). The large submarine freshwater lens under the shelf was first described by Hathaway et al. (1979) and subsequently attributed to trapped Pleistocene paleo-waters that were recharged during the last glacial maximum (LGM). Hydrogeological models suggested that the freshwater lens was emplaced by a

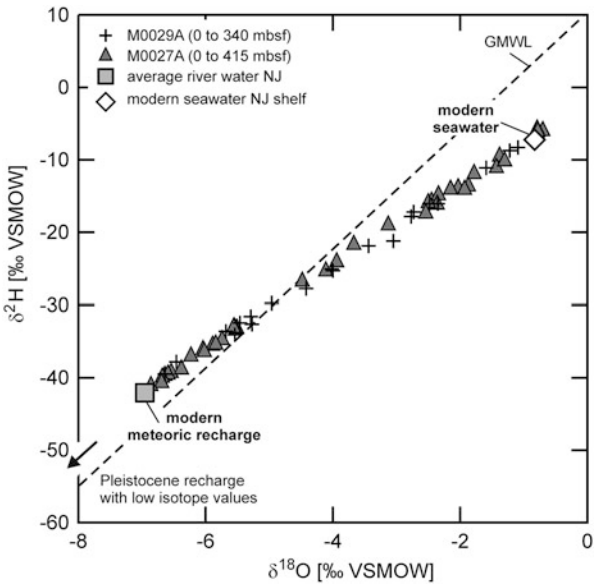

Fig. 7 Stable hydrogen and oxygen isotope values of drill sites and end members. Isotope data indicate mixing between modern seawater and onshore groundwater recharge. Pleistocene waters that have been postulated as a freshwater source would be characterized by lower isotope values (modified from van Geldern et al. 2013)

combination of meteoric recharge during sea-level low stands and highly elevated onshore infiltration of glacial meltwaters (Cohen et al. 2010). Therefore, the freshwater stored under the shelf was considered as a nonrenewable resource.

The study by van Geldern et al. (2013) used pore water samples retrieved during the Integrated Ocean Drilling Program (IODP) Expedition 313 in 2009. Their analyses indicated a previously unknown complex geometry of the underlying freshwater lens with alternating freshwater–saltwater intervals divided by sharp boundaries in the upper part of the drilling cores. The pore fluid $\delta^{18}O$ and $\delta^{2}H$ values defined a mixing line with freshwater and seawater as end members (Fig. 7). The isotopic compositions of the end members were found to be similar to the modern mean value of New Jersey precipitation and today's New Jersey shelf water, respectively. The freshwater most likely originated from onshore meteoric recharge through aquifer systems that crop out on the New Jersey mainland. These aquifers dip under the Atlantic shelf and drain into the ocean via submarine groundwater discharge (SGD) at marine canyons near the continental slope. An origin from Pleistocene glacial meltwaters with depleted isotope values could not be confirmed by stable isotope data.

Large volumes of low-salinity groundwater are not only found below the New Jersey shelf but also occur below continental shelves worldwide (Post et al. 2013). More than 40 % of the global population lives within 100 km from the coast (Martínez et al. 2007) and the exploitation of fresh groundwater resources has been pushed beyond sustainable limits in many coastal areas. To keep up with the growing demand for freshwater, particularly in coastal megacities, submarine low-salinity groundwater is considered as a potential source of usable natural

water for drinking water supply (Bakken et al. 2012). In this context, a clear definition of groundwater origin, migration pathways, and recharge conditions is fundamentally important.

Future Prospects

From the early beginnings in the late 1940s and early 1950s of the last century, stable isotopes played an important role in water research and proved to be essential for understanding fundamental hydrological processes. Notably, freshwater is one of the most essential resources humans depend upon and stable isotopes are a valuable tool for tracing sources of water and its dissolved and suspended constituents. New techniques such as the laser-based isotope ratio spectroscopy revolutionized the analytical capabilities for water and gases and now enable exciting new applications with compact, mobile analyzers that can be used directly in the field.

Isotope research currently faces intensive innovation and new discoveries in many fields including non-mass-dependent isotope geochemistry, clumped isotopes, or the emergence of infrared absorption spectroscopy and multi-collector plasma mass spectrometry (Eiler et al. 2014).

For example, the triple oxygen isotopic composition and the excess of ^{17}O in meteoric waters ($\Delta^{17}O$) have received much interest in the last years to learn more about past humidity or evaporative regimes (Landais et al. 2010; Luz and Barkan 2010; Winkler et al. 2012). Recently, the first laser-based instruments were presented, which allow for the direct measurement of $^{17}O_{excess}$ in the vapor phase, something that is impossible by traditional IRMS analyses.

In addition, the emerging application of *nontraditional* isotope systems such as calcium, lithium, or magnesium can provide important insights into sediment source and the geochemical evolution of fine suspended particulate matter through erosion and transport via rivers and streams. This information is helpful in understanding and managing transport of suspended material through river drainage basins to the coast where many large cities are located in river deltas that face multiple threats from subsidence, unsustainable extraction of groundwater, rising sea level, and coastal erosion.

With respect to the hydrologic cycle, new challenging monitoring programs have been initiated such as the IAEA's GNIR initiative (GNIR, IAEA 2012) that experienced a relaunch with a new Coordinated Research Project (CRP) in 2014 (IAEA 2014). As river networks integrate processes across the Earth's surface, long-term records of river geochemistry are needed to understand the magnitude and direction of ongoing environmental changes.

Another innovation in large-scale environmental monitoring was the compilation of a German nationwide map of the hydrogeochemical background values of groundwater under the European Community water framework directive (Wagner et al. 2011; BGR 2010). It is currently dedicated only to more traditional parameters such as major ion chemistry or electrical conductivity. First efforts of the federal

Bavarian Environment Agency (LfU), the GeoZentrum Nordbayern, and the Helmholtz Research Center Munich have recently been made to expand databases with stable and radiogenic isotope values for different aquifers. Together with isotope precipitation and river water data, this will allow for a detailed investigation of groundwater–surface water interaction and groundwater recharge processes on a larger, regional scale.

While stable isotopes have greatly improved our understanding of hydrologic processes and biogeochemical cycles, they are also important tools to unravel environmental conditions in the past. Climate models predict that the most rapid environmental change will occur over the coming decades (Doney et al. 2012). Only a profound understanding of the Earth system and the impact of human actions will enable mankind to cope with the effects of environmental change on water, food, and energy security, ecosystem health, and regional economic conditions (Reid et al. 2010). Large-scale monitoring programs of different hydrologic compartments together with studies of past environmental conditions and their changes will help us to better understand fundamental processes and how ongoing man-made modifications of hydrologic systems might affect the interaction of the hydrologic cycle with Earth's surface in the future.

Acknowledgments This work and the numerous analyses involved would not have been possible without the help of Irene Wein, Silke Meyer, Christian Hanke, Sonja Konrad, Melanie Hertel, Lars Wunder, Jasmin de Wendt, Bernd Schleifer, and Konrad Kunz. I thank all my coauthors for thorough and constructive reading of the manuscripts and their valuable inputs on the way to successful publication. Partial financial support was provided by the Universitätsbund of Friedrich-Alexander-Universität Erlangen-Nürnberg, the grant for major instrumentation to the chair of Applied Geology (INST 90/678-1 FUGG), and by the German Research Foundation (DFG grant BA 2207/6-1).

References

Aeschbach-Hertig W, Gleeson T (2012) Regional strategies for the accelerating global problem of groundwater depletion. Nat Geosci 5(12):853–861. doi:10.1038/ngeo1617

Baertschi P, Silverman SR (1951) The determination of relative abundances of the oxygen isotopes in silicate rocks. Geochim Cosmochim Acta 1(4–6):317–328. doi:10.1016/0016-7037(51)90006-3

Bakken TH, Ruden F, Mangset LE (2012) Submarine groundwater: a new concept for the supply of drinking water. Water Resour Manag 26(4):1015–1026. doi:10.1007/s11269-011-9806-1

BGR (2010) Bundesanstalt für Geowissenschaften und Rohrstoffe: WMS Information der BGR Hannover: Hydrogeologische Karte von Deutschland 1:200.000 (HÜK200). Thema: Hydrogeochemie (HGC)/Hintergrundwerte im Grundwasser. http://www.bgr.de/Service/grundwasser. Accessed 18 Aug 2014

Bigg GR, Rohling EJ (2000) An oxygen isotope data set for marine waters. J Geophys Res 105 (C4):8527–8535. doi:10.1029/2000JC900005

Bowen GJ (2010) Isoscapes: spatial pattern in isotopic biogeochemistry. Ann Rev Earth Planet Sci 38(1):161–187. doi:10.1146/annurev-earth-040809-152429

Bowen GJ, Wilkinson B (2002) Spatial distribution of $\delta^{18}O$ in meteoric precipitation. Geology 30:315–318. doi:10.1130/0091-7613(2002)030<0315:SDOOIM>2.0.CO;2

Brand WA, Coplen TB, Vogl J, Rosner M, Prohaska T (2014) Assessment of international reference materials for isotope-ratio analysis (IUPAC Technical Report). Pure Appl Chem 86(3):263–467. doi:10.1515/pac-2013-1023

Chandrajith R, Chaturangani D, Abeykoon S, Barth JC, van Geldern R, Edirisinghe EANV, Dissanayake CB (2014) Quantification of groundwater–seawater interaction in a coastal sandy aquifer system: a study from Panama, Sri Lanka. Environ Earth Sci 72:867–877. doi:10.1007/s12665-013-3010-y

Clark I, Fritz P (1997) Environmental isotopes in hydrology. Lewis, Boca Raton, FL

Cohen D, Person M, Wang P, Gable CW, Hutchinson D, Marksamer A, Dugan B, Kooi H, Groen K, Lizarralde D, Evans RL, Day-Lewis FD, Lane JW Jr (2010) Origin and extent of fresh paleowaters on the Atlantic continental shelf, USA. Ground Water 48(1):143–158. doi:10.1111/j.1745-6584.2009.00627.x

Coplen TB (2011) Guidelines and recommended terms for expression of stable-isotope-ratio and gas-ratio measurement results. Rapid Commun Mass Spectrom 25(17):2538–2560. doi:10.1002/rcm.5129

Craig H (1953) The geochemistry of the stable carbon isotopes. Geochim Cosmochim Acta 3 (2–3):53–92. doi:10.1016/0016-7037(53)90001-5

Craig H (1961) Isotopic variations in meteoric waters. Science 133:1702–1703

Dansgaard W (1954) The O^{18}-abundance in fresh water. Geochim Cosmochim Acta 6 (5–6):241–260. doi:10.1016/0016-7037(54)90003-4

Darling GW, Bath A, Gibson J, Rozanski K (2006) Isotopes in water. In: Leng MJ (ed) Isotopes in palaeoenvironmental research, vol 10, Developments in paleoenvironmental research. Springer, Dordrecht, pp 1–66. doi:10.1007/1-4020-2504-1_01

Doney SC, Ruckelshaus M, Emmett Duffy J, Barry JP, Chan F, English CA, Galindo HM, Grebmeier JM, Hollowed AB, Knowlton N, Polovina J, Rabalais NN, Sydeman WJ, Talley LD (2012) Climate change impacts on marine ecosystems. Annual Rev Marine Sci 4(1):11–37. doi:10.1146/annurev-marine-041911-111611

Edmunds WM (2001) Palaeowaters in European coastal aquifers—the goals and main conclusions of the PALAEAUX project. In: Edmunds WM (ed) Palaeowaters in Coastal Europe: evolution of groundwater since the Late Pleistocene, vol 189. Geological Society of London, London, pp 1–16. doi:10.1144/gsl.sp.2001.189.01.02

Eiler JM, Bergquist B, Bourg I, Cartigny P, Farquhar J, Gagnon A, Guo W, Halevy I, Hofmann A, Larson TE, Levin N, Schauble EA, Stolper D (2014) Frontiers of stable isotope geoscience. Chem Geol 372:119–143. doi:10.1016/j.chemgeo.2014.02.006

Emerson S, Hedges J (2008) Chemical oceanography and the marine carbon cycle. Cambridge University Press, Cambridge

Engelhardt I, Barth JAC, Bol R, Schulz M, Ternes TA, Schüth C, van Geldern R (2014) Quantification of long-term wastewater fluxes at the surface water/groundwater-interface: an integrative model perspective using stable isotopes and acesulfame. Sci Total Environ 466–467:16–25. doi:10.1016/j.scitotenv.2013.06.092

Epstein S, Mayeda T (1953) Variation of O^{18} content of waters from natural sources. Geochim Cosmochim Acta 4:213–224

Epstein S, Buchsbaum R, Lowenstam H, Urey HC (1951) Carbonate-water isotopic temperature scale. Geol Soc Am Bull 62(4):417–426. doi:10.1130/0016-7606(1951)62[417:cits]2.0.co;2

Friedman I (1953) Deuterium content of natural waters and other substances. Geochim Cosmochim Acta 4(1–2):89–103. doi:10.1016/0016-7037(53)90066-0

Giorgi F (2006) Climate change hot-spots. Geophys Res Lett 33:L08707. doi:10.1029/2006GL025734

Gleick PH (1996) Water resources. In: Schneider SH (ed) Encyclopedia of climate and weather, vol 2. Oxford University Press, New York, pp 817–823

Hathaway JC, Poag CW, Valentine PC, Miller RE, Schultz DM, Manheim FT, Kohout FA, Bothner MH, Sangrey DA (1979) U.S. geological survey core drilling on the Atlantic shelf. Science 206(4418):515–527

Hetzer T, Bräuning A, Leuschner HH (2014) High-resolution climatic analysis of wood anatomical features in Corsican pine from Corsica (France) using latewood tracheid profiles. Trees. doi:10.1007/s00468-014-1045-7

IAEA (2012) Monitoring isotopes in rivers: creation of the global network of isotopes in rivers (GNIR). IAEA-TECDOC-1673. International Atomic Energy Agency (IAEA), Vienna

IAEA (2014) Coordinated research project (CRP): application and development of isotope techniques to evaluate human impacts on water balance and nutrient dynamics of large river basins (CRP code F33021). International Atomic Energy Agency (IAEA). http://cra.iaea.org/cra/explore-crps/all-active-by-programme.html. Accessed 17 Aug 2014

IAEA/WMO (2006) Global network of isotopes in precipitation. The GNIP database. http://www.iaea.org/water. Accessed 18 Aug 2014

Kendall C, Coplen TB (2001) Distribution of oxygen-18 and deuterium in river waters across the United States. Hydrol Process 15:1363–1393. doi:10.1002/hyp.217

Landais A, Risi C, Bony S, Vimeux F, Descroix L, Falourd S, Bouygues A (2010) Combined measurements of $^{17}O_{excess}$ and d-excess in African monsoon precipitation: Implications for evaluating convective parameterizations. Earth Planet Sci Lett 298(1–2):104–112. doi:10.1016/j.epsl.2010.07.033

Luz B, Barkan E (2010) Variations of $^{17}O/^{16}O$ and $^{18}O/^{16}O$ in meteoric waters. Geochim Cosmochim Acta 74(22):6276–6286. doi:10.1016/j.gca.2010.08.016

Lykoudis SP, Argiriou AA, Dotsika E (2010) Spatially interpolated time series of $\delta^{18}O$ in Eastern Mediterranean precipitation. Glob Planet Change 71:150–159. doi:10.1016/j.gloplacha.2009.09.004

Martínez ML, Intralawan A, Vázquez G, Pérez-Maqueo O, Sutton P, Landgrave R (2007) The coasts of our world: ecological, economic and social importance. Ecol Econ 63(2–3):254–272. doi:10.1016/j.ecolecon.2006.10.022

Négrel P, Petelet-Giraud E (2011) Isotopes in groundwater as indicators of climate changes. TrAC Trend Anal Chem 30(8):1279–1290. doi:10.1016/j.trac.2011.06.001

Nier AO (1947) A mass spectrometer for isotope and gas analysis. Rev Sci Instrum 18(6):398–411. doi:10.1063/1.1740961

Post VEA, Groen J, Kooi H, Person M, Ge S, Edmunds WM (2013) Offshore fresh groundwater reserves as a global phenomenon. Nature 504(7478):71–78. doi:10.1038/nature12858

Reid WV, Chen D, Goldfarb L, Hackmann H, Lee YT, Mokhele K, Ostrom E, Raivio K, Rockström J, Schellnhuber HJ, Whyte A (2010) Earth system science for global sustainability: grand challenges. Science 330(6006):916–917. doi:10.1126/science.1196263

Rozanski K (1985) Deuterium and oxygen-18 in European groundwaters—links to atmospheric circulation in the past. Chem Geol 52(3–4):349–363. doi:10.1016/0168-9622(85)90045-4

Schotterer U, Oldfield F, Fröhlich K (1996) GNIP – global network for isotopes in precipitation. International Atomic Energy Agency (IAEA), Vienna

Stögbauer A, Strauss H, Arndt J, Marek V, Einsiedl F, van Geldern R (2008) Rivers of North-Rhine Westphalia revisited: tracing changes in river chemistry. Appl Geochem 23 (12):3290–3304. doi:10.1016/j.apgeochem.2008.06.030

Szymczak S, Joachimski MM, Bräuning A, Hetzer T, Kuhlemann J (2012) A 560 yr summer temperature reconstruction for the Western Mediterranean basin based on stable carbon isotopes from *Pinus nigra* ssp. laricio (Corsica/France). Clim Past 8(5):1737–1749. doi:10.5194/cp-8-1737-2012

Ternes TA (1998) Occurrence of drugs in German sewage treatment plants and rivers. Water Res 32(11):3245–3260. doi:10.1016/S0043-1354(98)00099-2

Terzer S, Wassenaar LI, Araguás-Araguás LJ, Aggarwal PK (2013) Global isoscapes for δ18O and δ2H in precipitation: improved prediction using regionalized climatic regression models. Hydrol Earth Syst Sci 17(11):4713–4728. doi:10.5194/hess-17-4713-2013

Urey HC (1947) The thermodynamic properties of isotopic substances. J Chem Soc (Resumed) 0:562–581. doi:10.1039/JR9470000562

Urey HC, Lowenstam HA, Epstein S, McKinney CR (1951) Measurement of paleotemperatures and temperatures of the Upper cretaceous of England, Denmark and the Southeastern United States. Geol Soc Am Bull 62(4):399–416. doi:10.1130/0016-7606(1951)62[399:mopato]2.0.co;2

van Geldern R, Hayashi T, Böttcher ME, Mottl MJ, Barth JAC, Stadler S (2013) Stable isotope geochemistry of pore waters and marine sediments from the New Jersey shelf: methane formation and fluid origin. Geosphere 9(1):96–112. doi:10.1130/GES00859.1

van Geldern R, Baier A, Subert HL, Kowol S, Balk L, Barth JAC (2014a) Pleistocene paleo-groundwater as a pristine fresh water resource – evidence from stable and radiogenic isotopes. Sci Total Environ 496:107–115. doi:10.1016/j.scitotenv.2014.07.011

van Geldern R, Kuhlemann J, Schiebel R, Taubald H, Barth JAC (2014b) Stable water isotope patterns in a climate change hotspot: the isotope hydrology framework of Corsica (western Mediterranean). Isot Environ Health Stud 50(2):184–200. doi:10.1080/10256016.2013.839559

van Geldern R, Schulte P, Mader M, Baier A, Barth JAC (2015) Spatial and temporal variations of pCO_2, dissolved inorganic carbon and stable isotopes along a temperate karstic watercourse. Hydrol Process 29:3423–3440. doi:10.1002/hyp.10457

Wagner B, Walter T, Himmelsbach T, Clos P, Beer A, Budziak D, Dreher T, Fritsche H-G, Hübschmann M, Marczinek S, Peters A, Poeser H, Schuster H, Steinel A, Wagner F, Wirsing G (2011) Hydrogeochemische Hintergrundwerte der Grundwässer Deutschlands als Web Map Service. Grundwasser 16(3):155–162. doi:10.1007/s00767-011-0161-1

Winkler R, Landais A, Sodemann H, Dümbgen L, Prié F, Masson-Delmotte V, Stenni B, Jouzel J (2012) Deglaciation records of ^{17}O-excess in East Antarctica: reliable reconstruction of oceanic normalized relative humidity from coastal sites. Clim Past 8(1):1–16. doi:10.5194/cp-8-1-2012

Toward an Integrated Isotope Zooarchaeology

Cheryl A. Makarewicz

Introduction

The study of ancient cultural remains such as animal and human bones, carbonized plant remains, ceramics, and lithics has formed the core of archaeological analyses for decades and has provided key insights into the ways in which people utilize, produce, and distribute resources; organize societies; command and negotiate political networks; and construct landscapes. These traditional analyses are now regularly complemented by novel biomolecular approaches that access genetic, dietary, and environmental information preserved in ancient DNA, bioapatite, proteins, and lipids, which are revealing previously inaccessible information on the diet, mobility, and evolutionary histories of ancient societies. No less important, archaeological materials and ancient biomolecular analyses are now regularly combined within cohesive research designs, demonstrating that the distinct perspectives provided by such approaches are required in order to adequately address major questions of archaeological interest. Even more significant, integrated approaches are helping transform the relationship between traditional and biomolecular analyses from a multidisciplinary undertaking that separately treats datasets as disconnected units interpreted independently of each other to a truly interdisciplinary mission that actively seeks to integrate datasets in order to examine core archaeological research themes. This analytical synergy is already generating new insights into some of the most enduring questions pursued by archaeologists over the past decades relating to the transition from hunting and gathering to food production, the spread of agropastoralism across Eurasia, and emergent political complexity in the Old and New Worlds.

C.A. Makarewicz (✉)
Institut für Ur- und Frühgeschichte, Christan-Albrechts-Universität Kiel, Johanna-Mestorf-Straße 2-6, 24118 Kiel, Germany
e-mail: c.makarewicz@ufg.uni-kiel.de

G. Grupe, G.C. McGlynn (eds.), *Isotopic Landscapes in Bioarchaeology*,
DOI 10.1007/978-3-662-48339-8_11

Along these lines, there has been a recent explosion in archaeological research that combines zooarchaeology and stable isotope biogeochemistry in order to investigate how human-animal relationships shape and direct the subsistence and surplus economies, sociopolitical organization, and ritual practices of ancient societies. Zooarchaeology is often described as the study of human and animal interaction through the analysis of faunal remains recovered from archaeological sites (Reitz and Wing 1999). Faunal analysis involves the quantification of taxonomic, skeletal part, ageing, metrical, and bone modification data collected from individual bone specimens derived from a faunal assemblage comprised of multiple bone specimens associated by their temporal and cultural context. Stable isotope biogeochemistry involves the study of environmental, physiological, and dietary change through the measurement of carbon, nitrogen, oxygen, sulphur, and strontium isotope ratios obtained from sediments, water, plants, and animal tissues. Stable isotopic analyses of animal skeletal tissues provide a direct measure of dietary intake and environmental inputs that document changes in diet and mobility in wild and domesticated animals.

Zooarchaeological and stable isotopic approaches, when employed simultaneously as part of the same study, have provided insights into animal exploitation strategies that would have been undetectable to either technique applied in isolation. Combined biometrical and stable isotope analyses have helped distinguish between the diets of wild and husbanded animals (Balasse et al. 2012; Lösch et al. 2006; Makarewicz and Tuross 2012; Noe-Nygaard et al. 2005), while concerted taxonomic abundance, skeletal part distribution, and isotopic analyses of bone specimens derived from the same faunal assemblage have provided insights into the impact of human predation and climate change on wild ungulate resource availability (Dusseldorp 2011; Fisher and Valentine 2012) and identify the transport, exchange, and circulation of animals on the hoof and their postmortem products in urban economic systems and ritual landscapes (Laffoon et al. 2013; Sayre et al. 2015; Sjögren and Price 2013; Thornton 2011).

The increasing use of stable isotope analysis to examine questions relating to human exploitation of animal resources, and the occasional juxtaposition of stable isotopic data with zooarchaeological data as described above, lends to the impression that zooarchaeology and stable isotope biogeochemistry are seamlessly interlinked. However, the degree to which results are integrated varies considerably, with some studies comprehensively combining zooarchaeological and stable isotopic data in their interpretations, while other studies remain asymmetrically weighted towards one type of data set. This reflects the lack of familiarity with the analytical and quantitative methods, interpretative models, and limitations of each approach by the practitioners of the other.

Overall, despite these integrative imbalances, there is a growing level of articulation between zooarchaeology and stable isotope analysis. This has been recognized with the production of special issue journals and the creation of an International Council of Archaeozoology (ICAZ) working group devoted to the topic (Zangrando et al. 2014; Pilaar Birch 2013). However, there has been little attention paid to the historical developments that took place within each discipline that contributed to their later integration or exploration of what constitutes the

integrative elements of isotope zooarchaeology. Here, I identify a path of increasing connectivity between zooarchaeology and stable isotope biogeochemistry that was facilitated by a convergence of research questions, shared materials, and methodological developments within each field. First, I detail the central role of modern and paleontological skeletal material in establishing some of the fundamentals of stable isotope biogeochemistry and then discuss how isotopic analyses of archaeological faunas were historically neglected unless required for human dietary reconstruction. I then argue that research agendas in Paleolithic archaeology concerned with animal resource availability encouraged the isotopic study of archaeological faunal remains, but primarily as a proxy for environmental reconstruction and as an indirect measure of available animal biomass rather than as a direct examination of human–animal interactions. Subsequent zooarchaeological research assessing the role of selective predation and opportunistic scavenging in Neanderthal subsistence marked a pivotal connection point, as it activated stable isotopic work that directly referred to zooarchaeological results and explicitly sought to further contribute to the debate through analyses of human and Neanderthal skeletal remains. Research agendas focused on tracing early animal management strategies and domestication processes provided the critical spark that reoriented stable isotope analysis toward questions concerned with human–animal interaction and, in doing so, become more directly involved with zooarchaeological datasets. Finally, I argue that the integration of zooarchaeology and stable isotope analysis is promoted by their complimentary scales of analysis, and, further integration depends on the use of human behavioral ecology, practice theory, and niche construction theory, which provide theoretical frameworks crucial for understanding micro- and macroscale developments in human-animal relationships.

Disciplinary Developments Within Zooarchaeology and Stable Isotope Analysis

Zooarchaeology has become a well-established and standard part of archaeological research agendas. Far from the days when superficial lists of relative taxonomic abundance were generated for the purposes of paleoecological reconstruction and, occasionally, coarse estimation of animal sources to the human diet, current zooarchaeological analyses address a diverse assortment of anthropologically oriented questions investigating human subsistence, social organization, ritual activity, and political complexity (Crabtree 1990; deFrance 2009; Russell 2012). Zooarchaeology today is an increasingly globalized field that represents an amalgamation of quantitative and qualitative approaches and theoretical frameworks that derive from a variety of research traditions, archaeological and otherwise, from all over the world.

The study of animal bones from archaeological sites has a surprisingly deep history that reaches back into the nineteenth century, but zooarchaeology became a

discipline within its own right as part of the emergence of a processual archaeology that emphasized cultural ecology, dynamic systems, and cultural process (Binford 1978; Higgs and Jarman 1975; Landon 2005; Lyman 2015). Transformed from a zoologically oriented method generally concerned with taxonomic identifications for the purposes of zoogeographical and coarse environmental reconstruction (Bartosiewicz 2001; Lyman 2015; Reitz and Wing 1999), zooarchaeology encapsulated the study of human–animal interactions and the processes associated with the evolution of this relationship. Zooarchaeology was further strengthened by the development of a zooarchaeological middle-range theory that sought to link patterning observed in faunal assemblages with human behaviors and assemblage formation processes, in part through actualistic research and experimental verification (Binford 1978, 1980; Blumenschine 1986, 1988; see Gifford-Gonzalez 1991 and citations within). Although it did not necessarily address all aspects of archaeological inquiry, as early processual zooarchaeological endeavors tended to align heavily with processualist questions related to subsistence and taphonomy, zooarchaeology was sufficiently integrated to benefit from and contribute to the analytical and theoretical currents of archaeology, including later developments in so-called post-processual archaeology which helped promote the creation of a social zooarchaeology (Russell 2012).

In contrast to zooarchaeology, with its relatively long gestation period within archaeology, stable isotope analysis was a relatively late arrival to archaeology due in part to the pace of methodological developments within stable isotope biogeochemistry, i.e., the development of continuous flow mass spectrometry, and the later theoretical developments within archaeology that expanded modes of archaeological inquiry beyond processual archaeology (Makarewicz and Sealy 2015). Isotopic analyses of animal skeletal tissues, both modern and paleontological, played an indispensable role in the initial development of stable isotope biogeochemistry. Early research provided foundational insights into diet-tissue carbon and nitrogen isotopic spacing in animal collagen (DeNiro and Epstein 1978, 1981), carbon isotopic differences between herbivores ingesting varying amounts of C_3 and C_4 plants (DeNiro and Epstein 1978; Schoeninger and DeNiro 1984; Cormie and Schwarcz 1994), carbon and nitrogen isotopic distinctions in animals feeding within marine, freshwater, and terrestrial environments (Schoeninger and DeNiro 1984), and the impact of trophic level on consumer $\delta^{15}N$ values (DeNiro and Epstein 1981; Minagawa and Wada 1984; Sealy et al. 1987). Foundational concepts characterizing the biological basis of oxygen isotopes in mineralized mammalian tissues were also established. In particular, the relationship between the oxygen isotope ratios of ingested water and $\delta^{18}O$ values expressed in bone phosphate (Longinelli 1984; Luz et al. 1984, 1990; Luz and Kolodny 1989), the influence of relative humidity levels on bone phosphate oxygen isotope ratios (Cormie et al. 1994; Luz et al. 1990), and slightly later, the sensitivity of oxygen isotopes in apatite carbonates and phosphates to seasonal changes in temperature and humidity (Bryant et al. 1996; Cerling et al. 1997; Koch et al. 1989, 1995; Kohn et al. 1998; Quade et al. 1992) were all established primarily through isotopic analyses of ungulate skeletal materials. These initial works were further

complemented by a series of experimental studies exploring the relationship between inter- and intraspecies carbon and nitrogen isotopic variation of animals characterized by similar physiologies and ingesting isotopically identical diets (DeNiro and Schoeniger 1983; Sponheimer et al. 2003), the impact of environmental factors such as aridity and floral nitrogen isotopes on herbivore $\delta^{15}N$ values (Ambrose 1986, 1991; Cormie and Schwarcz 1994; Schwarcz et al. 1999; Sealy et al. 1987), and carbon isotopic fractionation between diet, bioapatite, and collagen (Ambrose and Norr 1993; Cerling and Harris 1999; Lee-Thorp et al. 1989).

These principal studies, while largely using animal skeletal materials in order to test and authenticate the relationship between dietary, environmental, and metabolic inputs and isotopic change in animal tissues, only occasionally included archaeofaunal specimens as an investigative medium. In the rare cases when these materials were used, the analysis of archaeological faunal remains was simply a natural extension of research, conducted on paleontological remains, which focused on defining the impact of diagenetic alteration on carbon and oxygen isotope measurements derived from biogenic apatite (Chillón et al. 1994; Iacumin et al. 1996; Lee-Thorp et al. 1989; Wang and Cerling 1994). Ultimately, in keeping with their biogeochemical focus, these studies were not concerned with questions relating to human–animal relationships.

However, Ericson (1985) was particularly prescient in his observation that stable isotopes (in particular strontium) could provide valuable insights into human behaviors relating to animal exploitation. Despite this missive, animal remains were largely neglected in initial stable isotopic applications within archaeology save for a few sporadic archaeofaunal analyses that served to contextualize human isotope values and reconstruct human diets and mobility (Makarewicz and Sealy 2015). This distinctly human-centric archaeological isotope research paid particular attention to major dietary transitions associated with the spread of agriculture as well as dietary change elicited by the ingestion of foodstuffs from geographically distinct places of origin. For example, carbon isotopic analyses of human bone collagens revealed the uptake of C_4 maize agriculture by hunter-gatherers inhabiting ^{13}C-depleted C_3 North American woodland environments and, in northern Europe, a shift from a marine-based diet in Mesolithic hunter-gatherers to terrestrial based diets in Neolithic agriculturalists (Bender et al. 1981; Schwarcz et al. 1985; Tauber 1981; van der Merwe and Vogel 1978). Carbon and nitrogen isotope analyses of human collagen also helped establish the relative contribution of marine and terrestrial dietary resources in the diets of prehistoric hunter-gatherers located in coastal environments (Chisholm et al. 1982, 1983; Hobson and Collier 1984; Johansen et al. 1986; Walker and DeNiro 1986) and differentiate between marine, plant-based agricultural, and meat- and milk-based pastoralist dietary intake (Ambrose 1986; Ambrose and DeNiro 1986).

These early works were pioneering in their capacity to reconstruct directly aspects of ancient human dietary intake, but they rarely considered zooarchaeological (and paleoethnobotanical) datasets or how they could inform the isotopic interpretive framework. From the perspective of archaeological stable isotope analysis, it was important to establish the relative contribution of animal proteins

(and also plant foods) to the human diet, but less important to isolate the precise subsistence strategies used to construct that diet. Moreover, one of the perceived strengths of stable isotope-based human dietary reconstructions was their independence from zooarchaeological and paleobotanical analyses, which were implicitly perceived as less than accurate measures of human dietary composition due to the impact of taphonomic factors on faunal and botanical assemblages and the attendant challenges in quantifying those datasets.

The (Paleolithic) Outer Edge of Integration

The first stable isotope work that focused expressly on archaeological animal bone specimens for the purposes of understanding, if indirectly, the relationship between people and their animal resources materialized out of Paleolithic research evaluating Neanderthal and anatomically modern human dietary breadth, prey acquisition and carcass processing strategies (Stiner 1994), hominid mobility as adaptive responses to environmental constraints (Féblot-Augustins 1994; Rolland and Dibble 1990), and cultural and niche interaction between Neanderthals and humans (Bar-Yosef 1992; Bar-Yosef and Meignen 1992; d'Errico et al. 1998; Gambier 1997; Stiner 1992, 1994).

Characterizing Pleistocene climatic conditions, resource availability, and niche partitioning was key to resolving many of these issues, and stable isotopic analyses of faunal assemblages recovered from hominid occupation sites provided a medium through which paleoenvironments could be reconstructed at the regional and local scales required to contextualize Neanderthal and anatomically modern human subsistence and mobility choices. Drawing from experimental work on modern herbivores indicating an increase in $\delta^{15}N$ values with increasing aridity levels (Ambrose and DeNiro 1986; Heaton et al. 1986; Sealy et al. 1987), nitrogen isotopic analyses of Pleistocene herbivore collagens were commonly employed as a proxy for paleoclimatic change (Bocherens et al. 1995a; Fizet and Lange-Badré 1995; Fizet et al. 1995; Iacumin et al. 1997, 2000). The biomass productivity of local niches was further defined by herbivore carbon isotopes, based on the premise that shifting $\delta^{13}C$ values reflected changes in the density of forest canopy cover (Drucker et al. 2003; Iacumin et al. 1997). Oxygen isotope analyses of tooth enamel were also occasionally used for similar climate reconstruction purposes (Bocherens et al. 1995b; Reinhard et al. 1996).

Paralleling developments in archaeological stable isotope research focused on human dietary reconstruction, some of this early faunal isotopic work sought to establish the isotope ecology of Pleistocene foodwebs, primarily for the purposes of interpreting carbon and nitrogen isotopic values obtained from human and Neanderthal skeletal remains and, in particular, demonstrate the degree of carnivory in Neanderthals (Bocherens et al. 1991; Fizet et al. 1995). In order to establish the relative contribution of animal proteins in the Neanderthal diet, this work not only required a confirmation of the isotopic distinction between herbivores and

carnivores but also an estimation of the amplitude of ^{15}N enrichment in carnivores over herbivores (Bocherens et al. 1991; Fizet et al. 1995). Along these lines, a more precise understanding of the isotopic structuring of herbivore populations was needed in order to better define Neanderthal access to particular animal resources. This was achieved by sampling from a range of bone specimens representing animal taxa with different habitat and dietary preferences (Bocherens et al. 1991, 1994, 1995a, b, 1996, 1997; Fizet et al. 1995; Koch 1991; Matheus 1995).

These isotopic investigations of Paleolithic faunas emphasized that archaeofaunal specimens were needed in order to provide an isotopic context for the interpretation of isotope values obtained from human and Neandertal tissues. However, as animal bone specimens continued to be viewed primarily as archives of paleobiological and ecological information, stable isotopic analyses of faunal remains were not explicitly linked to research questions concerned with the animal resource acquisition strategies pursued by Paleolithic hominids, issues that were central to zooarchaeology at that time. However, the second wave of isotope research examining Neanderthal and modern human diets was heavily informed by zooarchaeological questions and approaches, especially those assessing Neanderthal meat consumption and animal procurement strategies relating to selective predation or opportunistic scavenging (Marean 1998; Marean and Kim 1998; Stiner 1991, 1992, 1994). Inspired by this contentious debate, stable isotope analyses explicitly sought to further test this hypothesis and concluded that the high nitrogen isotope values exhibited by Neanderthals reflected an extraordinarily high level of meat consumption that could not have been supported solely by scavenging (Richards et al. 2000). Slightly later isotope research was also similarly informed by zooarchaeological work evaluating Neanderthal and modern human dietary breadth (Stiner et al. 2000) and confirmed that Neanderthals obtained most of their protein from terrestrial resources while humans obtained a significant portion of their diets from marine resources by the mid-Upper Paleoltihic (Richards et al. 2001).

Animal Management Practices and the First Forays into Isotope Zooarchaeology

Ultimately, the use of stable isotope biogeochemistry to directly examine human–animal interaction was a late development. This new direction in stable isotope analysis was facilitated in part by zooarchaeological research agendas concerned with the emergence of animal domestication processes during the Neolithic, particularly in Near Eastern contexts. For decades, much zooarchaeological work focused on this issue was caught up in establishing the wild or domesticated status of animals represented in faunal assemblages and detangling anthropogenic from environmental factors in driving shifts in taxonomic abundance, demography, and animal body size observed in Neolithic faunal assemblages. These issues, among

others, diverted attention away from understanding the precise strategies that contributed to the successful husbandry and eventual domestication of sheep, goats, cattle, and pigs. The further development of zooarchaeological methods for computing sex-specific age profiles (initially proposed by Hesse 1984) permitted detection of the timing of animal age at slaughter and the intensity of male and female kill-off (Zeder and Hesse 2001). This new concern with management strategies opened the way for stable isotopic approaches, which had great potential to explore the human practices involved with animal exploitation, largely because it supported the fine-grained scale of analysis required to isolate such strategies.

The initial integration of zooarchaeology and stable isotope analysis was facilitated by a cohesive series of research conducted on modern animals that documented the ways in which different animal husbandry strategies influenced the isotopic composition of animal tissues (Balasse et al. 2001, 2002, 2003, 2006; Makarewicz and Tuross 2006). As a direct measure of dietary and environmental inputs, stable isotope analysis provided a means to document crucial aspects of livestock management systems that were previously invisible to zooarchaeological approaches. A number of animal husbandry strategies designed to increase the overall health, body condition, and productive and reproductive output of domesticated livestock involve direct human interference with the animal diet. Fodder provisioning, control of animal age at weaning, and moving animals to different pastures, for example, all directly impact the ingredients and quality of animal diet. The timing of animal birth can also be shifted by herders, who may do so in order to more closely shape herd demography or change the quantity and duration of meat or milk availability for their consumption.

Much initial research exploring the feasibility of stable isotope analysis as a way to identify ancient animal husbandry practices involved foundational work establishing the sensitivity of carbon, nitrogen, and oxygen isotopes recorded in skeletal tissues to dietary and environmental change provoked by human decisions concerned with livestock management (Balasse et al. 2001, 2002, 2003). Crucially, these studies, conducted on modern animals in controlled laboratory settings whose dietary intake was known, helped establish the influence of biological fractionation effects, tissue formation rates, lag between dietary intake and equilibriation of body amino acid and carbon pools, and sampling strategy (e.g. bulk sampling v. intra-tooth sequential sampling) on the isotope values obtained from the collagenous and mineral phases of teeth and bones. This work highlighted the variability in the scales of temporal resolution at which animal husbandry strategies could be documented through isotope analysis. Recently, a small but highly important body of research has emerged focused on better defining the precise dietary and non-dietary factors in driving isotopic change in animals and observed isotopic patterns. This includes work identifying the influence of tooth formation rates and tooth geometry on the seasonal isotopic variation observed in sequentially sampled teeth (Bendrey et al. 2015; Blaise and Balasse 2011; Zazzo et al. 2006; 2012), remodelling rates on the distribution of isotopes in bone collagen (Olsen et al. 2013), non-dietary sources of isotopic variation (Reynard and Tuross 2015), and the potential of osteon-level sampling of bone (Koon and Tuross 2013; Scharlotta et al. 2013). Such studies are crucial for interpreting

isotopic data generally and identifying distinctive animal management strategies in the ancient isotopic record more specifically.

This laboratory-based research was followed by studies that investigated the feasibility of detecting animal husbandry strategies in domesticates with known life histories and managed under traditional herding regimes (Balasse et al. 2005; Frémondeau et al. 2012; Makarewicz 2014; Makarewicz and Tuross 2006; Makarewicz 2014). The isotopic information collected from these studies reflect the complex and sometimes messy intersection of natural environmental inputs, and decisions made by herders that dictate the type, timing, and intensity of management strategies enacted on individual animals and herds. These kinds of studies are akin to ethnozooarchaeological studies (see Albarella and Trentacoste 2011) and provide a framework of interpretation analogous to zooarchaeological middle-range theory. It is important to emphasize, however, that they do not provide direct, one-to-one comparative reference sets or baseline isotopic values for interpreting isotopic patterns derived from archaeological faunal remains. Instead, independent and contemporaneous monitors of ancient floral biomes and environmental conditions are usually needed, although often neglected, in order to determine if changes in ancient animal diet, movement patterns, or season of birth are due to human managment decisions or changes in the local ecosystem.

Putting It All Together: Integrative Elements of Isotope Zooarchaeology

The broad trends in zooarchaeological and stable isotope research discussed above have illustrated how the gap between the two disciplines diminished as both converged on similar research themes. Research agendas focused on tracing early animal management strategies and domestication processes provided a strong bridge between stable isotope analysis and zooarchaeology by directing stable isotope analysis toward questions relating to human–animal interaction and encouraging its direct involvement with zooarchaeological datasets. However, the link between these two disciplines does not rely on shared research questions alone, but is further connected by physical, scalar, and theoretical linkages. Together, the shared sample assemblage and congruent flexibility in scales of analysis and interpretation, informed by inferential frameworks that consider individual agency and practice in constructing human behavioral strategies and broader evolutionary processes, are the core elements that create an integrated isotope zooarchaeology.

The datasets generated by zooarchaeology and stable isotope analysis provide independent lines of evidence detailing the human-animal relationship and are inherently united by the very bone specimens from which both these analyses draw. Less evident, however, is that the faunal assemblage itself contextualizes the interpretation of results and provides the conduit through which isotopic and

zooarchaeological data sets can be cross-referenced. The practical research benefits lie in the improved interpretative power of the combined data streams. For example, paired analyses of harvesting profiles computed from tooth wear data and animal birth seasonality established through oxygen isotope analyses of the same teeth used to calculate the profile would help further detangle the environmental, ontogenetic, and subsistence variables contributing to decisions regarding timing of animal slaughter.

Zooarchaeology and stable isotope biogeochemistry are further woven together by overlapping scales of analysis. Each mode of analysis can operate at different degrees of temporal resolution, which translates into different perspectives on human-animal relationships and how these were informed by environmental and socio-economic dynamics. Zooarchaeological data sets tend to lend themselves well to analyses seeking to reconstruct animal exploitation strategies at the level of the site or settlement for several reasons. Faunal assemblages frequently represent the concatenated outcomes of distinct primary and secondary processing, consumption, and discard behaviors and are generally approached analytically as representing a temporal and spatial "average" of subsistence production, social activities, and ritual actions carried out in (pre)historic communities. In addition, quantitative calculations of zooarchaeological datasets often demand the intentional aggregation of faunal bone specimens derived from different contexts (representing different events) in order to achieve the sample sizes required for statistically meaningful output. This analytical decision has the effect of further blurring the picture of animal exploitation strategies used by individuals, households and communities expressed in the zooarchaeological record. Given the appropriate archaeological contexts, however, zooarchaeological analyses can provide high resolution data sets that provide insights into small-scale activities associated with, for example, household production or ritual practice (Grosman et al. 2008; Johannesson 2015; Piccione et al. 2015; Wallis and Blessing 2015).

Stable isotope analysis produces quantitative results, scaled to different temporal resolutions, which offer the potential for exceptionally fine-grained insights into the ways in which ancient humans exploited their animal resources by providing dietary, seasonality, and mobility information at community, individual, and intra-individual scales. Calibration of isotopic results against the time dependant formation properties of the sampled biological tissue is key to building multi-scalar interpretations. For example, a bone collagen isotope value reflects the 'lifetime' dietary intake of an individual animal. This value provides some stand-alone information about the general life history of the individual animal depending on environmental context, but when referenced against a cohort of isotopic values derived from other animals (obtained from the appropriate spatial and temporal contexts), it contributes to a broader pool of isotopic information that allows for robust inferences about consumer dietary shifts at the community level similar to the scale of resolution achieved by most zooarchaeological analyses. An even higher degree of temporal resolution can be obtained through sequential sampling of tooth enamel and dentin to provide highly detailed individual assessments of

animal diet and mobility within a seasonal time frame. Such analyses directly track the outcomes of specific human decisions concerned with animal management strategies and, although the subsistence and social motivations provoking such choices may be clearly evident only through other archaeological lines of evidence, they provide an opportunity to chronicle the immediate products of human agency that underscore large scale processes.

This scalar flexibility provides analytical connections between zooarchaeology and stable isotope analysis and, together with a topical convergence on human-animal interaction and the ways in which people manipulate animal resources, constructs the integrated foundation of an isotope zooarchaeology. The two analytical approaches could be further woven together through an explicit utilization of theoretical frameworks that draw from human behavioral ecology (HBE) and practice theory to explain past human behaviors reflected in the isotopic and zooarchaeological records. HBE frameworks link together circumstance models (i.e. how socio-ecological variables influence the perceived costs and benefits associated with particular behavioral strategies) and mechanism models (i.e. how natural selection acts on those costs and benefits) (Winterhalder and Smith 2000). These interlinked models seek to explicate cultural and behavioral variation as phenotypic adaptations to varying social and ecological contexts. HBE models hold that human decision-making is steered by conditional decision rules oriented towards achieving a particular goal under extant social and environmental constraints and that optimizing behavioral strategies are selected for. Such HBE models are particularly pertinent for isotope zooarchaeology, as optimal foraging, competition, sharing, and costly-signaling theories provide a powerful inferential framework for understanding human production behaviors conducted in groups, which include resource acquisition and distribution through exchange, sharing and coercive transfers (Smith and Winterhalder 2006).

Human social relationships figure prominently into HBE theoretical frameworks, but the configuration and tenor of these relationships are framed as ecological strategies that redirect selective pressures and promulgate further adaptive behavioral responses. However, HBE perspectives neglect the specifics of distinctive community structures, political influences, and historical priors that frequently feature in subsistence-oriented animal exploitation decisions and human-animal relations more generally. Practice theory brings together agency and social structures, highlighting a dynamic relationship where, through routine engagement in daily tasks, agents actively compose their relational worlds while simultaneously being constrained and socialized by institutionalized rules (Bourdieu 1997). Practice theory provides an important complement to HBE in that it supplies a means to understand the selection and propagation of historically contingent behavioral strategies and how structuring and restructuring of practices cultivate shifts in the social and political relationships between people and communities (Barrett 1994; Giddens 1984). By asserting the role of social actors in shaping particular short- and long-term behaviors that are not necessarily part of normative rules, practice theory incorporates individual strategies, including those concerned with animal exploitation, as a modus for social and economic dynamism.

Niche construction theory (NCT) further draws out the individual as active agent and places human decisions that modify their ecological and cultural environments front and center of evolutionary processes ranging from animal domestication to the spread of farming (McClure 2015; Smith 2012; Zeder 2015a). Although NCT is derived from evolutionary biology, NCT could be conceived as an amalgamation of human behavioral ecology and practice theory in that it explicitly unites biological and social factors contributing to human evolutionary processes. Niche construction is a multi-scalar process where organisms modify their own niches through their own activities and decisions. The outcomes of these choices subsequently propagate throughout a particular environment and modify natural selection pressures within and outside a particular niche. The NCT framework provides humans and animals with an active role as co-directors of their own (and others) evolution and recognizes that niche construction initiates evolutionary processes within a context of reciprocal interactions between environment and behavioral strategies (O'Brian and Laland 2010). Rather than view human behaviors as adaptive responses to environmental changes, NCT places primacy on the agency of humans who proactively modify their niches in order to shape their own ecological and cultural environments (Zeder 2015b). Importantly, the outcomes of human decisions that alter a particular niche elicit shifts in the selective environments of other ecological, social, and cultural niches on both transient and trans-generational levels (Kendal et al. 2011; Laland et al. 2000). Critically, NCT defies HBE concepts that construe human resource acquisition strategies as largely driven by resource scarcity and human modification of the environment as an adaptive response to environmental change (Smith 2009; Zeder 2015b).

All three theoretical frameworks have their own strengths that lend themselves well to interpreting zooarchaeological and stable isotopic data sets, but NCT is perhaps best suited to isotope zooarchaeology, as it provides a scalable linkage between macro-evolutionary causal factors and the actual initiation of particular human-animal relationships. This, combined with the flexible scalar resolution of stable isotopic and zooarchaeological data sets, opens exciting new possibilities into understanding the mechanisms and motivations underscoring animal domestication processes, the spread of pastoralism, and emergent political complexity.

Toward a Practice of Isotope Zooarchaeology

It has been just over 10 years since there was a call to further integrate zooarchaeology more thoroughly into archaeology and bring greater attention to the strength of zooarchaeological research as a means to address broad archaeological issues relating to, for example, trade, production, urbanization, social organization, and land use (Maltby 2002). Stable isotope biogeochemistry has yet to similarly assert itself to the archaeological community (and likely never will given the astonishing number of stable isotopic studies now conducted on archaeological plant, animal, and human remains), but this is perhaps all the more a reason for practitioners of the

discipline to more deeply reflect upon the connective elements that join isotope analysis to archaeology. Encouragingly, recent research that explictly draws together zooarchaeological and stable isotopic approaches (e.g. Guiry et al. 2014; Sugiyama et al. 2015; Salmi et al. 2015) is a healthy sign of an increasingly integrative archaeology.

It is equally important to ensure that an integrated isotope zooarchaeology remains a balanced interdisciplinary endeavor. There is a danger of biomolecular approaches eclipsing more traditional zooarchaeological ones for a variety of reasons, in particular the considerable asymmetry in the pace of analysis, but also the inherent attraction of 'cutting-edge' approaches, which are perceived as exciting, both in their novelty and their capacity to address previously unresolvable questions. Zooarchaeology tends to generate results relatively slowly as analysts wait for the completion of excavations and stratigraphic analyses before commencing with faunal analyses. In addition, they also must contend with extremely large volumes of material in order to achieve adequate sample sizes. In contrast, stable isotope analysts can process a large number of bone and tooth specimens relatively quickly, sometimes over the course of only a few months. This disparity in the time to completion of analysis has certainly contributed to the uneven application of an integrated isotope zooarchaeological approach to a particular faunal assemblage. The relative novelty of stable isotope analysis, at least within zooarchaeology, and the production of what appear to be unequivocal results, may also contribute to its attractiveness. The apparent advantage of speedy results does not justify rushing into isotopic analyses of animal bone specimens at the expense of a thorough zooarchaeological investigation.

Extracting zooarchaeological and stable isotopic data from faunal assemblages appropriate for the purposes of addressing questions relating to human subsistence and social practices requires a good understanding of the cultural and natural taphonomic factors that formed the assemblage under analysis. Discrimination between patterns and trends that are produced through the outcomes of human activities and those caused by other processes demands identification of the pre- and post-depositional factors that overprint faunal assemblages. The impact of taphonomic processes on bone specimen representation in faunal assemblages and how these bias quantitative and qualitative faunal measures has long been an active area of zooarchaeological research (Bonnichsen 1998; Gilbert and Singer 1982; Lyman 1984, 1987; Marean and Kim 1998; Stiner 1991), but less so by stable isotope analysts who have yet to grapple with how taphonomy (which is distinct from diagenesis) impacts the sample universe and consequent distribution of stable isotopic results. Moreover, as in the case of faunal analyses, achieving an adequate sample size from the desired archaeological contexts may be challenged by poor preservational conditions that encourage diagenesis and reduce the number of samples producing reliable stable isotope values. What may have initially been a carefully thought out sampling strategy that considered the species, age, sex, and skeletal part of sampled faunal specimens, as well as archaeological context, may turn into a less than ideal representation.

The adoption of stable isotopic approaches by zooarchaeology is equally hazardous if it lacks a firm grip of isotope biogeochemistry and the architecture of isotopic research designs. Decoupling environmental from anthropogenic inputs, for example, remains one of the foremost challenges in interpreting stable isotopic values derived from the tissues of animals exploited by humans. Stable isotopic studies that attempt to identify dietary change and mobility in domesticated animals without an independent means to monitor isotopic variation and change at the floral base of the foodweb may suffer from equifinality. The use of a wild control may be useful, but identifying a suitable number of skeletal specimens belonging to wild taxa in a particular assemblage may be difficult, especially in later period contexts where over-hunting or extirpation of wild animals is likely. The construction of isoscapes from plant and animal specimens other than the animal domesticates under study can be of use if no wild control is available, but this approach requires a nuanced understanding of how seasonality, diet, and physiology influence isotopic values exhibited in the floras and faunas selected for analysis. Thick characterization of the isotopic structuring of ancient floral and faunal communities, which necessitates the analysis of a number of samples larger than many current (zoo)archaeological isotopic studies achieve, may help to further untangle environmental from anthropogenic sources in observed isotopic patterns. Additional clarification may be obtained by simultaneous analyses of multiple isotopes, which offers independent information on different geospatial and dietary facets of a particular ecological system.

The development of new analytical approaches within zooarchaeology and stable isotope biogeochemistry is key to expanding our understanding of ancient human–animal interaction. Geometric morphometrics is a particularly exciting development, and although there are inevitably aspects of the approach that need additional critical evaluation, analyses are providing provocative new insights into animal domestication processes and the transfer and exchange of domesticated animal technologies across environmental and cultural landscapes (Evin et al. 2013; Haruda 2014). Isoscape reconstruction, compound-specific analysis, and dietary mixing models are expanding arenas in stable isotope biogeochemistry that may open additional windows into understanding the ways in which people influenced animal mobility, dietary intake, and life cycles (Makarewicz and Sealy 2015).

Currently, there are relatively few individuals who are trained in both zooarchaeology and stable isotope biogeochemistry. While research interests, academic training, and time might conspire against "doing it all," zooarchaeologists who wish to integrate stable isotope analysis into their research frameworks not only need to keep pace with new developments in stable isotope analysis, but also understand the promises and limitations of the approach. Without a thorough grounding in stable isotope biogeochemistry, it is all too easy to produce naïve interpretations that ultimately undermine the credibility of stable isotope analysis in zooarchaeology. Conversely, practitioners of stable isotope analysis need to understand not only the research questions that have emerged from zooarchaeology but also the active debates within zooarchaeology concerning the utility of specific

analytical approaches used to reconstruct animal use strategies. Data quantification (e.g., the relationship between NISP and derived units), statistical testing and multivariate analysis, and indeterminacy in using demographic models to establish animal production are but a few of the analytical challenges facing zooarchaeology (Domínguez-Rodrigo 2011; Lyman 2015; Marom and Bar-Oz 2009; Vigne et al. 2005; Wolverton et al. 2014).

The goal of pursuing interdisciplinary research and developing a new cross-boundary discipline is to open new research avenues that would otherwise be inaccessible to each discipline on its own. The challenge now is to develop a common theoretical vernacular of isotope zooarchaeology that inclusively integrates existing theoretical frameworks and develops new ones in order to mutually contextualize stable isotopic and zooarchaeological results and thus enable a seamless study of human–animal relations. An integrated isotope zooarchaeology brings us closer to a more holistic documentation of ancient human-animal relationships by drawing simultaneously from two compatible analytical approaches that share an ecological interpretive framework, one which performs as the primary currency for initial interpretations of both isotopic and faunal datasets. Importantly, the intrinsic scalar flexibility of isotope zooarchaeology provides a good fit with the equally scalable theoretical frameworks of human behavioral ecology, practice theory, and cultural niche construction theory to generate a second level of interpretation that provide frames of reference into how humans incorporate animals into their daily subsistence, political networks, and social and symbolic worlds.

Acknowledgements I wish to thank Joshua Wright for insightful conversations on topics relating to those discussed in this chapter. I also thank Bill Finlayson and Ben Arbuckle for their constructive comments on the original version of this chapter.

References

Albarella U, Trentacoste A (2011) Ethnozooarchaeology: the present and past of human-animal relationships. Oxbow Books, Oxford

Ambrose SH (1986) Stable carbon and nitrogen isotope analysis of human and animal diet in Africa. J Hum Evol 15:707–731

Ambrose SH (1991) Effects of diet, climate and physiology on nitrogen isotope abundances in terrestrial foodwebs. J Archaeol Sci 18:293–317

Ambrose SH, DeNiro MJ (1986) Reconstruction of African human diet using bone collagen carbon and nitrogen isotope ratios. Nature 319:321–324

Ambrose SH, Norr L (1993) Isotopic composition of dietary protein and energy versus bone collagen and apatite: purified diet growth experiments. In: Lambert JB, Grupe G (eds) Molecular archaeology of prehistoric human bone. Springer, Berlin, pp 1–37

Balasse M, Bocherens H, Mariotti A, Ambrose SH (2001) Detection of dietary changes by intra-tooth carbon and nitrogen isotopic analysis: an experimental study of dentine collagen of cattle (*Bos taurus*). J Archaeol Sci 28:235–245

Balasse M, Ambrose SH, Smith AB, Price TD (2002) The seasonal mobility model for prehistoric herders in the south-western Cape of South Africa assessed by isotopic analysis of sheep tooth enamel. J Archaeol Sci 29:917–932

Balasse M, Smith AB, Ambrose SH, Leigh SR (2003) Determining sheep birth seasonality by analysis of tooth enamel oxygen isotope ratios: the Late Stone Age Site of Kasteelberg (South Africa). J Archaeol Sci 30:205–215

Balasse M, Tresset A, Dobney K, Ambrose SH (2005) The use of isotope ratios to test for seaweed eating in sheep. J Zool 266:283–291

Balasse M, Tresset A, Ambrose SH (2006) Stable isotope evidence ($\delta^{13}C$, $\delta^{18}O$) for winter feeding on seaweed by Neolithic sheep of Scotland. J Zool 270:170–76

Balasse M, Boury L, Ughetto-Monfrin J, Tresset A (2012) Stable isotope insights ($\delta^{18}O$, $\delta^{13}C$) into cattle and sheep husbandry at Bercy (Paris, France, 4th millennium BC): birth seasonality and winter leaf foddering. Environ Archaeol 17:29–44

Bartosiewicz L (2001) Archaeozoology or zooarchaeology? A problem from the last century. Archaeol Polona 39:75–86

Bar-Yosef O (1992) The role of western Asia in modern human origins. Philos Trans R Soc Lond B Biol Sci 337:193–200

Bar-Yosef O, Meignen L (1992) Insights into Levantine middle Palaeolithic cultural variability. In: Dibble HL, Mellars P (eds) The middle paleolithic: adaptation, behavior, and variability. The University Museum/University of Pennsylvania, Philadelphia, pp 163–182

Barrett J (1994) Fragments from antiquity. Blackwell, Oxford

Bender MM, Baerreis DA, Steventon RL (1981) Further light on carbon isotopes and Hopewell agriculture. Am Antiq 46:346–353

Bendrey R, Vella D, Zazzo A, Balasse M, Lepetz S (2015) Exponentially decreasing tooth growth rate in horse teeth: implications for isotopic analyses. Archaeometry 57:1104–1124

Binford L (1978) Nunamiut ethnoarchaeology. Academic, New York

Binford L (1980) Willow smoke and dog's tails: hunter-gatherer settlement systems and archaeological site formation. Am Antiq 45:1–17

Blaise E, Balasse M (2011) Seasonality and season of birth of modern and late Neolithic sheep from south-eastern France using tooth enamel $\delta^{18}O$ analysis. J Archaeol Sci 38:3085–3093

Blumenschine RJ (1986) Early hominid scavenging opportunities. Implications of Carcass availability in the Serengeti and Ngorongoro ecosystems, B.A.R. International Series. Archaeopress, Oxford

Blumenschine RJ (1988) An experimental model of the timing of hominid and carnivore influence on archaeological bone assemblages. J Archaeol Sci 15:483–502

Bocherens H, Fizet M, Mariotti A, Lange-Badre B, Vandermeersch B, Borel JP, Bellon G (1991) Isotopic biogeochemistry (^{13}C, ^{15}N) of fossil vertebrate collagen: application to the study of a past food web including Neanderthal man. J Hum Evol 20:481–492

Bocherens H, Fizet M, Mariotti A, Gangloff RA, Burns JA (1994) Contribution of isotopic biogeochemistry (^{13}C, ^{15}N, ^{18}O) to the paleoecology of mammoths (*Mammuthus primigenius*). Hist Biol 7:187–202

Bocherens H, Emslie SD, Billiou D, Mariotti A (1995a) Stable isotopes (^{13}C, ^{15}N) and paleodiet of the giant short-faced bear (*Arctodus simus*). C R Acad Sci II 320:779–784

Bocherens H, Fogel ML, Tuross N, Zeder M (1995b) Trophic structure and climatic information from isotopic signatures in Pleistocene cave fauna of Southern England. J Archaeol Sci 22:327–340

Bocherens H, Koch P, Mariotti A, Geraads D, Jaeger J (1996) Isotopic biogeochemistry (^{13}C, ^{18}O) of mammalian enamel from African Pleistocene hominid sites. Palaios 11:306–318

Bocherens H, Billiou D, Patou-Mathis M, Bonjean D, Otte M, Mariotti A (1997) Paleobiological implications of the isotopic signatures (^{13}C, ^{15}N) of fossil mammal collagen in Scladina Cave (Sclayn, Belgium). Quat Res 48:370–380

Bourdieu P (1997) Outline of a theory of practice. Cambridge University Press, Cambridge

Bryant JD, Koch PL, Froelich PN, Showers WJ, Genna BJ (1996) Oxygen isotope partitioning between phosphate and carbonate in mammalian apatite. Geochim Cosmochim Acta 24: 5145–5148

Cerling TE, Harris JM (1999) Carbon isotope fractionation between diet and bioapatite in ungulate mammals and implications for ecological and paleoecological studies. Oecologia 120:347–363

Cerling TE, Harris JM, Ambrose SH, Leakey MG, Solounias N (1997) Dietary and environmental reconstruction with stable isotope analyses of herbivore tooth enamel from the Miocene locality of Fort Ternan, Kenya. J Hum Evol 33:635–650

Chillón BS, Alberdi MT, Leone G, Bonadonna FP, Stenni B, Longinelli A (1994) Oxygen isotopic composition of fossil equid tooth and bone phosphate: an archive of difficult interpretation. Palaeogeogr Palaeoclimatol Palaeoecol 107:317–328

Chisholm BS, Nelson DE, Schwarcz HP (1982) Stable-carbon isotope ratios as a measure of marine versus terrestrial protein in ancient diets. Science 216:1131–1132

Chisholm BS, Nelson DE, Schwarcz HP (1983) Marine and terrestrial protein in prehistoric diets on the British Columbia coast. Curr Anthropol 24:396–398

Cormie AB, Schwarcz HP (1994) Stable isotopes of nitrogen and carbon of North American white-tailed deer and implications for paleodietary and other food web studies. Palaeogeogr Palaeoclimatol Palaeoecol 107:227–241

Cormie AB, Schwarcz HP, Gray J (1994) Determination of the hydrogen isotopic composition of bone collagen and correction for isotopic exchange. Geochim Cosmochim Acta 58:365–375

Crabtree PJ (1990) Zooarchaeology and complex societies: some uses of faunal analysis for the study of trade, social status, and ethnicity. J Archaeol Method Theory 2:155–205

d'Errico F, Zilhão J, Julien M, Baffier D, Pelegrin J (1998) Neanderthal acculturation in Western Europe? A critical review of the evidence and its interpretation. Curr Anthropol 39:1–44

deFrance SD (2009) Zooarchaeology in complex societies: political economy, status, and ideology. J Archaeol Res 17:105–168

DeNiro MJ, Epstein S (1978) Influence of diet on the distribution of carbon isotopes in animals. Geochim Cosmochim Acta 42:495–506

DeNiro MJ, Epstein S (1981) Influence of diet on the distribution of nitrogen isotopes in animals. Geochim Cosmochim Acta 45:341–351

DeNiro MJ, Schoeniger MJ (1983) Stable carbon and nitrogen isotope ratios of bone collagen: variations within individuals, between sexes, and within population raised on monotonous diets. J Archaeol Sci 10:199–203

Domínguez-Rodrigo M (2011) Critical review of the MNI (Minimum Number of Individuals) as a zooarchaeological unit of quantification. Archaeol Anthropol Sci 4:47–59

Drucker D, Bocherens H, Bridault A, Billiou D (2003) Carbon and nitrogen isotopic composition of red deer (*Cervus elaphus*) collagen as a tool for tracking palaeoenvironmental change during the Late-Glacial and Early Holocene in the northern Jura (France). Palaeogeogr Palaeoclimatol Palaeoecol 195:375–388

Dusseldorp GL (2011) Studying Pleistocene Neanderthal and cave hyena dietary habits: combining isotopic and archaeozoological analyses. J Archaeol Method Theory 18:224–255

Ericson JE (1985) Strontium isotope characterization in the study of prehistoric human ecology. J Hum Evol 14:503–514

Evin A, Cucchi T, Cardini A, Strand Vidarsdottir U, Larson G, Dobney K (2013) The long and winding road: identifying pig domestication through molar size and shape. J Archaeol Sci 40: 735–743

Féblot-Augustins J (1994) Mobility strategies in the late middle paleolithic of Central Europe and Western Europe: elements of stability and variability. J Anthropol Archaeol 12:211–265

Fisher JL, Valentine B (2012) Resource depression, climate change, and mountain sheep in the eastern Great Basin of western North America. Archaeol Anthropol Sci 5:145–157

Fizet M, Lange-Badré B (1995) $\delta^{13}C$ et $\delta^{15}N$ du collagène des mammifères: reconstitution des relations trophiques et du paléoenvironnement du gisement de Marillac (France, Pléistocène supérieur). Geobios 28:167–181

Fizet M, Mariotti A, Bocherens H, Lange-Badré B, Vandermeersch B, Borel JP, Bellon G (1995) Effect of diet, physiology and climate on carbon and nitrogen stable isotopes of collagen in a Late Pleistocene anthropic palaeoecosystem: Marillac, Charente, France. J Archaeol Sci 22: 67–79

Frémondeau D, Cucchi T, Casabioanca F et al (2012) Seasonality of birth and diet of pigs from stable isotope analyses of tooth enamel ($\delta^{18}O$, $\delta^{13}C$): a modern reference data set from Corsica, France. J Archaeol Sci 39:2023–2035

Gambier D (1997) Modern humans at the beginning of the upper Paleolithic in France: anthropological data and perspectives. In: Clark GA, Villermet CM (eds) Conceptual issues in modern human origins research. Walter de Gruyter, New York, pp 117–131

Giddens A (1984) The construction of society: an outline of the theory of structuration. University of California Press, Berkeley

Gifford-Gonzalez D (1991) Bones are not enough: analogues, knowledge, and interpretive strategies in zooarchaeology. J Anthropol Archaeol 10:215–254

Gilbert AS, Singer BH (1982) Reassessing zooarchaeological quantification. World Archaeol 14: 21–40

Grosman L, Munro ND, Belfer-Cohen A (2008) A 12,000-year-old shaman burial from the southern Levant (Israel). Proc Natl Acad Sci USA 105:17665–17669

Guiry EJ, Harpley B, Jones Z, Smith C (2014) Integrating stable isotope and zooarchaeological analyses in historical archaeology: a case study from the urban nineteenth-century Commonwealth Block Site, Melbourne, Australia. Int J Hist Archaeol 18:415–440

Haruda A (2014) The potential for detecting livestock exchange in Late Bronze Age Kazakhstan: tracking sheep breeds across the steppe. In: Poster, association for environmental archaeology conference, University of Plymouth

Heaton TH, Vogel JC, la Chevallerie G, Collett G (1986) Climatic influence on the isotopic composition of bone nitrogen. Nature 322:822–823

Hesse B (1984) These are our goats: the origins of herding in west central Iran. In: Clutton Brock J, Grigson C (eds) Animals and archaeology, vol 3: Early herders and their flocks, British Archaeological Reports International Series 24. Oxford, pp 424–464

Higgs ES, Jarman MR (1975) Palaeoeconomy. In: Higgs ES (ed) Palaeoeconomy. Cambridge University Press, Cambridge, pp 1–9

Hobson KA, Collier S (1984) Marine and terrestrial protein in Australian Aboriginal diets. Curr Anthropol 25:238–240

Iacumin P, Cominotto D, Longinelli A (1996) A stable isotope study of mammal skeletal remains of mid-Pleistocene age, Arago cave, eastern Pyrenees, France. Evidence of taphonomic and diagenetic effects. Palaeogeogr Palaeoclimatol Palaeoecol 126:151–160

Iacumin P, Bocherens H, Delgado Huertas A, Mariotti A, Longinelli A (1997) A stable isotope study of fossil mammal remains from the Paglicci cave, southern Italy. N and C as palaeoenvironmental indicators. Earth Planet Sci Lett 148:349–357

Iacumin P, Nikolaev V, Ramigni M (2000) C and N stable isotope measurements on Eurasian fossil mammals, 40000 to 10 000 years BP: Herbivore physiologies and palaeoenvironmental reconstruction. Palaeogeogr Palaeoclimatol Palaeoecol 163:33–47

Johannesson EG (2015) Animals, identity, and mortuary behavior in Late Bronze Age–Early Iron Age Mongolia. In: Kardulias PN (ed) The ecology of pastoralism. University Press of Colorado, Denver, CO, pp 97–116

Johansen OS, Gulliksen S, Nydal R (1986) $\delta^{13}C$ and diet: analysis of Norwegian human skeletons. Radiocarbon 28:754–761

Kendal J, Tehrani JJ, Odling-Smee J (2011) Human niche construction in interdisciplinary focus. Philos Trans R Soc London B Biol Sci 366:785–792

Koch PL (1991) The isotope ecology of Pleistocene proboscideans. J Vertebr Paleontol 11:40a

Koch PL, Fisher DC, Dettman DL (1989) Oxygen isotope variation in the tusks of extinct proboscideans: a measure of season of death and seasonality. Geology 17:515–519

Koch PL, Sachos JC, Dettman DL (1995) Stable isotope stratigraphy and paleoclimatology of the Paleogene Bighorn Basin (Wyoming USA). Palaeogeogr Palaeoclimatol Palaeoecol 115: 61–89

Kohn MJ, Schoeninger JW, Valley JW (1998) Variability in oxygen isotope compositions of herbivore teeth: reflections of seasonality or developmental physiology? Chem Geol 152: 97–112

Koon H, Tuross N (2013) The Dutch whalers: a test of human migration in the oxygen, carbon and nitrogen isotopes of cortical bone collagen. World Archaeol 44:360–372

Laffoon JE, Plomp E, Davies GR, Hoogland MLP, Hofman CL (2013) The movement and exchange of dogs in the prehistoric Caribbean: an isotopic investigation. Int J Osteoarchaeol. doi:10.1002/oa.2313
Laland KN, O'Brien MJ (2010) Niche construction theory and archaeology. J Archaeol Method Theory 17:303–322
Laland KN, O'Brien MJ (2012) Cultural niche construction. An introduction. Biol Theory 6: 191–202
Laland KN, Odling-Smee J, Feldman MW (2000) Niche construction, biological evolution, and cultural change. Behav Brain Sci 23:131–175
Landon DB (2005) Zooarchaeology and historical archaeology: progress and prospects. J Archaeol Method Theory 12:1–36
Lee-Thorp JA, Sealy JC, van der Merwe NJ (1989) Stable carbon isotope ratio differences between bone collagen and bone apatite, and their relationship to diet. J Archaeol Sci 16:585–599
Lösch S, Grupe G, Peters J (2006) Stable isotopes and dietary adaptations in humans and animals at pre-pottery Neolithic Nevalı Çori, Southeast Anatolia. Am J Phys Anthropol 131:181–193
Longinelli A (1984) Oxygen isotopes in mammal bone phosphate: a new tool for paleohydrological and paleoclimatological research? Geochim Cosmochim Acta 48:385–390
Luz B, Kolodny Y (1989) Oxygen isotope variation in bone phosphate. Appl Geochem 4:317–323
Luz B, Kolodny Y, Horowitz M (1984) Fractionation of oxygen isotopes between mammalian bone-phosphate and environmental drinking water. Geochim Cosmochim Acta 48:1689–1693
Luz B, Cormie AB, Schwarcz HP (1990) Oxygen isotope variation in phosphate of deer bones. Geochim Cosmochim Acta 54:1723–1728
Lyman RL (1984) Bone density and differential survivorship of fossil classes. J Anthropol Archaeol 3:259–299
Lyman RL (1987) Archaeofaunas and butchery studies: a taphonomic perspective. Adv Archaeol Method Theory 10:249–337
Lyman RL (2015) The history of "laundry lists" in North American zooarchaeology. J Archaeol Sci 39:42–50
Makarewicz C (2014) Winter pasturage and variable foddering detected in ($\delta^{15}N$) and carbon (δ13C) isotopes in sheep dentinal collagen. J Archaeol Sci 42:502–510
Makarewicz CA, Sealy J (2015) Dietary reconstruction, mobility, and the analysis of ancient skeletal tissues: expanding the prospects of stable isotope research in archaeology. J Archaeol Sci 56:146–158
Makarewicz C, Tuross N (2006) Foddering by Mongolian pastoralist is recorded in the stable carbon ($\delta^{13}C$) and nitrogen ($\delta^{15}N$) isotopes of caprine dentinal collagen. J Archaeol Sci 33:862–870
Makarewicz C, Tuross N (2012) Finding fodder and tracking transhumance: isotopic detection of goat domestication processes in the Near East. Curr Anthropol 53:495–505
Maltby M (2002) Integrating zooarchaeology: introduction. In: Maltby M (ed) Integrating zooarchaeology. Oxbow Books, Oxford, pp 1–4
Marean CW (1998) A critique of the evidence for scavenging by Neanderthals and early modern humans: new data from Kobeh cave (Zagros Mountains, Iran) and Die Kelders Cave 1 layer 10 (South Africa). J Hum Evol 35:111–136
Marean CW, Kim SY (1998) Mousterian and large-mammal remains from Kobeh Cave: behavioral implications for Neanderthals and early modern humans. Curr Anthropol 39:S79–S113
Marom N, Bar-Oz G (2009) Culling profiles: the indeterminacy of archaeozoological data to survivorship curve modelling of sheep and goat herd maintenance strategies. J Archaeol Sci 36: 1184–1187
Matheus PE (1995) Diet and co-ecology of Pleistocene short-faced bears and brown bears in Eastern Beringia. Quat Res 44:447–453
McClure SB (2015) The pastoral effect: niche construction, domestic animals, and the spread of farming in Europe. Curr Anthropol 56:901–910
Minagawa M, Wada E (1984) Stepwise enrichment of ^{15}N along food chains: further evidence and the relation between $\delta^{15}N$ and animal age. Geochim Cosmochim Acta 48:1135–1140

Noe-Nygaard N, Price TD, Hede SU (2005) Diet of aurochs and early cattle in southern Scandinavia: evidence from ^{15}N and ^{13}C stable isotopes. J Archaeol Sci 32:855–871

Olsen KC, White CD, Longstaffe FJ, von Heyking K, McGlynn G, Grupe G, Rühli FJ (2013) Intraskeletal isotopic compositions ($\delta^{13}C$, $\delta^{15}N$) of bone collagen: nonpathological and pathological variation. Am J Phys Anthropol 153:598–604

Piccione P, Corrado A, Bartosiewicz L, Lemorini C, Masi A, Sadori L (2015) Distribution of artifacts and ecofacts in an Early Bronze Age house in eastern Anatolia: space use and household economy at Arslantepe VI B2 (2900–2750 BCE). J Archaeol Sci Rep 4:8–22

Pilaar Birch SE (2013) Stable isotopes in zooarchaeology: in introduction. Archaeol Anthropol Sci. doi:10.1007/s112520-013-0126-7

Quade J, Cerling TE, Barry JC, Morgan ME, Pilbeam DR, Chivas AR, Lee-Thorp JA, van der Merwe NJ (1992) A 16-Ma record of paleodiet using carbon and oxygen isotopes in fossil teeth from Pakistan. Chem Geol 94:183–192

Reinhard E, De Torres T, O'Neil JR (1996) $^{18}O/^{16}O$ ratios of cave bear tooth enamel: a record of climate variability during the Pleistocene. Palaeogeogr Palaeoclimatol Palaeoecol 126:45–59

Reitz EJ, Wing ES (1999) Zooarchaeology. Cambridge University Press, Cambridge

Reynard LM, Tuross N (2015) The known, the unknown and the unknowable: weaning times from archaeological bones using nitrogen isotope ratios. J Archaeol Sci 53:618–625

Richards MP, Pettitt PB, Trinkaus E, Smith FH, Paunović M, Karavnić I (2000) Neanderthal diet at Vindija and Neanderthal predation: the evidence from the stable isotopes. Proc Natl Acad Sci 97:7663–7666

Richards MP, Pettitt PB, Stiner MC, Trinkaus E (2001) Stable isotope evidence for increasing dietary breadth in the European mid-Upper Paleolithic. Proc Natl Acad Sci 98:6528–6532

Rolland N, Dibble HL (1990) A new synthesis of middle paleolithic variability. Am Antiq 55: 480–499

Russell N (2012) Social zooarchaeology: Humans and animals in prehistory. Cambridge University Press, New York

Salmi A-K, Äikäs T, Fjellström M, Spangen M (2015) Animal offerings at the Sámi offering site of Unna Saiva – changing religious practices and human–animal relationships. J Anthropol Archaeol 40:10–22

Sayre MP, Miller MJ, Rosenfeld SA (2015) Isotopic evidence for the trade and production of exotic marine mammal bone artifacts at Chavín de Huántar, Peru. Archaeol Anthropol Sci 1–15. doi:10.1007/s12520-015-0230-y

Scharlotta I, Goriunova OI, Weber A (2013) Micro-sampling of human bones for mobility studies: diagenetic impacts and potentials for elemental and isotopic Research. J Archaeol Sci 40: 4509–4527

Schoeninger MJ, DeNiro MJ (1984) Nitrogen and carbon isotopic composition of bone collagen from marine and terrestrial animals. Geochim Cosmochim Acta 48:625–639

Schwarcz HP, Melbye J, Katzenberg MA, Knyf M (1985) Stable isotopes in human skeletons of southern Ontario: reconstructing palaeodiet. J Archaeol Sci 12:187–206

Schwarcz HP, Dupras TL, Fairgrieve SI (1999) ^{15}N enrichment in the Sahara: in search of a global relationship. J Archaeol Sci 26:629–636

Sealy JC, van der Merwe NJ, Lee-Thorp JA, Lanham JL (1987) Nitrogen isotopic ecology in southern Africa: implications for environmental and dietary tracing. Geochim Cosmochim Acta 51:2707–2717

Sjögren K-G, Price TD (2013) A complex Neolithic economy: isotope evidence for the circulation of cattle and sheep in the TRB of western Sweden. J Archaeol Sci 40:690–704

Smith BD (2009) Core conceptual flaws in human behavioral ecology. Commun Integr Biol 6: 533–534

Smith BD (2012) Cultural niche construction theory of initial domestication. Biol Theory 6: 260–271

Smith EA, Winterhalder B (2006) Human behavioral ecology. In: Encyclopedia of cognitive science. Wiley, New York

Sponheimer M, Robinson T, Ayliffe L, Passey B, Roeder B, Shipley L, Lopez E, Cerling T, Dearing D, Ehleringer J (2003) An experimental study of carbon-isotope fractionation between diet, hair, and feces of mammalian herbivores. Can J Zool 81:871–876

Stiner M (1991) Food procurement and transport by human and non-human predators. J Archaeol Sci 18:455–482

Stiner M (1992) Overlapping species "choice" by Italian upper Pleistocene predators. Curr Anthropol 33:433–451

Stiner M (1994) Honor among thieves: a zooarchaeological study of Neanderthal ecology. Princeton University Press, Princeton, p 422

Stiner CM, Munro N, Surovell TA (2000) The tortoise and the hare. Curr Anthropol 41:39–79

Sugiyama N, Somerville AD, Schoeninger MJ (2015) Stable isotopes and zooarchaeology at Teotihuacan, Mexico reveal earliest evidence of wild carnivore, management in Mesoamerica. PLoS One 10(9):e0135635

Tauber H (1981) ^{13}C evidence for dietary habits of prehistoric man in Denmark. Science 292: 332–333

Thornton EK (2011) Reconstructing ancient Maya animal trade through strontium isotope ($^{87}Sr/^{86}Sr$) analysis. J Archaeol Sci 38:3254–3263

van der Merwe N, Vogel JC (1978) ^{13}C content of human collagen as a measure of prehistoric diet in Woodland North America. Nature 276:815–816

Vigne J-D, Helmer D, Peters J (2005) New archaeological approaches to trace the first steps of animal domestication: general presentation, reflections and proposals. In: Vigne J-D, Peters J, Helmer D (eds) First steps of animal domestication: new zooarchaeological approaches. Proceedings of the 9th conference of the international council of archaeozoology, Durham, August 2002, Oxbow, Oxford, pp 1–17

Walker PL, DeNiro MJ (1986) Stable nitrogen and carbon isotope ratios in bone collagen as indices of prehistoric dietary dependence on marine and terrestrial resources in Southern California. Am J Physi Anthropol 71:51–61

Wallis NJ, Blessing ME (2015) Big feast and small scale foragers: pit features as feast events in the American Southeast. J Anthropol Archaeol 39:1–18

Wang Y, Cerling TE (1994) A model of fossil tooth and bone diagenesis: implications for paleodiet reconstruction from stable isotopes. Palaeogeogr Palaeoclimatol Palaeoecol 107: 281–289

Winterhalder B, Smith EA (2000) Analyzing adaptive strategies: human behavioral ecology at twenty-five. Evol Anthropol 9:51–72

Wolverton S, Chambers KJ, Veteto JR (2014) Climate change and ethnobiology. J Ethnobiol 34: 273–275

Zangrando AF, Tessone A, Ugan A, Gutiérrez MA (2014) Applications of stable isotope analysis in zooarchaeology: an introduction. Int J Osteoarchaeol 24:127–133

Zazzo A, Balasse M, Patterson WP (2006) The reconstruction of mammal individual history: refining high-resolution isotope record in bovine tooth dentine. J Archaeol Sci 33:1177–1187

Zazzo A, Bendrey R, Vella D, Moloney AP, Monahan FJ, Schmidt O (2012) A refined sampling strategy for intra-tooth stable isotope analysis of mammalian enamel. Geochim Cosmochim Acta 84:1–13

Zeder MA (2015a) Core questions in domestication research. Proc Natl Acad Sci USA 112: 3191–3198

Zeder MA (2015b) Reply to Mohlenhoff et al: Human behavioral ecology needs a rethink that niche-construction theory can provide. Proc Natl Acad Sci USA 112:E3094

Zeder MA, Hesse B (2001) The initial domestication of goats (*Capra hircus*) in the Zagros Mountains 10,000 years ago. Science 287:2254–2257

Part IV
Processing Multi-isotope Signatures

Assigning Elephant Ivory with Stable Isotopes

Stefan Ziegler, Bruno Streit, and Dorrit E. Jacob

Introduction

The illicit trade of ivory and the associated poaching of African elephants have received international attention since several decades, peaking in the listing of the African elephant on CITES Appendix I in 1989 [Convention on International Trade in Endangered Species (CITES) of Wild Fauna and Flora]. This effectively cut off the legal supply of ivory to markets around the world. Since then, only two so-called one-off sales had been applied, allowing some countries to officially trade parts of their ivory stocks. The distinction between officially traded and illegal ivory without further laboratory testing is difficult (UNOCD 2014). In 2011, an estimated 17,000 elephants were illegally killed to meet the increasing demand of ivory in Asian consumer countries (Wasser et al. 2008). The increasing illicit trade may be leading to a dramatic decline in some African elephant populations (Wittemyer et al. 2014).

In the past 30 years, isotopic ratios of carbon, oxygen, nitrogen, strontium, and lead in elephant tusks have been evaluated and used to determine the geographic source of ivory (Van der Merwe et al. 1988; Vogel et al. 1990; Cerling et al. 1999,

S. Ziegler (✉)
Department of Ecology and Evolution, Goethe University Frankfurt, 60438 Frankfurt/Main, Germany

WWF Germany, Reinhardtstr. 18, 10117 Berlin, Germany
e-mail: stefan.ziegler@wwf.de

B. Streit
Department of Ecology and Evolution, Goethe University Frankfurt, 60438 Frankfurt/Main, Germany

D.E. Jacob
Department of Earth and Planetary Sciences, Macquarie University, North Ryde, NSW 2109, Australia

Department of Geosciences, Johannes Gutenberg University, 55099 Mainz, Germany

G. Grupe, G.C. McGlynn (eds.), *Isotopic Landscapes in Bioarchaeology*,
DOI 10.1007/978-3-662-48339-8_12

2003, 2004, 2007), but attempts to conduct assignment tests of elephant ivory with stable isotopes have been limited. The isotope enrichment of certain chemical elements in the tusks or the bone material of the animals is a sound method to reliably identify the origin of elephant ivory (Van der Merwe et al. 1990). Isotopic analysis has the advantage of allowing insights into the origin of elephant ivory even when the sample is contaminated or if DNA material is not available (UNOCD 2014). Several authors referred to general expectations of biome characteristics associated with foodweb ^{13}C and ^{15}N values (Van der Merwe et al. 1990; Ishibashi et al. 1999), but one shortcoming of the current framework is that when applied across an entire community, the metrics do not fully incorporate the natural variability within the system into the subsequent summary statistics (Jackson et al. 2011). Presumably, many factors contribute to isotopic variability within elephant populations, such as migration, ecological change within a region, or seasonal dietary shifts (Hobson 1999).

Research projects are under way to trace the geographical origin of ivory as a potentially powerful countermeasure tool and to create related databases. Court-proof results will need internationally recognized analytical methods and reference materials to facilitate legal prosecution (UNOCD 2014). Thus, assignment tests are urgently required to validate the potential of the isotopes more quantitatively in order to provide predictable and complementary markers for determining the provenance of ivory. The purpose of this study was to analyze the variability of isotope ratios in ivory samples from within and between different locations in Africa to quantitatively validate their potential for forensic purposes. Isotopic source-area determination must have a secure scientific basis that can withstand legal scrutiny (Koch and Behrensmeyer 1992).

Methodology

Isotope ratios used here are stored in the online database www.ivoryid.org, jointly developed by the German Federal Agency for Nature Conservation (BfN) and WWF Germany. This database contains isotopic ratios of $\delta^{13}C$, $\delta^{15}N$, $\delta^{18}O$, $\delta^{2}H$, and $\delta^{34}S$ from more than 500 geo-referenced ivory tusks throughout Africa and Asia. We selected a subset of 293 data of ivory samples from 18 African elephant range states (Table 1), comprising 40 different locations. Sampling procedures, sample preparation, and isotopic analyses are described in Ziegler et al. (2013). One important difference to most other ivory analyses in the literature is that the data contain isotopic ratios that are measured on pulverized ivory powder directly. Isotopic ratios (R) are expressed in δ units in the conventional permil notation where $\delta = [(R_{\text{sample}}/R_{\text{standard}}) - 1] \times 1000$. Analytical uncertainties were 0.1‰ ($\delta^{13}C$, $\delta^{15}N$), 0.2‰ ($\delta^{34}S$), 0.4‰ ($\delta^{18}O$), and 2.3‰ ($\delta^{2}H$). Corresponding relative errors were 0.4 % ($\delta^{13}C$), 0.9 % ($\delta^{15}N$), 2.1 % ($\delta^{34}S$), 2.4 % ($\delta^{18}O$), and 5.2 % ($\delta^{2}H$).

Table 1 List of African elephant range states and no. of samples included in this study

Country	No. of samples	CITES
Angola	3	Appendix I
Botswana	82	Appendix II
Burkina Faso	38	Appendix I
Cameroon	5	Appendix I
Democratic Republic of Congo	24	Appendix I
Gabon	2	Appendix I
Ghana	2	Appendix I
Kenya	4	Appendix I
Liberia	2	Appendix I
Malawi	25	Appendix I
Mozambique	18	Appendix I
Namibia	3	Appendix II
Sudan	2	Appendix I
Sierra Leone	2	Appendix I
Togo	3	Appendix I
Tanzania	11	Appendix I
South Africa	56	Appendix II
Zimbabwe	11	Appendix II

Statistical Analysis

All statistical analyses were conducted using the *R* environment for statistical computing and graphics. Isotopic values were standardized and we tested each stable isotope distribution for normality using the Kolmogorov–Smirnov test. The isotopic values were first normalized and then each stable isotope distribution was tested with the Kolmogorov–Smirnov test against the normal distribution ($n = 293$; mean = 0, SD = 1) for normality. All p-values were greater $p = 0.01$ so that normal distribution of the stable isotopes was assumed.

The partitioning and setting of training categories followed the inclusion of both extant elephant species in the CITES Appendices. We built two classifiers, representing elephant populations, which are currently listed on Appendix I ($n = 143$) and Appendix II ($n = 150$) in CITES. A perfect predictor would be described as 100 % sensitive (i.e., all ivory samples from Appendix I populations are assigned to Appendix I populations) and a false-positive rate of zero (i.e., no samples from Appendix II populations are assigned to Appendix I populations). In order to address the problem of cutting natural variation due to limited sample size, we calculated the mean and standard deviation for each CITES Appendix to simulate $n = 1000$ isotopic ratios per class. We then applied the nearest neighbor (NN) rule as pattern classification algorithm and cross-validated the original ($n = 293$) and simulated data ($n = 2000$). We ran leave-one-out cross-validation by using a single observation from the original data set as validation data and the

remaining observations as training data. This step was repeated until each observation in the sample was used once as the validation data. The basic rationale for the NN rule, which was first developed by Fix and Hodges (1989), is that samples with small Euclidian distance belong to the same class, meaning that those samples are likely derived from the same place of origin. Given the vast spatial range and the ecological heterogeneity of the African elephant habitat, we assumed that the pattern classes do overlap to some extent, rendering the NN rule suboptimal. Thus, we also performed the *k*-nearest neighbor (*k*-NN) rule that classifies the vector to the class that appears most frequently among its *k* nearest neighbors (Stone 1977) and set the *k* value as $\sqrt{n}$.

Results

Isotopic Markers

We investigated the potential power of isotopic markers to avoid the intermixing of legal and illegal ivory, if decisions for a restricted legal ivory trade from CITES Appendix II elephant populations will be taken in future. The current geographic clustering of Appendix II populations is restricted to four range states in Southern Africa, namely (1) Botswana, (2) Namibia, (3) South Africa, and (4) Zimbabwe. The mean isotopic values of these populations show a distinct isotopic signature against all other elephant populations which are listed in CITES Appendix I (Table 2). This is particularly prominent in $\delta^{34}S$ where the difference of the mean ratio between the two classes is 4.5‰ so that in general, ivory from a CITES Appendix II population appears to be enriched in ^{34}S. Higher means and smaller standard deviations were also detected in other isotope ratios from Appendix II populations. Therefore, we created kernel density plots to better show the distribution of the isotope variables and superimposed the plots of the Appendix I and II elephant populations (Fig. 1). The Kernel density estimation is a nonparametric way to estimate the probability density function of the stable isotope variables. We also conducted a global Kruskal–Wallis test and found significant differences among the two groups over all stable isotopes (p-values < 0.001). However, the density functions of all isotopes show that Appendix I and II elephant populations do overlap widely (Fig. 1). Only in upper and lower ranges of $\delta^{34}S$ as well as lower

Table 2 Results of stable isotope analyses of 293 ivory samples grouped by CITES Appendices

	$\delta^{13}C$		$\delta^{15}N$		$\delta^{18}O$		$\delta^{2}H$		$\delta^{34}S$	
	Mean	SD	Mean	SD	Mean	SD	Mean	SD	Mean	SD
Appendix I	−21.7	1.92	7.5	2.16	16.8	1.89	−46.0	11.16	8.4	2.8
Appendix II	−20.3	1.28	9.5	1.38	17.9	2.98	−36.7	8.52	12.9	2.98

Isotope rations are expressed as means with standard deviations (SD)

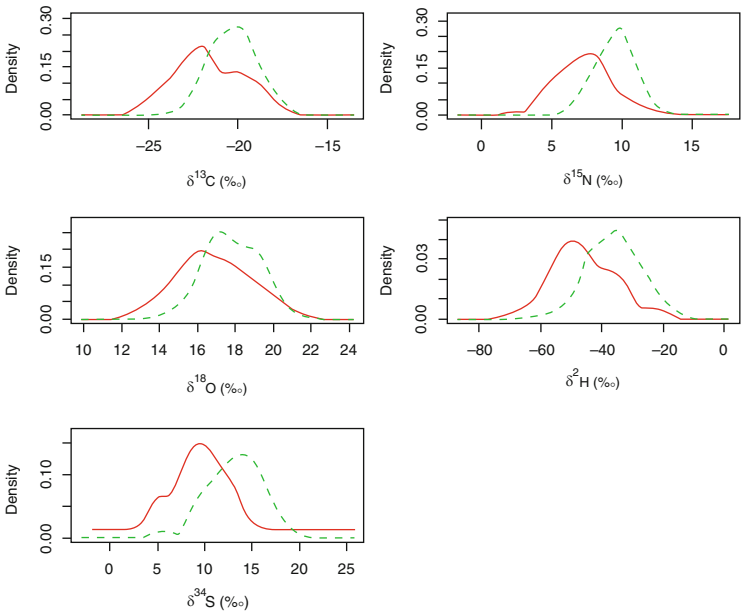

Fig. 1 Kernel density of isotope ratios of Appendix I (*solid line*) and Appendix II (*dotted line*) elephant populations

ranges of $\delta^{13}C$ and $\delta^{15}N$ do populations appear to show distinct signatures. However, it remains doubtful whether single isotopes provide satisfactory predictive power to clearly distinct sources of provenance from either CITES Appendices.

Assignments

Using all samples and vectorized isotope markers as training data, we conducted leave-one-out cross-validation with original and simulated Appendix I and II populations as classifiers and inserted the results in a contingent table (Table 3). Accuracy (overall number of correct classifications) for the *k*-NN rule was almost identical for both original and simulated data and scored in the range of 90 %. Sensitivity (i.e., all ivory samples from Appendix I populations are assigned to Appendix I populations) slightly increased by 2 %, whereas the false-positive rate (i.e., no samples from Appendix II populations are assigned to Appendix I populations) slightly decreased (2 %) for the simulated data. We also calculated the mean Euclidian distance and the tolerance limits (95 % confidence interval) of the *k*-NN ($k = 17$) for both Appendix I (mean: 1.366; SD: 0.570) and II (mean: 1.17; SD: 0.374) classes (Fig. 2).

Table 3 Results of leave-one-out cross-validation for real data ($n = 293$; $k = 17$) and simulated data with k-NN rule ($n = 2000$; $k = 44$)

	Real data		Simulated data	
	Appendix I	Appendix II	Appendix I	Appendix II
Appendix I	125	10	890	85
Appendix II	18	140	110	915
Accuracy (%)	90.4		90.3	

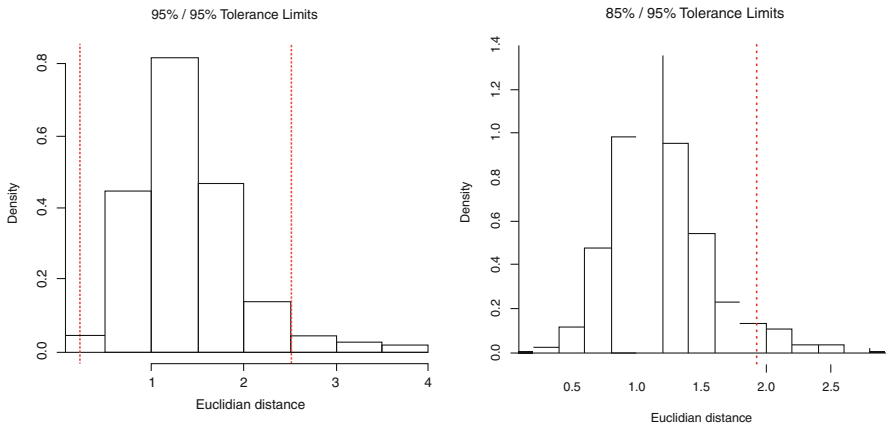

Fig. 2 (**a**, **b**) Tolerance limit (95 % confidence interval) of Euclidian distance of $k = 17$ nearest neighbors of Appendix I (**a**) and Appendix II (**b**) elephant populations

Discussion

Forensic Provenancing

Through the combination of isotopic markers used in our study, it is possible to increase the sensitivity of correctly assigned Appendix I samples to approximately 90 %. We also demonstrated that the predictive power remains stable if the sample size is increased in order to simulate natural variability within populations. With our simulation approach the risk of point estimates can be avoided (Jackson et al. 2011). Ideally, any statistical approach to distinguish legal from illegal elephant ivory by its isotopic signature would aim to correctly determine the place of origin. However, the consequences of such a statistical procedure that leads to incorrectly assigning ivory of stated origin must be carefully taken into account (Hoogewerff 2010). There are two possible ways in which a sample may be misassigned. On the one hand, the test may mask fraud, such as poaching or leaking of stockpiled ivory from Appendix I populations onto the market. This is a "false negative" and our simulated data have shown that this risk remains stable at a level

of approx. 10 %. Furthermore, samples from an Appendix II population can be wrongly assigned as "false positives." This interpretation could lead to false accusations against legitimate producers or buyers of legal ivory. Our simulated data show that this risk is also in the range of 8–9 %. This difference can likely be attributed to lower within population variance of Appendix II populations which can be postulated from the overall lower standard deviation of the mean isotopic values. It is also illustrated by the narrower tolerance interval (95 % confidence interval) of the *k*-NN Euclidian distance among ivory samples from Appendix II elephant range states (Fig. 2).

If decisions for a restricted legal ivory trade are in place, spot checks usually contain no additional information to help decide whether the sample derives from an Appendix I or II population. Thus, each of the two CITES Appendices can be considered equally likely, or having the a priori probability of 0.5. In our simulated model, the highest probability of assigning a tusk to any CITES Appendix population is approximately 0.9. Thus, the probability of not assigning it to that population is approximately 0.1. So the odds ratio of assigning a sample is 0.9/0.1 or 9, whereas the odds ratio for the a priori probability is 0.5/0.5 or 1. Thus, the odds ratio of our stable isotope model for assigning elephant ivory to either CITES category is 9/1 or 9. Or in other words, the geographic structure and associated isotopic signatures of current CITES listing of elephant populations are about nine times more informative than the uniform or random case. This value is above the fourfold improvement in odds ratio over random assignment which was given by Rocque et al. (2006) as a threshold for possible assignments of two locations. Therefore, our isotope-based results are promising for the aim of classifying elephant ivory according to its regional provenance under current CITES listing of elephant populations. In cases where knowledge of isotopic differences between elephant ivory is important for conservation activities and to better control contrabanded ivory trade, cost-effective isotopic markers and the statistical methods examined here may be used.

At the time of the last continent-wide assessment in 2007, the African elephant population was calculated to be at least 472,000 individuals, with possible numbers exceeding 690,000 elephants. One of the key findings in the latest African Elephant Status Report (Blanc et al. 2007) is that elephant numbers in East and Southern Africa are increasing by 4 % annually. These two subregions hold 88 % of all of the "definite" and "probable" elephant numbers in the African Elephant Database. In the medium term, some African countries, particularly those with increasing elephant numbers, might insist that trade of ivory from their stocks should be allowed in order to generate continuous revenues for nature conservation (Ziegler 2010). On the other hand, poaching of African elephants and illicit trade in ivory have accelerated in some African subregions during the recent years (Wittemyer et al. 2014). Well-organized and heavily armed criminal gangs not only endanger elephant populations but also constitute a threat to regional political stability, territorial integrity, and sustainable social and economic developments of the countries concerned (UNOCD 2014). Thus, the methods we have examined may also help international law enforcement and cross-border cooperation to uncover the structures and pathways of ivory smuggling.

References

Blanc JJ, Barnes RFW, Craig GC, Dublin HT, Thouless CR, Douglas-Hamilton I, Hart JA (2007) African elephant status report 2007: an update from the elephant database. Occasional paper series of the IUCN species survival commission, No. 33. IUCN/SSC African Elephant Specialist Group; IUCN, Gland, Switzerland, vi + 276 pp

Cerling TE, Harris JM, Leakey MG (1999) Browsing and grazing in elephants: the isotope record of modern and fossil proboscideans. Oecologia 120:364–374

Cerling TE, Harris JM, Passey BH (2003) Diets of East African Bovidae based on stable isotope analysis. J Mammal 84:456–470

Cerling TE, Hart JH, Hart TB (2004) Stable isotope ecology in the Ituri Forest. Oecologia 138:5–12

Cerling TE, Omondi P, Macharia AN (2007) Diets of Kenyan elephants from stable isotopes and the origin of confiscated ivory in Kenya. Afr J Ecol 45:614–623

Fix E, Hodges JL (1989) Discriminatory analysis – nonparametric discrimination: consistency properties. Int Stat Rev 57:238–247

Hobson KA (1999) Tracing origins and migration of wildlife using stable isotopes: a review. Oecologia 120:314–326

Hoogewerff J (2010) Trace elements and Sr-isotopes analyses to evaluate the geographical origin of food products. TRACE Newsl 5:8

Ishibashi H, Takeuchi T, Whyte I, Koike H (1999) Delta 15N and delta 13C measurements from the African elephant, Loxodonta Africana, used for ivory sourcing. Bull Grad Sch Soc Cult Stud Kyushu Univ 5:1–8

Jackson AL, Inger R, Pamell AC, Bearhop S (2011) Comparing isotopic niche widths among and within communities: SIBER – Stable Isotope Bayesian Ellipses in R. J Anim Ecol 80:595–602

Koch P, Behrensmeyer AK (1992) Determining the source-area of ivory through isotopic analysis. Afr Wildl Found: Elephant Ivory Inf Service 19:1–4

Rocque DA, Ben-David M, Barry RP, Winker K (2006) Assigning birds to wintering and breeding grounds using stable isotopes: lessons from two feather generations among three intercontinental migrants. J Ornithol 147:395–404

Stone CJ (1977) Consistent nonparametric regression. Ann Stat 5:595–645

UNOCD (2014) Guidelines on methods and procedures for ivory sampling and laboratory analysis. United Nations, New York, 119 pp

van der Merwe NJ, Lee-Thorp JA, Bell RHV (1988) Carbon isotopes as indicators of elephant diets and African environments. Afr J Ecol 26:163–172

van der Merwe NJ, Lee-Thorp JA, Thackeray JF, Hall-Martin A, Kruger FJ, Coetzee H, Bell RHV, Lindeque M (1990) Source-area determination of elephant ivory by isotopic analysis. Nature 346:744–746

Vogel JC, Eglington B, Auret JN (1990) Isotope fingerprints in elephant bone and ivory. Nature 346:747–749

Wasser SK, Clark WJ, Drori O, Kisamo ES, Mailand C (2008) Combating the illegal trade in African elephant ivory with DNA forensics. Conserv Biol 22:1064–1071

Wittemyer G, Northrup JM, Blanc J, Douglas-Hamilton I, Omondi P, Burnham KP (2014) Illegal killing for ivory drives global decline in African elephants. PNAS 111:13117–13121

Ziegler S (2010) Development of a spatial references database for ivory. TRAFFIC Bull 23:4

Ziegler S, Denkl C, Hornig K, Schupfner R (2013) Isotope databases for the determination of age and provenance of elephant ivory. CITES CoP16 Inf 19:1–11

Towards Predicting Places of Origin from Isotopic Fingerprints: A Case Study on the Mobility of People in the Central European Alps

Markus Mauder, Eirini Ntoutsi, Peer Kröger, and Hans-Peter Kriegel

Introduction

Isotopic analysis is used for dating skeletons, artifacts, and archaeological sites, as well as for the reconstruction of diet, climate, and migration patterns (Ambrose and Krigbaum 2003). More on general principles and limitations of stable isotope analysis can be found in Meier-Augenstein and Kemp (2009). The general idea behind these works is that the isotope measurements in the different samples reflect the environments where these samples were located. Indirectly, this means that different places can be characterized by different isotopic fingerprints or isotopic signatures based on the distribution of the different elements in these places. Determining the isotopic fingerprint for a specific location is requisite for providing useful information about this place and it can also be used as a template for classifying new samples to their most probable origin.

In this work, we base our calculations on the isotopic signatures of three elements, oxygen, strontium, and lead deriving from samples of animal bones recovered from various archaeological sites in the Alps.

The goal of the project is to build local isotopic fingerprint models thereby generating different isotopic profiles for the alpine area. Such profiling would be helpful for comprehending the specific characteristics of each area, how the different areas are isotopically connected, and whether the isotopic proximity corresponds to the spatial proximity of the areas. In the second step, this profiling could be used for associating the values taken from other samples of unknown origin with specific localities for which the isotopic fingerprint is mapped. It should be noted that mapping does not need to rely on profiling exclusively. In data mining terms, extracting the isotopic fingerprints is an unsupervised task (clustering), whereas

M. Mauder (✉) • E. Ntoutsi • P. Kröger • H.-P. Kriegel
Lehr-und Forschungseinheit für Datenbanksysteme, Ludwig-Maximilians-Universität München, Oettingenstraße 67, 80538 Munich, Germany
e-mail: mauder@dbs.ifi.lmu.de

G. Grupe, G.C. McGlynn (eds.), *Isotopic Landscapes in Bioarchaeology*,
DOI 10.1007/978-3-662-48339-8_13

predicting the origins of new samples is a supervised task (classification/regression).

A critical question at the current state of the project is the small size of the dataset, which at the moment comprises less than 100 samples. Therefore, caution is advised since these preliminary results could be misleading. Enriching the dataset with new samples would greatly benefit the analysis process. There are further samples which can be employed; however, these samples are acquired after cremation. $\delta^{18}O$ is known to be altered at high temperatures and therefore its measurement after cremation is not reliable for our analysis. Except for this "practical issue," the effect of oxygen stable isotopes on isotopic fingerprinting comprises an open discussion in the community. Therefore, in this chapter we focus on whether and how the inclusion/exclusion of $\delta^{18}O$ affects the results. To this end, we build (using clustering) different fingerprints for both the cases with and without oxygen and we compare how the cluster patterns change due to the exclusion of oxygen. We also study the effect of oxygen on the predictive accuracy of classification models.

The rest of the chapter is organized as follows: In section "Exploratory Analysis for Oxygen," we focus on $\delta^{18}O$ and examine how it is correlated to other isotopes in the dataset and on its spatial distribution in the under investigation area. In section "Building Isotopic Fingerprints (Clustering)" isotopic fingerprinting is presented and treated as an unsupervised learning task (clustering). Here, we distinguish between considering and omitting the oxygen attribute. Predicting the origin of new samples is treated as a supervised learning task (classification) and is discussed in section "Classification with and Without Oxygen." Outlier analysis was also performed and its effect on clustering and classification is evaluated in section "Outlier Removal." A summary and discussion is presented in section "Discussion."

Exploratory Analysis for Oxygen

When considering cremated and non-cremated material, we will face the problem that for the cremated material information on the oxygen isotopes is not available. In this section, we study the correlation of $\delta^{18}O$ to other isotopes and its spatial distribution in order to evaluate its impact on the data mining task.

Correlation of $\delta^{18}O$ to Other Isotopes

If all information to be gained from oxygen is apparent from other isotopes, they are either positively or negatively correlated.

The data plotted in Fig. 1 indicates that there is no apparent linear correlation between oxygen and the other isotopes. Colors indicate the position of the data

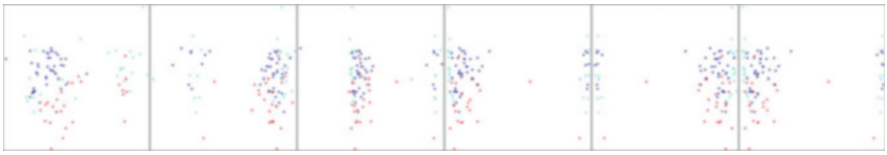

Fig. 1 Correlation of $\delta^{18}O$ (PO_4, *y*-axis) with other isotopes. From *left* to *right*: ^{87}Sr:^{86}Sr, ^{208}Pb:^{204}Pb, ^{207}Pb:^{204}Pb, ^{206}Pb:^{204}Pb, ^{208}Pb:^{207}Pb, ^{206}Pb:^{207}Pb. Colors correspond to spatial locations: *blue* (north), *red* (center), *cyan* (south) of the Alps

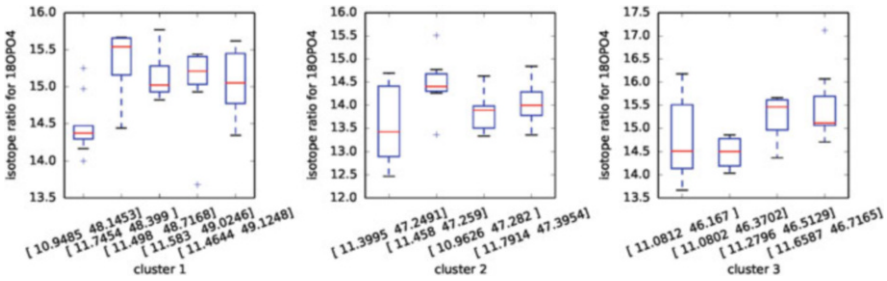

Fig. 2 Oxygen isotope distribution by location [clusters 1, 2, 3 correspond to regions 1 (north), 2 (inneralpine), 3 (south)]

point in question in the northern, central, or southern part of the surveyed area. A positive linear correlation would be indicated by the points falling on a diagonal from the origin to the top right and an inverse correlation by a line from top left to bottom right. Since the points in the diagram scatter along no apparent lines there is either a complex (non-linear) correlation or no correlation at all. If there is indeed no correlation, this may indicate one of two scenarios: either $\delta^{18}O$ is orthogonal to the other isotopes, and as such, highly relevant for differentiation between isotopes, or it is uncorrelated because it does not indicate any association.

Oxygen Distribution in Spatial Aggregations

The assumption underlying isotope fingerprint analysis is that there is a correlation between samples from the same spatial location. The dataset used in this study contains multiple locations represented by more than one sample. To viably contribute to the identification of a sample's origin, the distribution of isotopes between locations must be distinct.

In Fig. 2, the oxygen isotope distributions of several locations are displayed. Some displayed clusters have as little as five points to support their distribution, so the plots can be heavily influenced by outlying values. Despite the minimal support, it is apparent that the oxygen distribution overlaps between sites.

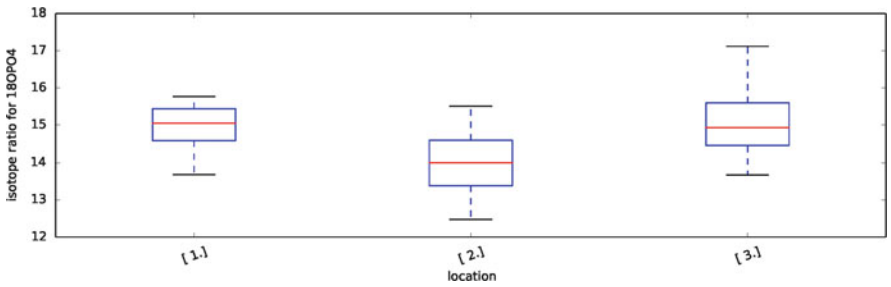

Fig. 3 Oxygen isotope distribution by region north (1), inneralpine (2), south (3)

Figure 3 aggregates regions north (1), inside (2), or south (3) of the Alps. Due to the aggregation of more points the image is better understandable. The overlap between regions is an indication that the oxygen isotope is not a strong contributor to the spatial association of isotopes.

Building Isotopic Fingerprints (Clustering)

Clustering was employed in order to place the samples into groups of similar samples and extract the isotopic fingerprints per group. For the clustering, we used all isotopic attributes (not the SE attributes though). Later, we used location information for the evaluation of the clustering results. Intuitively, we expect the extracted groups (without location information) to be spatially distinguishable.

The quality of clustering depends heavily on the quality of the underlying data. A "bad isotope" will decrease the quality of the model. A "good isotope" will function as a more realistic predictor. One without any descriptiveness will not influence the model at all.

Here we assume that data were generated by a Gaussian mixture model and we use the well-known EM algorithm (Bishop et al. 2006) to estimate the parameters of the model based on our dataset. EM alternates between an expectation E-step that reestimates the expected values of the hidden data (cluster assignments) under the current estimate of the model θ^{old} and the maximization (M-) step, which computes new model parameters θ maximizing the expected log-likelihood found on the E-step.

After an original guess of k Gaussian distributions parametrized by θ^{old} the improvement of a different parametrization θ is calculated by

$$Q\left(\theta, \theta^{\text{old}}\right) = \sum_{Z} p\left(Z \middle| X, \theta^{\text{old}}\right) \quad \ln p\left(X, Z \middle| \theta\right)$$

where X are samples in isotope space and Z are the latent variables of the model.

The highest improvement is accepted for the next round (Bishop et al. 2006 and the whole process is repeated until convergence.

We used the WEKA implementation of the EM algorithm (Hall et al. 2009), without specifying the number of clusters to be extracted. The optimal number of clusters is selected by cross-validation. In the following, we distinguish between clustering with oxygen and without oxygen. After that, we discuss their differences and the effect of oxygen.

Considering Oxygen

The samples were described in terms of all seven attributes: one oxygen isotopic ratio, one strontium isotopic ratio, and five lead isotopic ratios.

The algorithm resulted in six clusters, the smallest one containing three instances, and the largest one containing 29 instances. The cluster population is shown in Table 1. For cluster description, we provide the boxplots of the different attributes for each cluster. Boxplots are intuitive since they display the median, minimum, maximum values, quartiles, and outliers.[1] The results are shown in Fig. 4. From the resulting boxplots, it can be derived that none of the isotopic ratios alone can distinguish between all clusters. For example, if only strontium (top left) is considered, we would probably end up in only two clusters (the members of cluster 1 and cluster 6 are merged to one cluster; the instances of the remaining clusters form the second group). Similar observations can be made for the other isotopes except oxygen (bottom right). Considering only oxygen is not discriminative enough to detect the clusters since the ranges of values of the clusters significantly overlap each other.

We visualized the clusters versus the sample locations to show the spatial distribution of the isotope clusters; the results are shown in Fig. 5. Each pie in the figure indicates one location. The size of the slices indicates the ratio each of the represented clusters has in that location. Circles of a solid color indicate locations with a single cluster. Spatial distribution of points of a cluster can be estimated by the range of locations containing the color of that cluster.

We can see that some clusters consist of members which are spatially close like the red (\#14 instances) and purple (\#7 instances) cluster. However, there are clusters scattered over different places like the pink (\#27 in-stances) cluster

Table 1 The population of the extracted clusters (oxygen case)

Cluster-ID	0	1	2	3	4	5
# Instances	14 (15 %)	29 (30 %)	3 (3 %)	16 (17 %)	27 (28 %)	7 (7 %)

[1] http://flowingdata.com/2008/02/15/how-to-read-and-use-a-box-and-whisker-plot/

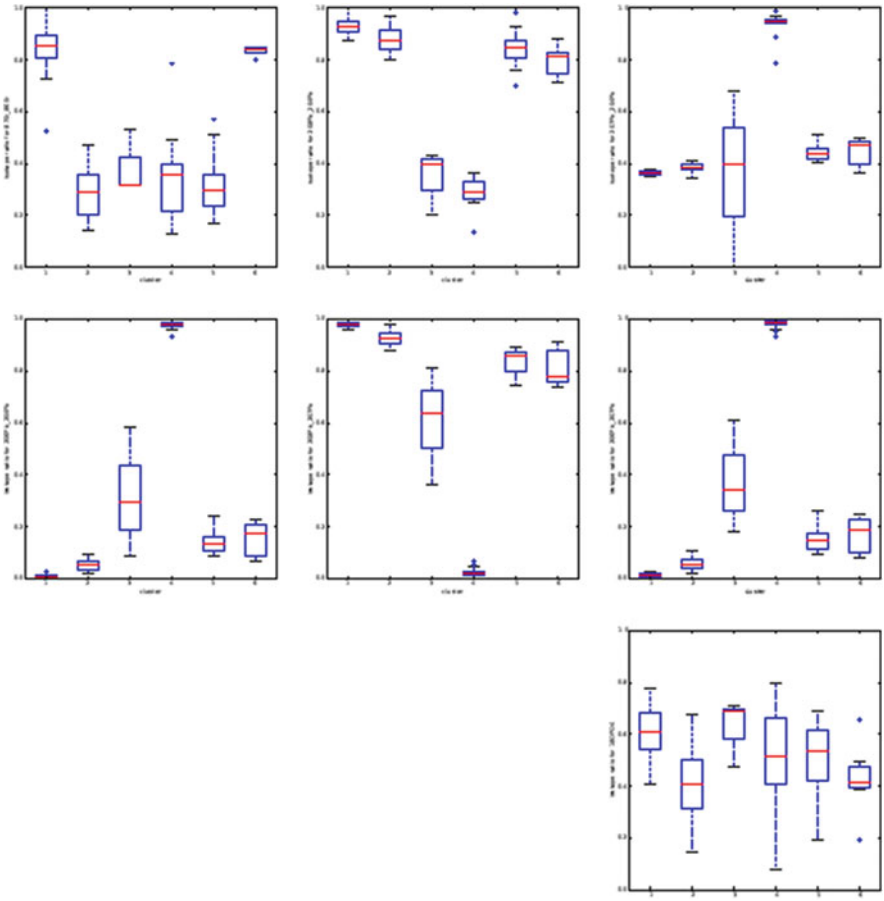

Fig. 4 Boxplots per attribute (from *top left*: $^{87}Sr/^{86}Sr$, $^{208}Pb/^{204}Pb$, $^{207}Pb/^{204}Pb$, $^{206}Pb/^{204}Pb$, $^{208}Pb/^{207}Pb$, $^{206}Pb/^{207}Pb$, $\delta^{18}O_{PO4}$) and cluster (oxygen case)

which is located in Germany–Austria, the green (\#29 instances) cluster that is located almost exclusively in Germany–Austria, and the blue (\#16 instances) cluster that is located in Germany–Italy.

So it seems that the resulted clusters based solely on isotopes are not as spatially connected as expected.

Omitting Oxygen

Oxygen is sensitive to cremation procedures, in contrast to strontium and lead isotopes. Therefore, we want to check how the clustering results, and therefore the isoscaping, are affected by excluding oxygen from clustering. To this end, we

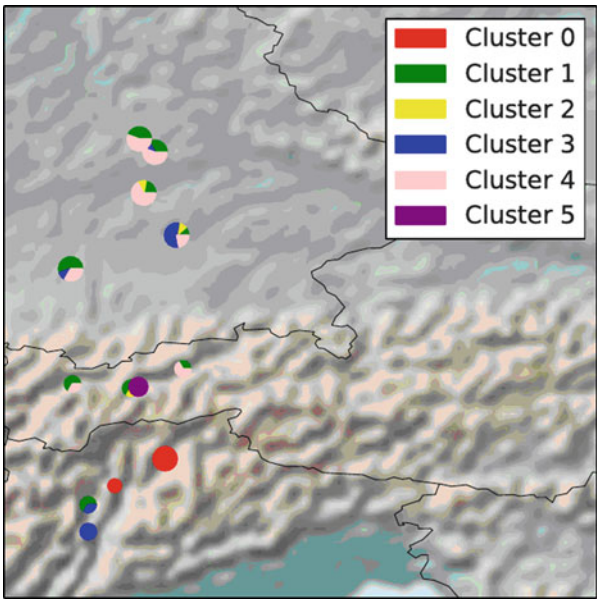

Fig. 5 Detected clusters versus location of the samples (oxygen case)

Table 2 The population of the extracted clusters (no-oxygen case)

Cluster-ID	0	1	2	3	4	5
# Instances	7 (7 %)	15 (16 %)	3 (3 %)	16 (17 %)	40 (42 %)	15 (16 %)

repeat the clustering experiment, but this time we leave out the oxygen attribute and we rely solely on strontium and lead isotopic values.

The new clustering also results in six clusters, whose population is displayed in Table 2. For a better comparison across the different clusters, we again display the boxplots for each cluster along each dimension in Fig. 6. Oxygen is included in the visualization (but not considered by the clustering algorithm).

We visualized the clusters versus the samples locations; the results are shown in Fig. 7. The picture is quite similar to what we observed for the no-oxygen case in Fig. 5.

The Effect of Oxygen on Clustering

A visual inspection of the clustering with oxygen and the clustering without oxygen indicates that some samples are co-clustered in both cases. However, in order to understand the exact mapping of the clusters from the oxygen to the no-oxygen clustering case, we relied upon the intersection of the cluster members following the MONIC framework (Spiliopoulou et al. 2006).

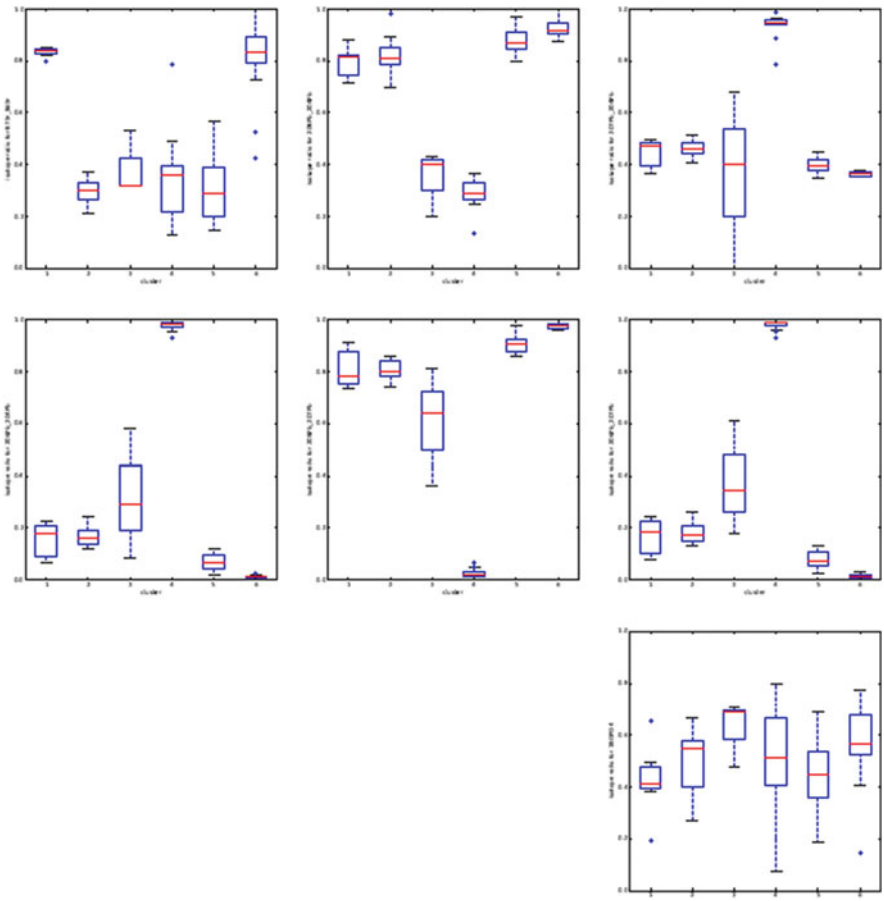

Fig. 6 Boxplots per attribute (from *top left*: $^{87}Sr/^{86}Sr$, $^{208}Pb/^{204}Pb$, $^{207}Pb/^{204}Pb$, $^{206}Pb/^{204}Pb$, $^{208}Pb/^{207}Pb$, $^{206}Pb/^{207}Pb$) and cluster (no-oxygen case)

For each cluster of the oxygen clustering, we found its intersection to all clusters of the no-oxygen clustering. The corresponding intersection matrix is displayed in Table 3.

As we can see, cluster 0 of the oxygen case (red color) survived entirely to cluster 5 of the no-oxygen case (pink color). Also, cluster 2 of the oxygen case (yellow color) survived entirely to cluster 2 of the no-oxygen case (gray color). Similarly, cluster 3 of the oxygen case (blue color) survived entirely to cluster 3 of the no-oxygen case (black color). Moreover, cluster 5 of the oxygen case (purple color) survived entirely to cluster 0 of the no-oxygen case (cyan color). Cluster 1 (green color) almost exclusively survived into cluster 4 (white color) and a tiny percentage to cluster 5 (pink color). A split occurred, namely cluster 4 of the oxygen case (pink color) was split into two clusters for the no-oxygen case: cluster 1 (orange

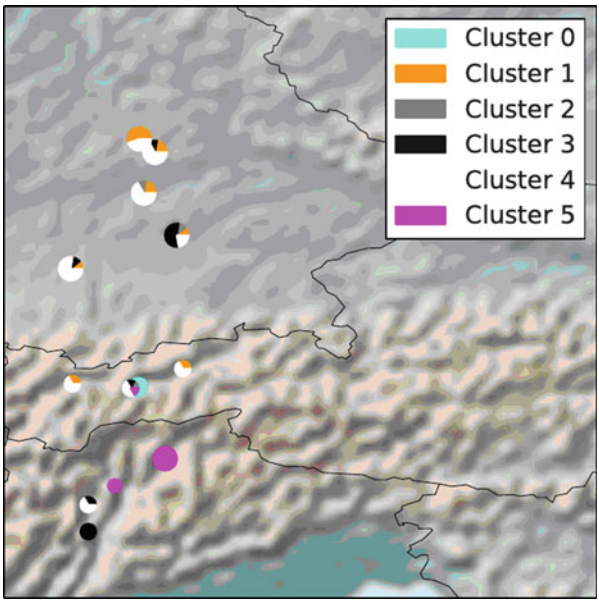

Fig. 7 Detected clusters versus locations of the samples (no-oxygen case)

Table 3 Migration of samples between clusters when using oxygen (*y*-axis) versus no oxygen (*x*-axis)

	No oxygen					
Oxygen	0	1	2	3	4	5
0	0	0	0	0	0	1
1	0	0	0	0	0.97	0.03
2	0	0	1	0	0	0
3	0	0	0	1	0	0
4	0	0.56	0	0	0.44	0
5	1	0	0	0	0	0

color) and cluster 4 (white color). Cluster 4 of the no-oxygen case (white color) is the result of a merging from cluster 1 (green color) and cluster 4 (pink color) of the oxygen case.

So, in total some clusters are entirely untouched by the omission of oxygen, whereas two others were involved in merge and split operations. The clusters merging and splitting are on the one hand spatially close and on the other they comprise a large region, indicating that they are very broad themselves. This explains some of the instability of these clusters and that they are susceptible to disruption by not very indicative isotopes. These findings support the notion that oxygen is not a key feature for isotopic fingerprinting.

Classification with and Without Oxygen

From the spatial information associated with samples, a class label can be derived, which can then be used to build a model for this set of samples. More specifically, we categorized the data based on their spatial coordinates into classes "north," "middle," and "south" of the Alps. This is termed a "supervised" data mining task. Based on these models, the association with a previously unseen sample can be established.

A classification model is built upon a training set of known class labels and its performance is evaluated over a test set of known labels which are employed during training. The idea is that the model should be able to best describe the training set but also to generalize in case of unseen instances by the model. By splitting a dataset with known class labels in non-overlapping training and test sets, we avoid the problem of overfitting.

To judge the effect of oxygen on classification, we build two classification models, one considering and one omitting oxygen, and we compare the classifiers performance. If the classification performance grows with the omission of oxygen, its inclusion had a detrimental effect on the quality of the classification model. If it shrinks, oxygen contributes to the performance. Finally, if the classification performance is not significantly affected, the omission of oxygen has no effect.

Table 4 shows a few indicating values about the quality of the classification with oxygen and without it.

A summarizing value that can be used for direct comparison is the F-Measure. It is defined as:

$$F_1 = 2 \times \frac{\text{precision} \times \text{recall}}{\text{precision} + \text{recall}}$$

In direct comparison, classification values with oxygen are a bit higher than the ones without oxygen, but not by a large margin (0.83 vs. 0.76). This seems to indicate that oxygen can indeed contribute to the classification result.

As a baseline, we re-ran the classification experiments considering each isotope alone, i.e., in an univariate setting. Table 5 shows the classification performance based on distinct isotopes. The performance of the univariate classifiers built upon single isotopes is very low and much lower compared to the multivariate classifier. Surprisingly, oxygen performed best of all isotopes tested in this experiment. This may indicate that it is helpful, but stands in direct opposition with the findings above, where its removal had relatively little effect. It is important to note that there

Table 4 Classification quality

	TP rate	FP rate	Precision	Recall	F-measure
Oxygen	0.833	0.115	0.837	0.833	0.832
No oxygen	0.76	0.168	0.768	0.76	0.759

Table 5 Classification performance when using only one isotope at a time

	TP rate	FP rate	Precision	Recall	*F*-measure	ROC area
$\delta^{18}O_{PO4}$	0.542	0.297	0.536	0.542	0.531	0.665
$^{87}Sr/^{86}Sr$	0.51	0.252	0.524	0.51	0.515	0.645
$^{208}Pb/^{204}Pb$	0.479	0.302	0.48	0.479	0.479	0.576

is no direct correlation between an attribute's individual classification power and the aggregation of multiple attributes.

Outlier Removal

Outliers (Hawkins 1980) have a negative effect on data mining tasks, and therefore, it is important to see whether outliers exist in our dataset. For the outlier detection, we rely on the interquartile range test and consider as extreme outliers all those points that belong to the lower outer fence ($Q1 - 3 \times IQ$) and the upper outer fence ($Q3 + 3 \times IQ$). IQ is the interquartile range (Q3–Q1), where Q1 is the lower quartile (the 25th percentile) and Q3 is the upper quartile (the 75th percentile).

Instances which contain at least one attribute with outlier values are considered as outlier instances. The outlier analysis resulted in 17 instances containing outlier values out of the 96 instances of our original dataset.

The outlier versus the inlier instances were spatially projected and are depicted in Fig. 8. One can see that the outliers (green color) are located in the south and in the north. A closer inspection of the results and an association with the clustering results presented in the previous sections shows that the outlier instances are mainly members of a single cluster (blue cluster for the oxygen case and black cluster for the no-oxygen case). This cluster seems quite "suspicious" spatially in the sense that its members reside in north or south and there are no members in the central Alps. This is in contrast to other spatially mixed clusters that are spread all over the three countries.

We filtered out the outlier instances and build a classifier model (*k*NN classifier, $k = 1$) over the cleaned instances (79 inlier instances remained after cleaning). On average, the accuracy improved by 5 % compared to considering the whole dataset case which also includes the outlier points.

Discussion

The number of data points analyzed is quite small (\#96 data points) and scattered over only few sites (\#13). This is particularly problematic when the goal is to build a model of the covered areas (isotopic fingerprinting) and use these models for

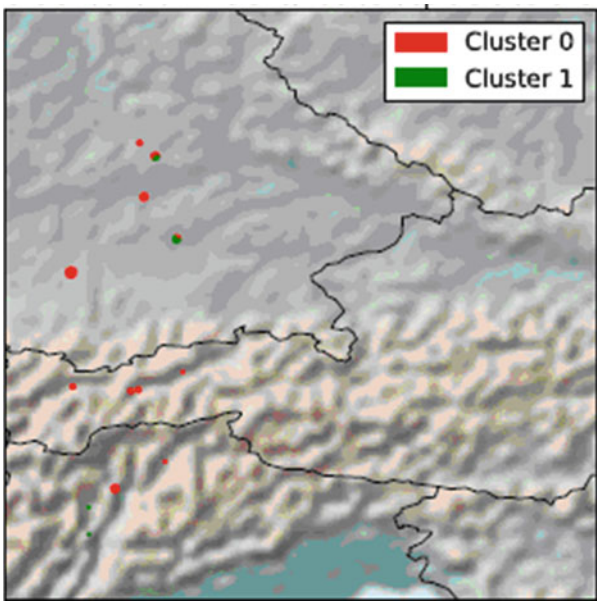

Fig. 8 Outlier instances (*green color*) versus non-outlier instances (*red color*)

origin prediction for future samples. To exacerbate the situation, some of the points stand out as different (outliers). If these points were spatially constrained, this would indicate a particularly clear fingerprint for that region. However, the outlier points are not constrained; rather they are scattered all over the covered area, allowing no such conclusion. Ignoring the outliers from the analysis results in further shrinkage of the training set and therefore the danger of overfitting is even larger.

Based on these limitations, we took a first step towards analyzing these data in terms of clustering, classification, and outlier detection for isotopic fingerprinting and origin prediction. We focused in this study on the effect of oxygen, which is sensitive to high temperatures, and how its inclusion/exclusion affects the results of the corresponding analysis. Our findings in terms of extracted cluster and classification models with and without oxygen indicate that oxygen does not contribute strongly to the results.

References

Ambrose SH, Krigbaum J (2003) Bone chemistry and bioarchaeology. J Anthropol Archaeol 22:193–199

Bishop CM et al (2006) Pattern recognition and machine learning, vol 1. Springer, New York

Hall M, Frank E, Holmes G, Pfahringer B, Reutemann P, Witten ICH (2009) The WEKA data mining software: an update. SIGKDD Explor Newsl 11:10–18

Hawkins D (1980) Identification of outliers, vol 1. Chapman and Hall, London
Meier-Augenstein W, Kemp HF (2009) Stable isotope analysis: general principles and limitations. Wiley, Hoboken
Spiliopoulou M, Ntoutsi E, Theodoridis Y, Schult R (2006) MONIC: modeling and monitoring cluster transitions. In: Proceedings of the 12th ACM international conference on knowledge discovery and data mining (SIGKDD), Philadelphia, PA, pp 706–711

Index

G. Grupe, G.C. McGlynn (eds.), *Isotopic Landscapes in Bioarchaeology*,
DOI 10.1007/978-3-662-48339-8